Geoscience BC

Summary of Activities

2019 Minerals

Geoscience BC

GEOSCIENCE BC SUMMARY OF ACTIVITIES 2019: MINERALS

Geoscience BC Report 2020-01

This publication is also available, free of charge, as colour digital files in Adobe Acrobat® PDF format from the Geoscience BC website: http://www.geosciencebc.com/s/SummaryofActivities.asp.

Every reasonable effort is made to ensure the accuracy of the information contained in this report, but Geoscience BC does not assume any liability for errors that may occur. Source references are included in the report and the user should verify critical information.

When using information from this publication in other publications or presentations, due acknowledgment should be given to Geoscience BC. The recommended reference is included on the title page of each paper. The complete volume should be referenced as follows:

Geoscience BC (2020): Geoscience BC Summary of Activities 2019: Minerals; Geoscience BC, Report 2020-01, 172 p.

Summary of Activities: Minerals (Geoscience BC)
Annual publication

ISSN 2562-8623 (Print)
ISSN 2562-8631 (Online)

Geoscience BC
1101–750 West Pender Street
Vancouver, British Columbia V6C 2T7
Canada

Front cover photo and credit: Mineral Deposit Research Unit (The University of British Columbia) field assistant, A. Boileau Morrison, at Alunite ridge, Toodoggone district, northern British Columbia (F. Bouzari, 2019).

Back cover photo and credit: Chalcopyrite and pyrite in quartz specimen from the Granisle copper mine, on display at the Lakes District Museum Society in Burns Lake, British Columbia (J. Moffat, 2019).

Foreword

Geoscience BC is pleased to once again present results from our ongoing projects and scholarship winners in our annual *Summary of Activities* publication. Papers are published in two separate volumes: *Energy and Water*, and this volume, *Minerals*. Both volumes are available in print and online via www.geosciencebc.com.

Summary of Activities 2019: Minerals

This volume, *Summary of Activities 2019: Minerals*, contains 20 papers from Geoscience BC–funded projects or scholarship recipients that are within Geoscience BC's strategic focus area of minerals. The papers are divided into two sections, based on Geoscience BC's strategic objectives of

1) Identifying New Natural Resource Opportunities, and
2) Advancing Science and Innovative Geoscience Technologies.

The first two papers in the 'Identifying New Natural Resource Opportunities' section focus on northern Vancouver Island. Clift et al. describe Geoscience BC's latest airborne magnetic and radiometric survey in the region, which adjoins an earlier Geoscience BC–supported magnetic survey flown in 2012. Morris and Canil examine skarn mineralization in the Merry Widow Mountain area.

Four papers present research into mineralization or coal in southern British Columbia (BC). Branson et al. highlight exploration for podiform chromite occurrences using ground magnetometry. Höy et al. discuss ongoing work on mineral potential in the east half of the Penticton map area (NTS 082E), and Rioseco et al. present new Ar/Ar ages for the Purcell Anticlinorium and the Kootenay Arc. Also in the Kootenay region, Kuppusamy and Holuszko introduce a new Geoscience BC–supported project to investigate the potential for extracting rare-earth elements from East Kootenay coal seams.

Two papers discuss the potential of machine-learning techniques to support mineral exploration in BC. In Grunsky and Arne, advanced data analytics and machine learning are applied to the results from regional stream-sediment sampling in southwestern BC. Murphy et al. introduce a project designed to develop a database of gold compositions from across the province, which can be interrogated using machine-learning techniques.

Finally, Sacco et al. highlight initial activities being undertaken in one of Geoscience BC's new Central Interior Copper-Gold Research series of projects. These projects, which will start new field activities in 2020, are focused on investigating the potential for undiscovered mineral deposits buried beneath thick glacial sediments between Mackenzie and Williams Lake.

In the 'Advancing Science and Innovative Geoscience Technologies' section, three papers highlight new methods in exploration geochemistry. Lett et al. present an investigation into the use of soil-gas detectors for mapping geological faults and detecting buried mineralization, as soil-gas anomalies have been reported above faulting and mineralization from a range of deposits across the northern hemisphere. Dunn and Heberlein took advantage of archived tree-top samples collected during the TREK project to further research the use of halogen elements as an exploration tool. Jackaman and Lett investigate a modified regional stream-sediment sampling methodology that integrates the collection of bulk-sediment samples to derive mineralogical information with trace-metal data in south-central BC.

Three papers describe research into new tools and techniques that will benefit exploration in BC. Bouzari et al. introduce a new project examining advanced argillic alteration associated with BC porphyry systems to identify key textural, mineralogical and geochemical trends to help guide exploration across the province. Mackay et al. discuss their ongoing study using the Roben Jig to clean exploration coal samples for analysis. Finally, Cutts et al. describe an exciting new project aimed at assessing the potential for rocks in BC to sequester atmospheric carbon dioxide in minerals.

Three papers describe new Geoscience BC initiatives focused on preserving BC's geological heritage. Barlow et al. describe the methods and benefits of capturing geoscience data contained in NI 43-101 reports pertaining to BC and making them searchable by location through a map layer hosted by Geoscience BC and also updating MINFILE occurrences. Randell et al. introduce a project aimed at digitally preserving key rock and mineral samples in BC through an online, interactive museum; and Ledwon and Ogryzlo highlight updates to the Smithers Exploration Group's Rock Room.

The final two papers present the results of ongoing mining-reclamation studies led by Thompson Rivers University. Gervan et al. examine the response of invertebrates to reclamation and soil-amendment treatments, and Fischer et al. consider microbial and geochemical changes within topsoil stockpiles set aside for post-mining reclamation.

Geoscience BC Minerals Publications 2019

In addition to the two *Summary of Activities* volumes, Geoscience BC releases interim and final products from our projects as Geoscience BC reports. The following seven Minerals reports and maps were published in 2019:

- Twelve technical papers in the *Geoscience BC Summary of Activities 2018: Minerals and Mining* volume (Geoscience BC Report 2019-01)
- **Bedrock Geology, Search Phase I Project Area, Western Skeena Arch, West-Central British Columbia,** by J.J. Angen, M. Rahimi, J.L. Nelson and C.J.R. Hart (Geoscience BC Map 2019-03-01 / MDRU Map 17-2018 / BCGS Open File 2019-07)
- **Aeromagnetic Correlation with Bedrock Geology, Search Phase I Project Area, Western Skeena Arch, West-Central British Columbia,** by J.J. Angen, M. Rahimi, J.L. Nelson and C.J.R. Hart (Geoscience BC Map 2019-03-02 / MDRU Map 18-2018 / BCGS Open File 2019-08)
- **Mineral Mapping Using ASTER Data, Search Phase I Project Area, Western Skeena Arch, West-Central British Columbia,** by M. Rahimi, J.J. Angen and C.J.R. Hart (Geoscience BC Map 2019-03-03 / MDRU Map 19-2018)
- **Geology of the Penticton Map Sheet (east half; NTS 082E/01, 02, 07, 08, 09, 10, 15, 16),** by T. Höy (Geoscience BC Map 2019-04)
- **Producing Clean Coal from Western Canadian Coal Fields using the Water-Based Roben Jig: Refining the Process,** by M. Mackay, R. Leeder, L. Giroux, M. Holuszko, H. Dexter and D. Thomas (Geoscience BC Report 2019-05)
- **An Exploration Framework for Porphyry to Epithermal Transitions in the Toodoggone Mineral District (094E),** by F. Bouzari, T. Bissig, C.J.R. Hart and H. Leal-Mejía (Geoscience BC Report 2019-08 / MDRU Publication 424)

All releases of Geoscience BC reports, maps and data are published on our website and are announced through e-mail updates. Most final reports and data can also be viewed or accessed through our Earth Science Viewer at https://gis.geosciencebc.com/esv/?viewer=esv.

Acknowledgments

Geoscience BC would like to thank all authors and reviewers of the *Summary of Activities* for their contributions to this volume. RnD Technical is also acknowledged for its work in editing and assembling both volumes. As well, Geoscience BC would like to acknowledge the Province of British Columbia and our project funding partners for their ongoing support of public geoscience, and express our appreciation for the leaders and volunteers in British Columbia's mineral exploration, mining and energy sectors who support our organization through their guidance, use and recognition of the information that we collect and distribute.

Christa Pellett
Vice President, Minerals
Geoscience BC
www.geosciencebc.com

Contents

Identifying New Natural Resource Opportunities

Advancing Science and Innovative Geoscience Technologies

Vancouver Island North Regional Project: Airborne Magnetic and Radiometric Survey, British Columbia (Parts of NTS 092E, F, K, L)

B.K. Clift, Geoscience BC, Vancouver, British Columbia, clift@geosciencebc.com

T.A. Ballantyne, in3D Geoscience Inc., Gabriola, British Columbia

C.L. Pellett, Geoscience BC, Vancouver, British Columbia

Clift, B.K., Ballantyne, T.A. and Pellett, C.L. (2020): Vancouver Island North Regional Project: airborne magnetic and radiometric survey, British Columbia (parts of NTS 092E, F, K, L); *in* Geoscience BC Summary of Activities 2019: Minerals, Geoscience BC, Report 2020-01, p. 1–4.

Introduction

The Vancouver Island North Regional Project (VIN) is designed to provide high-quality airborne geophysical data over 6127 km^2 of northern Vancouver Island, British Columbia (BC; Figure 1), an area with a long history of mining and mineral exploration. The project falls within the Wrangellia terrane—a mixture of Triassic through Jurassic volcanic and sedimentary sequences, including the Karmutsen Formation and Bonanza Group (Nixon et al., 2011a–c). The VIN project covers prospective trends for Jurassic and Miocene porphyry copper deposits, Eocene gold vein deposits, Jurassic iron and copper skarn deposits, and Paleozoic volcanogenic massive sulphide deposits (J. Houle, pers. comm., 2014).

Following in the Geoscience BC tradition of regional geophysical surveys such as Targeting Resources through Exploration and Knowledge (TREK) and Search, these new geophysical data will assist the mineral exploration community in identifying regional geological and structural mineral exploration targets, thereby providing new economic stimulation to the region. Geoscience BC is committed to engaging with communities in the region to share information during and after the project is completed.

Previous Work

The VIN covers an area that had not been surveyed as part of a regional geophysical program since the 1980s (Natural Resources Canada, 2019). Survey lines at that time were flown 1500 m apart. The project builds on the 2012 Northern Vancouver Island Exploration Geoscience Project, which was a partnership between Geoscience BC and the Island Coastal Economic Trust (ICET; Simpson et al., 2013). The 2012 airborne magnetic survey was conducted using a predefined drape surface with a nominal ground clearance of 80 m at 250 m line-spacing over the northwestern extent of Vancouver Island (Figure 1). The work carried out in 2012 included the collection of new regional geochemical data for northern Vancouver Island (Geo Data Solutions GDS Inc., 2013; Jackaman and Lett, 2013; Simpson et al., 2013). The geochemical survey covered a much larger area than the magnetic survey, which overlapped the northern part of the new VIN project area. Geological mapping in the region has been recently updated by the BC Geological Survey (Nixon et al., 2011a–c).

Vancouver Island North Regional Project

Covering approximately 20% of Vancouver Island, the airborne survey carried out under the VIN project collected horizontal gradient magnetic data as well as radiometric data. The survey was flown by Precision GeoSurveys Inc. of Langley, BC, between August and October 2019. The survey area is located between the communities of Port Alice and Zeballos on the west, Sayward on the east, Gold River on the south and Port McNeill on the north (Figure 1). In total, data were collected over 26 973.4 line-km at a constant height of 80 m above ground level. The sensors used were attached to an Airbus AS350 helicopter flying along lines 250 m apart and oriented at 56.5°, with tie lines flown every 2500 m, perpendicular to the main flight lines. Within the project area there are three large provincial parks, which were excluded from the survey, and communities within the survey area were flown at a minimum of 300 m above ground level. The survey overlaps slightly with the 2012 Northern Vancouver Island Exploration Geoscience Project magnetic survey so that the two surveys can be levelled.

The VIN 2019 survey height was maintained at a constant 80 m above ground surface, following the contours of the terrain as much as possible, within the limitations of pilot safety. In contrast, the 2012 Northern Vancouver Island Exploration Geoscience Project survey was flown using a pre-

This publication is also available, free of charge, as colour digital files in Adobe Acrobat® PDF format from the Geoscience BC website: http://www.geosciencebc.com/updates/summary-of-activities/.

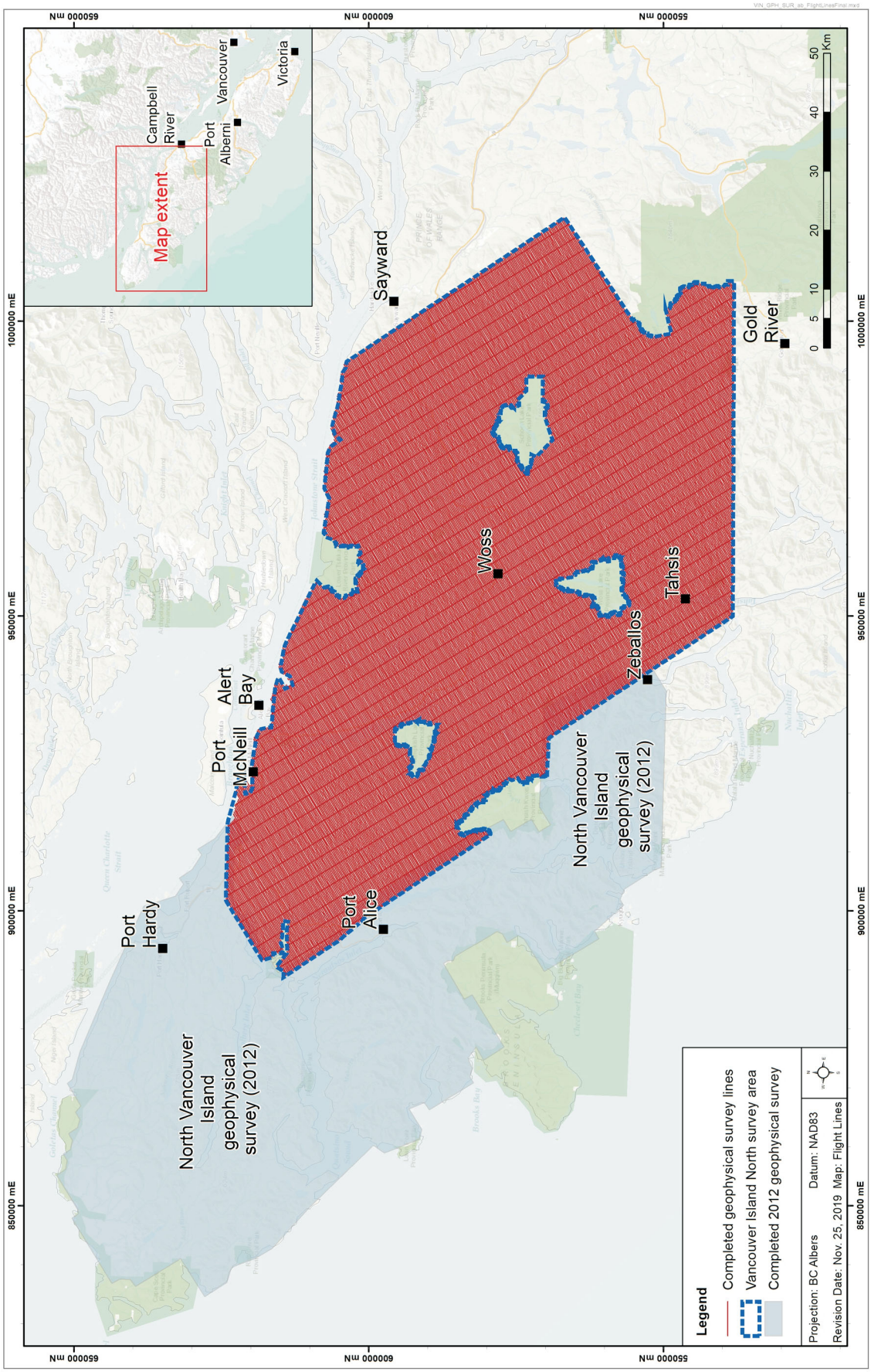

Figure 1. Vancouver Island North (VIN) Regional Project area, British Columbia. Geophysical survey lines (oriented at 56.5° and spaced 250 m apart) and tie lines (spaced 2500 m apart) are shown in red. The area covered by the geophysical survey undertaken by Geoscience BC in 2012 as part of the Northern Vancouver Island Exploration Geoscience Project is shown in blue. Background map created using ArcGIS® software by Esri. ArcGIS® and ArcMap™ are the intellectual property of Esri and are used herein under license. Copyright © Esri. All rights reserved. For more information about Esri software, please visit www.esri.com.

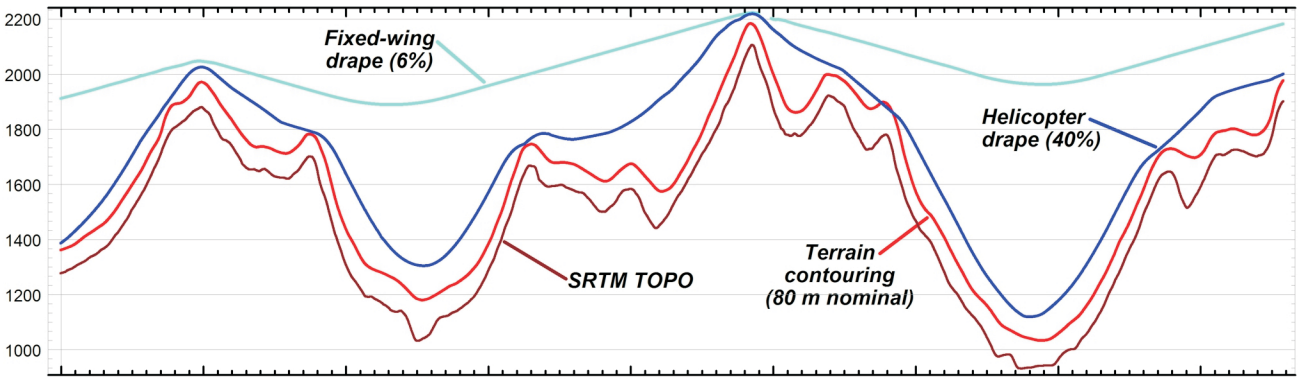

Figure 2. Example of airborne survey height above rugged topography using 'terrain contouring' (red line), which closely follows the contours of the terrain, within the limitations of pilot safety, compared to two examples of 2-D preplanned drape surveys (a fixed-wing drape surface using 6% slope, shown in light blue, and a hypothetical helicopter 40% drape surface, shown in dark blue). The 2-D drape surfaces were calculated using the Geological Survey of Canada's Drape DTM 2.0 software. Note that the vertical axis is exaggerated. All survey heights are relative to Shuttle Radar Topography Mission topography (SRTM TOPO).

defined drape surface (i.e., preplanned terrain clearance) and had a 20% rate of ascent and descent above the surface, resulting in a nominal ground clearance of 80 m. Figure 2 (reproduced from Madu and Ballantyne, 2018) illustrates the benefit of surveys flown at a constant height above ground in mountainous terrain, compared to a common alternative of preplanned flight surface. (Note that in this figure an example of a 40% helicopter drape is shown.)

Magnetic Survey

Three Scintrex CS-3 cesium-vapour airborne magnetometer sensors were arranged into a triple-boom magnetometer configuration on an Airbus AS350 helicopter (Figure 3). Sensor separation was 11.5 m perpendicular to the direction of flight (cross-line) and 7.3 m in the direction of flight (in-line), which allowed for simultaneous collection of magnetic data at three different locations with known and fixed separation. The magnetometers measure total magnetic field, cross-line magnetic gradient (transverse) and in-line gradient (longitudinal).

Figure 3. Precision GeoSurveys Inc.'s Airbus AS350 helicopter, which was used to fly the Vancouver Island North airborne survey. Survey equipment included three Scintrex CS-3 cesium-vapour airborne magnetometer sensors arranged into a triple-boom magnetometer configuration (shown), and 21 L of sodium iodide (NaI) gamma radiation detection crystals. Photo courtesy of Precision GeoSurveys Inc.

Radiometric Survey

Radiometric data, consisting of potassium, thorium and uranium gamma radiation naturally emitted from surface rocks and soils, were measured using an airborne gamma-ray spectrometer with 16.8 L of downward-looking sodium iodide (NaI) crystals. Radiometric data complement magnetic data, representing a different rock property, which contributes to more accurate mapping of lithology, alteration and geological structure.

Summary

The VIN project covers an area that had not been surveyed as part of a regional geophysical program since the 1980s; survey lines at that time were flown 1500 m apart. The VIN survey offers data with a much higher resolution and an exponential increase in the density of sampling. Northern Vancouver Island will now have a modern and highly detailed magnetic and radiometric survey to guide exploration, land use and planning decisions for a significant portion of the island.

Acknowledgments

The authors would like to acknowledge J. Houle for his technical input to the survey boundaries and enduring support of the Vancouver Island mineral exploration community. This paper benefited from the peer review conducted by C. Salas.

References

Geo Data Solutions GDS Inc. (2013): Heliborne high resolution aeromagnetic survey: northern Vancouver Island, BC; Geoscience BC, Report 2013-02, 26 p., URL <http://www.geosciencebc.com/reports/gbcr-2013-02/> [November 2019].

Jackaman, W. and Lett, R.E.W. (2013): Updating the British Columbia Regional Geochemical Survey database with new field survey and sample reanalysis data to support mineral exploration (NTS 082F,K, 092K, L, 093J, 102I); *in* Geoscience BC Summary of Activities 2012, Geoscience BC, Report 2013-1, p. 5–10, URL <http://cdn.geosciencebc.com/pdf/SummaryofActivities2012/SoA2012_Jackaman.pdf> [November 2019].

Madu, B.E. and Ballantyne, T. (2018): Search Project: Phase III activities in north-central British Columbia (Phase III, covering NTS 094C, D, E, F, 093M, N); *in* Geoscience BC Summary of Activities 2017: Minerals and Mining, Geoscience BC, Report 2018-01, p. 1–6, URL <http://cdn.geosciencebc.com/pdf/SummaryofActivities2017/MM/SoA2017_MM_Madu.pdf> [November 2019].

Natural Resources Canada 2019: Magnetics – total field; *in* Geoscience Data Repository for Geophysical Data, Magnetic-Radiometric-EM, Natural Resources Canada, URL <http://gdr.agg.nrcan.gc.ca/gdrdap/dap/search-eng.php?tree-0=Magnetic-Radiometric-EM+-+Magn%C3%A9tiques-Radioactivit%C3%A9-%C3%89M&tree-1=Click+here+for+more+options&tree-2=Click+here+for+more+options&tree-3=Click+here+for+more+options&datatype-ddl=MAG&layer_name=&submit_search=Submit+Search#results> [March 2019].

Nixon, G.T., Hammack, J.L., Koyanagi, V.M., Payie, G.J., Orr, A.J., Haggart, J.W., Orchard, M.J., Tozer, E.T., Friedman, R.M., Archibald, D.A., Palfy, J. and Cordey, F. (2011a): Geology, geochronology, lithogeochemistry and metamorphism of the Quatsino-Port McNeill area, northern Vancouver Island (NTS 92L/11, and parts of 92L/05, 12 and 13); BC Ministry of Energy, Mines and Petroleum Resources, BC Geological Survey, Geoscience Map 2011-02, scale 1:50 000, URL <http://webmap.em.gov.bc.ca/mapplace/minpot/Publications_Summary.asp?key=4652> [November 2019].

Nixon, G.T., Kelman, M.C., Larocque, J.P., Stevenson, D.B., Stokes, L.A., Pals, A., Styan, J., Johnston, K.A., Friedman, R.M., Mortensen, J.K., Orchard, M.J. and McRoberts, C.A. (2011b): Geology, geochronology, lithogeochemistry and metamorphism of the Nimpkish-Telegraph Cove area, northern Vancouver Island (NTS 92L/07 and part of 92L/10); BC Ministry of Energy, Mines and Petroleum Resources, BC Geological Survey, Geoscience Map 2011-05, scale 1:50 000, URL <http://webmap.em.gov.bc.ca/mapplace/minpot/Publications_Summary.asp?key=4678> [November 2019].

Nixon, G.T., Snyder, L.D., Payie, G.J., Long, S., Finnie, A., Orr, A.J., Friedman, R.M., Archibald, D.A., Orchard, M.J., Tozer, E.T., Poulton, T.P. and Haggart, J.W. (2011c): Geology, geochronology, lithogeochemistry and metamorphism of the Alice Lake area, northern Vancouver Island (NTS 92L/06 and part of 92L/03); BC Ministry of Energy, Mines and Petroleum Resources, BC Geological Survey, Geoscience Map 2011-04, scale 1:50 000, URL <http://webmap.em.gov.bc.ca/mapplace/minpot/Publications_Summary.asp?key=4677> [November 2019].

Simpson, K.A., Kowalczyk, P.L. and Kirkham, G.D. (2013): Update on Geoscience BC's 2012 geophysical programs; *in* Geoscience BC Summary of Activities 2012, Geoscience BC, Report 2013-1, p. 1–4, URL <http://cdn.geosciencebc.com/pdf/SummaryofActivities2012/SoA2012_Jackaman.pdf> [November 2019].

Skarn Mineralization along Magma-Carbonate Contacts in the Merry Widow Mountain Area, Vancouver Island, British Columbia (NTS 092L)

R.A. Morris[1], **School of Earth and Ocean Sciences, University of Victoria, Victoria, British Columbia, ramorri@uvic.ca**

D. Canil, School of Earth and Ocean Sciences, University of Victoria, Victoria, British Columbia

Morris, R.A. and Canil, D. (2020): Skarn mineralization along magma-carbonate contacts in the Merry Widow Mountain area, Vancouver Island, British Columbia (NTS 092L); *in* Geoscience BC Summary of Activities 2019: Minerals, Geoscience BC, Report 2020-01, p. 5–12.

Introduction

Wrangellia hosts nearly 50% (~350) of all documented skarn deposits within the Canadian Cordillera, the majority occurring on Vancouver Island (Ray, 2013). Many of these skarn deposits are economically significant and were historically mined for Cu-Au-Co-Ag and Fe (Merry Widow, Kingfisher, Old Sport, Zeballos, Iron Hill and Brynnor; MINFILE 092L 044, 045, 035 and 149; 092F 075 and 001; BC Geological Survey, 2019b).

The past-producing Merry Widow magnetite deposit (Merry Widow Mountain; Figure 1), along with other Fe-skarns in Wrangellia, commonly occur at the contact between intrusions of the Jurassic Bonanza arc and Upper Triassic carbonate rocks of the Quatsino Formation (i.e., the Quatsino limestone) and the Parson Bay Formation. Previous work highlights the association of nearby intrusions with skarn deposits (Sangster, 1964; Ray et al., 1995) but focused mainly on the extent of the mineralization and skarn classification rather than its cause. Attributes such as heat content, bulk composition and cooling history of the magma influence the type and endowment of skarn mineralization but were not the focus of prior studies. This research aims to quantify how these attributes influenced the extent of magma-carbonate reaction and related skarn mineralization. An end goal for this study is to establish the reacted volume per unit time between the magmas and carbonate rocks by investigating which elements are assimilated into the magma and sequestered in the intrusion (the endoskarn). This approach differs from previous efforts that targeted the development of exoskarn (the skarn mineralization that occurs within the wallrock), where most economic deposits are found.

This paper presents the preliminary results from mapping and sampling of the Merry Widow Mountain area during the 2019 summer field campaign. The Merry Widow Mountain area was selected for the initial study as it is easily accessed, has exceptional exposures and displays magma-carbonate interactions on a variety of scales (i.e., broader plutonic-carbonate interactions versus more localized dike-carbonate interactions). The study area is located on northern Vancouver Island, approximately 25 km southeast of Port Alice (Figure 1). Access is by truck from Port Alice along Highway 30 to Alice Lake Road, or via the Keogh Road from Port McNeill. Mapping and sampling were conducted along road cuts and exposures near both active and decommissioned logging roads.

Geological Setting

Wrangellia ranges from Devonian to Jurassic in age and comprises most of the Insular Belt of coastal western Canada. Most units within the terrane were first described by Muller (1977). Wrangellia accounts for the majority (~80%) of the exposed units on Vancouver Island (Figure 1; Muller and Yorath, 1977; Greene et al., 2009). A simplified summary of oldest to youngest stratigraphy on Wrangellia is as follows: Devonian island arc (Sicker Group), Mississippian to Permian siliciclastic and carbonate rocks (Buttle Lake Group), Middle to Upper Triassic large igneous province (Karmutsen Formation), Upper Triassic carbonate rocks (Quatsino Formation; herein referred to as the Quatsino limestone), Upper Triassic to Lower Jurassic calcsilicate and siliciclastic rocks (Parson Bay Formation), and Lower Jurassic arc volcanic rocks and associated intrusions (Bonanza arc; Jones et al., 1977; Muller, 1977; Massey and Friday, 1987; Nixon et al., 1993; Monger and Journeay, 1994; Nixon et al., 1995; Greene et al., 2009). Volcanic and plutonic rocks of the Jurassic Bonanza arc are the youngest units of Wrangellia.

The study area is ~7 km^2 on Merry Widow Mountain (Figure 2). The oldest rocks in the area are volcanic rocks associated with the Karmutsen Formation, just outside the northeastern part of the map area, which underlie the

[1]*The lead author is a 2019 Geoscience BC Scholarship recipient.*

This publication is also available, free of charge, as colour digital files in Adobe Acrobat® PDF format from the Geoscience BC website: http://www.geosciencebc.com/updates/summary-of-activities/.

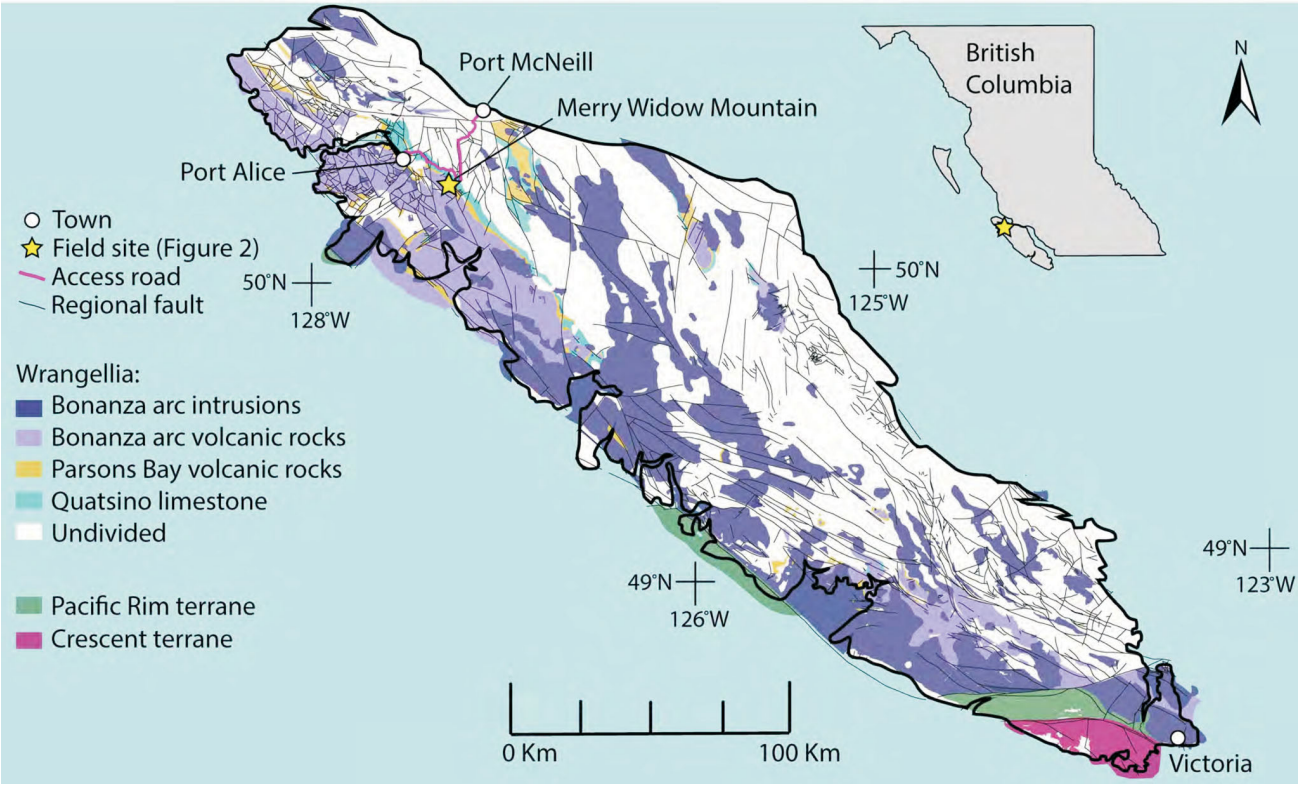

Figure 1. Regional geology of Vancouver Island, showing Wrangellia and the Pacific Rim and Crescent terranes. Wrangellia is stripped of its pre- and post-Jurassic rocks, except for Parson Bay volcanic rocks and Quatsino limestone (both Triassic), which immediately underlie the Jurassic Bonanza arc. Geological-unit boundaries and faults are from the BC Geological Survey (BCGS) MapPlace dataset (BC Geological Survey, 2019a). The Merry Widow Mountain area is located in NTS 092L.

Quatsino limestone (Figure 2; Lund, 1966; Ray and Webster, 1995; Nixon et al., 2011). Measured bedding of the Quatsino limestone and Parson Bay Formation dips gently (~20°) to the west. Mafic dikes crosscut the Quatsino limestone, the Parson Bay Formation (i.e., stratified tuff and volcanic breccia) and the Merry Widow Mountain pluton (Figure 2). Fieldwork was conducted in the eastern region of the Merry Widow Mountain pluton, where it is dominantly gabbroic.

The Merry Widow pit is situated along a prominent northeast-striking (035°), near-vertical fault (the Kingfisher fault) that propagates outward from the pluton margin (Nixon et al., 2011). Most regional faults in the area are near vertical and trend northeast (Figure 2).

Geochronology has been completed on two units within the study area and includes an $^{40}Ar/^{39}Ar$ date of 197.9 ±1.3 Ma on phlogopite within the limestone (presumably contact metamorphosed) and a U-Pb age of 197.1 ±0.3 Ma for zircon within the western region of the Merry Widow pluton (Nixon et al., 2011).

Carbonate

The Quatsino limestone is the oldest and stratigraphically lowermost unit mapped in the Merry Widow Mountain area. It is approximately 1 km in thickness and comprises massive to bedded, grey to white micrite. In some areas, the limestone is locally folded, showing evidence of ductile flow. Folding of the limestone is most apparent within graphite-rich layers (Figure 3a). Regional bedding dips gently (10–30°) to the west. The limestone is crosscut by various dikes and sills (described below) and, in some cases, forms drag folds at the contact with dikes (Figure 3b). These drag folds show evidence of slight normal offset of ~20 cm. Where present, skarn mineralization occurs at the contact of the limestone with dikes and sills, and is usually <25 cm in thickness.

Keystone Intrusion and Associated Dikes and Sills

The Keystone intrusion and associated dikes and sills weather a characteristic light green to buff colour. The groundmass is very fine grained to hypocrystalline. Mafic xenoliths with reaction rims are abundant within the unit and range in size from <1 cm to >20 cm (Figure 4a). Flow banding is common and is parallel to the margins of dikes, or of sills (Figure 4b). Sills follow limestone contacts and dip gently (~20°) to the northwest. Dikes crosscut the limestone bedding and have a moderate to steep southeast dip (~60–75°). Skarn mineralization is most common at contacts of the Keystone intrusion (and associated dikes/sills)

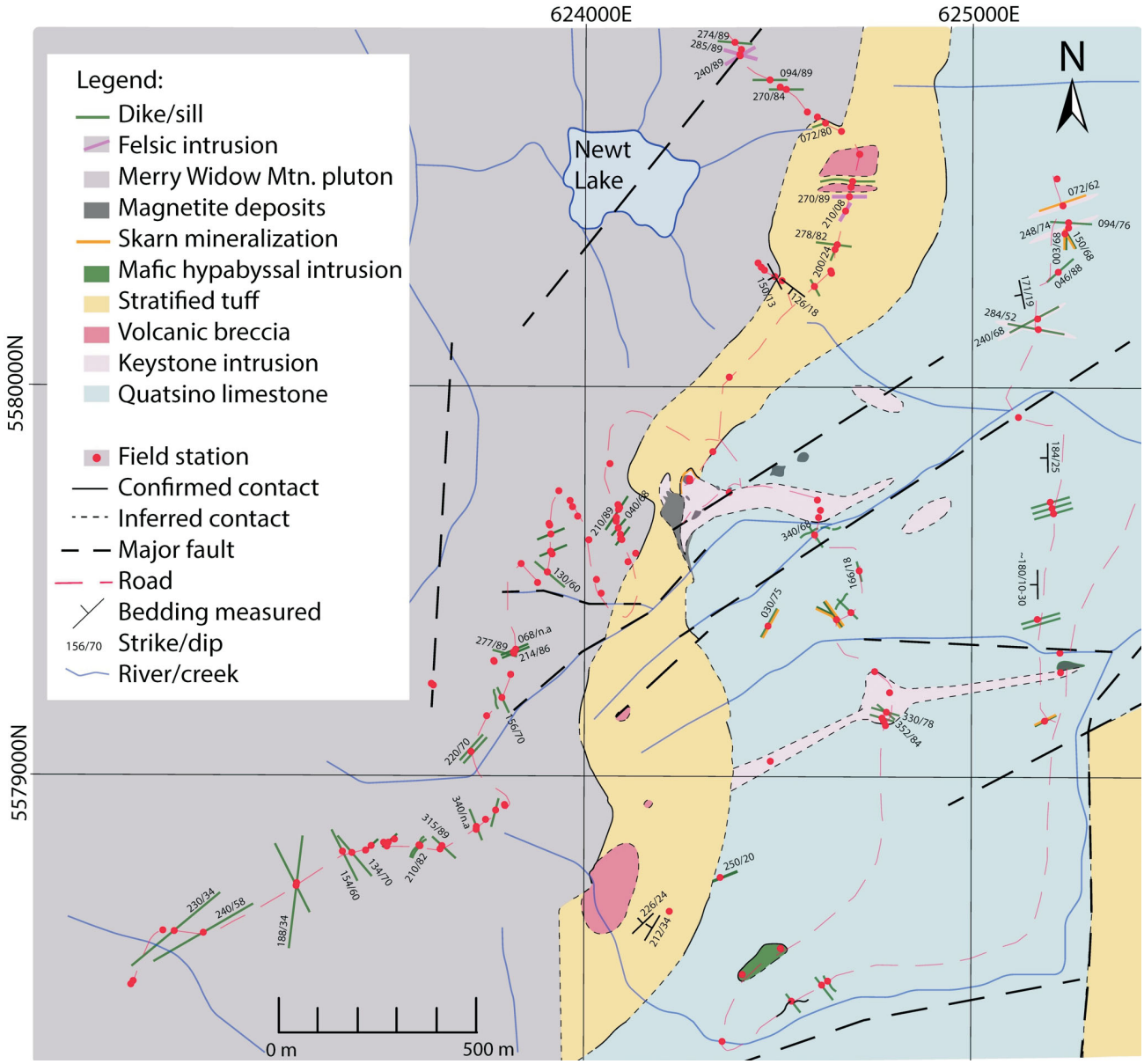

Figure 2. Detailed bedrock geology of the Merry Widow Mountain area, modified after Lund (1966), Ray and Webster (1991) and Nixon et al. (2011). Mapped volcanic breccia locations are from Ray and Webster (1991) and this study (see field stations). The mafic hypabyssal intrusion was previously defined by Ray and Webster (1991) as a pyroxenite. Other previously defined units include the Keystone intrusion (Ray and Webster, 1991) and the Merry Widow Mountain pluton (Nixon et al., 2011).

with the limestone (Figure 4c). The skarn contains assemblages of garnet-diopside-epidote±wollastonite±magnetite (Figure 4c, d). Calcite along the limestone–dike/sill contacts is coarse and frequently recrystallized, and can contain conspicuous void spaces (Figure 4d).

Stratified and Brecciated Volcanic Rocks

Stratified and brecciated volcanic rocks overlying the Quatsino limestone belong to the Parson Bay Formation (Nixon et al., 2011). The stratified unit is a crystal-poor, lithic-rich tuff with a hypocrystalline groundmass, and contains thin layers of quartz-feldspar (Figure 5a). The tuff weathers dominantly light green to buff, with lithic fragments weathering dark grey (Figure 5a). Measured bedding dips gently (~30°) to the northwest. Brecciated volcanic rocks are discordant with the surrounding stratified tuff and occur as near- to subvertical bodies interpreted as subvolcanic plugs (Figure 2). Boundaries between the tuff and volcanic breccia show both brecciation and flow banding. The breccia is polymictic (Figure 5b) and includes clasts that resemble the stratified tuff, plagioclase-phyric basalt and the nearby gabbro (the latter two described below). The groundmass within the breccia is fine grained and weathers dark grey. Previous mapping interpreted the Keystone intrusion (de-

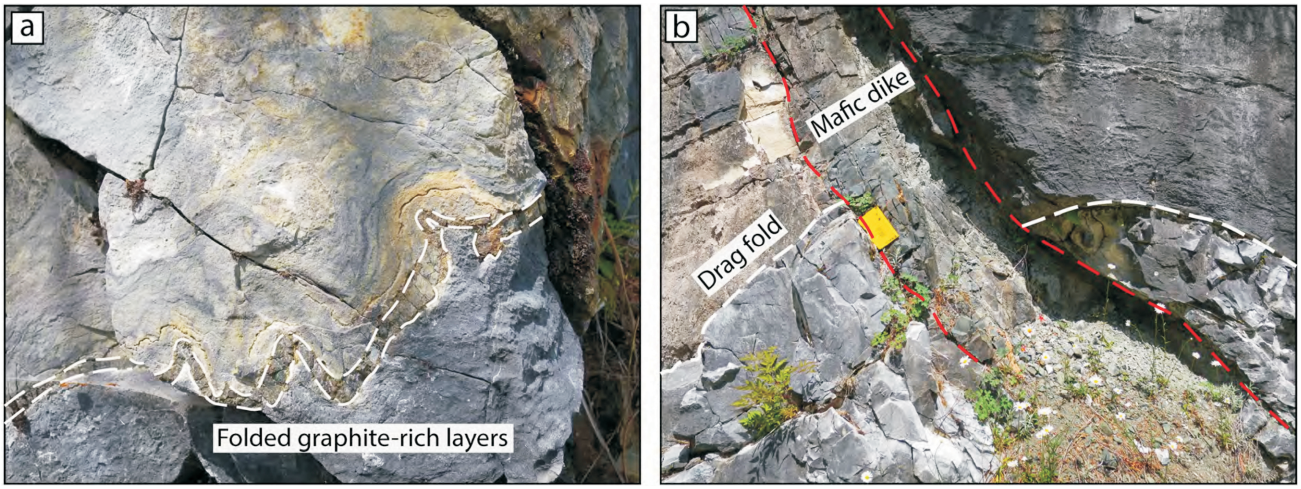

Figure 3. Field images of the Quatsino limestone, displaying **a)** folding of graphite-rich layers (outlined by dashed white line) and ductile behaviour of the surrounding massive limestone; and **b)** drag fold (dashed white line) within the limestone along the contact of a mafic dike (dashed red line); drag fold has a slight normal offset of ~20 cm.

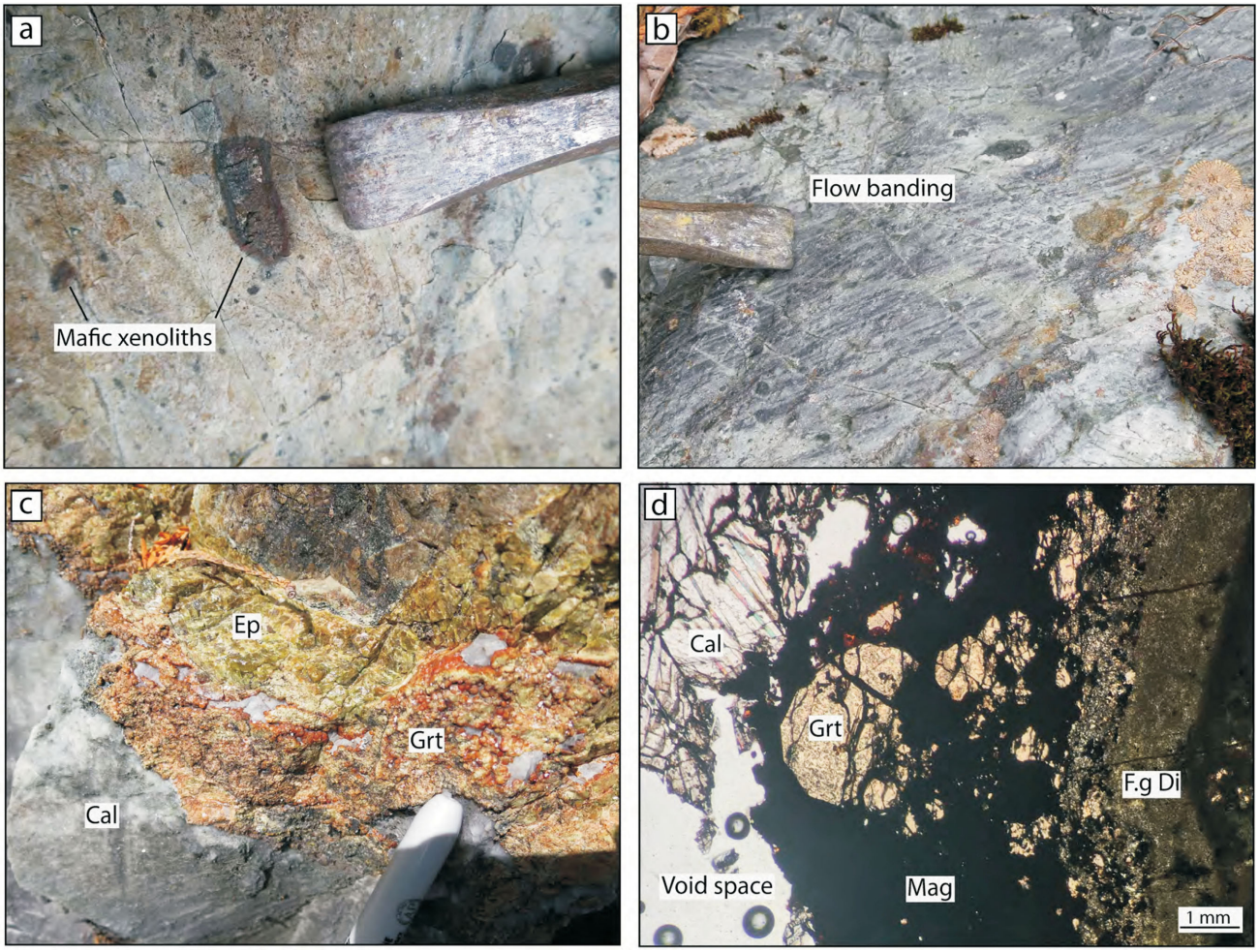

Figure 4. Field and petrographic images of the Keystone intrusion displaying **a)** mafic xenoliths with reaction rims; **b)** flow banding and preferentially oriented xenoliths; **c)** skarn development along the margin of the Keystone intrusion with the limestone (Cal), displaying irregular patches of epidote (Ep) and garnet (Grt); and **d)** the change in mineralogy (Cal-Mag-Grt-Di) shown in plane-polarized light from limestone (Cal) to skarn along the margin of the Keystone intrusion. The calcite is coarse and void spaces are common at the limestone (Cal) to skarn transition. Abbreviations: Cal, calcite; Ep, epidote; F.g. Di, fine-grained diopside; Grt, garnet; Mag, magnetite.

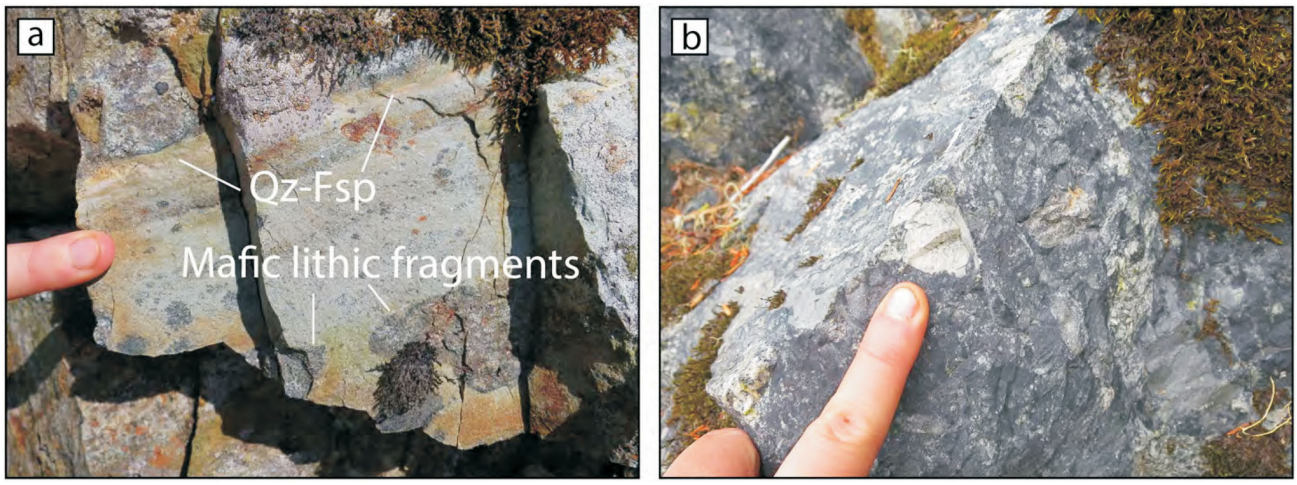

Figure 5. Field images of the Parson Bay Formation, displaying **a)** stratified tuff with thin quartz-feldspar (Qz-Fsp) layers and mafic lithic fragments; and **b)** polymictic volcanic breccia with clasts resembling the stratified tuff, a plagioclase-phyric basalt and the nearby gabbroic intrusion.

scribed above) as the feeder to both the stratified tuff and the volcanic breccia (Ray and Webster, 1991).

Plutonic Rocks

Plutonic rocks of the Merry Widow Mountain area have been previously described as the Coast Copper stock (Ray and Webster, 1991) or the Merry Widow Mountain pluton (Nixon et al., 2011). The present study mapped the eastern margin of the pluton in detail. The pluton is heterogeneous and ranges modally from dominantly gabbro to lesser occurrences of monzonite. Textures display both brittle (sharp, angular boundaries) and ductile (mingling) relationships between the gabbro and monzonite compositions.

The dominant gabbro of the Merry Widow Mountain pluton (Figure 6a, b) is hypidiomorphic, with euhedral plagioclase (45–60%), anhedral clinopyroxene (25–40%), hornblende (<10%), oxides (5–10%), ± olivine (5%). Grain size ranges from medium to pegmatitic, in which euhedral plagioclase crystals can reach up to 5 cm in length. Rare coarse-grained mafic cumulates occur along the margin of the pluton. These cumulates are hypidiomorphic, with altered (i.e., chloritized) hornblende (30%), plagioclase (40%), oxides (10–15%), apatite (5%), clinopyroxene (<5%), olivine (~1–3%) and titanite (~1%). Within these cumulates, apatite grains reaching 2 mm in diameter commonly have melt inclusions (Figure 6c). Titanite typically forms on the edges of apatite (Figure 6c). Fine-grained clinopyroxene along plagioclase boundaries also occurs in some marginal gabbro (Figure 6d).

Mafic Dikes and Sills

In the lower section of the study area, mafic dikes are discordant and sills are concordant with the surrounding limestone bedding (Figure 7a). There is evidence of two sets of dikes/sills. The late dikes/sills form sharp and brittle contacts with the surrounding limestone, whereas the earlier dikes/sills show evidence of ductile deformation at their margins and are commonly boundinaged. Dikes/sills occur as 1) aphyric with microphenocrysts of plagioclase and rare xenoliths that resemble the gabbro; or are 2) plagioclase phyric with euhedral plagioclase laths <1.5 cm in length. Both aphyric and plagioclase-phyric dikes/sills are interpreted to be basalt to basaltic andesite in composition. Aphyric dikes have a steep (~75°) dip to the southeast and the sills have a gentle (<20°) dip to the west. Both aphyric dikes and sills are typically <1–2 m in width. Plagioclase-phyric dikes have a steep (>65°) dip toward either the northeast or southeast and are larger (>2 m in width). Within the lower section of the field area, aphyric dikes commonly cut up through larger, earlier dikes of the Keystone intrusion (i.e., a dike within a dike). Sulphides (chalcopyrite and pyrite) are concentrated along some of these dike contacts with the limestone (Figure 7b).

In the upper section of the study area, mafic dikes crosscut the Merry Widow Mountain pluton (Figure 2). They range from <1 m to >5 m in width and are interpreted to be basalt to basaltic andesite in composition. The dikes dip gently to near vertically (<20° to >80°) between southwest and northwest. The dikes are 1) aphyric with microphenocrysts of plagioclase; 2) plagioclase phyric with euhedral plagioclase laths <1.5 cm in length; or have 3) abundant carbonate-silicate spherules interpreted as ocelli. These ocelli-rich dikes are confined to the upper section where they only crosscut the pluton, and display ocelli amalgamating (Figure 7c) near some of the dike centres. The ocelli are similar in grain size to the groundmass (fine grained) but are lighter in colour (Figure 7c, d). Glomerocrysts of clinopyroxene are common within the ocelli, as well as in the main groundmass. Both the glomerocrysts of clinopyroxene and the ocelli can be up to 3 mm in diameter.

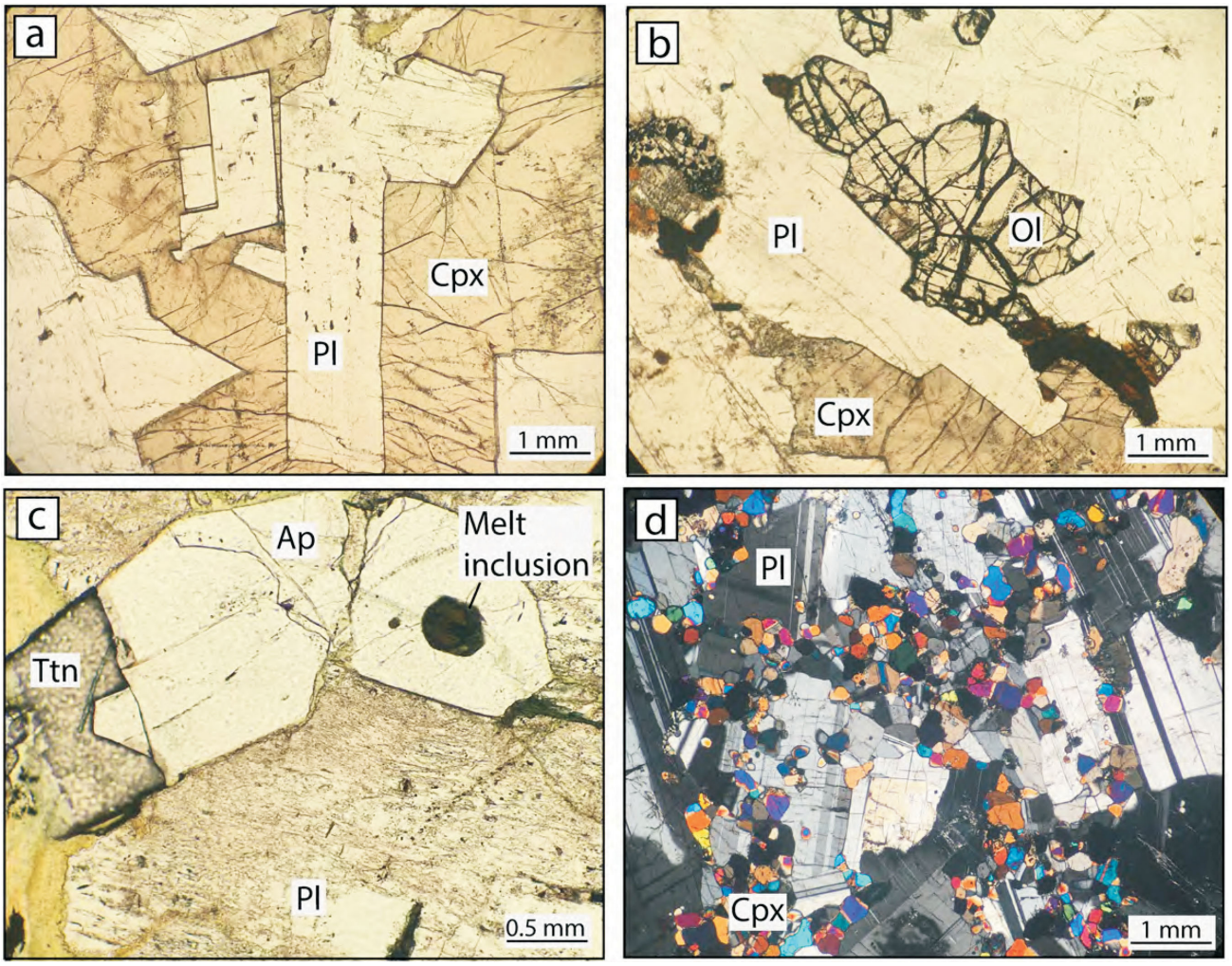

Figure 6. Petrographic images of the gabbro of the Merry Widow Mountain pluton, displaying **a)** euhedral plagioclase (Pl) and anhedral clinopyroxene (Cpx) in plane-polarized light; **b)** euhedral-subhedral olivine (Ol) grains in plane-polarized light; **c)** apatite (Ap) and titanite (Ttn) within mafic cumulates in a marginal gabbro in plane-polarized light; and **d)** fine-grained clinopyroxene (Cpx) along plagioclase (Pl) boundaries in a marginal gabbro in cross-polarized light.

Felsic aplite dikes also crosscut the Merry Widow Mountain pluton and are predominant closer to the plutonic margin and/or near faulted zones (northeast of Newt Lake; Figure 2).

Summary and Future Work

Detailed mapping and sampling during the 2019 summer field campaign in the Merry Widow Mountain area focused on the contacts of the Jurassic Bonanza arc intrusions, dikes and sills with the Quatsino limestone. The overall crustal section dips gently (~20°) to the west and from deepest to shallowest consists of ~1 km of limestone, ~250 m of stratified tuff and volcanic breccia, and ~500 m of gabbro. Skarn development, resulting in garnet-diopside-epidote±wollastonite±magnetite, is most prevalent along contacts between limestone and the Keystone intrusion. Some sulphide concentration (chalcopyrite+pyrite) occurs at the contact between limestone and dikes or sills. No skarn development or sulphide mineralization was observed within the stratified tuff or volcanic breccia. The Merry Widow Mountain pluton is dominantly a plagioclase-clinopyroxene–rich gabbro but displays heterogeneity in composition and texture. Heterogeneity along the margin of the gabbro includes conspicuous coarse-grained mafic cumulates containing abundant apatite (~5%) and occurrences of fine-grained clinopyroxene along plagioclase boundaries. Mafic dikes crosscut all units but have not yet been followed continuously across the exposed depth range. Aphyric and plagioclase-phyric dikes are observed at all levels (i.e., from limestone up to gabbro), whereas mafic dikes containing carbonate-silicate spherules (interpreted as ocelli) are only observed in the upper part of the section, where they crosscut the pluton.

The overarching project goal is to understand all parts of the magmatic system and heat source that led to skarn development at Merry Widow Mountain. It will be important

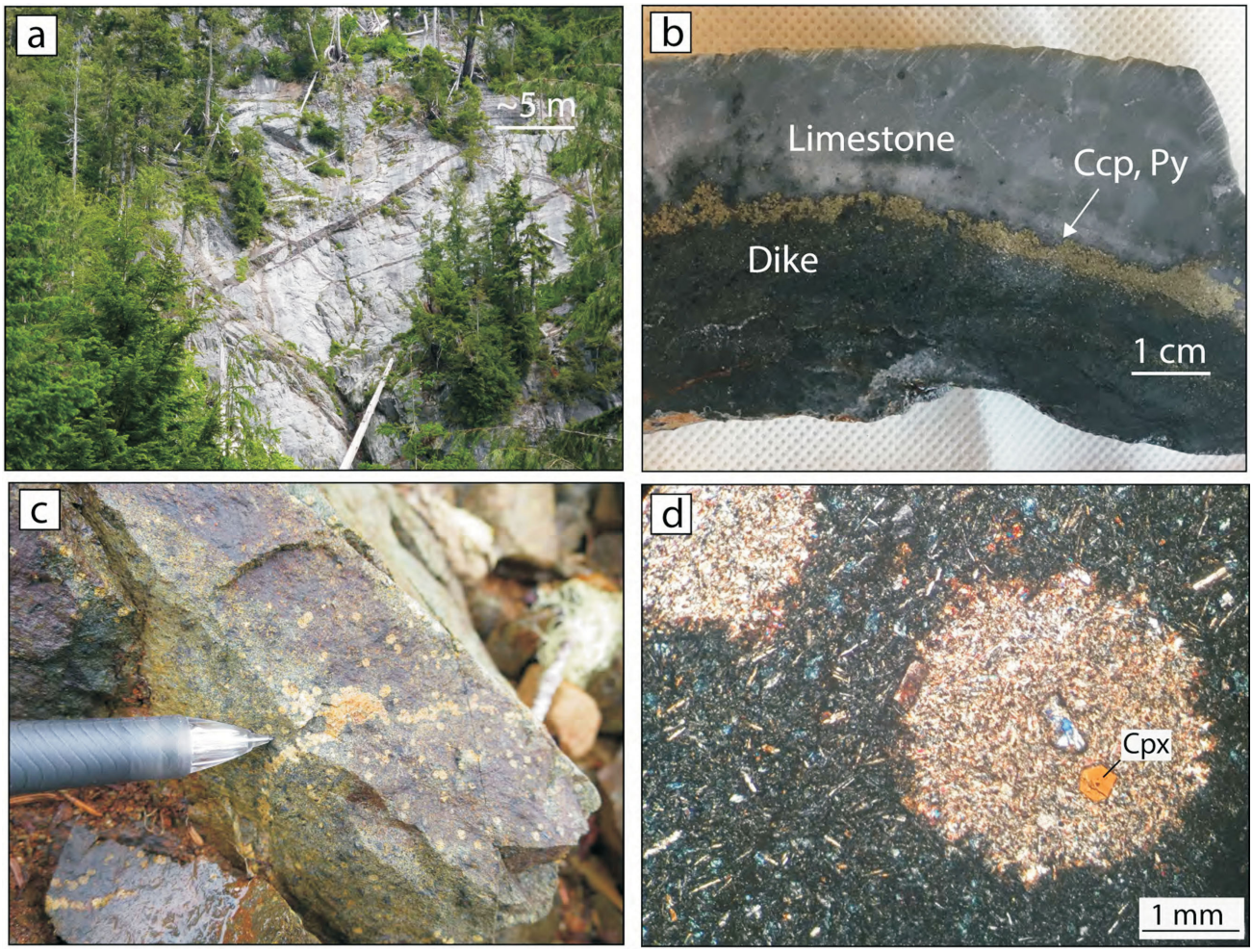

Figure 7. Field and petrographic images displaying **a)** aphyric mafic dikes and sills crosscutting the Quatsino limestone in the lower section; **b)** concentration of chalcopyrite (Ccp) and pyrite (Py) along the margin of an aphyric dike in limestone; **c)** carbonate-silicate spherules interpreted as ocelli amalgamate near the centre of a dike that crosscuts the Merry Widow Mountain pluton; and **d)** ocelli (lighter groundmass, circular) set in a mafic groundmass of similar grain size in cross-polarized light, with a phenocryst of clinopyroxene (Cpx) within one of the ocelli; glomerocrysts of pyroxene can occur within ocelli and in the main groundmass; both ocelli and glomerocrysts can reach up to 3 mm in diameter.

to establish whether the lower dikes that crosscut the limestone and stratified tuffs are related to the upper dikes that crosscut the pluton, and whether either is genetically related to mineralization. Lack of exposures impeded the tracing of dikes upsection into the pluton. It is a priority to complete geochemical analyses on sampled dikes at all crustal levels to identify compositional changes. Geochemical analyses will help assess 1) the extent to which assimilation of limestone into the magma has occurred; 2) the volume and extent of the endoskarn development within the pluton; and 3) relationships (if any) to endoskarn mineralization.

The study will produce details of contact mineralization, and related geochronological data will help to further refine the stratigraphy of Wrangellia, including the ages and groupings of Jurassic plutons and correlations of late Triassic carbonate wallrocks. This research aims to create a predictive tool to aid future exploration for Cu-Au-Co-Ag skarn deposits on Vancouver Island.

Acknowledgments

This project was supported by Geoscience BC scholarships (RM) and a Natural Sciences and Engineering Research Council of Canada (NSERC) Discovery Grant (DC). The authors thank M. Mihalynuk for his thoughtful reviews of this paper.

References

BC Geological Survey (2019a): MapPlace GIS internet mapping system; BC Ministry of Energy, Mines and Petroleum Resources, BC Geological Survey, MapPlace website, URL <http://www.MapPlace.ca> [November 2019].

BC Geological Survey (2019b): MINFILE BC mineral deposits database; BC Ministry of Energy, Mines and Petroleum Re-

sources, BC Geological Survey, URL <http://minfile.ca/> [November 2019].

Greene, A.R., Scoates, J.S., Weis, D., Nixon, G.T. and Kieffer, B. (2009): Melting history and magmatic evolution of basalts and picrites from the accreted Wrangellia oceanic plateau, Vancouver Island, Canada; Journal of Petrology, v. 50, p. 467–505, URL <https://doi.org/10.1093/petrology/egp008> [November 2019].

Jones, D.L., Silberling, N.J. and Hillhouse, J. (1977): Wrangellia – a displaced terrane in northwestern North America; Canadian Journal of Earth Sciences, v. 14, p. 2565–2577, URL <https://doi.org/10.1139/e77-222> [November 2019].

Lund, J.C. (1966): Structural geology of Empire mine, Empire Development Limited, Port McNeil, British Columbia; M.Sc. thesis, University of British Columbia, Vancouver, BC, URL <http://hdl.handle.net/2429/37080> [November 2019].

Massey, N.W.D. and Friday, S.J. (1987): Geology of the Cowichan Lake area, Vancouver Island (92C/16); *in* Geological Fieldwork 1986: A Summary of Field Activities and Current Research; BC Ministry of Energy, Mines and Petroleum Resources, BC Geological Survey Branch, Paper 1987-1, p. 223–229, URL <http://cmscontent.nrs.gov.bc.ca/geoscience/PublicationCatalogue/Paper/BCGS_P1987-01.pdf> [November 2019].

Monger, J.W.H. and Journeay, J.M. (1994): Basement geology and tectonic evolution of the Vancouver region; *in* Geology and Geological Hazards of the Vancouver Region, Southwestern British Columbia, J.W.H. Monger (ed.), Geological Survey of Canada, Bulletin 481, p. 3–25, URL <https://doi.org/10.4095/203245> [November 2019].

Muller, J.E. (1977): Evolution of the Pacific Margin, Vancouver Island, and adjacent regions; Canadian Journal of Earth Sciences, v. 14, p. 2062–2085, URL <https://doi.org/10.1139/e77-176> [November 2019]

Muller, J.E. and Yorath, C.J. (1977): Geology of Vancouver Island; Geological Association of Canada– Mineralogical Association of Canada, Joint Annual Meeting, April 21–24, 1977, Vancouver, BC, Field Trip 7 Guidebook, URL <https://www.gac-cs.ca/publications/FT_Geology_of_Vancouver_Island.pdf> [November 2019].

Nixon, G.T., Hammack, J.L., Hamilton, J. and Jennings, H. (1993): Preliminary geology of the Mahatta Creek area, northern Vancouver Island (92L/5); *in* Geological Fieldwork 1992, BC Ministry of Energy, Mines and Petroleum Resources, BC Geological Survey Branch, Paper 1993-1, p. 17–35, URL <http://cmscontent.nrs.gov.bc.ca/geoscience/PublicationCatalogue/Paper/BCGS_P1993-01.pdf> [November 2019].

Nixon, G.T., Hammack, J.L., Payie, G.J., Snyder, L.D., Archibald, D.A. and Barron, D.J. (1995): Quatsino–San Josef map area, northern Vancouver Island: geological overview (92L/12W, 1021/8, 9); *in* Geological Fieldwork 1994, BC Ministry of Energy, Mines and Petroleum Resources, BC Geological Survey Branch, Paper 1995-1, p. 9–21. URL <http://cmscontent.nrs.gov.bc.ca/geoscience/PublicationCatalogue/Paper/BCGS_P1995-01.pdf> [November 2019].

Nixon, G.T., Snyder, L.D., Payie, G.J., Long, S., Finnie, A., Orr, A.J., Friedman, R.M., Archibald, D.A., Orchard, M.J., Tozer, E.T., Poulton, T.P. and Haggart, J.W. (2011): Geology, geochronology, lithogeochemistry and metamorphism of the Alice Lake area, northern Vancouver Island, NTS 092L/06 and part of 092L/03; BC Ministry of Energy, Mines and Petroleum Resources, BC Geological Survey, Geoscience Map 2011-4, 1:50 000, URL <http://cmscontent.nrs.gov.bc.ca/geoscience/PublicationCatalogue/GeoscienceMap/BCGS_GM2011-04.pdf> [November 2019].

Ray, G.E. (2013): A review of skarns in the Canadian Cordillera; BC Ministry of Energy, Mines and Petroleum Resources, BC Geological Survey, Open File 2013-08, 50 p., URL <http://cmscontent.nrs.gov.bc.ca/geoscience/PublicationCatalogue/OpenFile/BCGS_OF2013-08.pdf> [November 2019].

Ray, G.E. and Webster, I.C.L. (1991): Geology and mineral occurrences of the Merry Widow skarn camp, northern Vancouver Island; BC Ministry of Energy, Mines and Petroleum Resources, BC Geological Survey, Open File 1991-08, 1:5000 scale map, URL <http://cmscontent.nrs.gov.bc.ca/geoscience/PublicationCatalogue/OpenFile/BCGS_OF1991-08.pdf> [November 2019].

Ray, G.E., Webster, I.C.L. and Ettlinger, A.D. (1995): The distribution of skarns in British Columbia and the chemistry and ages of their related plutonic rocks; Economic Geology, v. 90, p. 920–937, URL <https://doi.org/10.2113/gsecongeo.90.4.920> [November 2019].

Sangster, D.F. (1964): The contact metasomatic magnetite deposits of southwestern British Columbia; Ph.D. thesis, University of British Columbia, Vancouver, BC, URL <http://hdl.handle.net/2429/38943> [November 2019].

Geophysical Exploration for Podiform Chromite Occurrences in the Quesnel Terrane, South-Central British Columbia (NTS 082L/04)

A.R. Branson[1], **Queen's University, Kingston, Ontario, drew.branson@queesu.ca**

C.A. Walter, Queen's University, Kingston, Ontario

G.R. Olivo, Queen's University, Kingston, Ontario

A. Braun, Queen's University, Kingston, Ontario

G. Fotopoulos, Queen's University, Kingston, Ontario

Branson, A.R., Walter, C.A., Olivo, G.R., Braun, A. and Fotopoulos, G. (2020): Geophysical exploration for podiform chromite occurrences in the Quesnel terrane, south-central British Columbia (NTS 082L/04); *in* Geoscience BC Summary of Activities 2019: Minerals, Geoscience BC, Report 2020-01, p. 13–22.

Introduction

Podiform chromite deposits represent approximately 25% of global chromite production, a production share that has been consistent for the past 50 years (Mosier et al., 2012). Chromium is an essential metal for stainless-steel production and is one of the 35 minerals identified in the United States as being "critical" (i.e., a secure and reliable supply is needed; U.S. Department of the Interior, 2018). Worldwide, production of chromium is currently dominated by, in decreasing order of importance, South Africa, Turkey, Kazakhstan and India (U.S. Geological Survey, 2019). The last known chromite production in Canada was in 1948 from the Union Carbide Company's 'Montreal' pit in the Black Lake area of Quebec (Eardley-Wilmot, 1948). Its designation as a critical mineral with no domestic supply indicates the need to investigate possible domestic sources. The primary issue facing exploration for podiform chromite is the discontinuous nature and small size of the deposits. Podiform chromite occurs in lenticular bodies in the lower portions of ophiolitic sequences, particularly in the upper (500—1000 m) part of the tectonite zone in the host harzburgite (Eckstrand et al., 1995). British Columbia has demonstrated historical potential along a chain of obducted ophiolite sequences that runs parallel to the accretionary arc along the margins of the Quesnel Terrane. The correlation between the terrane margins and known podiform chromite occurrences is shown in Figure 1. This project investigates the region surrounding one such known occurrence, located on the Bart mineral claims (#1057772; Strafehl, 2019), 25 km northwest of Kelowna.

[1]*The lead author is a 2019 Geoscience BC Scholarship recipient.*

This publication is also available, free of charge, as colour digital files in Adobe Acrobat® PDF format from the Geoscience BC website: http://www.geosciencebc.com/updates/summary-of-activities/.

Obducted ophiolites are typically highly deformed and altered by serpentinization. The process of serpentinization results in the formation of magnetite, which leads to a strong residual magnetic-field anomaly over the ophiolitic ultramafic rocks (Parvar et al., 2017). The high magnetic susceptibility of these serpentinized rocks makes magnetic surveys an effective tool for mapping the extent and structure of ophiolitic sequences. It must be noted that chromite has a low magnetic susceptibility and therefore must be detected using an indirect approach: measuring the serpentinized areas and then investigating if chromite is present through non-geophysical means, such as geochemical sampling and drilling.

Geology

The Bart mineral claims are dominated by the Permian Chapperon Group, which is generally interpreted as a fault-bounded, obducted ophiolite complex (Cui et al., 2017). The regional-scale geology and ground-magnetic survey data may be seen in Figure 2. The Chapperon Group consists of metamorphosed siliceous and calcareous argillites, greenschists of volcanic and sedimentary origin, and minor serpentinized harzburgite (also identified as dunite by Cairnes, 1932) in pelitic and volcanic rocks (Cui et al., 2017). Within the Chapperon Group are oblong bands of ultramafic intrusive rocks striking approximately 330° and known to host podiform chromite occurrences. These ultramafic units are historically known as the Old Dave intrusions. These comprise primarily dark green serpentine that often weathers to a deep orange-red but is sometimes coated with a thin, semitransparent, whitish, talcose film (Cairnes, 1932). Thin-section analysis reveals different stages of alteration, from abundant small grains of olivine occurring in a meshwork of serpentine to instances in which no traces of unaltered olivine remain (Cairnes, 1932). Other common minerals include similarly altered pyroxene, talc, chlorite, magnetite, asbestos and chromite (Cairnes, 1932).

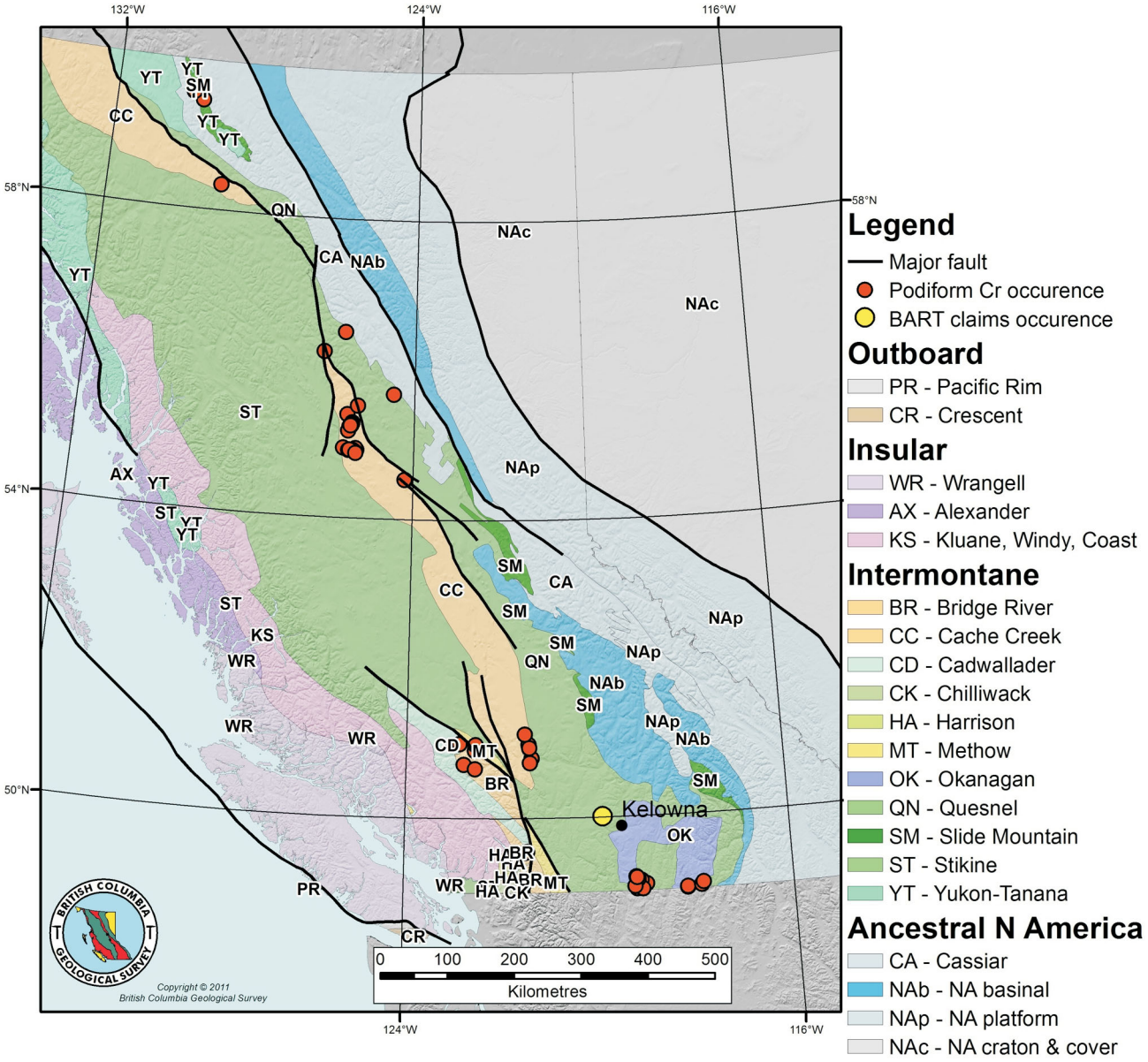

Figure 1. Terranes of British Columbia with known podiform chromite occurrences indicated. Base map from BC Geological Survey (2011), modified with MINFILE data from BC Geological Survey (2019).

The Devonian to Permian Harper Ranch Group, located east of the Chapperon Group, comprises Carboniferous to Permian arc clastic rocks (limestone, sandstone and mudstone) that form the basement to the Quesnel terrane (Beatty et al., 2006). The Chapperon and Harper Ranch groups are unconformably overlain by the Upper Triassic to Lower Jurassic Nicola Group (Cui et al., 2017). The Nicola Group comprises the following sedimentary facies of Upper Triassic age: shale, argillite, siltstone, sandstone, phyllite, tuff, local polymict conglomerate, limestone, greenstone and chloritic phyllite (Cui et al., 2017). These units were intruded into and are abutted by intermediate intrusive rocks to the southwest that comprise, in order of lessening abundance, granodiorite, quartz diorite, quartz monzonite and lesser monzonite, diorite and gabbro, emplaced during the late Triassic to early Jurassic (Cui et al., 2017). Overlying the region in the Eocene period is the Penticton Group, comprising volcanic rocks that include mixed alkalic and calcalkaline transtensional volcanic rocks and associated fluvial and lacustrine sedimentary rocks, hornblende-biotite-quartz-feldspar porphyry and biotite-hornblende-plagioclase porphyry (Cui et al., 2017). Abutted against the east side of the serpentinized belt is a parallel layer of discontinuous marble of sedimentary origin. Apart from the Penticton Group, all the geological units in the study area are components of the Quesnel terrane.

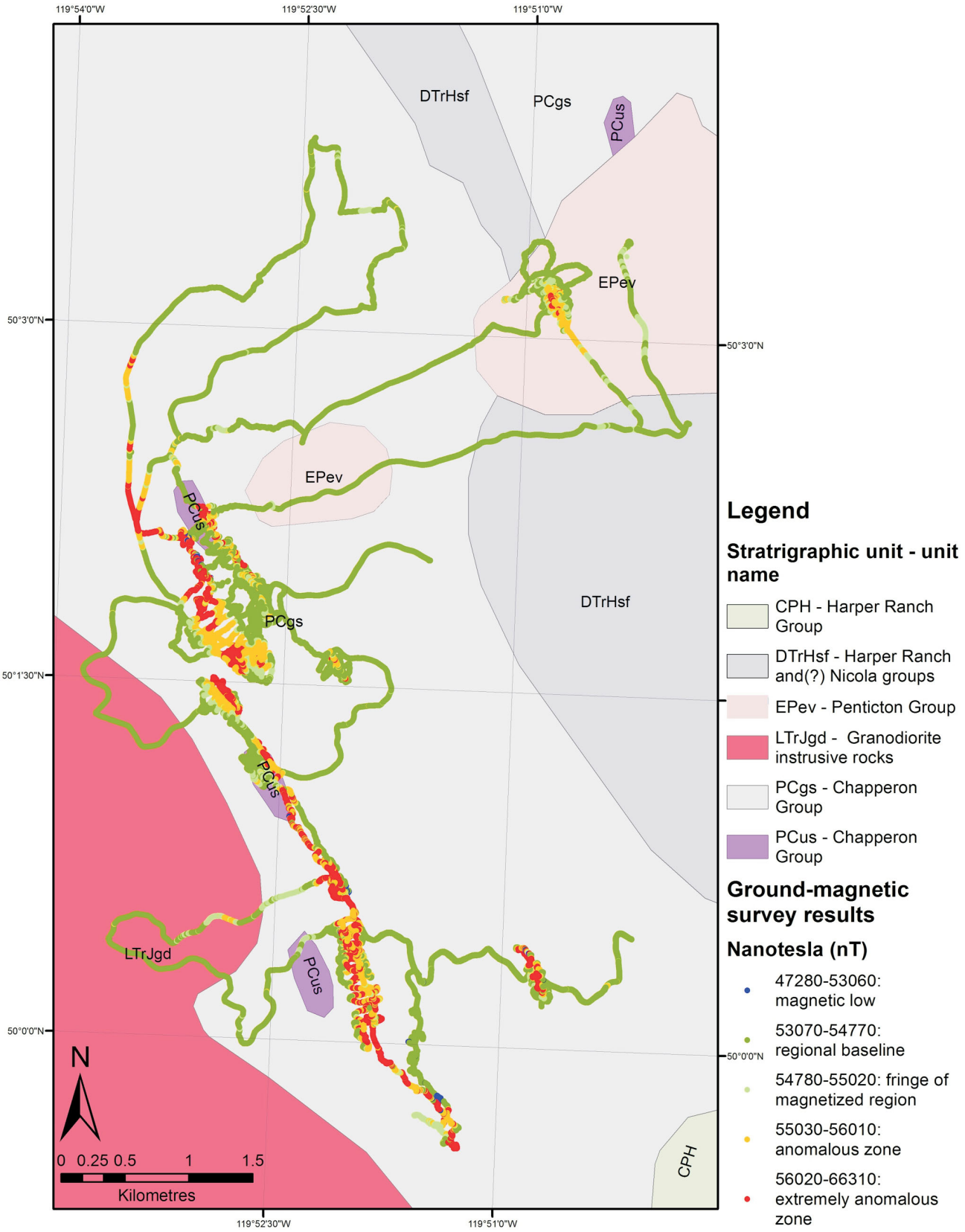

Figure 2. Regional geology of the Bart claims (#1057772; Strafehl, 2019) and ground-magnetic survey data with a manually defined discrete colour-scale, grouping distinct subsets of magnetic intensities (regional geological data from Cui et al., 2017).

Thin-section analysis was done on a sample taken from one of the known chromite pods on the property and a sample of the serpentinized ultramafic rocks that host the occurrence and are shown in Figures 3 and 4, respectively.

The clasts in Figure 3 comprise massive chromite dominated by a brittle fracture system, which was infilled by serpentine. The clasts also have inclusions of unknown opaque minerals, which exhibit a higher reflectance than

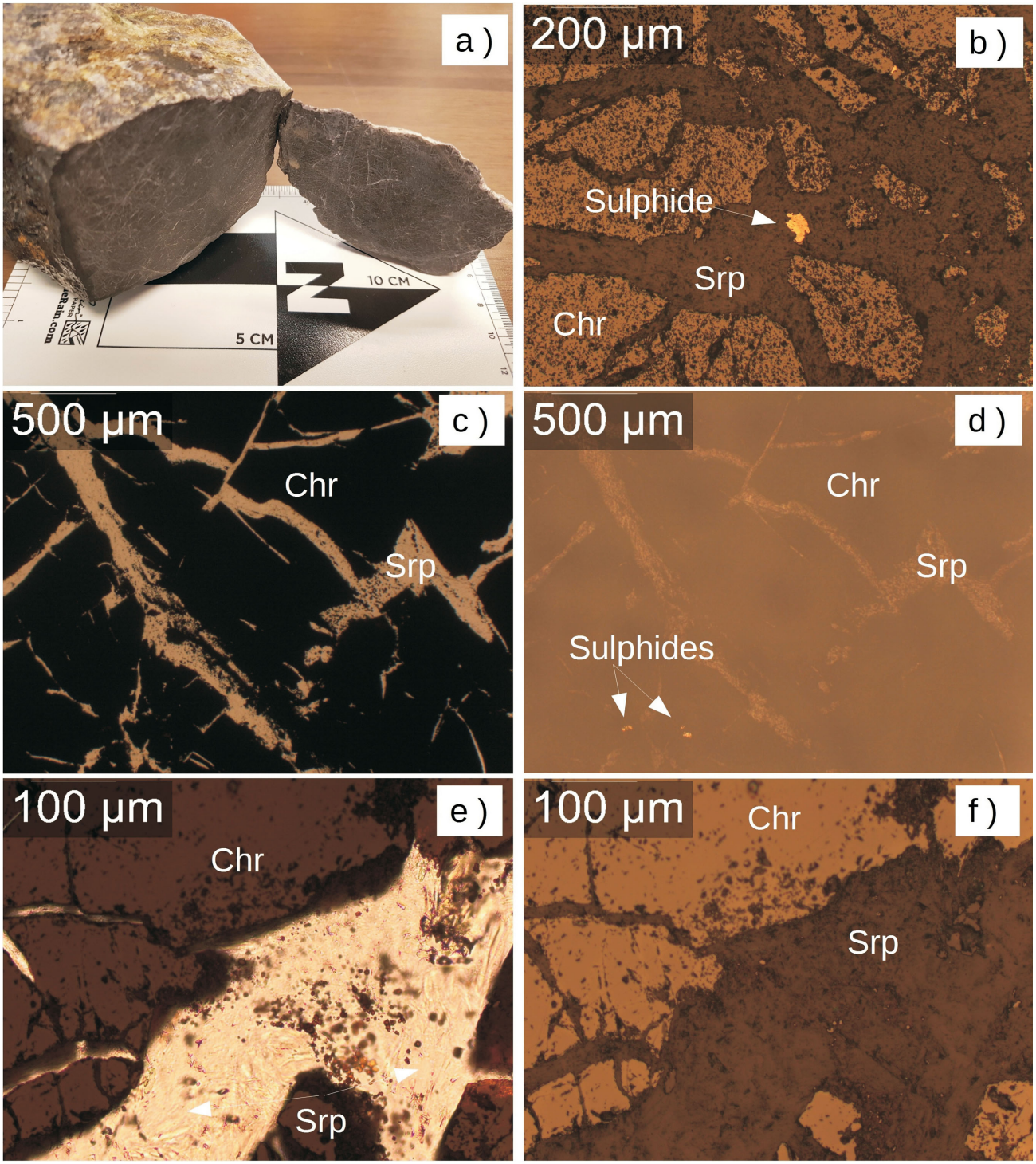

Figure 3. Sample **(a)** and photomicrographs from a known chromite pod: **b, d)** reflected-light images illustrating the fracture system that dominates the sample; chromite (Chr), which makes up 70–90% of the section, was brittlely deformed, resulting in serpentine (Srp)–filled fractures throughout the sample; unknown sulphide minerals occur throughout these fractures; **c)** transmitted-light image (with the same field of view as (d), illustrating the brittle deformation that the sample underwent; **e, f)** transmitted-light (e) and reflected light (f) views of the opaque grains hosted within the serpentine matrix.

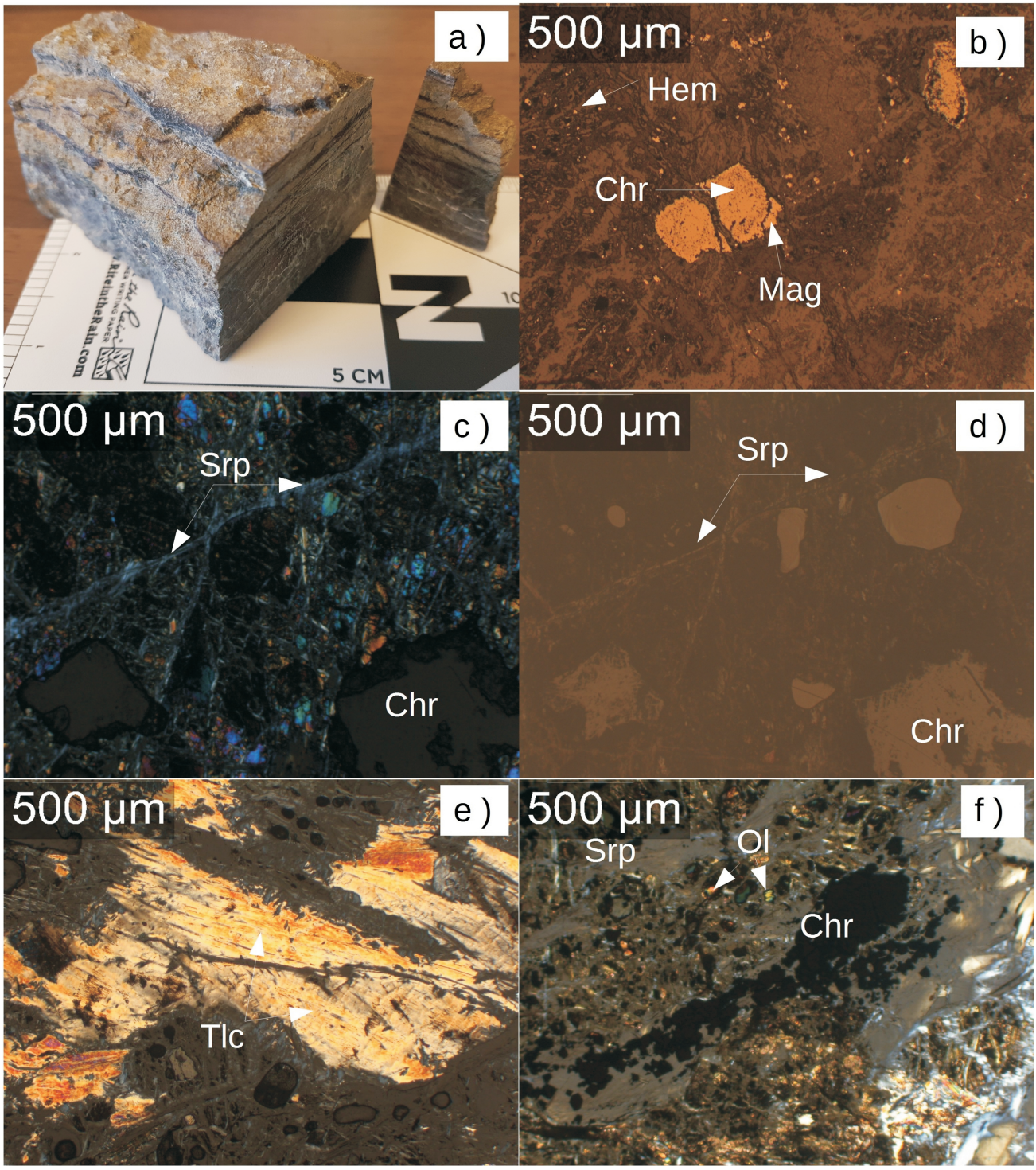

Figure 4. Typical sample **(a)** of the serpentinized ultramafic rocks that occur within the Chapperon Group and photomicrographs illustrating its mineralogy: **b)** reflected-light image of a large chromite (Chr) grain with replacement by magnetite (Mag) on the periphery of the grain, disseminated hematite (Hem) in the surrounding matrix; **c)** cross-polarized image illustrating serpentine (Srp)–filled fracture through heavily altered host; **d)** same field of view as (c) with reflected light, illustrating the moderately reflective chromite grains; **e)** cross-polarized image displaying talc (Tlc); **f)** cross-polarized image showing an accumulation of chromite grains along a heavily deformed trend in the section, hosted within remnant olivine (Ol) not destroyed by the serpentinization process.

the host chromite. The reflective inclusions may also be seen in several of the other fractures. These are likely to be sulphide minerals such as chalcopyrite or pentlandite, which will be investigated in the near future by scanning electron microscope (SEM) analysis.

The serpentinized ultramafic sample in Figure 4 was determined to consist primarily of serpentine and talc, with remnant olivine as well as opaque minerals in two modes of occurrence: disseminated throughout the section and hosted in concentrated layers as a result of metamorphic processes. These opaque minerals are believed to consist of chromite, magnetite and minor hematite. The chromite and magnetite are associated with each another, with chromite making up the core of the opaque grains and the outside altered to magnetite in many samples. This provides an explanation for the strong magnetic signal generated by these ultramafic rocks.

Ground Magnetometry Survey

The primary survey method used for delineating the extent of the serpentinized regions is ground magnetometry using a GEM Systems GSM-19T proton-precession magnetometer. Positioning was achieved using a NovAtel single-frequency GPS receiver with an advertised accuracy of 1.5 m in the horizontal plane. The GPS antenna was mounted on the GEM systems GSM-19T sensor staff, approximately 2 m above ground level. The magnetometer sampling frequency was set to 0.5 sample/second. Approximately 165 line-km were collected, assuming a 4 km/h walking speed, with 74 281 filtered observations collected in nanoteslas (nT) over the 10-day ground magnetic survey (June 18–28, 2019). A reference station for monitoring diurnal variations was not available. However, since the target anomalies were an order of magnitude larger than the diurnal signals, this was deemed to be a noncritical issue.

The primary targets for exploration were the regions of serpentinization within the ultramafic Chapperon Group, which follows a north-northwesterly structural trend. This trend dominates the joint patterns and schistosity, and controls the extent of the Chapperon and Harper Ranch groups in this region. This interpretation is based on the orientation of the purple lobes within the Chapperon Group shown in Figure 2. In order to target the north-northwest-trending serpentinized regions, large-scale (750–3000 m line spacing, depending on accessibility) perpendicular transects of this trend were made across the Chapperon Group. Anomalous zones were identified in the field and followed up with high resolution local grid surveys on subsequent days.

The magnetic data were interpolated using natural neighbour interpolation, and a discrete colour scale was applied based on geological interpretations from field observations (Figure 5). Natural-neighbour interpolation is an algorithm that, for a subset of data surrounding a query point, constructs a Voronoi diagram for the given data points and the Voronoi polygon for the query point. The proportion of overlap between the query polygon and the adjacent cells determines the weights applied for the calculation of the point value (Esri, 2016).

Interpretations

Geological interpretations were made based on a combination of magnetic signatures, field mapping and observations of geology. Based on field observations, the colour scale for magnetic intensity shown in Figures 2, 5 and 7 was selected to separate the magnetic data into geologically meaningful groups. This clustering resulted in the grouping of very high magnetic signals produced within the serpentinized zone (56 020–66 310 nT), the average signal observed within the serpentinized zone (55 030–56 010 nT) and the slightly lower signal on the fringe of this zone (54 660–55 010 nT). Based on the strong magnetic signal generated by the serpentinization of the ultramafic rocks and ground observations of the geology, the delineation of the serpentinized ultramafic rocks was reviewed as shown in Figure 6.

The geological interpretations in Figure 6 indicate several fault structures, along with strike-slip motion. These faults are oriented primarily in two parallel sets, one with sinistral strike-slip at approximately 300° and the other with dextral strike-slip at approximately 355°. Based on this pattern of strike-slip faults, it is interpreted that these faults make up a conjugate fault set, which is reacting to a north-northwest-oriented primary stress field as a result of regional-scale tectonic forces. This may be the result of a regional-scale dextral shear system that is present throughout the western cordillera (Mazzotti et al., 2008). Interpretations of the fault systems can be seen in Figure 7.

Conclusions

The data collected this field season provided the highest resolution magnetometer data to date for this area. The finer resolution of this survey has enabled more precise interpretations regarding the extent of the serpentinized zone and improved interpretations of the orientation of the fault structures. There remains some uncertainty regarding the exact orientation of these fault structures as observed during fieldwork, so these interpretations are based mainly on magnetic and topographic features. Detailing the full extent of the serpentinized ultramafic rocks will allow for more effective rock- and soil-sampling programs, which may result in the discovery of chromite pods of potential economic importance. Of additional interest, the faults in the area may have acted as fluid conduits for hydrothermal mineralization, evidence of which was observed in the area as glacially transported rock samples. Improved under-

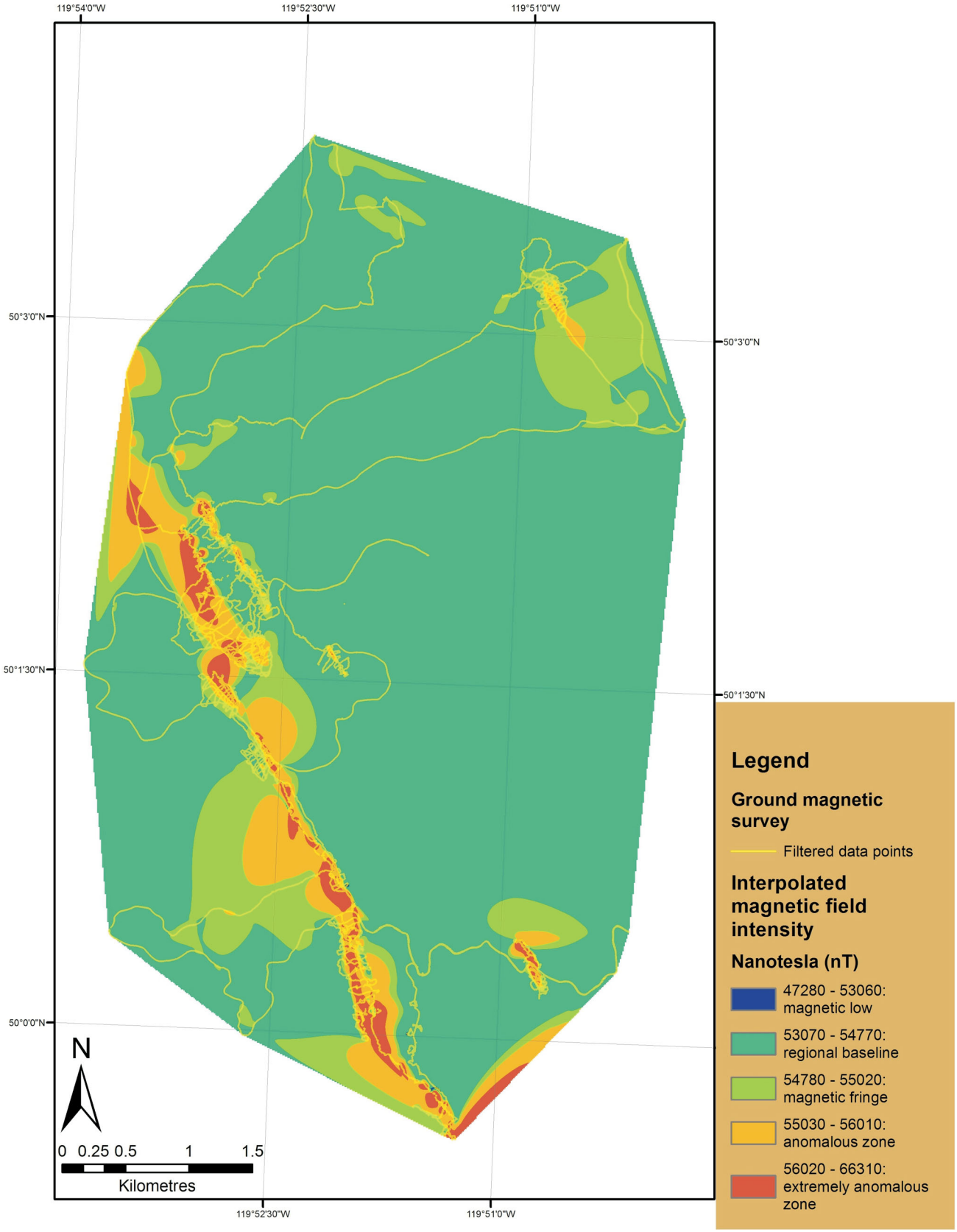

Figure 5. Natural-neighbour–interpolated magnetic-intensity data with a discrete colour scale reflecting field observations of distinct groups. Data points used in the interpolation are displayed in yellow to allow identification of interpolation and edge effects.

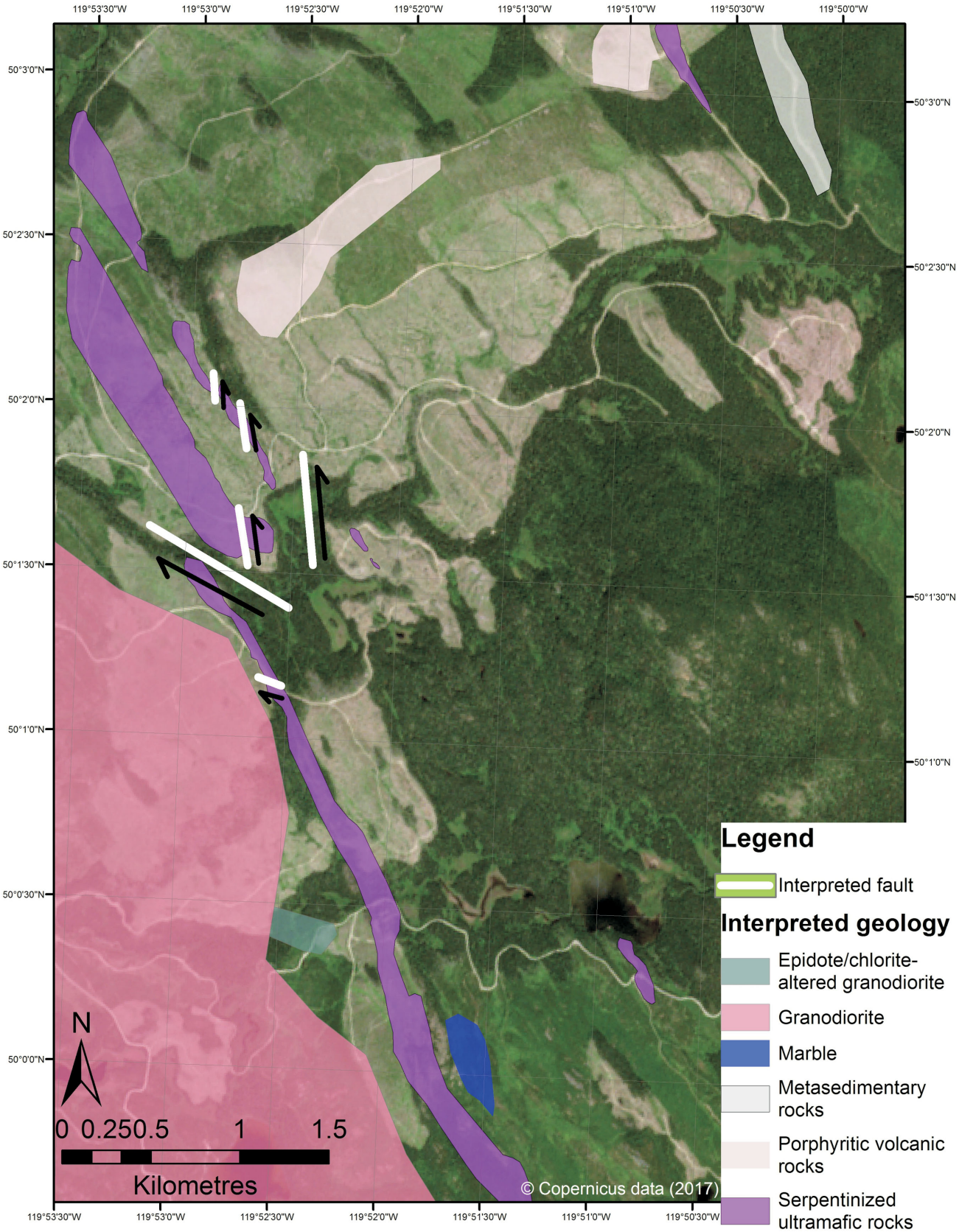

Figure 6. Geological and structural interpretations based on ground-magnetic survey and geological observations. Background imagery from Copernicus (2017).

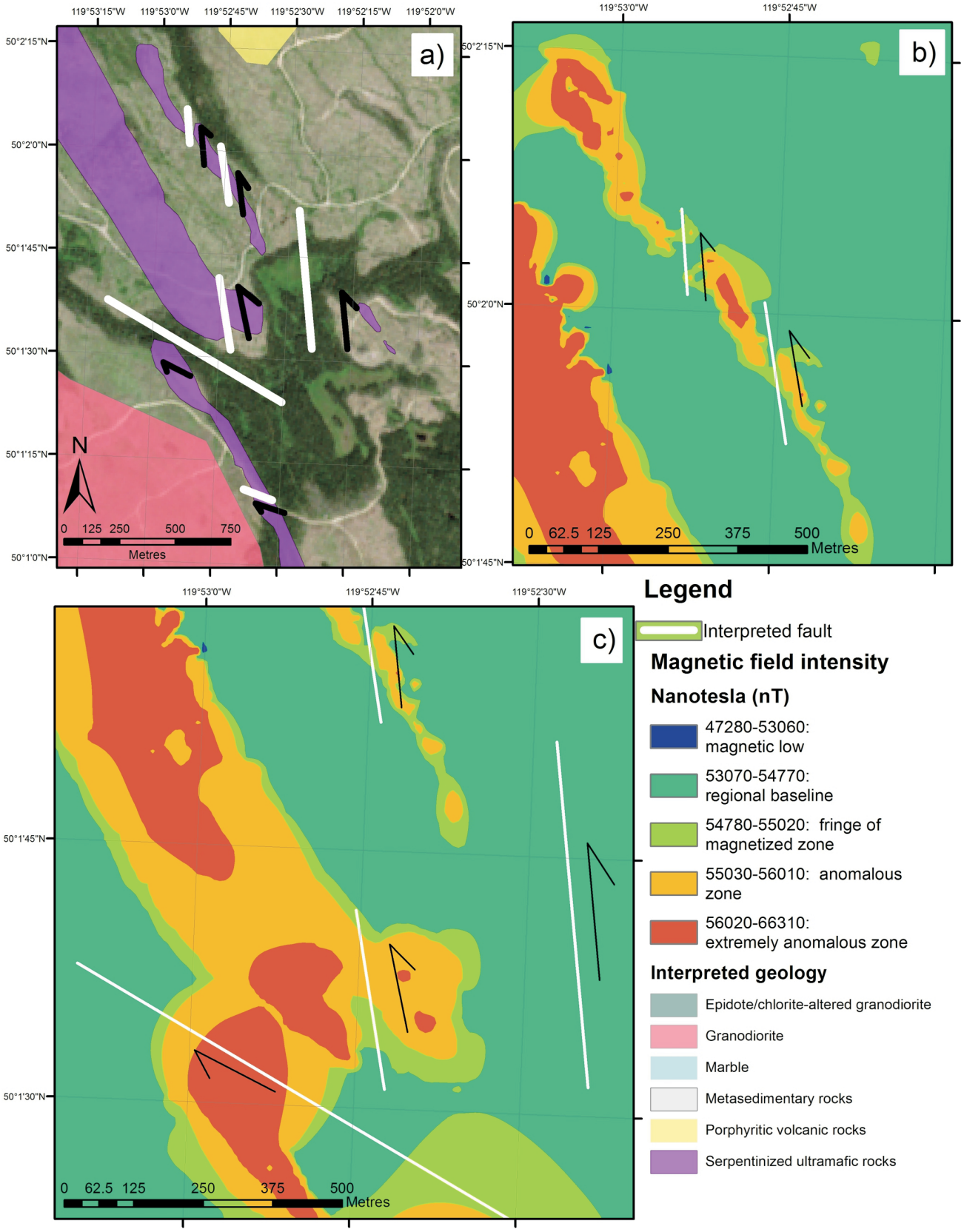

Figure 7. a) Interpreted geological and structural features in the northern part of the survey area, with supporting magnetic-field data, at 1:20 000 scale. Smaller scale subsets (1:8 000) of the data in (a), illustrating the structural interpretations with supporting interpolated and point (to illustrate data density used in interpolation) magnetic-field data for **b)** north-striking fault system in the northeastern ridge, and **c)** evidence of conjugate faults through the southern northwest-trending gully and the central lobe, which was displaced northward.

standing of these fault structures may generate targets for exploration of hydrothermal mineral occurrences.

Future Work

In order to better resolve the distribution of magnetic susceptibility within the serpentinized ultramafic belt, an unmanned aerial vehicle (UAV)–borne aeromagnetic survey is planned for the spring of 2020. This will allow total-magnetic-field data to be collected at a high resolution over the tops of densely forested areas and steep gullies where collecting terrestrial total-magnetic-field measurements was not physically possible. This UAV magnetometry is also capable of achieving higher spatial resolution than a manned airborne survey. This UAV-borne total-magnetic-field data will enable gaps in the terrestrial magnetic data to be filled, observation of additional fault structures and the ability to better resolve areas within the serpentinized ultramafic rocks that may host chromite. An SEM analysis will be conducted to verify mineral interpretations from the thin sections and to determine the composition of the observed sulphide inclusions.

Acknowledgments

The authors thank M. MacDougall for reviewing this paper and Geoscience BC, Redline Minerals Inc. and Mitacs for their support of this project. They also acknowledge the Society of Economic Geologists Foundation (SEGF) for a student research grant from the Hugo Dummet Discovery Fund to C.A. Walter for fieldwork.

References

BC Geological Survey (2011): BC terranes 2011; BC Ministry of Energy, Mines and Petroleum Resources, BC Geological Survey, map, 1:8 000 000 scale, URL <https://www2.gov.bc.ca/assets/gov/farming-natural-resources-and-industry/mineral-exploration-mining/bc-geological-survey/mineral-inventory/bc_terranes_2011.pdf> [November 2019].

BC Geological Survey (2019): MINFILE BC mineral deposits database; BC Ministry of Energy, Mines and Petroleum Resources, BC Geological Survey, URL <http://minfile.ca/> [November 2019].

Beatty, T.W., Orchard, M.J. and Mustard, P.S. (2006): Geology and tectonic history of the Quesnel terrane in the area of Kamloops, British Columbia; *in* Paleozoic Evolution and Metallogeny of Pericratonic Terranes at the Ancient Pacific Margin of North America, Canadian and Alaskan Cordillera, M. Colpron and J. Nelson (ed.), Geological Association of Canada, Geological Association of Canada, Special Paper 45, p. 483–504.

Cairnes, C.E. (1932): Mineral resources of northern Okanagan Valley, BC; *in* Geological Survey, Summary Report, 1931, Part A, Canada Department of Mines, Ottawa, Ontario, p. 66A–109A, URL <http://ftp.geogratis.gc.ca/pub/nrcan_rncan/publications/ess_sst/293/293756/sum_rep_1931_a.pdf> [November 2019].

Copernicus (2017): Sentinel-2A satellite true colour image: image granule s2a_msil1c_20170702t185921_n0205_r013_t10uga_20170702t190708; Copernicus, European Space Agency, Open Access Hub, URL <https://scihub.copernicus.eu/dhus/#/home> [November 2019].

Cui, Y., Miller, D., Schiarizza, P. and Diakow, L. J. (2017): British Columbia digital geology. BC Ministry of Energy, Mines and Petroleum Resources, BC Geological Survey, Open File 2017-8, 9 p. (data version 2018-04-05), URL <https://www2.gov.bc.ca/gov/content/industry/mineral-exploration-mining/british-columbia-geological-survey/geology/bcdigitalgeology> [November 2019].

Eardley-Wilmot, V.L. (1948): Chromium; *in* The Canadian Mineral Industry in 1948, Canada Department of Mines and Technical Surveys, no. 829, p. 9–11.

Eckstrand, O.R., Sinclair, W.D. and Thorpe, R.I., editors (1995): Geology of Canadian Mineral Deposit Types; Geological Survey of Canada, Geology of Canada, no. 8, 640 p. (also Geological Society of America, The Geology of North America, v. P-1), URL <https://doi.org/10.4095/207944> [November 2019].

Esri (2016): How Natural Neighbor works; Environmental Systems Research Institute, URL <http://desktop.arc gis.com/en/arcmap/10.3/tools/spatial-analyst-toolbox/how-natural-neighbor-works.htm> [November 2019].

Mazzotti, S., Leonard, L.J., Hyndman, R.D. and Cassidy, J.F. (2008): Tectonics, dynamics, and seismic hazard in the Canada-Alaska cordillera; *in* Active Tectonics and Seismic Potential of Alaska, J. Freymueller, P.J. Haeussler, R. Wesson and G. Ekstrom (ed.), American Geophysical Union (AGU), Geophysical Monograph Series, Volume 179, p. 297–319, URL <https://doi.org/10.1029/179GM17> [November 2019].

Mosier, D., Singer, D., Moring, B. and Galloway, J. (2012): Podiform chromite deposits—database and grade and tonnage models; U.S. Geological Survey Scientific Investigations Report 2012-5157, 45 p., URL <https://pubs.usgs.gov/sir/2012/5157/sir2012-5157_text.pdf?fbclid=IwAR0YxIvRJNfRUJ8iyFVPs-iGgpSMgvvP781XNFTQmU0lTIw-SD_O29hSBxw> [November 2019].

Parvar, K., Braun, A., Layton-Matthews, D. and Burns, M. (2017): UAV magnetometry for chromite exploration in the Samail ophiolite sequence, Oman; Journal of Unmanned Vehicle Systems, v. 6, no. 1, p. 57–69, URL <https://doi.org/10.1139/juvs-2017-0015> [November 2019].

Strafehl, R. (2019): Geologic and geochemical assessment report on the Bart claims (NTS 082L/04W); BC Ministry of Energy, Mines and Petroleum Resources, BC Geological Survey, Assessment Report Indexing System (ARIS), Assessment Report 38145, 89 p., URL <https://aris.empr.gov.bc.ca/search.asp?mode=repsum&rep_no=38145> [November 2019].

U.S. Department of the Interior (2018): Final list of critical minerals 2018; Federal Register, v. 83, no. 97, May 18, 2018, p. 23295–23296, URL <https://www.govinfo.gov/content/pkg/FR-2018-05-18/pdf/2018-10667.pdf> [November 2019].

U.S. Geological Survey (2019): Mineral commodity summaries 2019: chromium; U.S. Geological Survey, Washington, DC, p. 46–47, URL <https://doi.org/10.3133/70202434> [November 2019].

Porphyry, Base-Metal and Gold Potential in the Boundary Area, Southern British Columbia (NTS 082E)

T. Höy, Geological Consultant, Sooke, British Columbia, thoy@shaw.ca

R. Friedman, The University of British Columbia, Vancouver, British Columbia

J. Gabites, The University of British Columbia, Vancouver, British Columbia

Höy, T., Friedman, R. and Gabites, J. (2020): Porphyry, base-metal and gold potential in the Boundary area, southern British Columbia (NTS 082E); *in* Geoscience BC Summary of Activities 2019: Minerals, Geoscience BC, Report 2020-01, p. 23–34.

Introduction

The Boundary area in southern British Columbia (BC) has an extended history of exploration and mining, particularly in the Greenwood, Franklin and Beaverdell camps, where intermittent production of base and precious metals continued from the late 1890s to the early 1990s. Exploration continues to be active throughout most of the area, although it is largely concentrated in the Greenwood camp for a variety of deposit types, including epithermal gold, skarn and base- and precious-metal vein deposits.

This project is a continuation and enhancement of systematic 1:50 000 geological mapping of the eastern half of the Penticton map area (NTS 082E) that has resulted in publication of six maps (Figure 1): Grand Forks (NTS 082E/01), Greenwood (NTS 082E/02), Almond Mountain (NTS 082E/07), Deer Park (NTS 082E/08), Burrell Creek (NTS 082E/09) and Christian Valley (NTS 082E/10). The focus of the project has been to determine the ages of and controls on the various types of deposits that occur throughout the eastern half of the Penticton map area and to provide updated regional base maps and deposit models that may direct ongoing and future exploration. All new radiometric ages reported in this paper were obtained by J. Gabites (Ar-Ar) or R. Friedman (U-Pb) at the University of British Columbia; some of this data has been previously released in a summary report by Höy et al. (2019) and included in a regional compilation map by Höy and Jackaman (2019).

A large part of the Penticton map area is underlain by poorly dated granitic and alkalic intrusive rocks that have been variously assigned to largely undifferentiated granodiorite of the Jurassic 'Nelson' Complex, granite of the Okanagan batholith or Coryell syenite. However, numerous small, generally unrecognized, high-level stocks occur within some of the intrusive complexes and these have the potential to host metallic-mineral deposits. The 2018–2019 project was largely directed toward examining several examples of mineral occurrences related to these stocks to determine their age and thereby provide impetus for further exploration within areas that are largely underlain by these undifferentiated batholiths. Efforts focused on several areas and work included sample collection for radiometric dating, geological mapping and data compilation. In this paper, the Franklin camp, the Beaverdell–Carmi–Tuzo Creek area, the Lightning Peak camp and the Midas–Bulldog area (Figure 1) are briefly described. These areas highlight the range in ages and the variety of deposit types throughout the district, with mineralization related to small Jurassic, Cretaceous, Paleocene and Eocene stocks respectively, and host-rocks that range from granite to syenite.

This publication is also available, free of charge, as colour digital files in Adobe Acrobat® PDF format from the Geoscience BC website: http://www.geosciencebc.com/updates/summary-of-activities/.

Franklin Camp

Introduction

Mineralization in the Franklin mining camp, located in the southern part of the Burrell Creek map area (Figure 1), was discovered in the early 1900s (Drysdale, 1915). The only significant deposit in the camp, the Union mine, produced 122 555 t grading 14.1 g/t Au and 353.4 g/t Ag, primarily in the early 1930s. Recent exploration in the camp has included soil sampling, geological mapping and prospecting by Tuxedo Resources Ltd. in 2001–2004 (Caron, 2004), and rock sampling, trenching and limited diamond drilling by Solitaire Minerals Inc. in 2004 (Caron, 2005).

The geology in the vicinity of the Franklin camp is shown in Figure 2. The area is in the hangingwall of the Granby fault and underlain by dominantly Jurassic rocks that intrude metavolcanic and metasedimentary rocks of the late Paleozoic Franklin group. These are locally intruded by Eocene Coryell syenite stocks and numerous dikes. Eocene Penticton group conglomerate and feldspathic grit of the Kettle River formation and overlying Marron formation alkalic volcanic rocks unconformably overlie the Paleozoic metasediments and Jurassic intrusions. Mineralization is spatially related to the Averill Plutonic Complex, a suite of mafic alkalic intrusions that was originally interpreted as

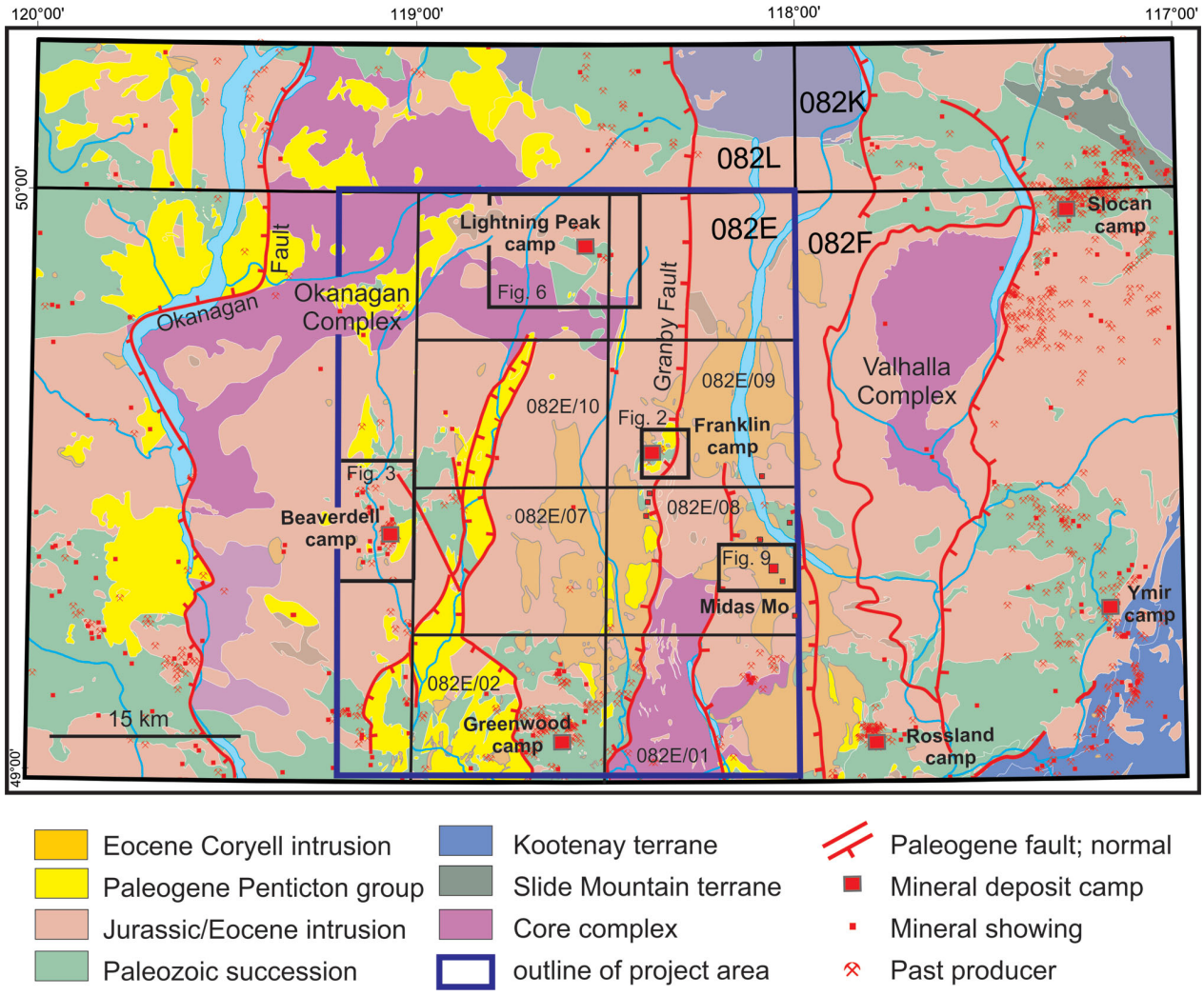

Figure 1. Regional terrane map of the Boundary area of British Columbia, showing the location of mineral occurrences, study areas covered in this paper and published 1:50 000 Geoscience BC maps (locations of figures 2, 3, 6 and 9 are also outlined).

Eocene in age based in large part on its similarity to Coryell intrusive rocks (Drysdale, 1915) but is now recognized as Jurassic, based on a K-Ar date reported in Keep (1989) and several new Ar-Ar dates that range from ca. 176 Ma to 161 Ma (Höy et al., 2019).

Several styles of mineralization are recognized in the camp. These include skarns in altered late Paleozoic metasediments and metavolcanic rocks of the Franklin group, minor platinum-group minerals (Pt, Pd) in the Averill Complex, and base- and precious-metal mineralization in shears and faults (Drysdale, 1915).

Discussion on the Franklin Camp

The Averill Plutonic Complex is a zoned alkalic intrusion within the dominantly calcalkaline, middle to early Jurassic plutonic suite in the eastern half of the Penticton map area. Other exposures of smaller mineralized Jurassic intrusions are common throughout the area. For example, the ca. 179.9 Ma Greenwood stock (Massey et al., 2010) hosts several deposits and showings. Also, numerous precious- and base-metal vein occurrences in the northwestern part of the Almond Mountain map area east of Beaverdell, which are hosted by Middle Jurassic granodiorite and diorite, are assumed to be related to these early intrusions. These deposits appear to have a regional structural control, aligned along prominent northwest structural trends that are marked by the alignment of late faults and orientations of host intrusive rocks. They are within relative structural highs; the Franklin camp is in the hangingwall of the Eocene Granby fault and occurrences east of Beaverdell are within a north-northwest-trending, fault-bounded structural zone that crosses the more northerly trending Rock Creek graben (Höy and Jackaman, 2016).

Beaverdell Area

The Beaverdell area (Figure 1) is located immediately west of the Almond Mountain map area (NTS 082E/07), straddling the West Kettle River (Figure 3). The area includes

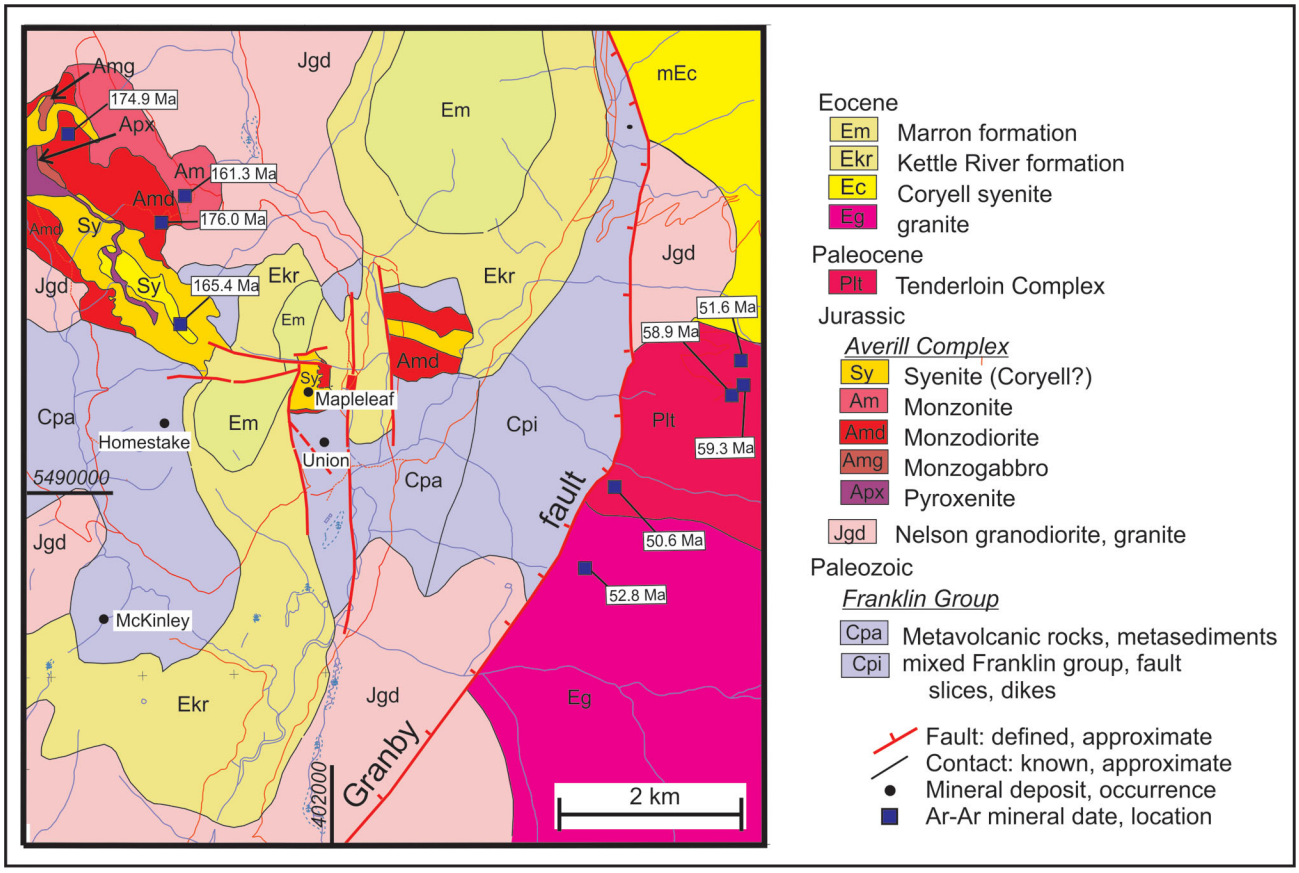

Figure 2: Geology of the Franklin mining camp and surrounding area; all dates are Ar-Ar mineral dates from Höy et al. (2019). Map is modified from Keep (1989) and Höy and Jackaman (2013).

the past-producing Beaverdell silver-lead-zinc camp and several gold occurrences, including Carmi (MINFILE 082ESW029; BC Geological Survey, 2019) in the north. Two prominent molybdenite porphyry deposits also occur in the area, the Carmi deposit just north of Carmi township and the Tuzo Creek deposit south of Beaverdell.

The Beaverdell area was mapped initially by Reinecke (1915) and this work largely provided the basis for later regional compilation maps by Cairnes (1940), Little (1961) and Tempelman-Kluit (1989). The area east of Beaverdell was mapped more recently by Massey and Duffy (2008a, b). This paper and map (Figure 3) are a compilation of those previously published maps, several provincial assessment reports, mapping by the senior author this past field season and new radiometric dates.

The area is underlain mainly by Middle Jurassic granodiorite that has intruded Late Paleozoic metasedimentary rocks, referred to as the 'Wallace formation' by both Reinecke (1915) and Massey and Duffy (2008b). Massive to porphyritic granite of the Paleogene Okanagan batholith intrudes and surrounds the Jurassic exposures as well as forms several small, isolated stocks within the central mass of granodiorite (Figure 3). These stocks are the loci for mineralization in the main deposits or camps within the area.

Beaverdell Camp

Mineral deposits in the Beaverdell camp were mined intermittently from 1913 to 1991, producing approximately 99.2 million grams of silver (35 million oz.) and 481 941 grams of gold (17 000 oz.) from narrow, high-grade lead-zinc veins. Mineralization and associated alteration occur mainly within Middle Jurassic granodiorite but extend into a small granitic stock that is essentially centred on the town of Beaverdell. The Ar-Ar dating method using hornblende yielded an age of 168.4 Ma for a sample of the Middle Jurassic granodiorite and the same method using muscovite yielded an age of 59.2 Ma for an unaltered sample of the Beaverdell stock (Figure 3). Supporting evidence for a Paleocene age for mineralization in the camp is provided by galena lead-isotope data that indicated a ca. 0.05 Ga age (Watson et al., 1982).

Carmi Area

The Carmi area, located approximately 8 km north of Beaverdell, hosts a variety of mineral occurrences and deposits. These include base- and precious-metal veins as well as the Carmi molybdenum deposit (MINFILE 082ENE036). Gold-bearing veins within the Westkettle batholith and host Paleozoic Wallace formation have been

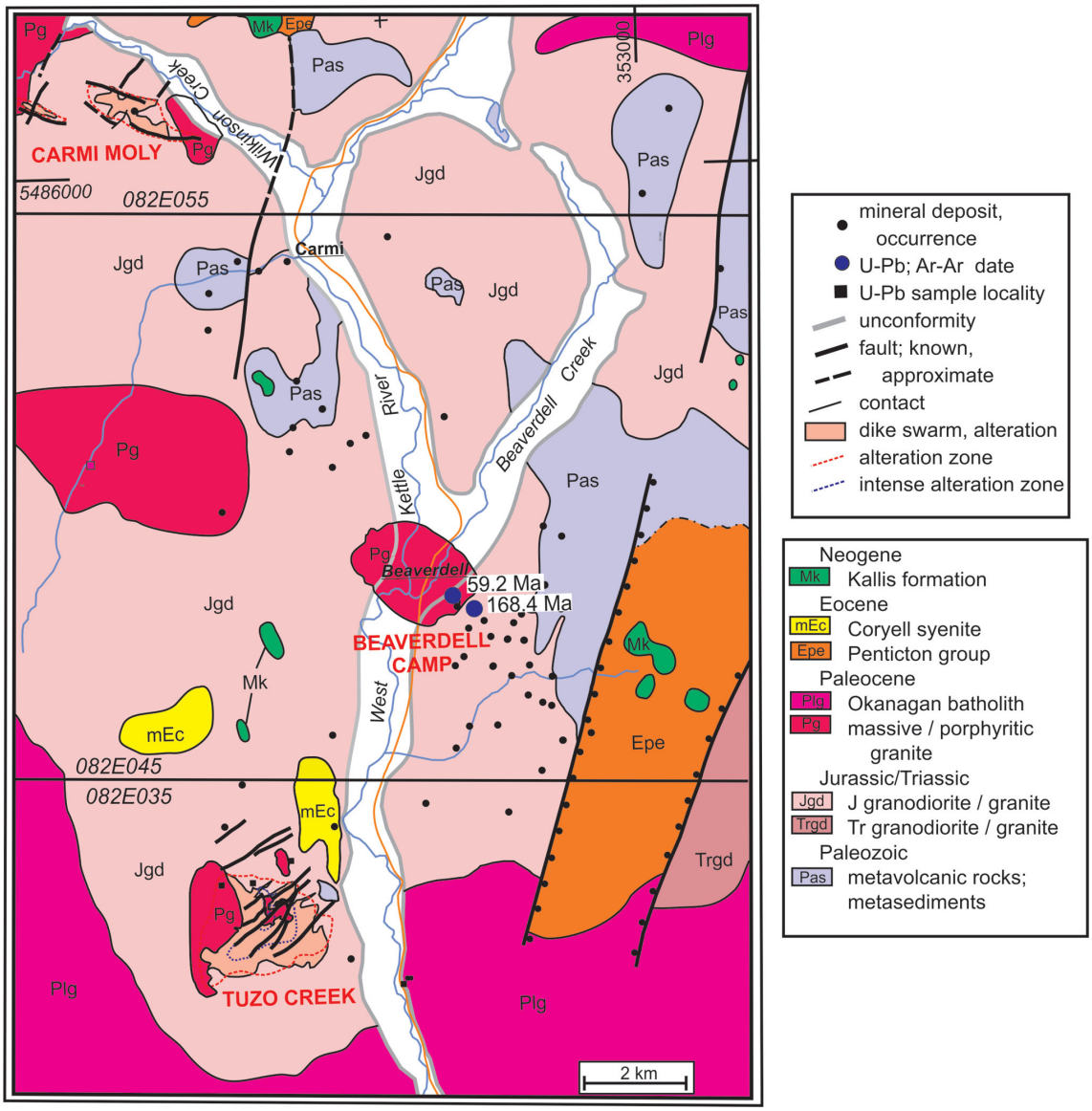

Figure 3: Geology of the Beaverdell camp, Carmi and Tuzo creeks areas. Geology modified from Reinecke (1915), Leary (1987) and Massey and Duffy (2008b); Ar-Ar radiometric dates are from Höy et al., (2019).

interpreted to be Jurassic in age based on galena lead-isotope data (Watson et al., 1982).

The Carmi molybdenum deposit was discovered in 1960 by Kennco Exploration Ltd. and since then has been explored fairly intensely by various companies, defining two zones referred to as the 'E zone' and the 'Lake zone' (summarized in Leary, 1987). Recent work, including diamond drilling, has defined an open pit indicated resource of 12.96 Mt grading 0.058% Mo and an inferred resource of 27.38 Mt grading 0.066% Mo (Reynolds, 2009).

The deposit is within an area largely underlain by Middle Jurassic granodiorite (Figure 3) that is cut by monzonite to granodiorite dikes and an underlying granitic stock (Leary, 1987). A late quartz monzonite stock, lithologically similar to phases of the Beaverdell stock, occurs immediately east of the Carmi molybdenum deposit and a similar stock along the western edge of the Lake zone. Molybdenum-copper mineralization comprises molybdenite with pyrite, magnetite, chalcopyrite and minor bornite in west-northwest-trending shear and breccia zones in Jurassic granodiorite and within the younger quartz monzonite stocks and dikes. The age of mineralization is assumed to be Paleocene based on correlation of the younger intrusive phases with the Valhalla Complex (Okanagan batholith; Leary, 1987). A sample of medium-grained, equigranular quartz monzonite from the E zone has been submitted for radiometric dating; the results will more closely constrain the age of mineralization in the Carmi molybdenum deposit.

Tuzo Creek

A molybdenite deposit (MINFILE 082ESW058) has been explored in the Tuzo Creek area, west of the West Kettle River, approximately 7 km south-southwest of Beaverdell (Figures 3, 4). The deposit was discovered in 1961 by Kennco Explorations (Canada) Ltd. and drilled by Amax Exploration Inc. from 1964 to 1966 and by E&B Explorations Ltd. in 1981. The property was the subject of an M.Sc. thesis, which remains to date the most comprehensive study of the deposit (Leary, 1970).

The regional geology in the vicinity of the deposit is shown in Figure 3. A generally north-trending porphyritic granite/quartz monzonite stock, the Tuzo Creek stock, is lithologically similar to Okanagan batholith rocks farther west (Figure 5). It intrudes the Middle Jurassic Westkettle batholith that also hosts the Beaverdell stock and quartz monzonite intrusions at Carmi. A small syenite stock, similar to many phases of the Eocene Coryell intrusive suite, is exposed a few kilometres northeast of the Tuzo Creek stock.

A large zone of molybdenite mineralization, associated with pyrite and specular hematite, quartz stockwork and veining, and widespread zones of argillic and potassic alteration, occur within and along the eastern side of the Tuzo Creek quartz monzonite. Leary (1970) described several phases of hydrothermal activity and mineralization, spatially and temporally associated with prominent southwest-trending shear and breccia zones, and both pre- and postmineral dikes and 'sills'. Leary (op. cit.) concluded that molybdenite mineralization, controlled by the dominant southwest-trending shears, occurred during and immediately after intrusion of the porphyritic stock, followed locally by minor overprinting of galena-sphalerite-pyrite quartz veining.

Figure 4: View to the south-southwest, from a waste dump in the Beaverdell camp to the Tuzo Creek deposit located on the rounded hill in the centre left of the photo.

Discussion on the Beaverdell Area

Two porphyry molybdenite deposits occur within small Paleocene(?) stocks that are located along the margins of the Paleogene Okanagan batholith in the central part of the Penticton map area. The stocks intrude Middle Jurassic granodiorite in the central part of the Okanagan batholith. Approximately 6 km south of the Tuzo Creek deposit, the Chenier copper-porphyry occurrence appears to share a similar setting, associated with Paleocene(?) megacrystic K-feldspar dikes that intrude Middle Jurassic granodiorite (Kennedy, 2006; Höy, 2007). The Beaverdell silver-lead-zinc camp is associated with a similar granitic stock, dated at 59.2 Ma (muscovite Ar-Ar dating) that intrudes Jurassic granodiorite.

The deposits within the Beaverdell–Carmi–Tuzo Creek area are structurally controlled. On a regional scale they appear to be in a structural zone that extends northwest from the Greenwood area, crossing the Rock Creek graben and into the Beaverdell area, where Jurassic rocks and Paleozoic metasediments of the Wallace formation are exposed. A number of northwest-trending faults parallel the zone, and these seem to have localized the intrusion of small outlying Paleocene stocks. On property scales, the deposit areas are

Figure 5: Sample of fresh porphyritic granite of the Tuzo Creek stock; note subhedral K-feldspar phenocryst in a granular quartz, K-feldspar, plagioclase matrix.

characterized by numerous shears and faults, commonly with little displacement; many of these are schematically shown in both the Carmi and Tuzo Creek areas (Figure 3). These faults typically have two prominent trends, north-northeasterly parallel to the trend of the Eocene Rock Creek graben extensional faults farther east and northwesterly, parallel to the trend of the regional structural high.

Lightning Peak

The Lightning Peak gold camp is located in the northern part of the Penticton map area (Figure 1), between the Kettle River and the northern headwaters of the Granby River (Figure 6). Regional maps show the area to be underlain by undifferentiated Middle Jurassic intrusive rocks with occasional small scattered exposures of basement Monashee

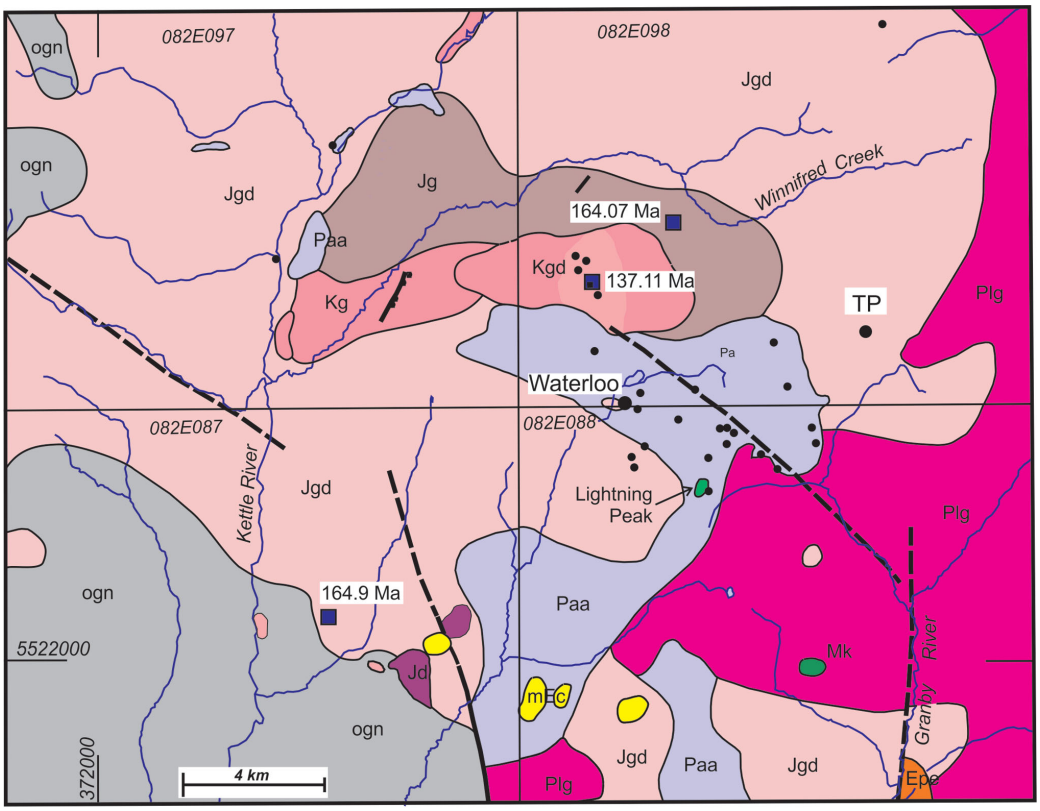

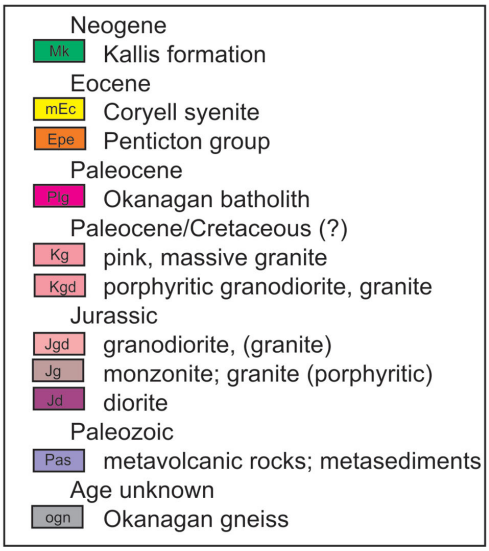

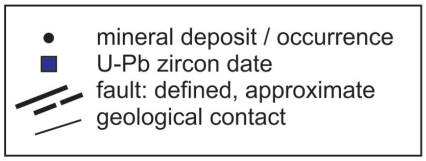

Figure 6: Geology of the Lightning Peak camp and surrounding area; geology is modified from Cairnes (1931) and Tempelman-Kluit (1989); U-Pb zircon dates were obtained at The University of British Columbia (R. Friedman, unpublished data, 2019).

gneiss and, to the southeast, Paleozoic volcanic and sedimentary rocks of the Harper Ranch group (Cairnes, 1931; Little, 1957; Tempelman-Kluit, 1989). This paper focuses mainly on gold-vein occurrences that occur in the porphyritic granodiorite (unit Kgd) shown in the central part of the 1:20 000 scale TRIM map 082E/098 (Figure 6).

The first claims in the Lightning Peak area (Figure 7) were staked in 1897 and, by the early 1900s, many of the showings were being developed and worked (Cairnes, 1931). Work has continued intermittently to the present and has included considerable diamond drilling, underground exploration in the 1930s and 1940s and a small amount of production. Recent work on the property (Callaghan and York-Hardy, 1996; Peterson, 2013) was concentrated mainly on the southern showings, referred to as the 'Waterloo tenures', which are hosted by Paleozoic Harper Ranch group rocks (Figure 6).

Mineral Occurrences and Deposits

The first comprehensive report of mineralization in the Lightning Peak camp describes two main vein types (Cairnes, 1931). East-west trending veins in shear zones, such as the Waterloo mine area (MINFILE 082ENE017; Figure 6), have been traced in surface and underground for several hundred metres within limestone and metasediments of the Harper Ranch group. The veins comprise mainly galena, sphalerite, pyrite and chalcopyrite, with high silver content in the form of ruby silver, argentite and native silver, in a gangue of quartz and minor calcite (Figure 8). A second style of veins, more common to the north, are north-trending gold-quartz veins that have been traced locally for several hundred metres. They occur in a light grey, megacrystic Cretaceous granodiorite (unit Kgd; Figure 6) and farther south, in Paleozoic rock commonly within or parallel to quartz-porphyry dikes. These veins contain variable amounts of pyrite and generally only minor galena and sphalerite.

The veins in the northern part of the Lightning Peak camp are hosted by an east-trending, generally leucocratic granodiorite stock that commonly contains large euhedral pink to tan K-feldspar phenocrysts up to 4 cm in length. Minor amounts of fresh to chloritic biotite and hornblende occur in a medium-grained matrix of plagioclase, quartz and K-feldspar. The stock appears to have a gradational contact in the north, with massive to porphyritic pink granite or monzonite (unit Jg) that also commonly contains large subhedral pink K-feldspar phenocrysts and, to the west, with massive pink granite (unit Kg). These units are not easily differentiated but all appear to be intrusive into the more typical, massive Middle Jurassic granodiorite (Figure 6).

Uranium-lead zircon ages are shown for several of the intrusive phases in Figure 6. The leucocratic ('white') granodiorite that hosts the north-trending gold veins has a Early Cretaceous age of 137.11 Ma, whereas the granite to the north has a Middle Jurassic age (164.07 Ma) similar to the host granodiorite (164.9 Ma). Hence, gold-bearing quartz veins hosted by the white granodiorite are no older

Figure 7: View to the southeast to Lightning Peak, which is capped by Miocene basalt of the Kallis formation that rests unconformably on Paleozoic basement.

Figure 8: Dump from workings of the AU silver-rich polymetallic veins (MINFILE 082ENE027) located approximately 3 km northwest of Lightning Peak and immediately northeast of the Waterloo deposit, shown on Figure 6.

than Early Cretaceous. The veins found further southeast along the northern margin of the Paleogene Okanagan batholith are very similar to the silver-rich sulphide veins in the Beaverdell camp; hence it is possible that they also represent a Paleocene mineralizing event.

Summary on the Lightning Peak camp

The Lightning Peak veins form a northwest-trending belt that extends from the northern margin of the Paleogene Okanagan batholith through a northwest-trending exposure of Paleozoic basement into the Early Cretaceous stock that hosts the main gold-rich veins. This mineralization may represent a zoned camp, marginal to the Paleogene Okanagan batholith, with more proximal silver-rich base-metal mineralization in the southeast and distal gold-vein mineralization in the northwest. Of note, examination of recent work undertaken in the area immediately northwest and northeast of Lightning Peak camp suggests the presence of a zoned mineral camp centred on porphyry-style molybdenite-copper mineralization in the vicinity of the TP mineral occurrence (MINFILE 082ENE049; Figure 6; Callaghan and York-Hardy, 1996). Furthermore, the same study identified prominent north-northeast- and northwest-trending linears, based on both ground topography and an airborne geophysical survey; these are inferred to be faults that parallel the northerly trend of the extensional graben faults and the northwest trends of controlling mineralizing structures, respectively, throughout the eastern half of the Penticton map area.

Midas Deposit Area

The Midas property (Figure 1) is located in the southern Monashee Mountains, southwest of Lower Arrow Lake (Figure 9). The area is included in the regional compilation maps of Tempelman-Kluit (1989) and Höy and Jackaman (2019), and the 1:50 000 scale Deer Park map (NTS 082E/08; Höy and Jackaman, 2010). Figure 9 shows the geology in the vicinity of the Midas molybdenum property and the Bulldog vein occurrence farther west.

The eastern part of the area is underlain by Eocene Coryell syenite dated at ca. 51 Ma (Carr and Parkinson, 1989). Granitic rocks of the Valhalla or Okanagan Complex, previously included as part of the Middle Jurassic Nelson Plutonic Suite, are exposed in the southwestern part of the map area. These are separated from the Proterozoic(?) Grand Forks Complex by the Kettle River extensional fault. Detailed mapping (Figure 9) shows that the Coryell and Okanagan batholiths are composite intrusions that can be separated into distinct intrusive phases. Late high-level stocks, essentially similar in age to the host batholiths, can be differentiated and these commonly localize mineralization.

The Midas porphyry-style molybdenum property (MINFILE 082ESE162) lies within a differentiated feldspar porphyry that is intruded by a swarm of northwest-trending feldspar porphyry dikes; this complex is cut by an east-trending breccia complex with stockwork quartz-magnetite mineralization and peripheral pyrite-argillic alteration. Mineralization, mainly within the breccia complex, includes molybdenite, minor chalcopyrite, and rare scheelite and sphalerite (summarized from MINFILE 082ESE162). Considerable work has been done on the property since its discovery in the early 1900s; the history of this exploration, including recent work, is summarized in recent assessment reports (e.g., Kennedy and Höy, 2010).

The Bulldog occurrence is a 2009 discovery 8 km west of the Midas property and is described in Kennedy and Höy (2010). A series of northwest-trending shears associated with intense propylitic alteration cut a small isolated body of Coryell syenite, dated at 51.99 Ma (Figure 9). Several parallel faults located to the northeast trend eastward toward the Midas property. Mineralization in the Bulldog area occurs as thin quartz veins and silicification, commonly with pyrite and jarosite alteration as well as elevated gold values.

Discussion on the Midas Deposit Area

The Midas property is a porphyry molybdenum prospect of Eocene age in a high-level quartz-feldspar porphyry complex within coarser grained Eocene Coryell syenite. Its location is structurally controlled along a series of northwest-trending faults; similar faults are also evident at the Bulldog gold occurrence to the west. Farther north, a zoned monzonite-monzodiorite intrusive complex cuts massive coarse-grained syenite. Megacrystic porphyritic granite surrounded by more massive granite is located southwest of the Coryell complex (Figure 9) and appears to correspond to an earlier phase than the syenite complex. The small syenite stock that hosts Bulldog mineralization is intrusive into the granite and a new U-Pb zircon date indicates a slightly younger age (Figure 9; R. Friedman, pers. comm. 2019).

Summary

This project was designed to demonstrate that large areas of the eastern half of the Penticton map area, underlain by largely undifferentiated and commonly poorly dated intrusive batholithic rocks, have the potential to include previously unrecognized stocks that may host mineralization. Several deposits and mineral camps were investigated, and all are shown to occur within or be related to isolated, generally high-level stocks that intrude Middle Jurassic, Paleocene or Eocene batholiths. These camps include dominantly polymetallic-vein mineralization in the Franklin camp, porphyry-style molybdenite deposits and high-grade silver base-metal–vein mineralization in the Beaverdell

area, gold and silver base-metal mineralization in the Lightning Peak area, and the Midas molybdenite porphyry deposit in the Deer Park map area. These camps illustrate the variety in both deposit types and ages of mineralization related to these small stocks.

An integral part of the project was to date the batholithic rocks and host stocks to better constrain the ages of associated mineralization. The results of U-Pb zircon and Ar-Ar mineral analyses have been summarized in Höy et al. (2019) and are included on the recently published compila-

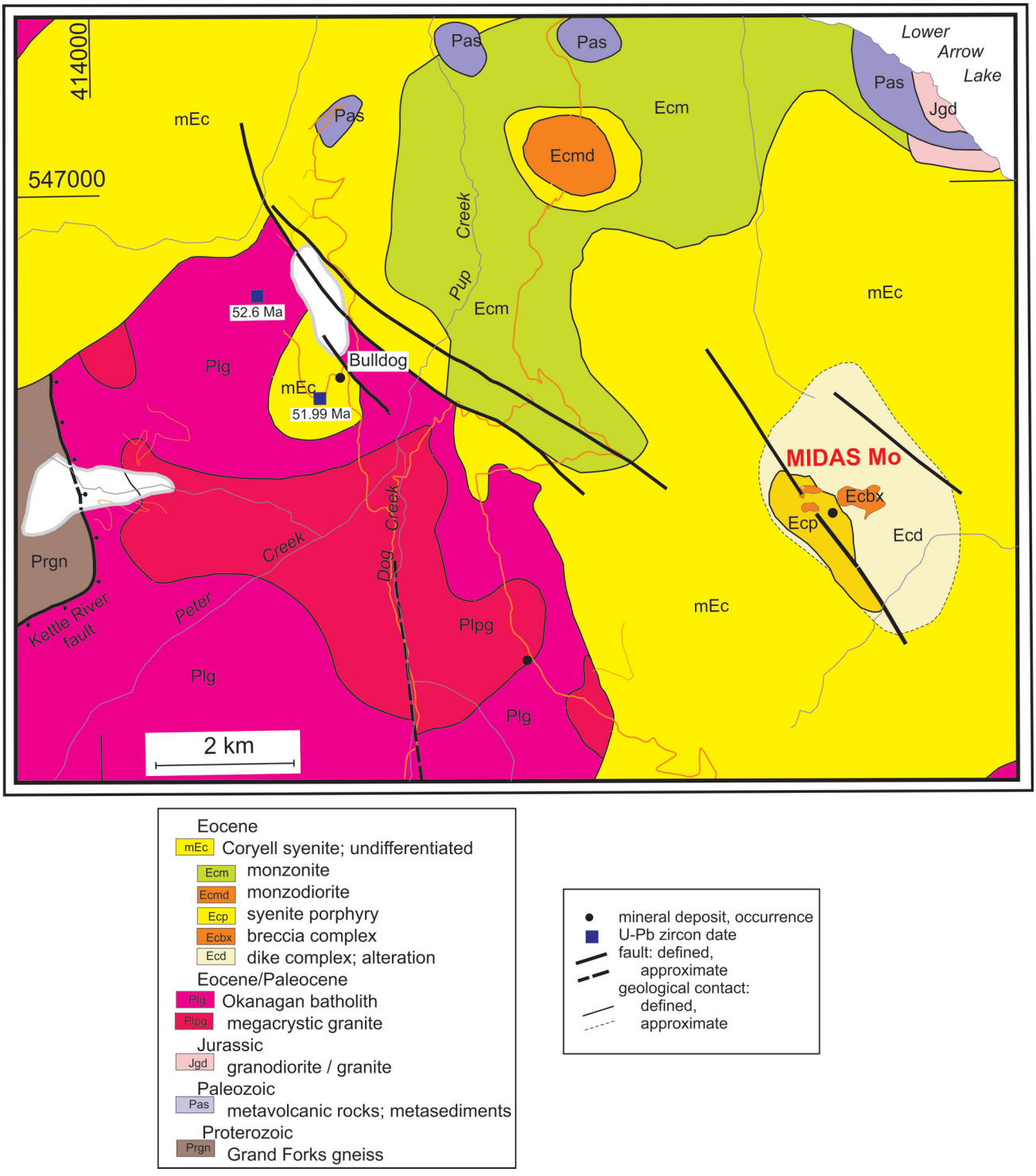

Figure 9: Geology of the Midas property and Bulldog mineral occurrence area. Geology modified from Tempelman-Kluit (1989) and Höy and Jackaman (2010); U-Pb zircon dates were obtained at The University of British Columbia (R. Friedman, unpublished data, 2019).

tion of the eastern half of the Penticton map area (Höy and Jackaman, 2019). Unpublished U-Pb zircon dates that appear in this paper will be included in a separate paper to be released by Geoscience BC.

Several Ar-Ar mineral analyses of various phases of the mafic alkalic Averill Complex, host to much of the vein mineralization in the Franklin camp, confirm a Middle Jurassic age for the complex and, by inference, the age of Franklin camp mineralization.

Mineralization in the Lightning Peak camp is hosted by Jurassic granodiorite and a small, Early Cretaceous stock. The age of mineralization may be Cretaceous, or Paleocene, and related to the margins of the Paleogene Okanagan batholith that occurs immediately south of the camp.

The Beaverdell camp is located along the margins and within a granitic stock that was dated at ca. 59 Ma, a Paleocene age similar to that of many of the massive to porphyritic granites that occur to the east in the Almond Mountain (NTS 082E/07) map area. The Carmi and Tuzo Creek porphyry molybdenite deposits, located several kilometres north and south of the Beaverdell camp, respectively, are hosted within similar granitic stocks and are assumed to have a similar Paleocene age.

The Midas porphyry-style molybdenite deposit occurs in a small, late Coryell syenite porphyry that intrudes the central part of the Eocene Coryell batholith. A small Coryell stock several kilometres to the west contains minor gold-quartz vein mineralization.

Discussion

Large regions of the Penticton map area are underlain by granitic terrane and their exploration can potentially lead to the discovery of new base- and precious-metal mineralization that is controlled by north- and northwest-trending structures. These structures are commonly the loci for late, high-level intrusions within similar-age batholithic bodies. Other than in existing mineral camps, the presence of these stocks often remains unrecognized and they do not appear on regional federal or provincial geological maps. Structures can also localize regional tectonic highs that expose contacts of batholithic rocks and country hostrocks, as well as being a favourable environment for mineralization. Features that help recognize these favourable areas within large terranes of dominantly granitic rock include:

- isolated exposures of basement rock
- marked changes in rock type as, for example, granodiorite to granite or syenite to monzonite
- textural changes, including porphyry or finer grained textures
- alteration zones, including typical K-feldspar, argillic or propylitic zones
- an increase in the density of dikes
- structures, including faults and shears, and possibly foliation within granitic rocks
- presence of mineralization.

Granitic and syenitic batholiths dominate the geology of the Penticton area; these record repeated magmatic episodes during Triassic and Jurassic time, locally in the Cretaceous, and throughout the Paleocene and Eocene. The recent mapping undertaken, in conjunction with radiometric dating, has concentrated largely on Paleogene events and their relationship to mineralization. It has demonstrated that the Okanagan batholith, also referred to as the Valhalla Complex, is a composite batholith that includes massive to porphyritic megacrystic granite of Paleocene age (ca. 59–67 Ma) that was locally exposed in early Eocene time and unconformably overlain by graben-controlled Penticton group conglomerate and volcanic rocks (ca. 52–57 Ma). Following burial, these were intruded by Eocene granite, also commonly included within the Okanagan batholith terrane, and similar-age syenite of the Coryell batholith (ca. 48–52 Ma). The large variety in igneous rock types, levels of exposure and ages is a direct function of vertical tectonics prevalent during regional extension in the central Okanagan in Paleogene time, and these have fundamentally controlled the distribution of base- and precious-metal mineralization.

Acknowledgments

Geoscience BC is gratefully acknowledged for financial support of this study. The authors also thank G.M. DeFields for his assistance in the field. The manuscript benefited considerably from reviews by G.E. Ray and G.M. DeFields.

References

BC Geological Survey (2019): MINFILE BC mineral deposits database; BC Ministry of Energy, Mines and Petroleum Resources, BC Geological Survey, URL <http://minfile.ca/> [September 2019].

Cairnes, C.E. (1931): Lightning Peak area, Osoyoos District, B.C.; *in* Summary report, 1930, Part A, Geological Survey of Canada, p. 79–115.

Cairnes, C.E. (1940): Kettle River, west half, Similkameen and Osoyoos districts, British Columbia; Geological Survey of Canada, Map 538A, scale 1:253 440.

Callaghan, B. and York-Hardy, R.W. (1996): Airborne geophysical surveys, detailed interpretation report and related geological mapping on the Zalmac property; BC Ministry of Energy, Mines and Petroleum Resources, Assessment Report 24 416, 73 p., URL <http://aris.empr.gov.bc.ca/search.asp?mode=repsum&rep_no=24416> [September 2019]

Caron, L. (2004): Assessment report on the Franklin property, Greenwood Mining Division: geology, geochemistry, trenching, diamond drilling; BC Ministry of Energy, Mines and Petroleum Resources, Assessment Report 27 328, 47 p., URL <http://aris.empr.gov.bc.ca/search.asp?mode=repsum&rep_no=27328> [November 2012].

Caron, L. (2005): Assessment report on the 2004 exploration program: rock sampling, trenching, diamond drilling, Union property, Franklin camp, Greenwood Mining Division, British Columbia; BC Ministry of Energy, Mines and Petroleum Resources, Assessment Report 27 604, 37 p., URL <http://aris.empr.gov.bc.ca/search.asp?mode=repsum&rep_no=27604> [November 2012].

Carr, S.D. and Parkinson, D.L. (1989): Eocene stratigraphy, age of the Coryell batholith, and extensional faults in the Granby valley, southern British Columbia; *in* Current Research Part A, Geological Survey of Canada, Paper 89-1E, p. 79-87.

Drysdale, C.W. (1915): Geology of the Franklin mining camp, southern British Columbia; Geological Survey of Canada, Memoir 15, 246 p.

Höy, T. (2007): Geology and rock geochemistry, Chenier property, Kelly Creek area, southern British Columbia; BC Ministry of Energy, Mines and Petroleum Resources, Assessment Report 28 960, 32 p., URL <http://aris.empr.gov.bc.ca/search.asp?mode=repsum&rep_no=28960> [September 2019].

Höy, T. and Jackaman, W. (2010): Geology of the Deer Park map sheet (NTS 82E/08); Geoscience BC, Map 2010-7-1, scale 1:50 000, URL <http://cdn.geosciencebc.com/project_data/GBC_Report2010-7/GBC_Map2010-7-1_Deer-Park.pdf> [November 2019].

Höy, T. and Jackaman, W. (2013): Geology of the Burrell Creek map sheet (NTS 82E/09); Geoscience BC, Map 2013-07-1, scale 1:50 000, URL <http://www.geosciencebc.com/i/project_data/GBC_Report2013-07/GBC_Map2013-07-1_Burrell.pdf> [November 2019].

Höy, T. and Jackaman, W. (2016): Geology of the Almond Mountain map sheet (NTS 82E/07); Geoscience BC, Map 2016-08, scale 1:50 000, URL <http://cdn.geosciencebc.com/project_data/GBCReport2016-08/GBC_Map2016-08_Almond.pdf> [November 2019].

Höy, T. and Jackaman, W. (2019): Geology of the Penticton mapsheet (east-half); Geoscience BC map 2019-04, scale 1:150 000, URL < http://cdn.geosciencebc.com/project_data/GBCR2019-04/GBCMap2019-04.pdf> [November 2019].

Höy, T., Gabites, J. and Friedman, R. (2019): Summary report, U-Pb and Ar-Ar age dating, Penticton east-half (082E½); supplementary report to Geoscience BC Map 2019-04, Geoscience BC, 122 p., URL <http://cdn.geosciencebc.com/project_data/GBCR2019-04/GBCMap2019-04-Supp_Geochronology_PetrographyRpt.pdf> [November 2019].

Keep, M. (1989): The geology and petrology of the Averill alkaline complex, near Grand Forks, British Columbia; M.Sc. thesis, The University of British Columbia, 110 p.

Kennedy, T. (2006): Assessment report, prospecting program, Chenier property, Greenwood and Osoyoos Mining Divisions; BC Ministry of Energy, Mines and Petroleum Resources, Assessment Report 28 578, 11 p., URL <http://aris.empr.gov.bc.ca/search.asp?mode=repsum&rep_no=28578> [September 2019.

Kennedy, T. and Höy, T. (2010): Geology and soil geochemistry, CP/Bully property, southern British Columbia; BC Ministry of Energy, Mines and Petroleum Resources, Assessment Report 31 485, 52 p., URL <http://aris.empr.gov.bc.ca/search.asp?mode=repsum&rep_no=31485> [September 2019].

Leary, G. (1970): Petrology and structure of the Tuzo Creek molybdenite deposit near Penticton, British Columbia; M.Sc. thesis, The University of British Columbia, 177 p.

Leary, G. (1987): Report on high grade molybdenite potential of the Lake zone, Carmi Molybdenum deposit, Greenwood Mining Division, British Columbia; BC Ministry of Energy, Mines and Petroleum Resources, Assessment Report 16 102, 56 p., URL <http://aris.empr.gov.bc.ca/search.asp?mode=repsum&rep_no=16102> [September 2019].

Little, H.W. (1957): Kettle River, east half, Similkameen, Kootenay and Osoyoos districts, British Columbia; Geological Survey of Canada, Map 6-1957, scale 1:253 440, URL <https://doi.org/10.4095/108451> [November 2019].

Little, H.W. (1961): Kettle River (west-half), British Columbia; Geological Survey of Canada, Preliminary map 15-1961, scale 1:253 440, URL <https://doi.org/10.4095/108762> [November 2019].

Massey, N.W. and Duffy, A. (2008a): Boundary project: McKinney Creek (NTS 82E/03) and Beaverdell (NTS 82E/06, 07W, 10W, 11W) areas, south-central British Columbia; *in* Geological Fieldwork 2007, BC Ministry of Energy, Mines and Petroleum Resources, Paper 2008-1, p. 87–101, URL <http://cmscontent.nrs.gov.bc.ca/geoscience/PublicationCatalogue/Paper/BCGS_P2008-01-10_Massey.pdf> [November 2019].

Massey, N.W.D. and Duffy, A. (2008b): Geology and mineral deposits of the area east of Beaverdell, British Columbia; BC Ministry of Energy, Mines and Petroleum Resources, BC Geological Survey Branch, Open File 2008-9, scale 1:250 000, URL <http://cmscontent.nrs.gov.bc.ca/geoscience/PublicationCatalogue/OpenFile/BCGS_OF2008-09.pdf> [November 2019].

Massey, N.W.D., Gabites, J.E., Mortenson, J.K. and Ullrich, T.D. (2010): Boundary project: geochronology and geochemistry of Jurassic and Eocene intrusions, southern British Columbia (NTS 082E); *in* Geological Fieldwork 2009, BC Ministry of Energy, Mines and Petroleum Resources, Paper 2010-1, p. 127–142, URL <http://cmscontent.nrs.gov.bc.ca/geoscience/PublicationCatalogue/Paper/BCGS_P2010-01-11_Massey.pdf> [November 2019].

Peterson, N. (2013): 2012 drilling, geochemical, geological and geophysical report on the Waterloo property, southeast British Columbia, Vernon Mining Division, British Columbia; BC Ministry of Energy, Mines and Petroleum Resources, Assessment Report 33 907, 306 p., URL <http://aris.empr.gov.bc.ca/search.asp?mode=repsum&rep_no=33907> September 2019].

Reynolds, P. (2009): Diamond drilling report on the Carmi molybdenum property, Kettle River project, British Columbia; BC Ministry of Energy, Mines and Petroleum Resources, Assessment Report 30 806, 211 p., URL <http://aris.empr.gov.bc.ca/search.asp?mode=repsum&rep_no=30806> [September 2019].

Reinecke, L. (1915): Ore deposits of the Beaverdell map area; Geological Survey of Canada, Memoir 79, 172 p.

Tempelman-Kluit, D.J. (1989): Geology, Penticton, west of the sixth meridian, British Columbia; Geological Survey of Canada, Map 1736A, scale 1:250 000.

Watson, P.H., Godwin, C.I. and Christopher, P.A. (1982): General geology and genesis of silver and gold veins in the Beaverdell area, south-central British Columbia; Canadian Journal of Earth Sciences, v. 19, p. 1264–1274.

Biotite and Muscovite $^{40}Ar/^{39}Ar$ ages from the Purcell Anticlinorium and the Kootenay Arc, Southeastern British Columbia (NTS 082F, G)

N.A. Rioseco, Department of Geoscience, University of Calgary, Calgary, Alberta, nicole.rioseco@ucalgary.ca

D.R.M. Pattison, Department of Geoscience, University of Calgary, Calgary, Alberta

A. Camacho, Department of Geological Science, University of Manitoba, Winnipeg, Manitoba

Rioseco, N.A., Pattison, D.R.M. and Camacho, A. (2020):Biotite and muscovite $^{40}Ar/^{39}Ar$ ages from the Purcell Anticlinorium and the Kootenay Arc, southeastern British Columbia (NTS 082F, G); *in* Geoscience BC Summary of Activities 2019: Minerals, Geoscience BC, Report 2020-01, p. 35–50.

Introduction

This paper presents new $^{40}Ar/^{39}Ar$ ages for biotite and muscovite from metasedimentary and meta-igneous rocks from the region between the towns of Creston, Kimberley and Crawford Bay in southeastern British Columbia (BC). This region comprises the interface between two major tectonic domains (Figure 1) in the southern Omineca Belt of the Canadian Cordillera: the Purcell Anticlinorium (PA) and the Kootenay Arc (KA). Geochronological data are combined with structural and metamorphic information to provide an improved understanding of the nature and significance of the interface.

The PA occupies the eastern and central portion of the study area. It is a regional-scale north-northwesterly-plunging Mesozoic fold-and-thrust structure that is cored by Mesoproterozoic rocks of the Belt-Purcell Supergroup (Price, 2000). The Belt-Purcell Supergroup comprises rift-related clastic rocks and synsedimentary mafic sills that are interpreted to have been deposited in an intracratonic rift basin between ca. 1470 and 1400 Ma (Höy, 1989; Anderson and Davis, 1995; Sears et al., 1998; Evans et al., 2000). On the eastern and western flanks of the PA, the Belt-Purcell Supergroup is unconformably overlain by the Neoproterozoic Windermere Supergroup, a sequence of rift-related clastic rocks that were deposited on the margin of ancient North America (Devlin et al., 1988; Warren, 1997; Lund et al., 2003).

In the western portion of the study area, the PA interfaces with the KA, an arcuate salient of polydeformed and polymetamorphosed rocks. The KA comprises Neoproterozoic to Paleozoic strata that were deposited on the rifted margin of ancestral North America as well as Paleozoic to Jurassic volcanic and sedimentary rocks of the Quesnel terrane that were accreted to the margin (Devlin and Bond, 1988). In general, the stratigraphy of the KA is younger than that of the PA. In the northern part of the area shown in Figure 2, the westward transition from the PA to the KA is continuous, whereas in the southern part of the area, such as in the vicinity of the town of Creston, BC, the transition is abrupt and marked by the Purcell Trench fault, which dies out going north from Creston and disappears in the vicinity of Crawford Bay.

A younging in stratigraphy between the two domains is complemented by a change in structural style, metamorphic grade and magmatism. Widespread cleavage development in the PA is stratigraphically restricted to Mesoproterozoic rocks of the Belt-Purcell Supergroup (Leech, 1962). Additionally, the PA is characterized by extensive low-grade metamorphism in the biotite zone of the greenschist facies (~450 °C and 3.5–4 kbar; Figure 2; DePaoli and Pattison, 1995; Pattison and Seitz, 2012;). In the northwestern area of Figure 2, where the transition between the PA and the KA is continuous, there is an intensification in deformation and an increase in metamorphic grade. Rocks of the KA are characterized by fabrics that are indicative of at least three Mesozoic regional-scale deformation events (Fyles, 1964; Moynihan and Pattison, 2013; Webster and Pattison, 2018). Metamorphic grade in the KA reaches upper-amphibolite facies (sillimanite+K-feldspar zone) and is marked by elongated, bull's-eye–shaped Barrovian metamorphic culmination zones (Figure 2; Moynihan and Pattison, 2013). The metamorphic grade on the eastern flank of the metamorphic culmination diminishes to that of the biotite zone, where the KA interfaces with the western flank of the PA. The KA experienced two major Mesozoic magmatic episodes resulting in the Middle Jurassic Nelson suite (Ghosh, 1995; Webster et al., 2017) and the mid- to late-Cretaceous Bayonne suite (Logan, 2001). Within the study area (Figure 2), intrusions of the Bayonne magmatic suite occur on both sides of the interface.

Papers in previous Geoscience BC reports (Rioseco and Pattison, 2018; Rioseco et al., 2019) have characterized the structural and metamorphic features of the PA and KA and the interface between them (discussed below). In this pa-

This publication is also available, free of charge, as colour digital files in Adobe Acrobat® PDF format from the Geoscience BC website: http://www.geosciencebc.com/updates/summary-of-activities/.

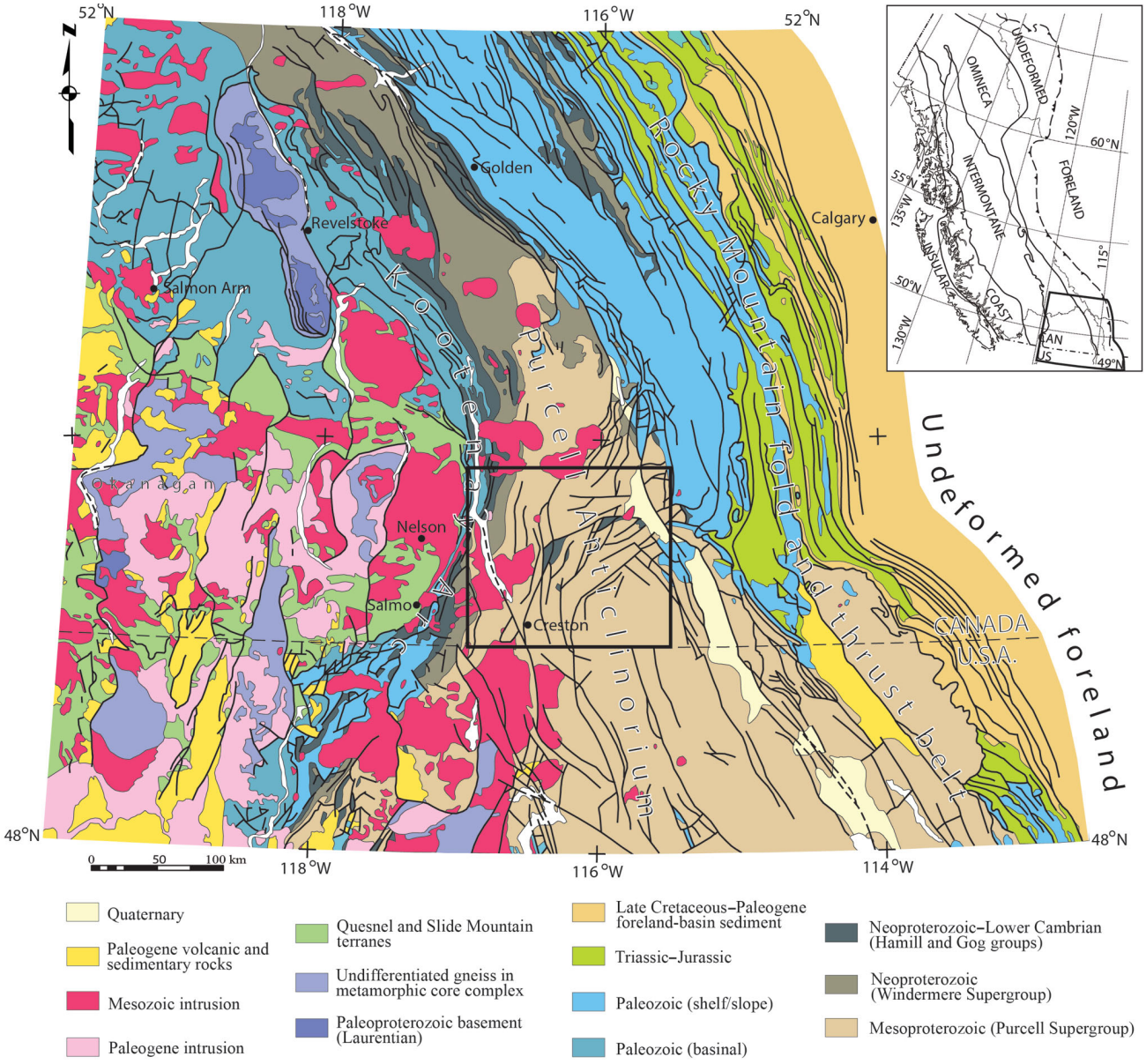

Figure 1. Regional geology of southeastern British Columbia. Geology modified from Wheeler and McFeely (1991), Moynihan and Pattison (2013) and Webster and Pattison (2018). The extent of the study area in Figures 2 and 7 is indicated by the box outlined in black.

per, new mica $^{40}Ar/^{39}Ar$ ages are presented to further constrain the nature of the two domains and their interface.

Structure and Metamorphism

Purcell Anticlinorium–type deformation is characterized by the development of penetrative slaty cleavage (S_1) that is present within argillaceous portions of turbidites of the lowermost Belt-Purcell unit. This S_1 cleavage is geographically widespread in Mesoproterozoic rocks of the PA (Figure 3a); it is not present in younger strata, indicating that it developed prior to deposition of the overlying Neoproterozoic Windermere Supergroup. The dominant Kootenay Arc–type structure is a penetrative phyllitic to fine-grained schistose foliation (S_2) that is subparallel to bedding and dips steeply (~60°–vertical) to the east and west (Figure 3a). Development of S_2 occurred during the second deformation phase (D_2), which is interpreted to be an Early Cretaceous deformation event (Moynihan and Pattison, 2013; Webster and Pattison, 2018) that overprinted an earlier, Mesozoic D_1 nappe-forming event.

Both the PA and KA were affected by a third episode of deformation (D_3) that is characterized by folding and the development of crenulations of S_1 or S_2 that define a spaced cleavage (S_3) and lineations (L_3). The development of S_3 and L_3 has only been observed in the northern portion of the study area (Figure 3b). The D_3 structures are thought to have developed in association with the formation of the overall anticlinorial structure of the PA and to have over-

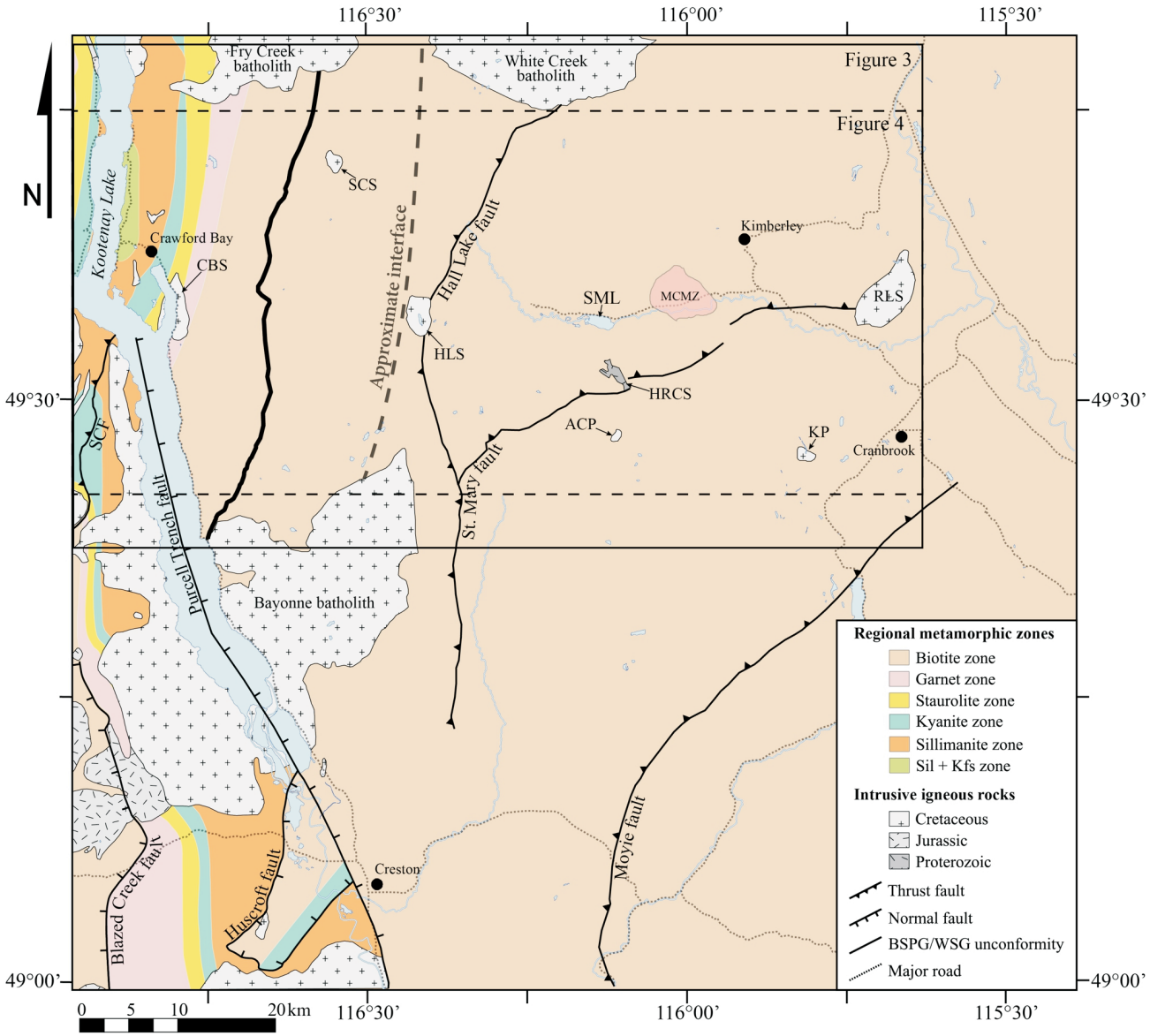

Figure 2. Distribution of metapelitic metamorphic zones within the study area (modified from Moynihan and Pattison, 2013; Webster and Pattison, 2018). The solid black outline indicates the area shown in Figures 3 and the dashed black outline indicates the area shown in Figure 4. Abbreviations: ACP, Angus Creek stock; BPSG, Belt-Purcell Supergroup; CBS, Crawford Bay stock; HLS, Hall Lake stock; Kfs, potassium feldspar; HRCS, Hellroaring Creek stock; KP, Kiakho stock; MCMZ, Matthew Creek metamorphic zone; RLS, Reade Lake stock; SCF, Seeman Creek fault; SCS, Sawyer Creek stock; Sil, sillimanite; SML, St. Mary Lake; WSG, Windermere Supergroup.

printed the D_2 structures in the KA (Price, 1984; Rioseco et al., 2019). Therefore, the structural interface between the PA and KA is best defined as the most easterly development of S_2 structures, which occurs in Belt-Purcell rocks roughly 15 km east of the unconformity between the Windermere and Belt-Purcell supergroups, at the latitude of St. Mary Lake (Figure 3).

There is no noticeable difference in metamorphic grade across the structural interface; the rocks in the PA east of the interface and the rocks on the eastern flank of the KA metamorphic culmination to the west of the interface both lie within the biotite zone (Figure 2). Therefore, a study of mineral growth with respect to microstructures is required to identify the boundary between the PA and KA metamorphic domains. In the PA, biotite and chlorite porphyroblasts are randomly oriented in rocks that do not contain a cleavage. When S_1 is present in the rock, biotite and chlorite are aligned within the plane of S_1 (Figure 4a, b), indicating that metamorphism predated or was contemporaneous with deformation, constraining it to the Mesoproterozoic. In the KA, straight inclusion trails in biotite were inherited from S_2, indicating that biotite formed during or slightly after this event (Figure 4c–e). In addition, S_2 is folded into microlithons between the spaced-cleavage planes of S_3 (Figure 4d, e) and the path of S_3 is deflected by biotite porphyro-

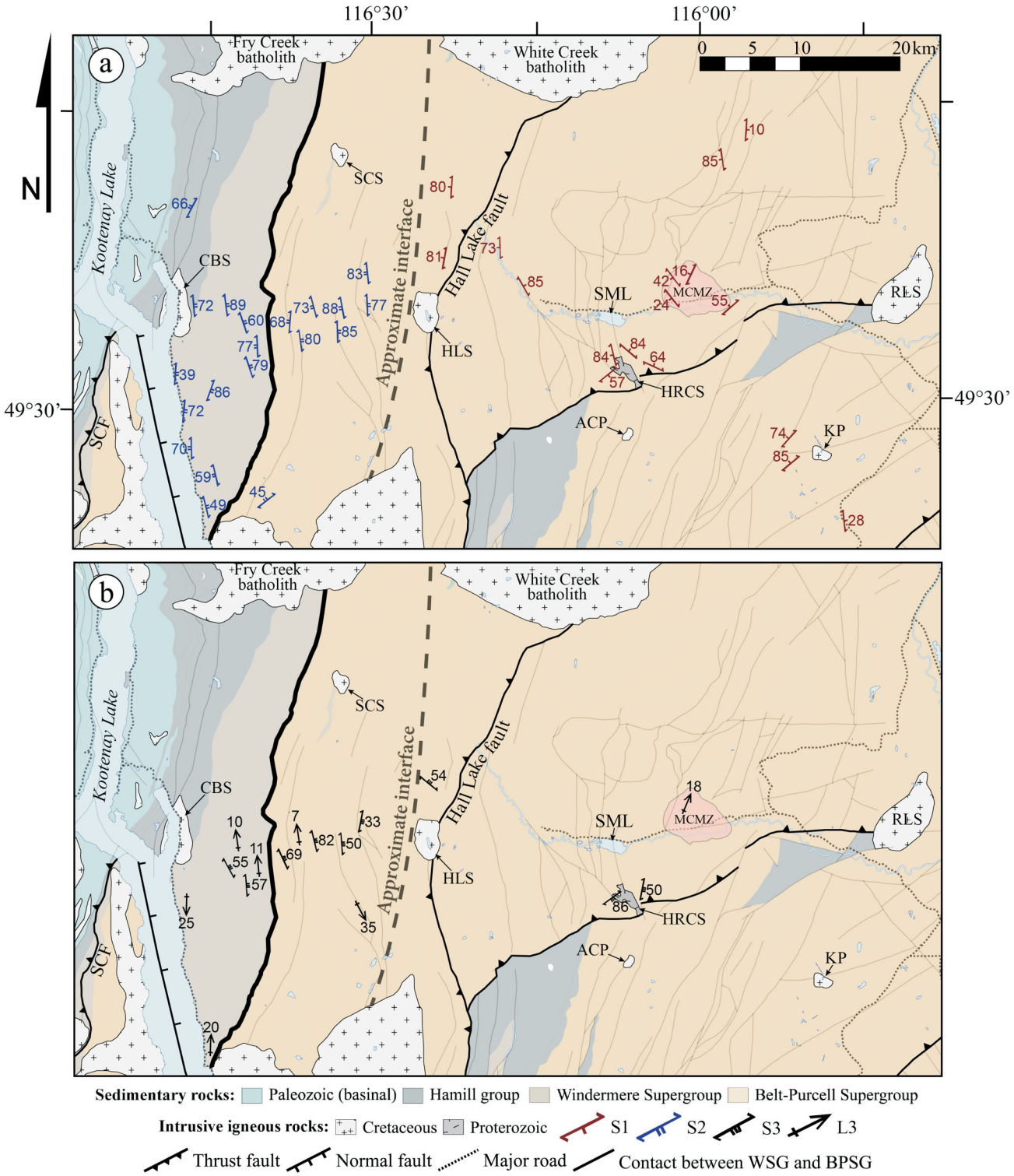

Figure 3. Distribution of structures across the northern portion of the study area: **a)** S_1 (red) and S_2 (blue) across the field area; **b)** D_3-related structures (S_3 and L_3) across the field area. Abbreviations: ACP, Angus Creek stock; BPSG, Belt-Purcell Supergroup; CBS, Crawford Bay stock; HLS, Hall Lake stock; HRCS, Hellroaring Creek stock; KP, Kiakho stock; MCMZ, Matthew Creek metamorphic zone; RLS, Reade Lake stock; SCF, Seeman Creek fault; SCS, Sawyer Creek stock; SML, St. Mary Lake; WSG, Windermere Supergroup.

blasts (Figure 4c–e). Fine-grained biotite aligned within the plane of S_2 was also subsequently deformed by D_3 (Figure 4f). The occurrence of these fabrics suggests that biotite development in this part of the KA either postdated or was approximately contemporaneous with D_2 and preceded the folding associated with D_3. The location of the metamorphic interface defined by the change in timing of development of the biotite, as defined by the above microstructures, coincides approximately with the structural interface (Figure 4); it occurs west of the most westerly Mesoproterozoic porphyroblasts, which predate the development of S_1, and east of the most easterly porphyroblasts that are related to Early Cretaceous D_2 deformation.

^{40}Ar/^{39}Ar Thermochronology

Sample Petrography

Samples for biotite and muscovite ^{40}Ar/^{39}Ar geochronology were selected to provide as broad a spatial coverage as possible in the PA and across the interface with the KA. Metasedimentary rocks sampled for this study range from fine-grained quartz-mica schist and phyllite to metamorphosed argillaceous sandstone. Metamorphic grade for most samples, whether from the PA or the KA, is within the biotite zone; samples 17NR168 and 17NR169 are the exception as they come from the garnet zone. Biotite and muscovite grains in these rocks are typically <0.5 mm in size. Biotite typically occurs as randomly oriented grains in massive rocks of the PA that show no sign of S_1 (Figure 5a) and as grains that lie within the dominant schistosity (S_2) in rocks of the KA (Figure 5b). Biotite also typically contains quartz inclusions and shows some degree of chloritization, though the latter is only obvious on backscattered electron images. Care was taken when hand-picking grains to assure that those analyzed contained as few inclusions and as little chloritization as possible. Muscovite from both PA and KA samples defines the dominant schistosity (Figure 5c) but in the KA samples, muscovite is more deformed than in the PA samples (Figure 5d). Meta-igneous rocks used for this study are predominantly intermediate to mafic phases of the Moyie Sill that were emplaced in the lowermost Belt-Purcell units. Mafic sills contain the mineral assemblage amphibole(hornblende±actinolite)+plagioclase+quartz and contain variable amounts of fine-grained (~0.25 mm) biotite±chlorite±epidote (Figure 5e). Bishop (1973) described a plagioclase-quartz-biotite granophyre phase of the Moyie Sill, which lacks amphibole but contains a much greater abundance of biotite. In these rocks, biotite occurs in aggregates (individual grains range from 0.10 to 0.45 mm in size; Figure 5f).

Mineral Compositions

Mineral compositions of samples were analyzed using a JEOL Limited JXA-8200 electron-probe microanalyzer at the University of Calgary Laboratory for Electron Microprobe Analysis. Mineral compositions for biotite and muscovite are presented in Table 1. The Mg/(Mg+Fe) ratio across all samples is in the range of 0.31 to 0.83, with most samples clustering between 0.35 and 0.5. The F/(F+Cl+OH) ratio across all samples is between 0.00 and 0.08. There is no discernible difference between the compositions of biotite in metamorphosed igneous versus sedimentary rocks or the compositions of biotite in the metasedimentary rocks of the PA versus the KA.

^{40}Ar/^{39}Ar Analytical Methods

Samples analyzed by the ^{40}Ar/^{39}Ar method were crushed using standard rock-crushing techniques and micas were separated from the bulk of the sample on a shaking table. Grains were then sieved, washed and subsequently hand picked. Separated grain sizes typically ranged from 250 to 297 µm, but larger (297–420 µm) grains were picked when possible and smaller (<250 µm) grains, when necessary.

The following methodology is reproduced from the supplementary material provided by Larson et al. (2017):

> *"The ^{40}Ar/^{39}Ar analytical work was performed at the University of Manitoba using a multi-collector Thermo Fisher Scientific ARGUS VI mass spectrometer, linked to a stainless steel Thermo Fisher Scientific extraction/purification line and Photon Machines (55 W) Fusions 10.6 CO2 laser. Argon isotopes (from mass 40–37) were measured using Faraday detectors with low noise 1 x 1012 Ω resistors and mass 36 was measured using a compact discrete dynode (CDD) detector. The sensitivity for argon measurements is ~6.312 x 1017 moles/fA as determined from measured aliquots of Fish Canyon Sanidine (Dazé et al., 2003; Kuiper et al., 2008).*
>
> *Standards and unknowns were placed in 2-mm-deep wells in 18-mm-diameter Al disks, with standards placed strategically so that the lateral neutron flux gradients across the disk could be evaluated. Planar regressions were fit to the standard data, and the 40Ar/39Ar neutron fluence parameter, J, was interpolated for the unknowns. Uncertainties in J are estimated at 0.1–0.2% (1), based on Monte Carlo error analysis of the planar regressions (Best et al., 1995). All specimens were irradiated in the Cd-lined, in-core CLICIT facility of the Oregon State University TRIGA reactor (Corvallis, Oregon, USA)."*

The duration of irradiation was 20 hours and included Fish Canyon sanidine (28.2 Ma; Kuiper et al., 2008) and GA1550 biotite (98.5 Ma; Spell and McDougall, 2003) reference standards.

> *"Irradiated samples were placed in a Cu sample tray, with a KBr cover slip, in a stainless steel high vacuum extraction line and baked with an infrared lamp for 24 hours. Single crystals were either fused…"*

or step-heated

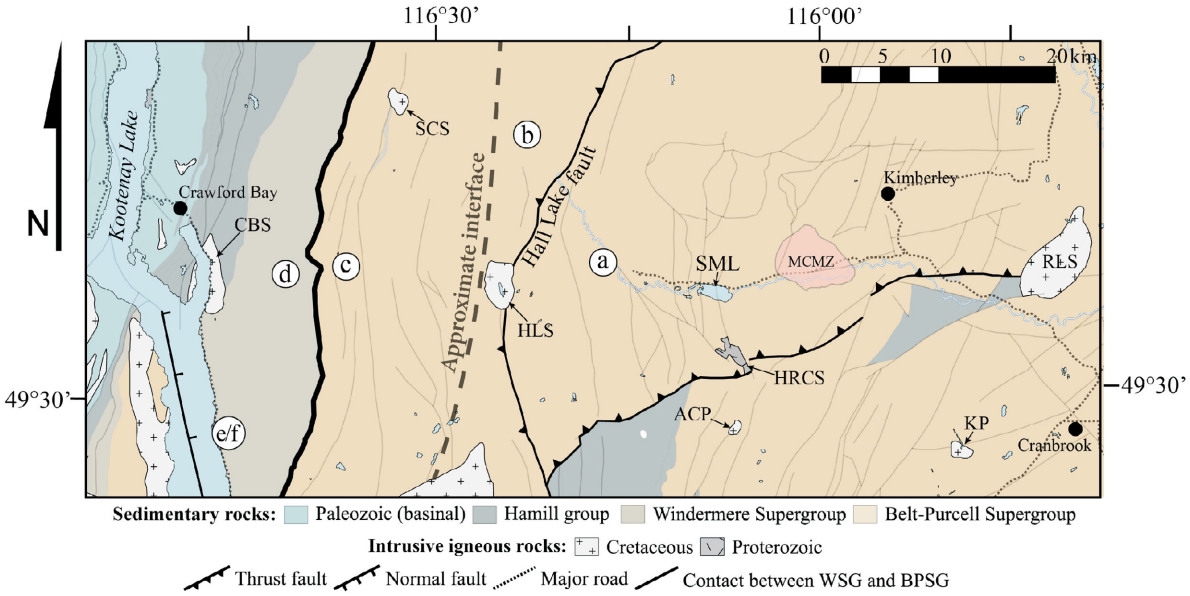
116°30'
116°00'
0 5 10 20 km
N
49°30'
49°30'
Kootenay Lake
Crawford Bay
CBS
SCS
Approximate interface
Hall Lake fault
HLS
Kimberley
SML
MCMZ
RLS
HRCS
ACP
KP
Cranbrook
a
b
c
d
e/f
Sedimentary rocks: Paleozoic (basinal) Hamill group Windermere Supergroup Belt-Purcell Supergroup
Intrusive igneous rocks: Cretaceous Proterozoic
Thrust fault Normal fault Major road Contact between WSG and BPSG

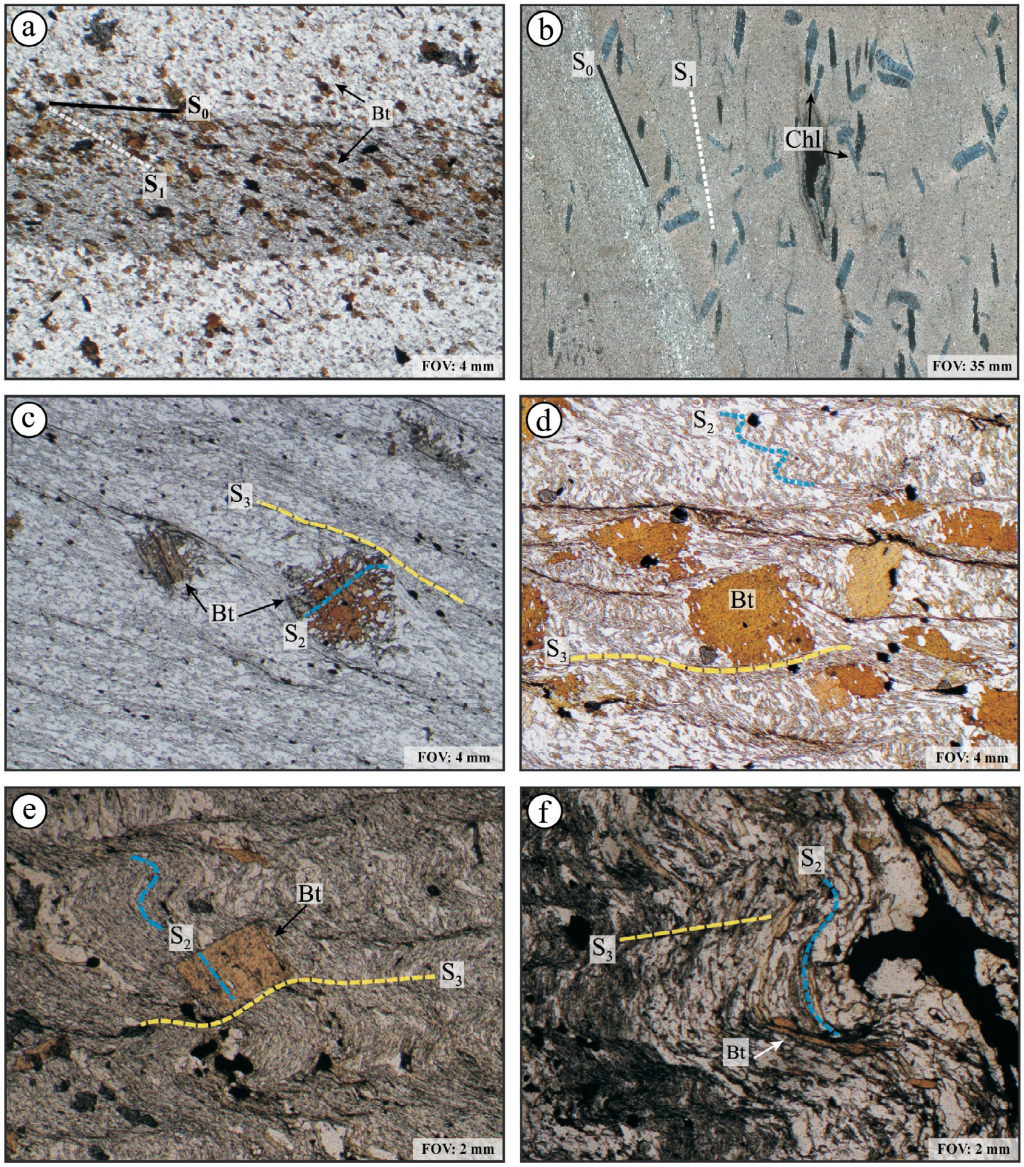
a
S0
S1
Bt
FOV: 4 mm
b
S0
S1
Chl
FOV: 35 mm
c
S3
Bt
S2
FOV: 4 mm
d
S2
Bt
S3
FOV: 4 mm
e
Bt
S2
S3
FOV: 2 mm
f
S2
S3
Bt
FOV: 2 mm

> *"…using the laser, and reactive gases were removed, after ~3 minutes, by three NP-10 SAES getters (two at room temperature and one at 450 °C) prior to being admitted to the mass spectrometer by expansion. Five argon isotopes were measured simultaneously over a period of 6 min. Measured isotope abundances were corrected for extraction line blanks, which were determined before every sample analysis."*

Line blanks averaged ~5.77 fA for mass 40 and ~0.02 fA for mass 36.

Detector intercalibration (IC) between the different faraday cups (H1 = ^{40}Ar, AX = ^{39}Ar, L1 = ^{38}Ar, L2 = ^{37}Ar) was monitored (in Qtegra) every four days by peak hopping ^{40}Ar. Calculated values are ICH1: 1.0000, ICAX: 1.0745, ICL1: 1.0637 and ICL2: 1.0534, with an error of approximately 0.2%. The intercalibration factor between H1 and the CDD was measured with the unknowns resulting in ICCDD: 1.0056 ±0.0006 per atomic mass unit. Additionally, as outlined in Larson et al. (2017):

> *"A value of 295.5 was used for the atmospheric ^{40}Ar/^{36}Ar ratio (Steiger and Jager, 1977) for the purposes of routine measurement of mass spectrometer discrimination using air aliquots, and correction for atmospheric argon in the ^{40}Ar/^{39}Ar age calculation. Corrections are made for neutron-induced ^{40}Ar from potassium, ^{39}Ar and ^{36}Ar from calcium, and ^{36}Ar from chlorine (Roddick, 1983; Renne et al., 1998; Renne and Norman, 2001)."*

Data collection was performed using Pychron software (Ross, 2017), and data reduction, error propagation, age calculation and plotting were performed using MassSpec software (version 8.091; Deino, 2013). The decay constants used were those recommended by Steiger and Jager (1977).

Criteria for Defining Ages

Argon release patterns for micas analyzed in this study are complex and they fall into five groups: 1) age spectra that define plateaus (Figure 6a), 2) relatively flat age spectra with 'forced plateaus' (Figure 6b), 3) monotonically increasing age spectra (Figure 6c), 4) half-saddle–shaped age spectra (Figure 6d), and 5) relatively flat age spectra, in which large portions of the ^{39}Ar were released in single steps (Figure 6e, f). As a result, interpreted ages presented in Table 2 represent a best estimate of the cooling age. A distinction is made between a date and an age in that a date lacks any sort of significance, whereas the term 'age' is reserved for what is interpreted to be in some way significant. Isoplot (Ludwig, 2008) was used to calculate plateau ages and the criteria set for a plateau was three or more contiguous steps, representing >50% ^{39}Ar released, with dates that are within uncertainty of each other at the 2σ level (Dalrymple and Lanphere, 1974; Lee et al., 1991). However, several samples did not meet these criteria.

An 'interpreted age' resulting from a forced plateau was calculated from three or more consecutive steps that produce a relatively flat profile but do not overlap in uncertainty at the 2σ level. In the cases where the step dates do not define a plateau or forced plateau, the interpreted age is an 'integrated age', which is determined by weighing the dates of the individual steps by the fraction of ^{39}Ar released. Calculation of an integrated age was typically reserved for experiments where a large portion of ^{39}Ar was released in a single step.

Half-saddle–shaped age spectra are characterized by a pattern of high initial ^{40}Ar/^{39}Ar dates that decrease to a trough at the end of the spectrum. This type of Ar-release pattern is interpreted as reactor-induced recoil loss of ^{39}Ar. Lanphere and Dalrymple (1976) suggested that the step or average of multiple steps comprising the trough of the saddle results in the best estimate of an age for the mineral. In this study, the age spectra with troughs consisting of fewer than three are considered as having no plateau. The interpreted age is determined from the step or steps in the trough that define a plateau segment; plateau segments defined in this study comprise between 15 and 40% of the total ^{39}Ar released.

Biotite and muscovite results will be discussed together in the following sections. For clarity, sample numbers that correspond to muscovite will be followed by '-Ms'.

Results and Interpretation

The ^{40}Ar/^{39}Ar ages obtained from rocks in the PA, east of the structural and metamorphic interface, have been subdivided into three domains separated by major north-northeast-trending thrust faults (Figure 1): the Moyie and the St.

Figure 4. Photomicrographs from across the structural and metamorphic interface, along with a map (top) indicating sample locations (letters match those identifying the photomicrographs): **a)** biotite-bearing metasediment from the Aldridge Formation, with biotite randomly oriented in arenaceous beds and aligned within the plane of S_1 in argillaceous parts of the rock; **b)** Aldridge Formation metasediments, with randomly oriented chlorite porphyroblasts that have been deformed in the orientation of S_1; **c)** argillaceous sandstone of the Dutch Creek Formation, in which biotite contains inclusion trails that are interpreted to have been inherited from S_2 and S_3 cleavage wraps around biotite porphyroblasts; **d)** crenulated fine-grained schist from the Horsethief Creek Group, with biotite porphyroblasts that predate the development of S_3; **e)** crenulated phyllite from the Horsethief Creek Group, with biotite porphyroblasts that predate the development of S_3; **f)** crenulated phyllite from the Horsethief Creek Group, with fine-grained biotite within the primary foliation plane (S_2) that predates the development of S_3. All samples are shown under plane-polarized light. Abbreviations: ACP, Angus Creek stock; BPSG, Belt-Purcell Supergroup; Bt, biotite; CBS, Crawford Bay stock; Chl, chlorite; HLS, Hall Lake stock; HRCS, Hellroaring Creek stock; FOV, field of view; KP, Kiakho stock; MCMZ, Matthew Creek metamorphic zone; RLS, Reade Lake stock; SCF, Seeman Creek fault; SCS, Sawyer Creek stock; SML, St. Mary Lake; WSG, Windermere Supergroup.

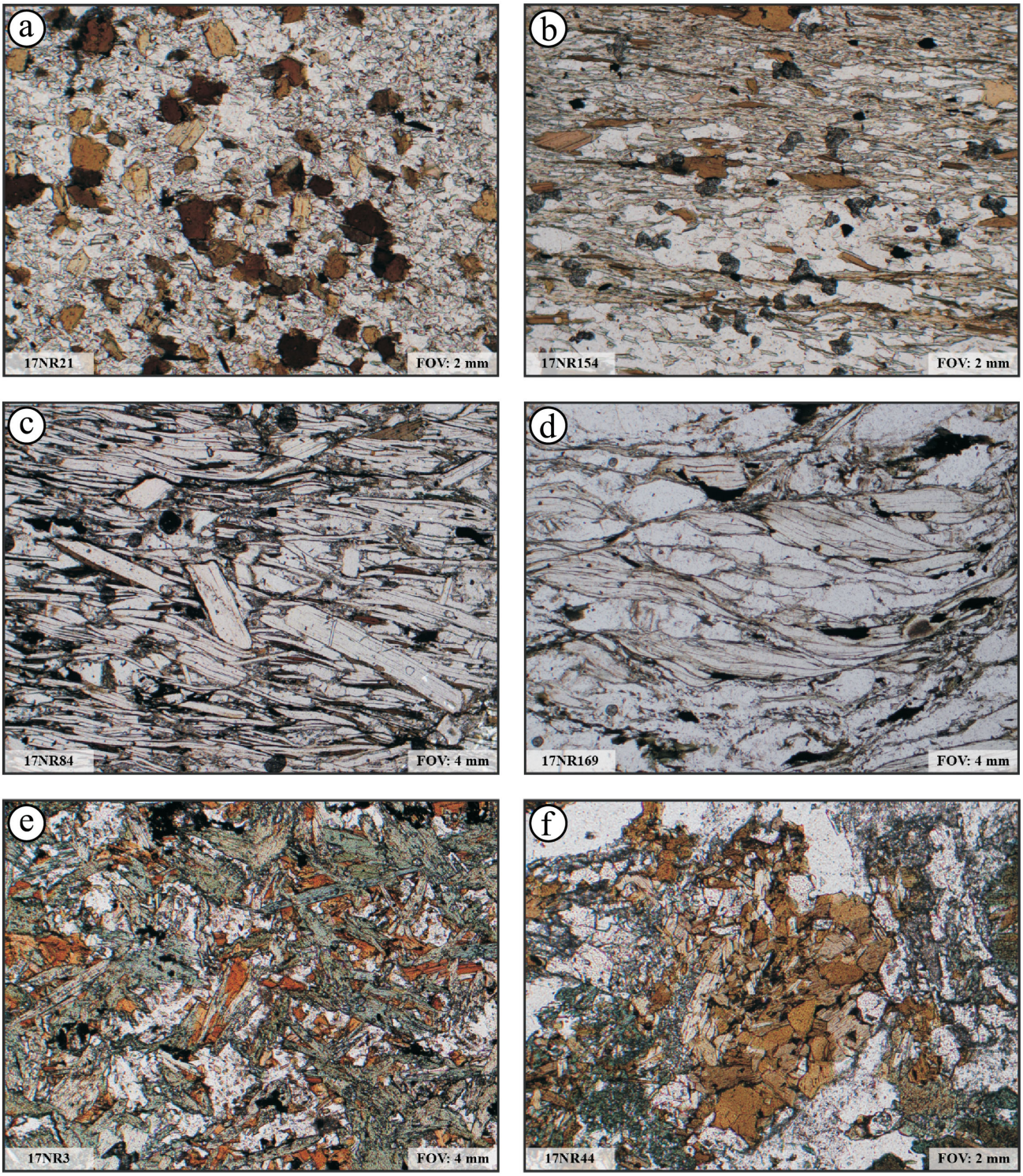

Figure 5. Representative photomicrographs of samples from the study area analyzed by the $^{40}Ar/^{39}Ar$ method: **a)** biotite-bearing metasediments from the middle Aldridge Formation near Yahk, BC; **b)** biotite-bearing fine-grained schist from the Horsethief Creek Group east of Gray Creek, BC; **c)** fine-grained muscovite schist of the lower Aldridge Formation from near the Hellroaring Creek stock; **d)** fine-grained muscovite schist of the Hamill group from near Crawford Bay, BC; **e)** metagabbro of the Moyie Sill, northeast of Yahk, BC; **f)** granophyre phase from the Moyie Sill, east of Creston, BC. Abbreviation: FOV, field of view.

Table 1. Representative mineral compositions for biotite and muscovite samples analyzed by the $^{40}Ar/^{39}Ar$ method. Abbreviations: Bt, biotite; Ms, muscovite.

Sample mineral	04K9A	08MC3A	11MOS1A	12MS20	17NR3	17NR6	17NR14b	17NR21	17NR44	17NR45	17NR72	17NR74	17NR86	17NR132	17NR136	17NR154	17NR161	12HRC2A	17NR84	17NR101C	17NR168	17NR169
	Bt	Bt	Bt	Bt	Bt	Bt	Bt	Bt	Bt	Bt	Bt	Bt	Bt	Bt	Bt	Bt	Bt	Ms	Ms	Ms	Ms	Ms
Oxide:																						
SiO_2	39.53	36.93	35.29	34.98	36.76	35.41	34.39	35.02	35.52	34.65	36.60	35.79	35.55	35.73	39.00	37.22	35.84	45.98	45.97	45.80	46.16	46.64
TiO_2	1.15	1.76	1.58	1.71	1.56	1.63	2.21	2.22	1.67	1.61	1.84	2.73	2.43	1.60	2.30	1.67	2.03	1.31	0.90	0.53	0.56	0.70
Al_2O_3	15.85	16.65	19.24	17.56	17.07	17.63	17.80	17.57	16.55	17.55	17.12	17.65	17.67	17.92	14.50	17.07	16.02	34.50	34.75	36.67	32.98	31.94
Fe_2O_3	0.00	0.00	0.00	0.00	0.00	0.00	0.00	0.00	0.00	0.00	0.00	0.00	0.00	0.00	0.00	0.00	0.00	0.00	0.00	0.00	0.00	0.00
FeO	11.95	15.63	22.72	24.77	19.67	21.66	24.99	24.09	23.25	25.44	19.88	20.86	19.64	19.22	7.56	18.50	23.00	1.25	1.41	0.91	3.40	3.84
MnO	0.05	0.18	0.16	0.38	0.19	0.29	0.35	0.34	0.24	0.43	0.19	0.42	0.47	0.33	0.04	0.13	0.23	0.01	0.02	0.00	0.00	0.00
MgO	16.60	13.22	7.51	6.42	10.59	9.15	6.39	6.69	8.52	6.65	10.46	8.22	9.79	10.69	21.26	11.33	8.57	1.09	0.82	0.38	0.99	1.03
CaO	0.00	0.01	0.01	0.00	0.03	0.00	0.05	0.02	0.04	0.06	0.04	0.03	0.03	0.01	0.05	0.03	0.05	0.02	0.01	0.00	0.01	0.03
Na_2O	0.03	0.03	0.15	0.05	0.04	0.11	0.00	0.07	0.02	0.00	0.08	0.05	0.08	0.03	0.37	0.09	0.06	0.59	0.63	1.61	1.62	0.97
K_2O	9.25	9.82	8.39	9.28	9.18	9.29	9.12	9.13	9.37	8.81	8.97	9.16	9.37	9.52	9.44	9.16	9.18	10.17	10.57	9.17	9.57	9.99
BaO	0.07	0.16	0.12	0.20	0.41	0.19	0.16	0.10	0.16	0.15	0.25	0.18	0.09	0.05	0.48	0.01	0.07	0.38	0.25	0.36	0.31	0.35
F	0.72	0.28	0.14	0.17	0.08	0.13	0.02	0.29	0.19	0.09	0.00	0.34	0.32	0.34	0.41	0.44	0.36	0.18	0.11	0.09	0.00	0.00
Total	**95.18**	**94.68**	**95.33**	**95.52**	**95.58**	**95.48**	**95.49**	**95.52**	**95.52**	**95.44**	**95.43**	**95.44**	**95.42**	**95.45**	**95.40**	**95.66**	**95.41**	**95.48**	**95.42**	**95.51**	**95.58**	**95.49**
Cations calculated on the basis of 11 oxygen:																						
Si	2.91	2.80	2.72	2.74	2.80	2.73	2.70	2.74	2.77	2.72	2.79	2.75	2.73	2.73	2.83	2.81	2.79	3.07	3.07	3.03	3.11	3.15
Ti	0.06	0.10	0.09	0.10	0.09	0.09	0.13	0.13	0.10	0.09	0.11	0.16	0.14	0.09	0.13	0.09	0.12	0.07	0.05	0.03	0.03	0.04
Al	1.37	1.49	1.75	1.62	1.53	1.60	1.65	1.62	1.52	1.63	1.54	1.60	1.60	1.61	1.24	1.52	1.47	2.72	2.74	2.86	2.62	2.54
Fe	0.74	0.99	1.46	1.63	1.25	1.40	1.64	1.57	1.51	1.67	1.27	1.34	1.26	1.23	0.46	1.17	1.50	0.07	0.08	0.05	0.19	0.22
Mn	0.00	0.01	0.01	0.03	0.01	0.02	0.02	0.02	0.02	0.03	0.01	0.03	0.03	0.02	0.00	0.01	0.02	0.00	0.00	0.00	0.00	0.00
Mg	1.82	1.49	0.86	0.75	1.20	1.05	0.75	0.78	0.99	0.78	1.19	0.94	1.12	1.22	2.30	1.28	0.99	0.11	0.08	0.04	0.10	0.10
Ca	0.00	0.00	0.00	0.00	0.00	0.00	0.00	0.00	0.00	0.01	0.00	0.00	0.00	0.00	0.00	0.00	0.00	0.00	0.00	0.00	0.00	0.00
Na	0.00	0.00	0.02	0.01	0.01	0.02	0.00	0.01	0.00	0.00	0.01	0.01	0.01	0.00	0.05	0.01	0.01	0.08	0.08	0.21	0.21	0.13
K	0.87	0.95	0.82	0.93	0.89	0.91	0.91	0.91	0.93	0.88	0.87	0.90	0.92	0.93	0.87	0.88	0.91	0.87	0.90	0.77	0.82	0.86
Ba	0.00	0.00	0.00	0.01	0.01	0.01	0.01	0.00	0.00	0.00	0.01	0.01	0.00	0.00	0.01	0.00	0.00	0.01	0.01	0.01	0.01	0.01
F	0.17	0.07	0.04	0.04	0.03	0.03	0.01	0.07	0.05	0.02	0.00	0.08	0.08	0.08	0.09	0.11	0.09	0.04	0.02	0.02	0.00	0.00
Total	**7.95**	**7.90**	**7.78**	**7.86**	**7.83**	**7.87**	**7.81**	**7.86**	**7.89**	**7.84**	**7.79**	**7.83**	**7.88**	**7.92**	**7.99**	**7.89**	**7.91**	**7.02**	**7.03**	**7.02**	**7.08**	**7.04**
F/(F+Cl+OH)	0.08	0.03	0.02	0.02	0.02	0.02	0.00	0.04	0.02	0.01	0.00	0.04	0.04	0.04	0.05	0.05	0.04	0.02	0.01	0.01	0.00	0.00
Mg/(Mg+Fe)	0.71	0.60	0.37	0.32	0.51	0.43	0.31	0.33	0.40	0.32	0.48	0.41	0.47	0.50	0.83	0.52	0.40	-	-	-	-	-

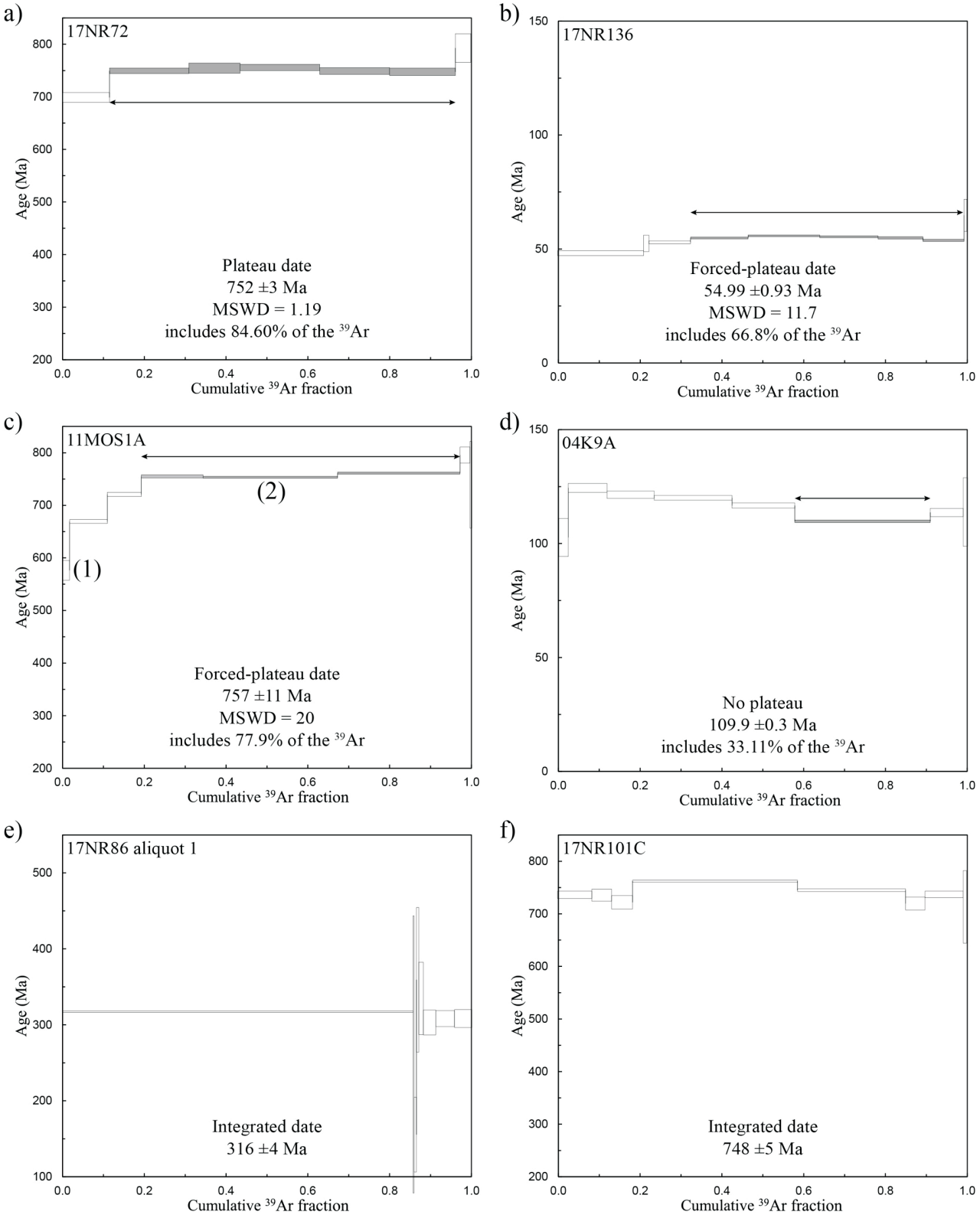

Figure 6. Representative $^{40}Ar/^{39}Ar$ age spectra for select samples from the study area: **a)** plateau date for sample 17NR72 from near Yahk, BC; **b)** forced plateau from a relatively flat age spectrum from near Boswell, BC; **c)** forced plateau from a monotonically increasing age spectrum from east of Yahk, BC, where point 2 indicates the best estimate for the age of the sample and point 1 indicates the time of final closure to argon diffusion; **d)** half-saddle–shaped spectrum, in which the age is interpreted from the results in the trough at the end of the spectrum; **e)** relatively flat spectrum with a large portion of ^{39}Ar released in a single step from near the Hellroaring Creek stock; **f)** relatively flat spectrum with a calculated integrated age from within the Matthew Creek metamorphic zone. Abbreviation: MSWD, mean square of weighted deviates.

Table 2. Summary of $^{40}Ar/^{39}Ar$ results (where n is the number of grains analyzed) from the study area. Abbreviations: Bt, biotite; Fm., Formation; FP, forced plateau; I, integrated date; Ms, muscovite; MSWD, mean square of weighted deviates; NP, no plateau; P, plateau. Unless otherwise noted, error is reported at the 2σ level.

Sample	Easting	Northing	Unit	Rock type	Mineral analyzed	Grain diameter (µm)	n	Age spectrum					Type	J value	±1σ
								Date (Ma)	^{39}Ar fraction	MSWD	Integrated date (Ma)	Interpreted age (Ma)			
04K9A	515505	5483628	Horsethief Creek Fm.	Metasediment	Bt	<250	5	109.9 ±0.3	33.11	N/A	115.81 ±1.57	109.9 ±0.3	NP	5.32E-03	3.76E-06
08MC3A	565318	5495890	Aldridge Fm.	Metasediment	Bt	297-250	4	432 ±5	18.11	N/A	496 ±5	432 ±5	NP	5.33E-03	2.28E-06
11MOS1A	584333	5439814	Aldridge Fm.	Metasediment	Bt	297-250	3	757 ±11	77.90	20	744 ±3	757 ±11	FP	5.29E-03	3.62E-06
12MS20	547277	5444841	Moyie Sills	Granophyre	Bt	420-297	2	366 ±8	36.70	4.1	377 ±5	366 ±8	FP	5.29E-03	3.55E-06
17NR3	572345	5449092	Moyie Sills	Mafic	Bt	297-250	2	489 ±2	70.22	N/A	567 ±7	489 ±2	NP	5.28E-03	6.52E-06
17NR6	548155	5444349	Moyie Sills	Granophyre	Bt	297-250	2	-	-	-	633 ±14	~600	NP	5.28E-03	4.32E-06
17NR14B	556865	5429592		Granodiorite	Bt	420-297	2	82.42 ±0.89	58.15	2	78.20 ±2.25	82.42 ±0.89	FP	5.28E-03	2.87E-06
17NR21	565449	5437346	Aldridge Fm.	Metasediment	Bt	<250	2	837 ±13	95.20	1.6	824 ±42	837 ±13	P	5.29E-03	6.06E-06
17NR44	541523	5439802	Moyie Sills	Granophyre	Bt	297-250	2	606 ±17	88.40	8.9	610 ±14	606 ±17	FP	5.29E-03	6.06E-06
17NR45	542208	5440222	Aldridge Fm.	Metasediment	Bt	<250	3	305 ±2	89.61	N/A	306 ±10	305 ±2	NP	5.30E-03	5.32E-06
17NR72	570325	5439259	Moyie Sills	Mafic	Bt	297-250	3	752 ±3	84.60	1.19	749 ±9	752 ±3	P	5.31E-03	6.04E-06
17NR86 aliquot 1	558368	5490387	Aldridge Fm.	Metasediment	Bt	297-250	2	-	-	-	316 ±4	316 ±4	I	5.28E-03	3.53E-06
17NR86 aliquot 2	558368	5490387	Aldridge Fm.	Metasediment	Bt	297-250	2	240.60 ±3.4	23.70	2.4	265 ±5	240 ±3	FP	5.28E-03	3.53E-06
17NR132	570840	5498230	Aldridge Fm.	Metasediment	Bt	297-250	4	582 ±15	40.40	7.8	668 ±10	582 ±15	FP	5.32E-03	4.14E-06
17NR136	517814	5475451	Horsethief Creek Fm.	Metasediment	Bt	707-420	1	54.99 ±0.93	66.80	11.7	53.41 ±0.68	54.99 ±0.93	FP	5.31E-03	4.18E-06
17NR154	520954	5496147	Horsethief Creek Fm.	Metasediment	Bt	297-250	4	-	-	-	84.04 ±2.75	84.04 ±2.75	NP	5.33E-03	4.77E-06
17NR160	523416	5492041	Horsethief Creek Fm.	Metasediment	Bt	297-250	4	139.8 ±1.6	96.50	13	139.23 ±1.06	139.8 ±1.6	FP	5.32E-03	3.56E-06
17NR161	525329	5495116	Dutch Creek Fm.	Metasediment	Bt	297-250	3	64.1 ±1.8	90.70	15	62.61 ±1.13	64.1 ±1.8	FP	5.32E-03	4.98E-06
12HRC2A	560553	5490222	Aldridge Fm.	Metasediment	Ms	707-420	1	704 ±2	83.50	2.7	700 ±6	704 ±2	FP	5.32E-03	4.10E-06
17NR84 aliquot 1	559419	5492015	Aldridge Fm.	Metasediment	Ms	420-297	2	-	-	-	674 ±6	674 ±6	I	5.28E-03	3.83E-06
17NR84 aliquot 2	559419	5492015	Aldridge Fm.	Metasediment	Ms	420-297	3	-	-	-	524 ±6	524 ±6	I	5.28E-03	3.83E-06
17NR101C	566235	5499982	Aldridge Fm.	Metasediment	Ms	420-297	3	-	-	-	748 ±5	748 ±5	I	5.33E-03	4.79E-06
17NR168 aliquot 1	516540	5506707	Hamill group	Metasediment	Ms	420-297	4	-	-	-	79.82 ±1.14	79.82 ±1.14	I	5.32E-03	4.27E-06
17NR168 aliquot 2	516540	5506707	Hamill group	Metasediment	Ms	420-297	3	-	-	-	77.68 ±1.14	77.68 ±1.14	I	5.32E-03	4.27E-06
17NR169	516614	5506727	Hamill group	Metasediment	Ms	420-297	3	-	-	-	83.60 ±0.89	83.60 ±0.89	I	5.33E-03	2.59E-06

Mary–Hall Lake faults. The southeastern domain is in the footwall of the Moyie fault. The western domain occurs between the Moyie and St. Mary faults, with data coming from its western portion near the town of Creston, BC, in the immediate hangingwall of the Purcell Trench fault. The northern domain is bounded by the St. Mary and Hall Lake faults in the vicinity of St. Mary Lake. The KA, more specifically rocks west of the structural and metamorphic interface, is referred to as a single domain. Representative age spectra are presented in Figure 6 and $^{40}Ar/^{39}Ar$ results are summarized in Table 2.

Four biotite separates from the eastern domain were analyzed in this study. Two samples, 17NR21 and 17NR72 returned plateau ages interpreted at 837 ±13 Ma and 752 ±3 Ma (Figure 6a), respectively. Sample 11MOS1A yielded a monotonically increasing spectrum with an 'forced plateau' age of 757 ±11 Ma (Figure 6c). This type of age spectrum is typically interpreted to reflect argon loss either to partial resetting (time point 1;~580 Ma) or protracted cooling (between time points 2 [~757 Ma] and 1 [~580 Ma]; McDougall and Harrison, 1999). In the fourth sample, 17NR3, a large portion (>70%) of the ^{39}Ar was released in a single step, so an integrated age of 489 ±2 Ma is reported for this sample.

Four biotite separates from the western domain near the town of Creston yielded $^{40}Ar/^{39}Ar$ ages between ca. 305 and ca. 606 Ma. Sample 17NR44 returned a forced-plateau age of 606 ±17 Ma, whereas sample 17NR6 (~600 Ma) is characterized by a half-saddle–shaped spectrum. Samples 17NR45 and 12MS20 yielded integrated ages of ca. 305 Ma and ca. 366 Ma, respectively. Biotite separates from a small, unmapped tonalitic intrusive body (17NR14B) located in the hangingwall of the Moyie fault (~2 km from the fault trace) returned a forced plateau age of 82 ±1 Ma. This age is interpreted from a monotonically increasing spectrum that indicates final closure to Ar loss at approximately 25 Ma. The significance of this sample will be discussed further below.

Mica from six samples from the northern domain were dated by $^{40}Ar/^{39}Ar$: three muscovites and three biotites. Sample 17NR101C-Ms does not yield a plateau; the integrated age is 748 ±5 Ma (Figure 6f). The age spectrum for sample 12HRC2A-Ms monotonically increases from ca. 105 Ma in the low-temperature steps to ca. 704 Ma in the higher temperature steps. Two aliquots of muscovite from sample 17NR84-Ms did not return age plateaus; the integrated age for aliquot 1 is 674 ±6 Ma and that for aliquot 2 is 524 ±6 Ma. Petrographic observations indicate that there may be two populations of muscovite in this sample (Figure 5c); however, the inconsistency between the two aliquots renders the significance of this age uncertain. Biotite-cooling ages from the northern domain are typically characterized by a half-saddle shape (17NR132: ca. 582 Ma; 08MC3A: ca. 432 Ma; 17NR86 [aliquot 2]: 240 Ma). The first aliquot analyzed for sample 17NR86 (aliquot 1) returned an integrated cooling age of 316 ±4 Ma (Figure 6e), significantly older than the second aliquot; however, unlike the muscovite in sample 17NR84-Ms, there is no evidence of two populations of biotite. The variation in cooling ages across aliquots will be addressed further below.

Mica cooling ages for the KA are much younger than those from the PA, between ca. 139 and ca. 55 Ma. In this region, two muscovite samples (17NR168-Ms, comprising two aliquots, and 17NR169-Ms) produced age spectra, in which a large portion of ^{39}Ar was released in a single step. Nevertheless, spectrum profiles are relatively flat so an integrated age was calculated for each; the two aliquots of separates for 17NR168 returned similar ages of 79.8 ±1.1 Ma and 77.7 ±1.1 Ma, whereas 17NR169 yielded an age of 83.6 ±0.9 Ma. Three of the five biotite samples returned forced-age plateaus from relatively flat spectra; (17NR160: 139 ±1.6 Ma, 17NR161: 64 ±1.8 Ma, 17NR136: 55 ±0.93 Ma; Figure 6b). The interpreted age for 04K9A is ca. 110 Ma from a half-saddle–shaped spectrum (Figure 6d). Sample 17NR154 did not return a plateau, so the calculated integrated date (84 ±2.75 Ma) is the interpreted age for this sample.

Discussion

$^{40}Ar/^{39}Ar$ Ages in the Purcell Anticlinorium

The significance of each individual cooling age in the PA is difficult to assess due to complex Ar-diffusion profiles of individual analyses and the nonsystematic distribution of ages across the PA (Figure 7). Several processes, individually or collectively, may have influenced the cooling history observed in the age spectra associated with rocks from the PA. The Belt-Purcell Supergroup was affected by three tectonic events prior to deposition of the Neoproterozoic Windermere Supergroup. These include: 1) the ca. 1350 Ma East Kootenay orogeny, which has been recognized as an extensional event (Anderson and Davis, 1995; Doughty and Chamberlain, 1996; McFarlane, 2015); 2) a cryptic, Grenville-age event that resulted in ca. 1100–1000 Ma U-Pb ages in metamorphic zircon, monazite and titanite (Anderson and Davis,1995; Doughty and Chamberlain, 1996; McFarlane, 2015); and 3) the ca. 900–800 Ma Goat River orogeny, which was described by McMechan and Price (1982) as a period of uplift and block faulting. Following the deposition of the Windermere Supergroup, the region was differentially uplifted and eroded, both of which were interpreted to have been caused by the rifting of Rodinia. The Montania (Deiss, 1941; Norris and Price, 1966; Benvenuto and Price, 1979) and Windermere highs (Price, 2000) are two of several topographic 'highs', or regions of high topographic relief, that

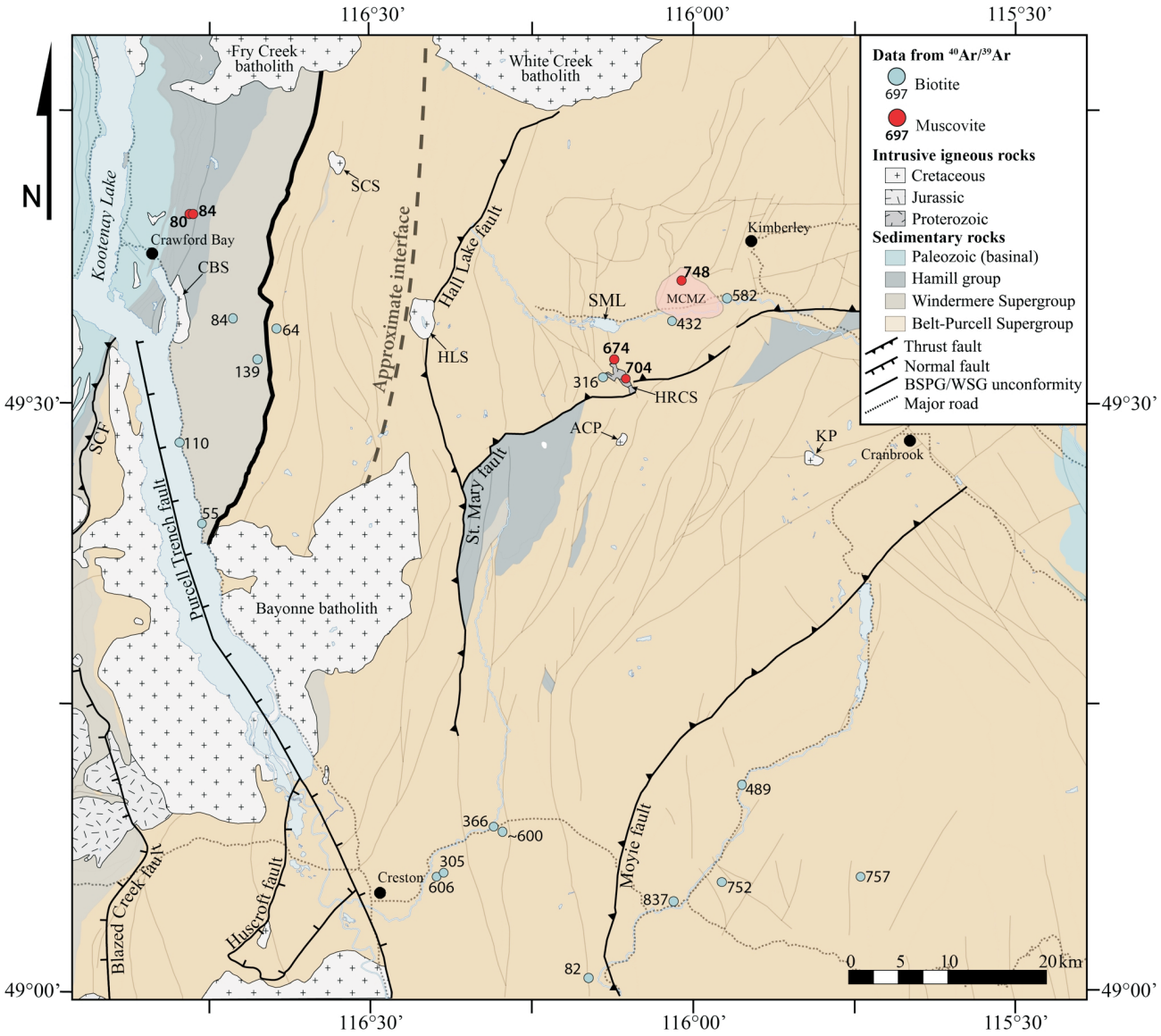

Figure 7. Map of $^{40}Ar/^{39}Ar$ mica cooling ages (reported in Ma) from the study area. Abbreviations: ACP, Angus Creek stock; BPSG, Belt-Purcell Supergroup; CBS, Crawford Bay stock; HLS, Hall Lake stock; HRCS, Hellroaring Creek stock; KP, Kiakho stock; MCMZ, Matthew Creek metamorphic zone; RLS, Reade Lake stock; SCF, Seeman Creek fault; SCS, Sawyer Creek stock; SML, St. Mary Lake.

developed during this time. Both regions have been identified either by the presence of a thin cover of Paleozoic strata or by their absence altogether, indicating that these blocks were uplifted and, as a result, not buried by the deposition of sediments at that time. Furthermore, the region may have been affected by possible episodes of partial reheating from sediment loading related to deposition of Windermere and potentially Paleozoic strata, possible partial reheating associated with Cordilleran tectonic thickening in the Mesozoic, and possible partial reheating associated with Mesozoic magmatism. However, the degree to which each process or set of processes influenced the age spectra is difficult to assess.

Of the three samples in which duplicates were analyzed, the ages of ca. 78 and ca. 80 Ma for 17NR168-Ms from the KA are within error of each other. On the other hand, ages for samples 17NR84-Ms and 17NR86 from the PA differ by more than 75 Ma (17NR84-Ms: ca. 674 and ca. 524 Ma; 17NR86: ca. 316 and ca. 240 Ma). Although it is possible that two generations of mica growth are present in sample 17NR84-Ms, there is no simple explanation as to why these aliquots yielded such different ages. Taking into consideration the wide spread of ages across the PA, in conjunction with the fact that samples from the KA yielded much younger, relatively flat reproducible spectra, it seems that the spread in ages across these two samples from the PA indicates that argon retentivity varies greatly in these samples, likely due to some combination of slow cooling and partial reheating. The inconsistent distribution of ages from across the PA is likely a regional-scale reflection of the variable ef-

fects of the different episodes of cooling and/or partial reheating.

The results of this study indicate that argon retention in biotite from rocks in the PA is unpredictable. Cooling ages from the PA range from 837 Ma to 240 Ma, with no systematic pattern of distribution (Figure 7). This observation most likely reflects variable degrees of resetting since the formation of the biotite in the Mesoproterozoic. Monotonically increasing age spectra indicate that some of the grains analyzed were subject to argon loss due to slow cooling. Additionally, sample 17NR14B from a previously undated, small granodioritic intrusive body returned a cooling age of 82 Ma from a monotonically increasing age spectrum that indicated final closure to ^{39}Ar loss at ca. 25 Ma. The interpreted cooling age for this sample overlaps with a population of cooling ages for intrusive rocks of the Bayonne magmatic suite (E. Webster, pers. comm., 2019). Localized domains of heating related to the emplacement of intrusions from the mid- to late-Cretaceous Bayonne magmatic suite may have led to partial reheating or partial resetting of ^{40}Ar/^{39}Ar cooling ages in rocks of the PA adjacent to the intrusions.

^{40}Ar/^{39}Ar Ages in the Kootenay Arc

Across the portion of the field area that is occupied by the KA, the spread in cooling ages spans a much shorter time interval in comparison to the PA (139 to 55 Ma). The spectra for KA samples are defined by relatively flat release patterns, and the ages returned span the interval between regional metamorphism (144–134 Ma; Moynihan, 2012) and final exhumation (90–40 Ma; E. Webster, pers. comm., 2019) in this region.

Contrasts in Cooling Ages between the Purcell Anticlinorium and the Kootenay Arc

Interpretation of the results of this study, indicates that the PA and KA represent two different cooling domains. Interpretation of the geochronology data suggests that the PA appears to involve variable degrees of resetting of originally Mesoproterozoic cooling ages. The Neoproterozoic to latest Paleozoic/earliest Mesozoic cooling ages indicate that this region was never buried sufficiently, either through Neoproterozoic or Paleozoic sedimentation or Mesozoic Cordilleran tectonic thickening (folding and faulting) associated with the development of the PA, to uniformly exceed temperatures of approximately 300–400°C (closure temperature of argon in biotite and muscovite). For an average geothermal gradient of 30°C/km, this temperature corresponds to a depth of approximately 10–13 km. Conversely, cooling ages for the KA indicate that this portion of the study area was affected by Mesozoic Cordilleran tectonothermal processes between 139 and 55 Ma. In combination with the identification of the structural and metamorphic interface between the KA and PA, the implication is that an important thermotectonic interface between the KA and PA existed at the time of Cordilleran tectonism. The PA, comprising a thick Mesoproterozoic stratigraphic package of turbidites and Moyie Sill, appears to have acted as a rigid backstop or 'buttress', perhaps to the east of a deep-crustal ramp, against which the elongate domain of thickening and Barrovian metamorphism in the KA was localized.

Conclusions

Deformation and metamorphism in the PA was widespread during the Mesoproterozoic and resulted in low-grade metamorphism and the development of an S_1 cleavage. The KA, on the other hand, was polydeformed and polymetamorphosed during the Mesozoic. Within the study area, the most conspicuous phases of Kootenay Arc–type deformation are D_2, which resulted in a primary foliation (S_2), and deformation (D_3), which led to the development of upright folds, a crenulation cleavage, and regional-scale thrusting and folding of the PA. Evidence of structural modification and metamorphic mineral growth related to the D_2M_2 event is restricted to the northwestern portion of the field area, and dies out roughly 15 km east of the unconformity between the Windermere and Belt-Purcell supergroups. East of this interface, the observed deformation and metamorphism is ascribed to Mesoproterozoic processes.

New ^{40}Ar/^{39}Ar results for biotite and muscovite samples from rocks of the PA and eastern KA indicate that the two regions are also characterized by different cooling histories. The ^{40}Ar/^{39}Ar cooling ages for the PA span the interval from the Neoproterozoic to the latest Paleozoic/earliest Mesozoic (837–240 Ma). The nonsystematic distribution of ages across the PA indicates that this region was never deeply buried since the Mesoproterozoic and most likely experienced a multifaceted history of tectonothermal modification, including several episodes of uplift and erosion, sediment loading, crustal thickening and magmatism. Cooling ages for rocks of the KA, on the other hand, indicate that the region was affected by Cordilleran thickening, metamorphism and exhumation between 139 and 55 Ma. This contrast suggests that the PA may have acted as a relatively rigid buttress, against which the rocks of the KA were thickened and metamorphosed in the Mesozoic.

Acknowledgments

First and foremost, the authors would like to thank Geoscience BC for their support of this study. This work was funded by a Geoscience BC grant to D. Pattison and N. Rioseco, and a Natural Sciences and Engineering Research Council of Canada Discovery Grant to D. Pattison. They would also like to thank C. Padget, J. Forshaw and M. Lazzarotto of their insightful reviews of this manuscript.

References

Anderson, H.E. and Davis, D.W. (1995): U-Pb geochronology of the Moyie sills, Purcell Supergroup, southeastern British Columbia: implications for the Mesoproterozoic geological history of the Purcell (Belt) basin; Canadian Journal of Earth Sciences, v. 32, p. 1180–1193, URL <https://pubs.geoscienceworld.org/cjes/article-abstract/32/8/1180/52667> [November 2019].

Benvenuto, G.L. and Price, R.A. (1979): Structural evolution of the Hosmer thrust sheet, southeastern British Columbia; Bulletin of Canadian Petroleum Geology, v. 27, p. 360–394.

Best, M., Christiansen, E.H., Deino, A.L., Gromme, C.S. and Tingey, D.G. (1995): Correlation and emplacement of a large, zoned, discontinuously exposed ash flow sheet; the $^{40}Ar/^{39}Ar$ chronology, paleomagnetism, and petrology of the Pahranagat Formation, Nevada; Journal of Geophysical Research: Solid Earth, v. 100, p. 24 593–24 609.

Bishop, D.T. (1973): Petrology and geochemistry of the Purcell sills in Boundary country, Idaho and adjacent areas; *in* Proceedings of the Belt Symposium, Volume 2, D.T. Bishop (ed.), Idaho Bureau of Mines and Geology–Idaho University Department of Geology, Moscow, Idaho, Special Publication, p. 15–66.

Dalrymple, B.G. and Lanphere, M.A. (1974): $^{40}Ar/^{39}Ar$ age spectra of some undisturbed terrestrial samples; Geochimica et Cosmochimica Acta, v. 38, p. 715–738.

Dazé, A., Lee, J.K.W. and Villeneuve, M. (2003): An intercalibration study of the Fish Canyon sanidine and biotite $^{40}Ar/^{39}Ar$ standards and some comments on the age of the Fish Canyon Tuff; Chemical Geology, v. 199, p. 111–127.

Deino, A.L. (2013): Users' manual for Mass Spec v7.961; Berkeley Geochronology Center, Berkeley, California, Special Publication 1a, 132 p.

Deiss, C. (1941): Cambrian geology and sedimentation in the central Cordilleran region; Bulletin of the Geological Society of America, v. 52, p. 1085–1116, URL <https://pubs.geoscienceworld.org/gsa/gsabulletin/article-pdf/52/7/1085/3416174/BUL52_7-1085.pdf> [August 2019].

DePaoli, G.R. and Pattison, D.R.M. (1995): Constraints on temperature-pressure conditions and fluid composition during metamorphism of the Sullivan orebody, Kimberley, British Columbia, from silicate-carbonate equilibria; Canadian Journal of Earth Sciences, v. 32, p. 1937–1949, URL <https://doi.org/10.1139/e95-148> [September 2019].

Devlin, W.J. and Bond, G.C. (1988): The initiation of the early Paleozoic Cordilleran miogeocline: evidence from the uppermost Proterozoic–Lower Cambrian Hamill Group of southeastern British Columbia; Canadian Journal of Earth Sciences, v. 25, p. 1–19, URL <https://doi.org/10.1139/e88-001> [September 2019].

Devlin, W.J., Brueckner, H.K. and Bond, G.C. (1988): New isotopic data and a preliminary age for volcanics near the base of the Windermere Supergroup, northeastern Washington, USA; Canadian Journal of Earth Sciences, v. 25, p. 1906–1911, URL <http://doi.org/10.1139/e88-179> [August 2019].

Doughty, P.T. and Chamberlain, K.R. (1996): Salmon River Arch revisited: new evidence for 1370 Ma rifting near the end of deposition in the Middle Proterozoic Belt basin; Canadian Journal of Earth Sciences, v. 33, p. 1037–1052, URL <https://doi.org/10.1139/e96-079> [October 2019].

Evans, K.V., Aleinikoff, J.N., Obradovich, J.D. and Fanning, C.M. (2000): SHRIMP U-Pb geochronology of volcanic rocks, Belt Supergroup, western Montana: evidence for rapid deposition of sedimentary strata; Canadian Journal of Earth Sciences, v. 37, p. 1287–1300, URL <https://doi.org/10.1139/e00-036> [October 2019].

Fyles, J.T. (1964): Geology of the Duncan Lake area, Lardeau District, British Columbia; BC Ministry of Energy, Mines and Petroleum Resources, BC Geological Survey, Bulletin 49, 87 p., URL <http://cmscontent.nrs.gov.bc.ca/geoscience/PublicationCatalogue/Bulletin/BCGS_B049.pdf> [June 2019].

Ghosh, D.K. (1995): U-Pb geochronology of Jurassic to early Tertiary granitic intrusives from the Nelson–Castlegar area, southeastern British Columbia, Canada; Canadian Journal of Earth Sciences, v. 32, p. 1668–1680, URL <https://doi.org/10.1139/e95-132> [October 2019].

Höy, T. (1989): The age, chemistry, and tectonic setting of the Middle Proterozoic Moyie sills, Purcell Supergroup, southeastern British Columbia; Canadian Journal of Earth Sciences, v. 26, p. 2305–2317, URL <https://doi.org/10.1139/e89-196> [June 2019].

Kuiper, K.F., Deino, A., Hilgen, F.J., Krijgsman, W., Renne, P.R. and Wijbrans, J.R. (2008): Synchronizing rock clocks of Earth history; Science, v. 320, p. 500–504, URL <https://doi.org/10.1126/science.1154339> [October 2019].

Lanphere, M.A. and Dalrymple, B.G. (1976): Identification of excess ^{40}Ar by the $^{40}Ar/^{39}Ar$ age spectrum technique; Earth and Planetary Science Letters v. 32, p. 141–148, URL <https://doi.org/10.1016/0012-821X(76)90052-2> [August 2019].

Larson, K.P., Camacho, A., Cottle, J.M., Coutand, I., Buckingham, H.M., Ambrose, T.K. and Rai, S.M. (2017): Cooling, exhumation, and kinematics of the Kanchenjunga Himal, far east Nepal; Tectonics, v. 36, p. 1037–1052, URL <https://doi.org/10.1002/2017TC004496> [November 2019].

Lee, J.K.W., Onstott, T.C., Cashman, K.V., Cumbest, R.J. and Johnson, D. (1991): Incremental heating of hornblende in vacuo: implications for $^{40}Ar/^{39}Ar$ geochronology and the interpretation of thermal histories; Geology, v. 19, p. 872–876, URL <https://pubs.geoscienceworld.org/gsa/geology/article-pdf/19/9/872/3512548/i0091-7613-19-9-872.pdf> [October 2019].

Leech, G.B. (1962): Metamorphism and granitic intrusions of Precambrian age in southeast British Columbia; Geological Survey of Canada, Paper 62-13, 11 p., URL <https://doi.org/10.4095/101124> [November 2019].

Logan, J.M. (2001): Prospective areas for intrusion-related gold-quartz veins in southern British Columbia; *in* Geological Fieldwork 2000, BC Ministry of Energy, Mines and Petroleum Resources, BC Geological Survey, Paper 2001-1, p. 231–252.

Ludwig, K.R. (2008): User's manual for ISOPLOT 3.60: a geochronological toolkit for Microsoft Excel; Berkeley Geochronology Center, Special Publication 4, 54 p.

Lund, K., Aleinikoff, J.N., Evans, K. V. and Fanning, C.M. (2003): SHRIMP U-Pb geochronology of Neoproterozoic Windermere Supergroup, central Idaho: implications for rifting of western Laurentia and synchroneity of Sturtian glacial deposits; Bulletin of the Geological Society of America, v. 115, p. 349–372, URL <https://doi.org/10.1130/

0016-7606(2003)115<0349:SUPGON>2.0.CO;2> [June 2019].

McDougall, I. and Harrison, T.M. (1999): Geochronology and Thermochronology by the $^{40}Ar/^{39}Ar$ Method (2nd edition); Oxford University Press, New York, New York, 269 p.

McFarlane, C.R.M. (2015): A geochronological framework for sedimentation and Mesoproterozoic tectono-magmatic activity in lower Belt-Purcell rocks exposed west of Kimberley, British Columbia; Canadian Journal of Earth Sciences, v. 52, p. 444–465, URL <https://doi.org/10.1139/cjes-2014-0215> [October 2019].

McMechan, M.E. and Price, R.A. (1982): Superimposed low-grade metamorphism in the Mount Fisher area, southeastern British Columbia – implications for the East Kootenay orogeny; Canadian Journal of Earth Sciences, v. 19, p. 476–489, URL <https://doi.org/10.1139/e82-039> [October 2019].

Moynihan, D.P. (2012): Metamorphism and Deformation of the Central Kootenay Arc, southeastern British Columbia; Ph.D. thesis, University of Calgary, 279 p.

Moynihan, D.P. and Pattison, D.R.M. (2013): Barrovian metamorphism in the central Kootenay Arc, British Columbia: petrology and isograd geometry; Canadian Journal of Earth Sciences, v. 50, p. 769–794, URL <https://doi.org/10.1139/cjes-2012-0083> [October 2019].

Norris, D.K. and Price, R.A. (1966): Middle Cambrian lithostratigraphy of southeastern Canadian Cordillera; Bulletin of Canadian Petroleum Geology, v. 14, p. 385–404.

Pattison, D.R.M. and Seitz, J.D. (2012): Stabilization of garnet in metamorphosed altered turbidites near the St. Eugene lead-zinc deposit, southeastern British Columbia: equilibrium and kinetic controls; Lithos, v. 134–135, p. 221–235, URL <https://doi.org/10.1016/j.lithos.2011.12.007> [October 2019].

Price, R.A. (1984): Tectonic evolution of the Purcell (Belt) rocks of the southeastern Canadian Cordillera and adjacent parts of the United States; *in* The Belt, W. Hobbs (ed.), Belt Symposium II 1983, Montana Bureau of Mines and Geology, abstracts and summaries, Special Publication 90, p. 47–48.

Price, R.A. (2000): The southern Canadian Rockies: evolution of a foreland thrust and fold belt; GeoCanada 2000, Calgary, May 29–June 2, 2000, Field Trip Guidebook no. 13, 246 p., URL <https://doi.org/10.13140/2.1.2910.2887> [September 2019].

Renne, P.R. and Norman, E.B. (2001): Determination of the half-life of ^{37}Ar by mass spectrometry; Physical Review C, v. 63, 3 p., URL <https://doi.org/10.1103/PhysRevC.63.047302> [August 2019].

Renne, P.R., Swisher, C.C., Deino, A.L., Karner, D.B., Owens, T.L. and DePaolo, D.J. (1998): Intercalibration of standards, absolute ages and uncertainties in $^{40}Ar/^{39}Ar$ dating; Chemical Geology, v. 145, p. 117–152, URL <https://doi.org/10.1016/S0009-2541(97)00159-9> [August 2019].

Rioseco, N.A. and Pattison, D.R.M. (2018): Preliminary investigations of the metamorphic and thermochronological interface between the Purcell Anticlinorium and the Kootenay Arc, southeastern British Columbia (NTS 082F, G); *in* Geoscience BC Summary of Activities 2017: Minerals and Mining, Geoscience BC, Report 2018-01, p. 47–56, URL <http://www.geosciencebc.com/i/pdf/SummaryofActivities2017/MM/SoA2017_MM_Rioseco.pdf> [November 2019].

Rioseco, N.A., Pattison, D.R.M. and Ashton, R.E. (2019): The Relationship between Deformation and Metamorphism in the Interface between the Purcell Anticlinorium and the Kootenay Arc, southeastern British Columbia (NTS 082F, G); *in* Geoscience BC Summary of Activities 2018: Minerals and Mining, Geoscience BC, Report 2019-01, p. 1–14, URL <http://cdn.geosciencebc.com/pdf/SummaryofActivities2018/MM/2017-009_SoA2018_MM_Rioseco.pdf> [November 2019].

Roddick, J.C. (1983): High precision intercalibration of ^{40}Ar-^{39}Ar standards; Geochimica et Cosmochimica Acta, v. 47, p. 887–898, URL <https://doi.org/10.1016/0016-7037(83)90154-0> [August 2019].

Ross, J. (2017): Pychron software, URL <https://doi.org/10.5281/zenodo.9884> [November 2019].

Sears, J.W., Chamberlain, K.R. and Buckley, S.N. (1998): Structural and U-Pb geochronological evidence for 1.47 Ga rifting in the Belt basin, western Montana; Canadian Journal of Earth Sciences, v. 35, p. 467–475, URL <https://doi.org/10.1139/e97-121> [September 2019].

Spell, T.L. and McDougall, I. (2003): Characterization and calibration of $^{40}Ar/^{39}Ar$ dating standards; Chemical Geology, v. 198, p. 189–211, URL <https://doi.org/10.1016/S0009-2541(03)00005-6> [August 2019].

Steiger, R.H. and Jager, E. (1977): Subcommission on geochronology: convention on the use of decay constants in geo- and cosmochronology; Earth and Planetary Science Letters, v. 36, p. 359–362.

Warren, M.J. (1997): Crustal extension and subsequent crustal thickening along the Cordilleran rifted margin of ancestral North America, western Purcell Mountains, southeastern British Columbia; Ph.D. thesis, Queen's University, 360 p.

Webster, E.R. and Pattison, D.R.M. (2018): Spatially overlapping episodes of deformation, metamorphism, and magmatism in the southern Omineca Belt, southeastern British Columbia; Canadian Journal of Earth Sciences, v. 55, p. 84–110, URL <https://doi.org/10.1139/cjes-2017-0036> [October 2019].

Webster, E.R., Pattison, D.R.M. and DuFrane, S.A. (2017): Geochronological constraints on magmatism and polyphase deformation and metamorphism in the southern Omineca; Canadian Journal of Earth Sciences, v. 54, p. 529–549, URL <https://doi.org/10.1139/cjes-2016-0126> [August 2019].

Development of a Database of Rare-Earth Element Occurrences and Characteristics for the East Kootenay Coalfields of Southeastern British Columbia (NTS 082G/10, 15): Proposed Work

V.K. Kuppusamy, NBK Institute of Mining Engineering, The University of British Columbia, Vancouver, British Columbia, vinothkumar@alumni.ubc.ca

M.E. Holuszko, NBK Institute of Mining Engineering, The University of British Columbia, Vancouver, British Columbia

Kuppusamy, V.K. and Holuszko, M.E. (2020): Development of a database of rare-earth element occurrences and characteristics for the East Kootenay coalfields of southeastern British Columbia (NTS 082G/10, 15): proposed work; *in* Geoscience BC Summary of Activities 2019: Minerals, Geoscience BC, Report 2020-01, p. 51–54.

Introduction

Rare-earth elements (REE) are a group of 17 elements in the periodic table that include 15 lanthanides and two chemically similar transition metals—scandium and yttrium. Using their atomic number, REE are classified as heavy or light, with elements from Tb to Lu and Y belonging to the former group, and La to Gd and Sc belonging to the latter group (Moldoveanu and Papangelakis, 2013; Zhang et al., 2015). With the emergence of new clean energy and defence-related technologies, consumption of REE has increased rapidly (Tse, 2011). For example, it is projected that the demand for dysprosium will increase by as much as 2600% by 2025 (Standing Committee on Natural Resources, 2014). In addition to increased demand, it is expected that traditional rare earth ore deposits will be exhausted in the near future (Seredin and Dai, 2012). Based on this projected increased demand and dwindling supply, the United States (U.S.) and the European Union have classified REE as critical elements, due to their importance in clean energy and defence applications (U.S. Department of Energy, 2010; European Commission, 2017). The National Energy Technology Laboratory (NETL) in the United States has conducted a prospective analysis of coal deposits as a source of REE using the coal database of the U.S. Geological Survey (USGS), which contains concentrations of rare-earth elements from coalfields across the United States (Bryan et al., 2015). The NETL has launched the 'Feasibility of Recovering Rare Earth Elements' program to demonstrate the technological and economic (techno-economic) feasibility of developing domestic technologies for separation of REE from coal and/or its byproducts. The study uses samples that contain a minimum of 300 ppm total REE and attempts to concentrate the REE to a level greater than or equal to 2% (by weight) in processed streams (U.S. Department of Energy, 2016). The program will focus on areas of research such as resource sampling and characterization, separation technology development, REE sensor development, process and systems modelling, and techno-economic analyses (U.S. Department of Energy, 2016).

The presence of REE has been documented in some Canadian coal deposits, especially in British Columbia (BC) coalfields (Goodarzi, 1988; Birk and White, 1991; Goodarzi et al., 2009); however, there is no proper quantification of their concentration, nor is there characterization or extraction analysis currently available for coal deposits in BC, or for coal deposits in other parts of Canada. Therefore, the first objective of this study is to develop a database of REE occurrences in the East Kootenay coalfields of southeastern BC (Figure 1), using samples collected in the field, and to identify the potential best coal sources of REE in the area. Using the data collected in the first phase, Phase 2 of the study will explore the possibility of extracting the REE from these sources. Some of the initial results of the study were reported previously (Kumar et al., 2018; Kuppusamy and Holuszko, 2019).

Background

U.S. Geological Survey's COALQUAL Database

During the 1970s energy crisis, the USGS developed the National Coal Resources Data System (NCRDS), which is a comprehensive database of coal resources in the United States (Finkelman et al., 1994). The USCHEM (United States geochemical database) is an interactive digital version of the NCRDS that contains information for more than 13 000 samples from major coal basins in the United States (Palmer et al., 2015). The COALQUAL database, which is a subset of 7430 samples from the USCHEM database (Bragg et al., 1994), was published in 1994. For each sample in the COALQUAL database, 136 parameters were collected, including coal type, proximate analysis data, ulti-

This publication is also available, free of charge, as colour digital files in Adobe Acrobat® PDF format from the Geoscience BC website: http://www.geosciencebc.com/updates/summary-of-activities/.

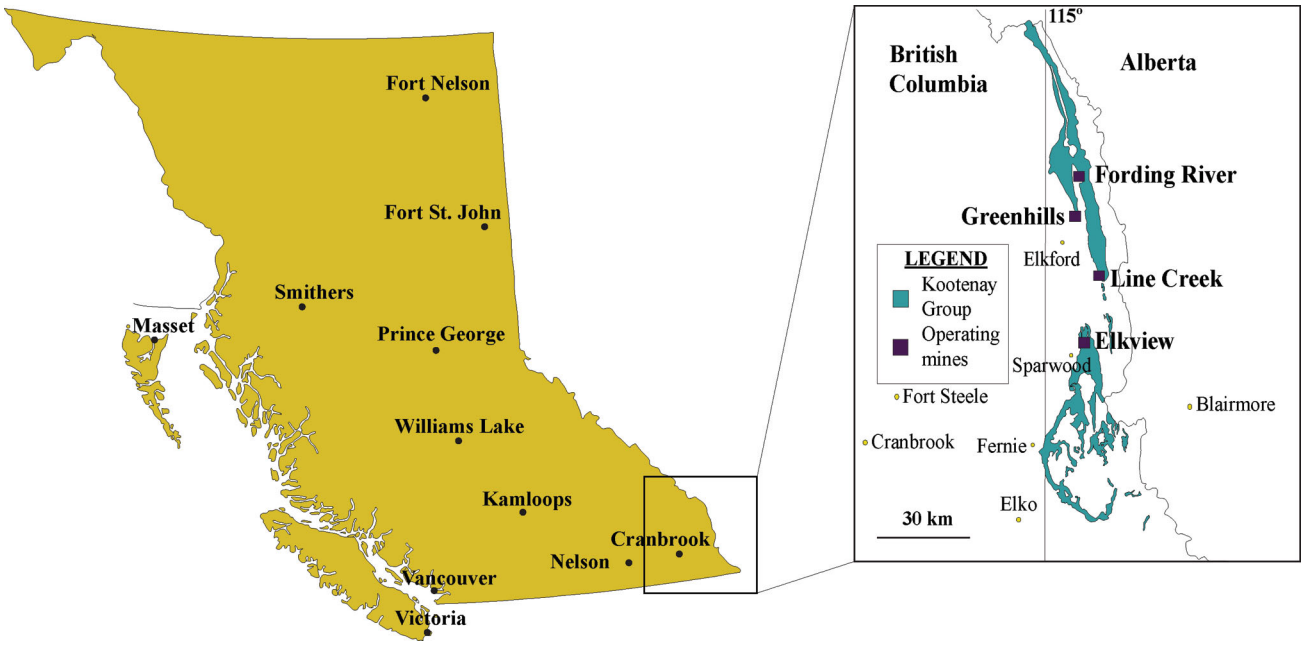

Figure 1. Location of East Kootenay coalfields and operating coal mines in southeastern British Columbia (adapted from BC Geological Survey, 2019).

mate analysis data, and major-, minor- and trace-elements analysis data (Finkelman et al., 1994). Figure 2 is an example of a COALQUAL sample detail page.

In 2015, an updated version (3.0) of the COALQUAL database was published, with 7657 samples (Palmer et al., 2015). Using the original database as a guideline, further investigations had been carried out to characterize and physically enrich the data on REE from coal-related feedstocks (e.g., produced coals, coal waste, coal ash from power plants) in the United States (Akdogan and Ghosh, 2014; Honaker et al., 2015; Miskovic, 2015; Soundarrajan et al., 2015).

Project Description

The purpose of this investigation is to assess BC coal deposits as possible sources of REE for extraction. During the first phase of the project, a database of REE distribution in the East Kootenay coalfields of southeastern BC will be created, one similar to the USGS COALQUAL database, but more simplified in terms of number of parameters collected and focusing on characteristics of REE in the study area. To develop the database, various samples of coal will be collected from different mines in the study area and analyzed for their REE concentration using inductively coupled plasma–mass spectrometry.

Further, stratigraphic variation in REE concentration has been reported in some United States coal deposits (Hower et al., 1999; Rozelle et al., 2016). Figure 3 shows the stratigraphic variation in REE concentration in samples from the West Kentucky No. 13 coal seam. To capture possible similar stratigraphic variations in REE content in the study area, for each coal seam sample collected, the associated roof, floor and partings waste rock samples will also be collected and analyzed for their REE concentration. Understanding these variations in REE concentration is important, since the mined coal is generally processed to remove undesirable impurities, such as deleterious minerals and sulphur, to meet market quality requirements. During coal processing, REE tend to concentrate in clean coal or waste tailings, depending on the nature of the REE association in the feed (Kumar et al., 2018; Kuppusamy and Holuszko, 2019); REE in coal can occur in several different modes, such as ion-adsorbed minerals, aluminosilicate minerals, accessory minerals, authigenic minerals, submicron minerals and in organic association (Hower et al., 1999, 2018; Dai et al., 2002; Seredin and Finkelman, 2008; Seredin and Dai, 2012; Zhang et al., 2015). To identify the nature of the REE mineral carriers in the study area, a select few samples will be characterized using techniques such as X-ray diffraction analysis, scanning electron microscope–energy dispersive spectrometry, and electron probe microanalyzer.

This first phase of work, which consists of database development and preliminary characterization of REE in the samples collected, is currently being carried out and is anticipated to be completed by March or April 2020. Based on the results, the second phase of the project will focus on advanced characterization of selected samples, and lab-scale extraction of the REE in the coal-related feedstocks. This will enable an assessment of the possibility of using BC coal deposits as potential resources for REE extraction.

USGS science for a changing world — COAL QUAL Database

Sample Detail for W218790

View Definitions of Qualifiers and Parameters

Sample Description		Proximate & Ultimate		Oxide		Trace Element	
Sample ID	W218790	Sample ID	W218790	Sample ID	W218790	Sample ID	W218790
State	Kentucky	Moisture	3.53	Remnant Moisture	1.23	GS Ash Dry	4.15
County	CLAY	Moisture Q		Remnant Moisture Q	r	GS Ash Dry Q	
Latitude	37.2203	Volatile Matter	39.99	GSAsh	4.1	Si	9550
Longitude	-83.8561	Volatile Matter Q		GSAsh Q		Si Q	
Province	EASTERN	Fixed Carbon	52.34	SiO_2	49.2	Al	7180
Region	CENTRAL APPALACHIAN	Fixed Carbon Q		SiO_2 Q	o	Al Q	
Field		Standard Ash	4.14	Al_2O_3	32.7	Ca	490
District	SOUTHWESTERN	Standard Ash Q		Al_2O_3 Q	o	Ca Q	
Formation	BREATHITT	Proximate Validation	Acceptable	CaO	1.65	Mg	191
Group		Hydrogen	5.38	CaO Q	o	Mg Q	
Bed	MANCHESTER	Hydrogen Q		MgO	0.764	Na	286
Member		Carbon	77.2	MgO Q	o	Na Q	
Coal Zone		Carbon Q		MnO	0.0057	K	436
Depth (in)	0	Nitrogen	1.8	MnO Q		K Q	
Thickness (in)	9.4	Nitrogen Q		Na_2O	0.932	Fe	951
System	Pennsylvanian	Oxygen	7.39	Na_2O Q	o	Fe Q	
Series/Epoch		Oxygen Q		K_2O	1.26	Ti	370
Literature		Sulfur	0.56	K_2O Q	o	Ti Q	
Comments		Sulfur Q		Fe_2O_3	3.27	TS	
Map	MANCHESTER (7.5')	Ultimate Validation	Excellent	Fe_2O_3 Q	o	TS Q	B
Collector	KYGS-CURRENS J C	Btu	13915	TiO_2	1.49	Ag	0.0145
Mine/Power Plant	SURFACE MINE	Btu Q		TiO_2 Q	o	Ag Q	
Drill Core No		Sulfate Sulfur	0.01	P_2O_5		As	0.506
Point Id	KGS 698	Sulfate Sulfur Q		P_2O_5 Q	B	As Q	
Submit Date	12/16/1982	Pyritic Sulfur	0.03	SO_3		Au	0.29
Sample Description	BITUMINOUS COAL	Pyritic Sulfur Q		SO_3 Q	B	Au Q	L
Estimated Rank	BITUMINOUS	Organic Sulfur	0.52	LOI		B	17.4
Apparent Rank	High volatile A bituminous	Organic Sulfur Q				B Q	
Analytical Labs	GT and USGS	Ash Deformation	2800			Ba	15.4
Sample Type	Channel	Ash Deformation Q	G			Ba Q	
Analysis Type	As Received	Ash Softening	2800			Be	2.78
Values Represent	Single sample	Ash Softening Q	G			Be Q	
Township		Ash Fluid	2800			Bi	0.42
Range		Ash Fluid Q	G			Bi Q	L

Figure 2. Example of a 'Sample Detail' page from the U.S. Geological Survey's (USGS) COALQUAL database.

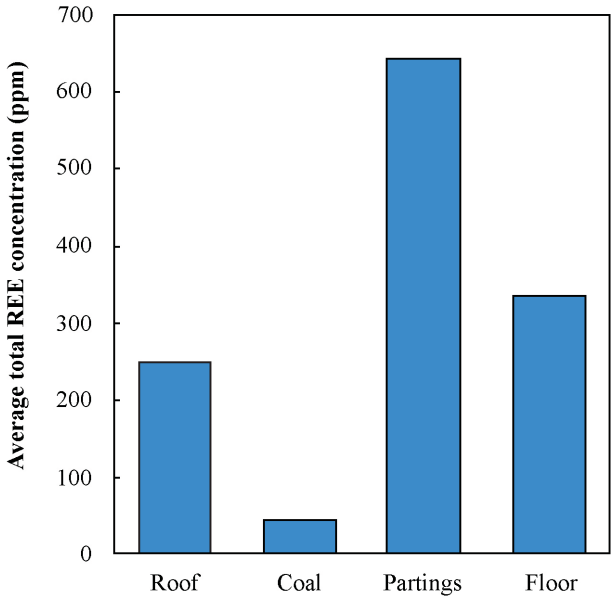

Figure 3. Average rare-earth element (REE) concentration (whole-coal basis, ppm) in roof, coal, partings and floor core samples from the West Kentucky No. 13 seam (data used is from Yang et al., 2019).

Acknowledgments

Financial support for the project from Geoscience BC is greatly appreciated. The authors gratefully acknowledge a scholarship from Geoscience BC in 2017-2018. Sincere gratitude is extended to industrial partner Teck Coal Limited. The authors would also like to thank M. Mastalerz, Indiana University, for her valuable comments and suggestions to improve this manuscript.

References

Akdogan, G. and Ghosh, T. (2014): Identification of REE in some Alaskan coal and ash samples; NETL REE Technical Reports, 27 p., URL <https://edx.netl.doe.gov/dataset/netl-ree-technical-reports/revision_resource/1a79ca45-91e6-e388-f46a-0fc523ae3396> [September 2019].

British Columbia Geological Survey (2019): British Columbia coal industry overview 2018; British Columbia Ministry of Energy, Mines and Petroleum Resources, Information Circular 2019-2, URL <http://cmscontent.nrs.gov.bc.ca/geoscience/PublicationCatalogue/InformationCircular/BCGS_IC2019-02.pdf> [September 2019].

Birk, D. and White, J.C. (1991): Rare earth elements in bituminous coals and underclays of the Sydney Basin, Nova Scotia: Ele-

ment sites, distribution, mineralogy; International Journal of Coal Geology, v. 19, p. 219–251.

Bragg, L.J., Oman, J.K., Tewalt, S.J., Oman, C.L., Rega, N.H., Washington, P.M. and Finkelman, R.B. (1994): U.S. Geological Survey coal quality (COALQUAL) database version 1.3; U.S. Geological Survey, Open-File Report 94-205, URL <https://pubs.er.usgs.gov/publication/ofr94205> [October 2019].

Bryan, R.C., Richers, D., Andersen, H.T. and Gray, T. (2015): Assessment of rare earth elemental contents in select United States coal basins; US National Energy Technology Laboratory, 47 p.

Dai, S., Ren, D. and Li, S. (2002): Occurrence and sequential chemical extraction of rare earth elements in coals and seam roofs; Journal of China University of Mining & Technology, v. 31, no. 5, p. 349–353.

European Commission (2017): Study on review of the list of critical raw materials; British Geological Survey, Bureau de Recherches Géologiques et Minières, Deloitte Sustainability, Directorate-General for Internal Market, Industry, Entrepreneurship and SMEs (European Commission), TNO, 92 p., URL <https://publications.europa.eu/en/publication-detail/-/publication/08fdab5f-9766-11e7-b92d-01aa75ed71a1/language-en> [September, 2017].

Finkelman, R.B., Oman, C.L., Bragg, L.J. and Tewalt, S.J. (1994): The U.S. Geological Survey coal quality data base (COALQUAL); U.S. Geological Survey, Open-File Report 94-177, 46 p., URL <https://pubs.er.usgs.gov/publication/ofr94177> [October 2019].

Goodarzi, F. (1988): Elemental distribution in coal seams at the Fording coal mine, British Columbia, Canada; Chemical Geology, v. 68, no. 1–2, p. 129–154, URL <https://doi.org/10.1016/0009-2541(88)90092-7> [October 2017].

Goodarzi, N.N., Goodarzi, F., Grieve, D.A., Sanei, H. and Gentzis, T. (2009): Geochemistry of coals from the Elk Valley coalfield, British Columbia, Canada; International Journal of Coal Geology, v. 77, p. 246–259.

Honaker, R., Hower, J.C., Eble, C.F., Weisenfluh, J., Groppo, J., Rezaee, M., Bhagavatula, A., Luttrell, G.H., Bratton, R.C., Kiser, M. and Yoon, R.H. (2015): University of Kentucky laboratory and bench scale testing for rare earth elements final report; NETL REE Technical Reports, 537 p., URL <https://edx.netl.doe.gov/dataset/netl-ree-technical-reports/revision_resource/37fea531-580e-665c-388a-4cfc09296bb9> [September 2019].

Hower, J.C., Berti, D., Hochella, M.F., Rimmer, S.M. and Taulbee, D.N. (2018): Submicron-scale mineralogy of lithotypes and the implications for trace element associations: Blue Gem coal, Knox County, Kentucky; International Journal of Coal Geology, v. 192, p. 73–82.

Hower, J.C., Ruppert, L.F. and Eble, C.F. (1999): Lanthanide, yttrium, and zirconium anomalies in the Fire Clay coal bed, Eastern Kentucky; International Journal of Coal Geology, v. 39, no. 1–3, p. 141–153.

Kumar, V., Kumar, A. and Holuszko, M.E. (2018): Occurrence of rare earth elements in selected British Columbian coal deposits and their processing products; *in* Geoscience BC Summary of Activities 2017: Minerals and Mining, Geoscience BC, Report 2018-01, p. 87–100, URL <http://cdn.geosciencebc.com/pdf/SummaryofActivities2017/MM/SoA2017_MM_Kumar.pdf> [February 2018].

Kuppusamy, V.K. and Holuszko, M.E. (2019): Characterization and extraction of rare earth elements from East Kootenay coalfield samples, southeastern British Columbia; *in* Geoscience BC Summary of Activities 2018: Minerals, Geoscience BC, Report 2019-01, p. 33–44, URL <http://cdn.geosciencebc.com/pdf/SummaryofActivities2018/MM/Schol_SoA2018_MM_Kuppusamy.pdf> [October 2019].

Miskovic, S. (2015): University of Utah REE recovery from western coals final report; NETL REE Technical Reports, 85 p., URL <https://edx.netl.doe.gov/dataset/netl-ree-technical-reports/revision_resource/e46fb2ed-fba7-b1bf-db80-56d77edcd5b0> [September 2019].

Moldoveanu, G. and Papangelakis, V. (2013): Recovery of rare earth elements adsorbed on clay minerals: II. leaching with ammonium sulfate; Hydrometallurgy, v. 131, p. 158–166.

Palmer, C.A., Oman, C.L., Park, A.J. and Luppens, J.A. (2015): The U.S. Geological Survey coal quality (COALQUAL) database version 3.0; U.S. Geological Survey, Data Series 975, URL <https://pubs.er.usgs.gov/publication/ds975> [June 2019].

Rozelle, P.L., Khadilkar, A.B., Pulati, N., Soundarrajan, N., Klima, M.S., Mosser, M.M., Miller, C.E. and Pisupati, S.V. (2016): A study on removal of rare earth elements from U.S. coal by-products by ion exchange; Metallurgical and Materials Transactions E, v. 3, no. 1, p. 6–17.

Seredin, V. and Dai, S. (2012): Coal deposits as potential alternative sources for lanthanides and yttrium; International Journal of Coal Geology, v. 94, p. 67–93.

Seredin, V.V. and Finkelman, R.B. (2008): Metalliferous coals: A review of the main genetic and geochemical types; International Journal of Coal Geology, v. 76, no. 4, p. 253–289.

Soundarrajan, N., Pulati, N., Klima, M.S., Ityokumbul, M. and Pisupati, S.V. (2015): Penn State separation of rare earth elements from coal and coal products final report; NETL REE Technical Reports, 70 p., URL <https://edx.netl.doe.gov/dataset/netl-ree-technical-reports/revision_resource/a2c1d4be-eae7-a2a7-a547-850c15db2815> [September 2017].

Standing Committee on Natural Resources (2014): The rare earth elements industry in Canada - summary of evidence; Standing Committee on Natural Resources, 26 p., URL <http://www.parl.gc.caiii> [December 2016].

Tse, P.K. (2011): China's rare-earth industry; U.S. Geological Survey, Open-File Report 2011-1042, p. 11, URL <https://pubs.usgs.gov/of/2011/1042/of2011-1042.pdf> [September 2017].

U.S. Department of Energy (2010): U.S. Department of Energy critical materials strategy, 190 p., URL <https://energy.gov/sites/prod/files/DOE_CMS2011_FINAL_Full.pdf> [September 2017].

U.S. Department of Energy (2016): Rare Earth Elements Program, 19 p., URL <https://www.netl.doe.gov/File Library/Research/Coal/Rare Earth Elements/REE-Project-Portfolio-2016.pdf> [September 2017].

Yang, X., Werner, J. and Honaker, R.Q. (2019): Leaching of rare earth elements from an Illinois basin coal source; Journal of Rare Earths, v. 37, no. 3, p. 312–321.

Zhang, W., Rezaee, M., Bhagavatula, A., Li, Y., Groppo, J. and Honaker, R. (2015): A review of the occurrence and promising recovery methods of rare earth elements from coal and coal by-products; International Journal of Coal Preparation and Utilization, v. 35, p. 295–330.

Mineral-Resource Prediction Using Advanced Data Analytics and Machine Learning of the QUEST-South Stream-Sediment Geochemical Data, Southwestern British Columbia (Parts of NTS 082, 092)

E.C. Grunsky, Department of Earth and Environmental Sciences, University of Waterloo, Waterloo, Ontario, egrunsky@gmail.com

D.C. Arne, Telemark Geosciences, Yackandandah, Victoria, Australia

Grunsky, E.C. and Arne, D.C. (2020): Mineral-resource prediction using advanced data analytics and machine learning of the QUEST-South stream-sediment geochemical data, southwestern British Columbia (parts of NTS 082, 092); *in* Geoscience BC Summary of Activities 2019: Minerals, Geoscience BC, Report 2020-01, p. 55–76.

Introduction

The QUEST-South project area in southern British Columbia (BC) was a focus for geochemical and geophysical research by Geoscience BC in 2009 and 2010 (Figure 1). Regional stream-sediment samples, originally collected under the Regional Geochemical Survey (RGS) program between 1976 and 1979 from the QUEST-South project area, were reanalyzed in 2009. This was done using an aqua-regia digestion followed by a combination of inductively coupled plasma–emission spectrometry (ICP-ES) and inductively coupled plasma–mass spectrometry (ICP-MS; Jackaman, 2010a). These samples were analyzed by ALS Global (North Vancouver, BC) using method ME-MS41L. An infill stream-sediment survey was also undertaken in 2009 and the samples analyzed using similar digestions and instrumental finishes at Eco Tech Laboratories Ltd. (Kamloops, BC; Jackaman, 2010b). The use of two different laboratories for analyses from the QUEST-South project area raises some issues in terms of data quality, as will be discussed in the following section.

The newly acquired stream-sediment data for 9321 samples were interpreted by Arne and Bluemel (2011) using a catchment-analysis approach. Of these samples, 8536 were originally collected between 1976 and 1979 and the locations transcribed from hard copy 1:50 000 scale topographic maps. Global positioning satellite (GPS) receivers were used to locate only the 785 new infill stream-sediment samples. The historical sample locations are known to be inconsistent with the 1:20 000 scale provincial Terrain Resource Information Management Program (TRIM I) hydrology data (Cui, 2010). As a result, considerable effort was expended by Arne and Bluemel (2011) to validate the recorded sample locations using scanned images of the archived topographic maps that had been used in the original sampling programs. Sample locations were adjusted where they were inconsistent with the original survey maps, and each sample location was given a confidence ranking. Catchment polygons for each sample were delineated by the British Columbia Geological Survey (BCGS) for the adjusted sample locations using the approach described by Cui et al. (2009), which involves computing the total drainage area for an individual sample from the nearest downstream stream junction for the adjusted sample location.

The catchment polygons thus obtained were used by Arne and Bluemel (2011) to query the bedrock types of the catchments and to determine the dominant rock type for each catchment area. It has previously been established that the dominant control on regional stream-sediment geochemistry is catchment rock type (Bonham-Carter and Goodfellow, 1986; Bonham-Carter et al., 1987; Carranza and Hale, 1997). Dominant catchment rock types were therefore used to level the geochemical data for the effects of variable background influence on stream-sediment geochemistry. Exploratory data analysis indicated that there were positive correlations between some elements and Fe and/or Mn, suggestive of scavenging of metals by secondary hydroxides. Positive residuals from linear-regression analysis of these metals against Fe were also used to identify areas of anomalous metal concentrations. Additive indices for several common ore-deposit types from the QUEST-South project area were then calculated using residuals and/or levelled Z-scores.

The approach used by Arne and Bluemel (2011), as well as by other previous studies (see references therein), relies on the use of drainage catchments for constraining bedrock type to define background values. Several assumptions are implied by the catchment-analysis approach:

1) The samples are accurately located and thus can be attributed to the correct catchment area.
2) The bedrock geology of the area is well known and accurately represented by the available geological mapping.

This publication is also available, free of charge, as colour digital files in Adobe Acrobat® PDF format from the Geoscience BC website: http://www.geosciencebc.com/updates/summary-of-activities/.

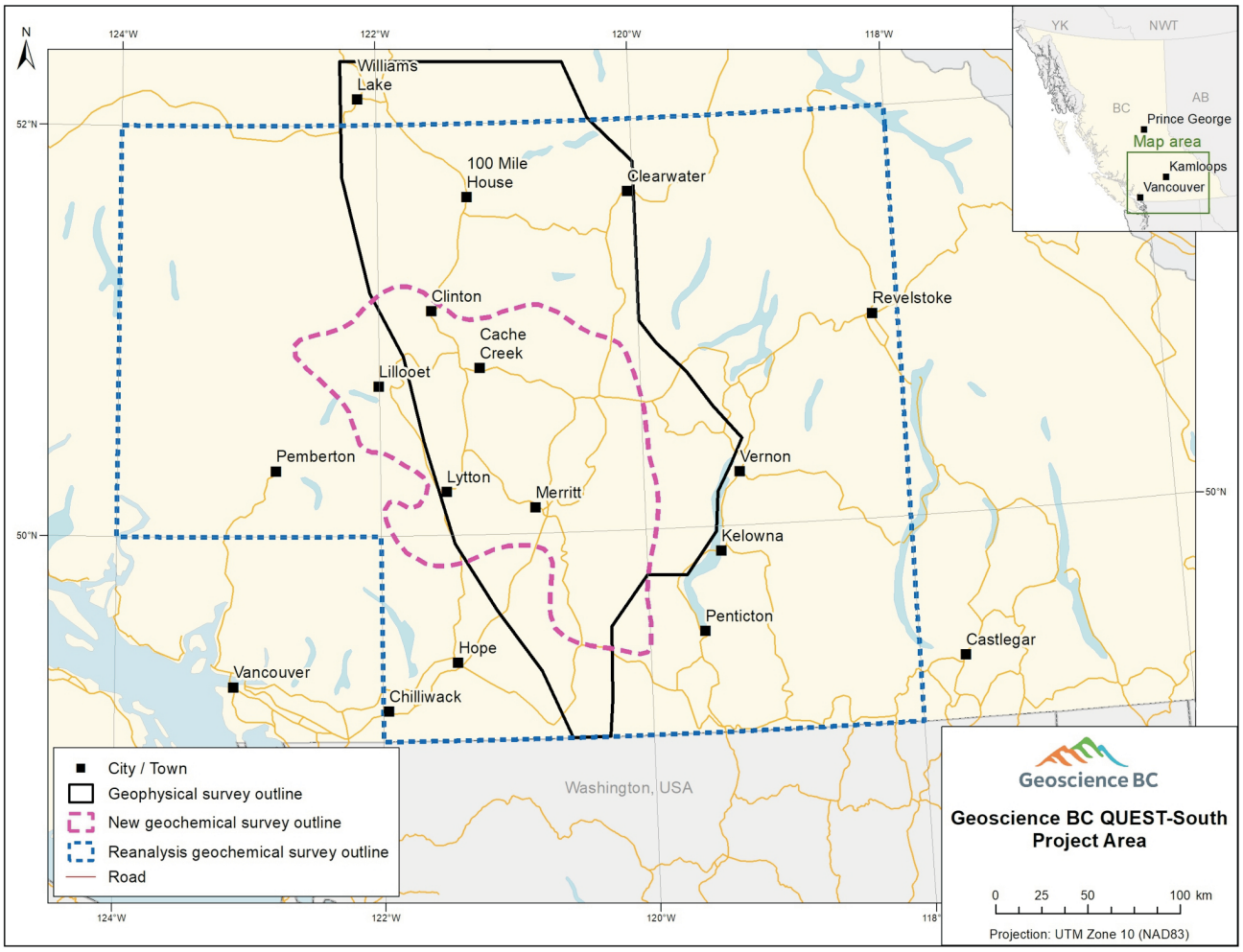

Figure 1. Location of the QUEST-South project area, showing the map areas from which archived stream-sediment samples were obtained (outlined in blue dashes), the area of infill stream-sediment sampling (outlined in pink dashes) and the area of geophysical surveys (outlined in solid black).

3) All areas of the catchment, and thus all rock types, contribute equally to the sediment load of the stream draining past the sample location.
4) The influence of transported materials such as till or glaciofluvial sediments is minimal.

Grunsky et al. (2010), de Caritat and Grunsky (2013), and Grunsky et al. (2014) demonstrated that the lithological controls on the geochemistry of regional drainage-sediment samples can be extracted from the data, particularly using principal-component analysis. Arne et al. (2018a) used regression analysis of key pathfinder or target-commodity elements against those principal components in which they were strongly represented to calculate residual values for those elements that were elevated above what would be expected, given lithological and other geochemical controls. Given that geological processes, including responses related to exposed mineralization, are inherent in the data (e.g., de Caritat et al., 2016), Harris et al. (2015) and Arne et al. (2018b) demonstrated that the use of machine-learning algorithms could provide useful predictions of where mineralization is likely to be found using publicly available regional geochemical data. These predictions can then be applied to catchment polygons in the case of stream-sediment surveys to generate predictive maps for mineral exploration. This project extends that work and applies it to the QUEST-South project area.

Data Quality

The analyses from standard reference materials (SRMs) submitted with the samples during the original survey and analyses were not provided in Jackaman (2010a, b). Therefore, only a perfunctory review of data accuracy could be made by Arne and Bluemel (2011) using the available field duplicates and blind (pulp) duplicate data. They did note, however, that there was poor correlation (Spearman Rank correlation coefficient of 0.44) between ICP-MS Au and the historical instrumental neutron activation (INAA) data for Au. Digestions for the ICP-MS data involved 0.5 g of –177 µm sediment, whereas the historical INAA samples averaged 23 g. The INAA Au data were preferred for data

interpretation, given the larger sample mass. Despite this preference, the precision of the INAA Au analyses is considered to be poor.

Reanalyzed SRM data from the original survey and data from the SRMs submitted with the infill samples were made available by Jackaman (2018), including the Regional Geochemical Survey (RGS) SRMs Red Dog (84) and SQ (22), and a small number of samples of certified reference material (CRM) Canmet STSD-2 (7). A larger number of Geological Survey of Canada (GSC) SRMs were also reanalyzed from the original surveys but were generally not available for inclusion with the infill survey samples to provide overlapping SRM data sets for comparison.

A comparison of SRM data for the Red Dog and SQ SRMs for selected elements indicates systematic relative biases for several elements of significance for mineral deposits in the QUEST-South region (Figure 2), including As, Ag, Mo and Sb. The elements Ba and La also show significant relative biases. Those elements with significant biases (i.e., ±5%) have been adjusted using the RGS Red Dog median data, so that the data remain in the unit of measurement to allow a centred-log transformation of the data. This correction was validated on the stream-sediment data from samples located in the area of infill sampling and was found to make only a slight difference.

A comparison was made of the three analytical methods used on the stream-sediment samples: ICP-MS/ES, INAA and atomic absorption (AA). The AA results were not considered further for this study due to the limited number of elements analyzed, which were already present in the reanalyzed ICP results and have higher detection limits for AA compared to the more recent ICP-MS results. The ICP data are based on an aqua-regia digestion, which is a partial extraction for many elements. The INAA results in a 'complete' analysis. A comparison of the detection limits and ranges of the analytical results generated by the two methods indicates that, although INAA data reflect a 'complete' composition, there are fewer elements available and the detection limits for some of the elements are higher than for the same elements analyzed by ICP-MS. Previous studies have shown that the material dissolved with aqua regia provides a multi-element signature that reflects silicate-bearing assemblages, most likely through partial dissolution of the silicates (Grunsky et al., 2014). The decision was made to use only the ICP-MS data in this study for the sake of consistency. Data from the following 35 elements were used: Au, Ag, Al, As, Ba, Bi, Ca, Cd, Co, Cr, Cu, Fe, Ga, Hg, K, La, Mg, Mn, Mo, Na, Ni, P, Pb, S, Sb, Sc, Se, Sr, Th, Ti, Tl, U, V, W and Zn. In total, data from 8545 stream-sediment sites were used in the study.

Methods

Data Screening and the Compositional Nature of Geochemical Data

Geochemical data require quality-assurance and quality-control (QA-QC) screening prior to the application of statistical methods and subsequent interpretation. A sequence of data QA-QC strategies (Grunsky, 2010) was applied to the data. All data processing was carried out using the R programming and statistical environment (R Core Team, 2019), and geospatial rendering was carried out using the Quantum Geographic Information System (QGIS Development Team, 2019). Of the 9321 geochemical analyses assembled, 496 were blind (pulp) duplicates and 280 were field duplicates. The duplicate analyses were removed to provide 8545 analyses for evaluation.

Major-element concentrations, reported as percentages, were converted to parts per million (ppm). Geochemical data reported at less than the lower limit of detection (censored data) can bias the estimates of mean and variance. Therefore, a replacement value that more accurately reflects an estimate of the true mean is preferred. Replacement values for censored geochemical data can be determined using several methods (Grunsky, 2010; Hron et al., 2010; Palarea-Albaladejo et al., 2014). In this study, the lrEM function from the zCompositions package (Palarea-Albaladejo et al., 2014) was used to estimate replacement values. Values reported at greater than the upper limit of detection were not addressed in this study. The 'maximum' value reported by the laboratory was used.

Integration of Geology and MINFILE Attributes with the Stream-Sediment Geochemistry

The QGIS software was used for the integration of various data sources and the geospatial rendering of the results. The projection used to manage and display the data is based on the North American Datum of 1983 (NAD 83) and the Universal Transverse Mercator (UTM) Zone 10.

Digital files of the bedrock geology (Cui et al., 2017), regional terranes (Nelson et al., 2013) and MINFILE data were obtained from the website of the BC Geological Survey (https://www2.gov.bc.ca/gov/content/industry/mineral-exploration-mining/british-columbia-geological-survey) in May 2019. The focus of this study was on metallic mineral deposits. An initial selection from the MINFILE database yielded 4877 records. MINFILE data that were classified as industrial minerals were dropped from further consideration, resulting in a total of 4108 records. Polymetallic Ag-Pb-Zn veins (deposit type I05) are by far the most common mineral occurrence in the QUEST-South area (31.5% of all MINFILE occurrences) but have geo-

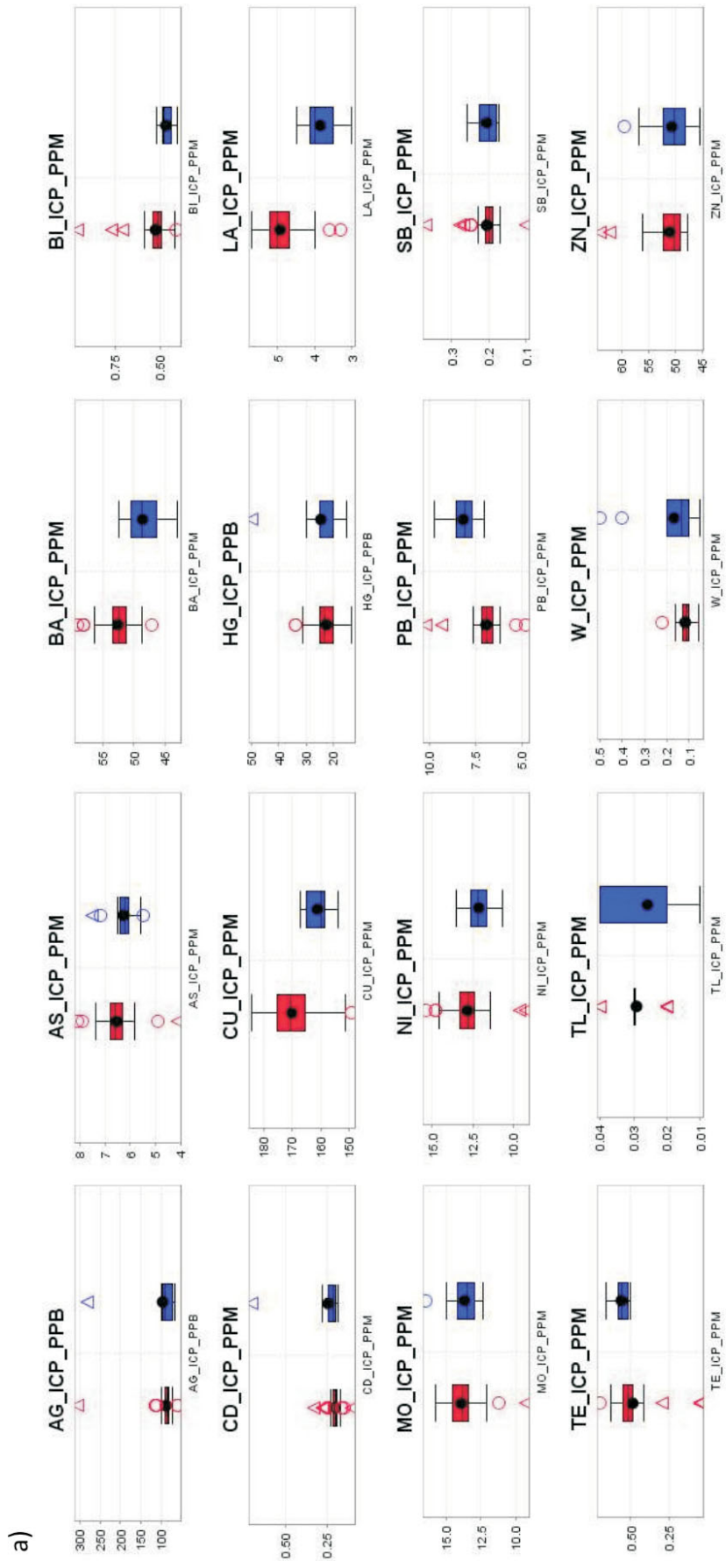
a)
AG_ICP_PPB
AS_ICP_PPM
BA_ICP_PPM
BI_ICP_PPM
CD_ICP_PPM
CU_ICP_PPM
HG_ICP_PPB
LA_ICP_PPM
MO_ICP_PPM
NI_ICP_PPM
PB_ICP_PPM
SB_ICP_PPM
TE_ICP_PPM
TL_ICP_PPM
W_ICP_PPM
ZN_ICP_PPM

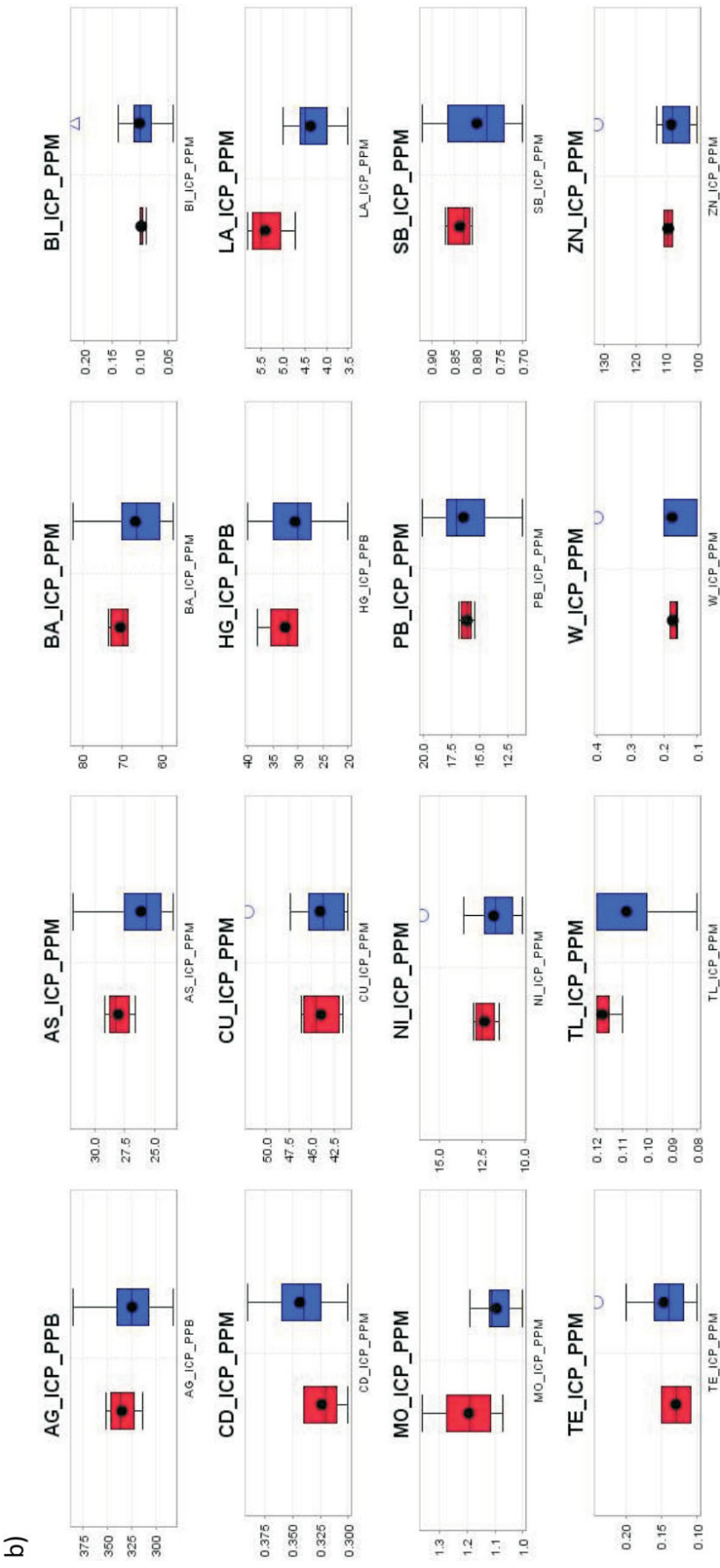

Figure 2. Box and whisker plots of selected elements from ICP-MS analysis of the Red Dog **(a)** and SRM SQ **(b)** standard reference materials. Data in red are from ALS Global and data in blue are from EcoTech.

chemical characteristics that overlap with several mineral-deposit types that are more economically significant.

The QGIS function 'NNJoin' was used to find the closest MINFILE point to each stream-sediment sampling site. Each RGS site was tagged with the nearest distance to a MINFILE site. These distances range from 0.7 to 42 848 m. A histogram of distance values is shown in Figure 3. Figure 4 shows a map of the stream-sediment sites and a summary of the distances between a stream-sediment site and the closest MINFILE site.

The QGIS function 'Intersect' was used to merge the bedrock geology and terrane designation with the stream-sediment geochemical data and the closest MINFILE point. The tagging of a MINFILE site with a stream-sediment site is based on the closest distance between the two sites, regardless of the MINFILE 'Status' designation and catchment delineation. Thus, MINFILE sites with the status of Producer or Past Producer may not be tagged with the closest stream-sediment site if another MINFILE site with the status of Developed Prospect, Prospect, Showing or Anomaly is closer. Because some MINFILE sites (Producer, Past Producer, Developed Prospect) may not be tagged if there is no stream-sediment site nearby, the likelihood of a geochemical expression of the mineralization may be difficult to estimate. Table 1 lists the number of stream-sediment sample sites associated with each MINFILE Status attribute. If the measured distance between a stream-sediment site and a MINFILE site was greater than 2500 m, the stream-sediment site MINFILE Model designation was tagged as 'Unknown'.

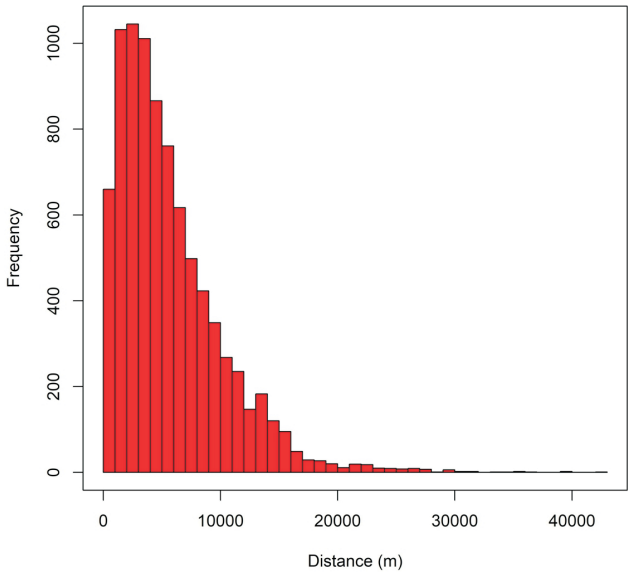

Figure 3. Histogram of the distances between stream-sediment sites and MINFILE sites, based on the QGIS function 'NNJoin'.

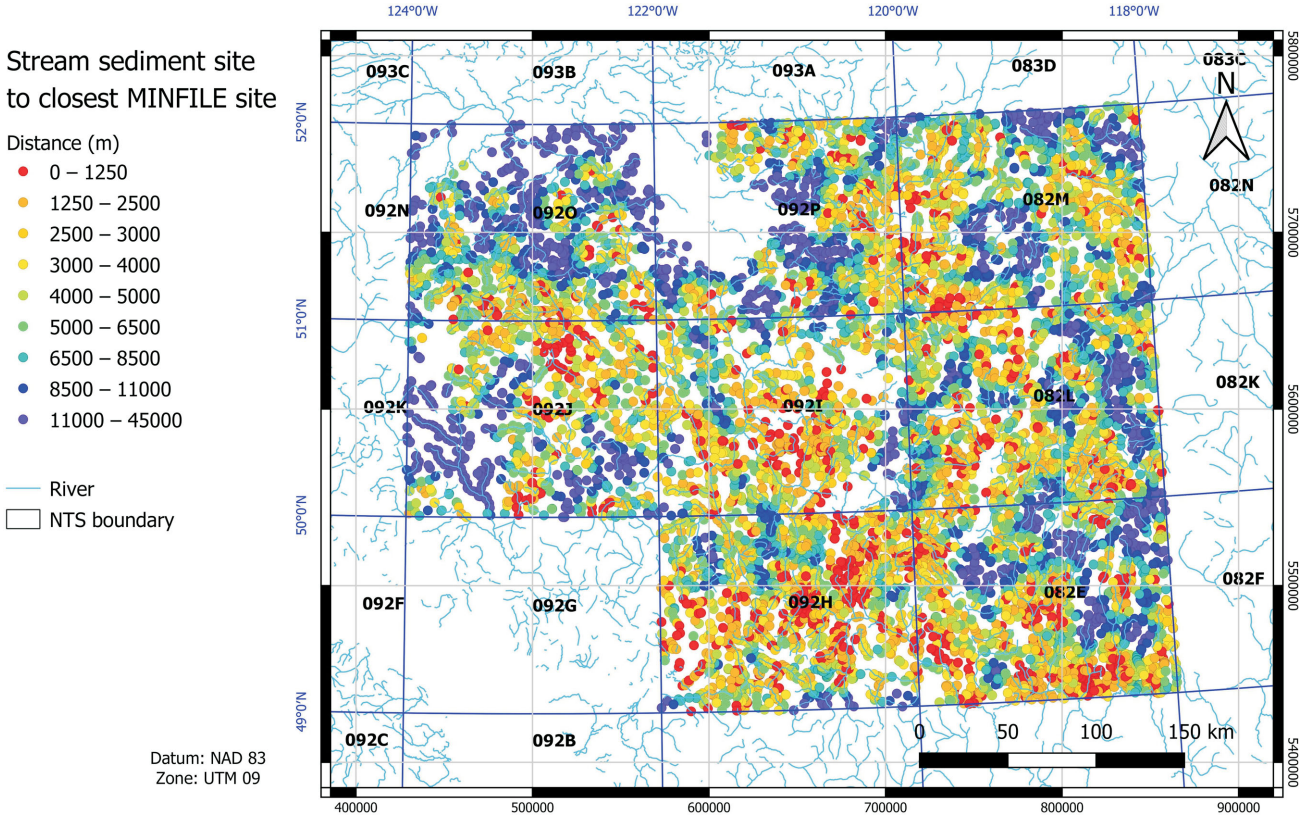

Figure 4. Geographic distribution of the distance measures between a stream-sediment site and the closest MINFILE site, based on the QGIS function 'NNJoin'.

Table 1. MINFILE Status for the tagged Quest-South stream-sediment data.

MINFILE status	Frequency
Anomaly	116
Developed Prospect	341
Past Producer	682
Producer	38
Prospect	1144
Showing	6224
Total	**8545**

Interpolation of principal-component scores and random forests posterior probabilities was carried out using a geostatistical framework. The gstat package for R (Pebesma, 2004) was used to generate and model semi-variograms with sufficient parameters to produce interpolated images through kriging. The cell size used for image interpolation was chosen as 5.0 km for the images generated by principal-component analysis (PCA) and a cell size of 2.5 km was used for the images generated by the Random Forest predictions. This paper contains only the results of the application of PCA and the posterior probabilities of the mineral-deposit prediction derived from the application of random forests.

Characterizing Mineral Occurrence Information

Each MINFILE record lists a mineral-deposit model derived from the BCGS Mineral Deposit Profiles (BC Geological Survey, 1996). The number of MINFILE sites associated with each model is shown in Table 2.

The large number of mineral-deposit types for which there are only a few sites was considered to create difficulty in a statistical assessment of the data. Consequently, the models were merged as shown in Table 3. These merged models, termed 'GroupModels', were the basis for assessing the multivariate geochemical patterns. Figure 5a shows the GroupModel designation for each of the tagged stream-sediment sites and Figure 5b shows the Status of the MINFILE sites, labelled with the BCGS Mineral Deposit Profile that is listed in the MINFILE record variable 'Deposit Type'. Figure 6 shows a graphical legend for the GroupModel classes that are used in the subsequent figures of this paper, where the left legend is the mnemonic category of the BCGS Mineral Deposit Profile and the right legend provides a description of the respective BCGS Mineral Deposit Profile.

Mineral-Deposit Models and Their Geospatial Footprint

An important consideration in the use of machine-learning methods for resource-potential prediction is the geospatial extent of the footprint of the mineral-deposit model. For many types of mineral deposits, namely vein (I01–I06), skarn (K01–K05), carbonatite (N01) and rare-earth elements (REE; O01–O04), the geospatial extent is quite limited, typically less than 200 m. As a result, the geochemistry

Table 2. Number of stream-sediment sites associated with a MINFILE model.

Model[1]	Frequency	Model[1]	Frequency	Model[1]	Frequency	Model[1]	Frequency
C01	118	G03	1	I11	7	L05	52
D03	115	G04	34	I12	4	L07	1
D04	13	G05	6	I14	3	L08	14
D06	6	G06	102	J01	11	M01	1
E01	2	G07	2	J04	2	M02	26
E03	2	H02	13	K01	151	M03	21
E04	3	H03	2	K02	28	M04	2
E05	2	H05	44	K03	20	M05	26
E12	12	H08	10	K04	54	N01	15
E13	5	I01	311	K05	25	N03	1
E14	92	I02	30	K07	5	O01	8
E15	1	I05	988	K09	6	O02	24
E16	2	I06	82	L01	61	S01	7
F01	7	I07	3	L02	7	Unknown[2]	901
G01	5	I08	4	L03	198		
G02	2	I09	24	L04	384		

[1]MINFILE 'Model' designation (see 'Deposit' section of 'Mineral Occurrence' tab of MINFILE Search page at <http://minfile.ca/>.

[2]Unknown means no mineral deposit model was assigned to the MINFILE record.

Note: . For many types of mineral deposits, namely, vein (I01 – I06), skarn (K-01 – K05), carbonatite (N01) and REE (O01 – O04), the geospatial extent is quite limited, typically less than 200 m. As a result, the geochemistry of stream sediment sites that are tagged with MINFILE sites with these models may not reflect the geochemical signature of the mineral deposit. Other deposit types such as placer (C01 – C04), volcanic-hosted Cu (D03), basal U (D04- D06), sediment-hosted massive sulphides (E01, E02, E05, E12, E13, E14, E15), volcanic-hosted massive sulphides (G04, G05, G06), porphyry systems (L01 – L08) and mafic volcanic/ intrusive-hosted Ni, Cu, Cr (M01 – M05) may have broader geospatial signatures (> 200 m).

Table 3. Merged mineral-deposit models (GroupModels) for statistical processing of the Quest-South stream-sediment data.

Models[1]	GroupModel
C01, C04	C01C04
D03	D03
D04, D06	D04D06
E01, E02, E05	E01E02E05
E12, E13, E14, E15, S01	E12E13E14E15
G04, G05	G04G05
G06	G06
G07, H02, H03	G07H02H03
H05	H05
I01	I01
I02	I02
I05	I05
I06	I06
K01, K03	K01K03
K02	K02
K04	K04
K05	K05
L01	L01
L02, L04	L02L04
L03	L03
L05, L08	L05L08
M01, M02, M03, M05	M01M02M03M05
N01	N01
O01, O02, O04	O01O02O04

[1]MINFILE 'Model' designation (see 'Deposit' section of 'Mineral Occurrence' tab of MINFILE Search page at <http://minfile.ca/>.

of stream-sediment sites that are tagged with MINFILE sites with these models may not reflect the geochemical signature of the mineral deposit. Other deposit types, such as placer (C01–C04), volcanic-hosted Cu (D03), basal U (D04- D06), sediment-hosted massive sulphides (E01, E02, E05, E12, E13, E14, E15), volcanic-hosted massive sulphides (G04, G05, G06), porphyry systems (L01–L08) and mafic volcanic/intrusive–hosted Ni, Cu and Cr (M01–M05), may have broader geospatial signatures (>200 m). Consequently, the ability to predict the various types of mineral deposits will depend on the proximity of the stream-sediment sample site to the MINFILE site.

Selecting the Training and Test Datasets

In this study, mineral-deposit prediction is based on the selection of a training set of stream-sediment sites that are tagged with the nearest MINFILE site (as described previously). Additionally, MINFILE Status designations of Anomaly or Occurrence were classed as Unknown. A stream-sediment site that is more than 2500 m from a MINFILE site is also classed as Unknown for the associated MINFILE Status and Model classes.

Table 4 shows the frequency of the MINFILE GroupModel class for all stream-sediment sites that met the criteria of being less than 2500 m from a MINFILE site with the Status class, as described above. Table 2 shows that, for the 61 Model deposit types that were identified, many are associated with less than 10 sites. As a result, the Model classes were merged into the GroupModels, as shown in Table 3, with the corresponding number of sites shown in Table 4.

After some experimentation, it was decided that the Mineral Deposit Model I05 (Polymetallic Veins) created a significant amount of confusion in the prediction of the other mineral-deposit types. This issue was noted in a previous study (Arne et al., 2018b). Consequently, stream-sediment sites that were labelled as I05 were re-labelled as Unknown. The training set contains all stream-sediment sites where the GroupModel is not classed as Unknown. The test set contains all of the stream-sediment sites where the GroupModel class is Unknown. It is unrealistic to consider that every stream-sediment site must have a MINFILE Model or GroupModel designation. Thus, a random selection of 100 stream-sediment sites with a GroupModel of Unknown was made. In this way, sites that do not have a geochemical signature that reflects a form of mineralization may have the possibility of being assigned as belonging to an Unknown GroupModel class. This resulted in a training set of 474 sites and a test set of 8071 sites. Table 4 summarizes the GroupModel classes that are part of the training dataset.

Process Discovery – Empirical Investigation of Geochemistry

After QA-QC, the geochemical data were subjected to an empirical investigation in which the assumptions about the data were minimal. Because geochemical data, by definition, are compositions, the issue of closure also becomes important. As compositional data sum to a constant (i.e., 100%, 1 000 000 ppm), then by definition, when one value changes, all others must change to maintain the constant sum. Thus, the data are 'closed' and the variables are not independent, but standard statistical methods are based on variables that are independent. For geochemical data, this lack of independence can result in meaningless statistical results. To deal with the effect of closure, data for the 35 selected elements were log-centred (clr) transformed (Aitchison, 1986).

Multivariate methods were applied to the clr-transformed data for the purposes of discovering patterns and features that potentially describe relationships among geochemical, geological and geophysical parameters, as well as the effects of gravitational processes (Grunsky et al., 2010). These methods included principal-component analysis (PCA), independent-component analysis (ICA; Comon, 1994) and t-distributed stochastic neighbour embedding (t-SNE; van Maaten and Hinton, 2008). Each of these methods provides different co-ordinate systems that can reveal features and patterns related to geochemical processes. Only the PCA results are presented in this paper.

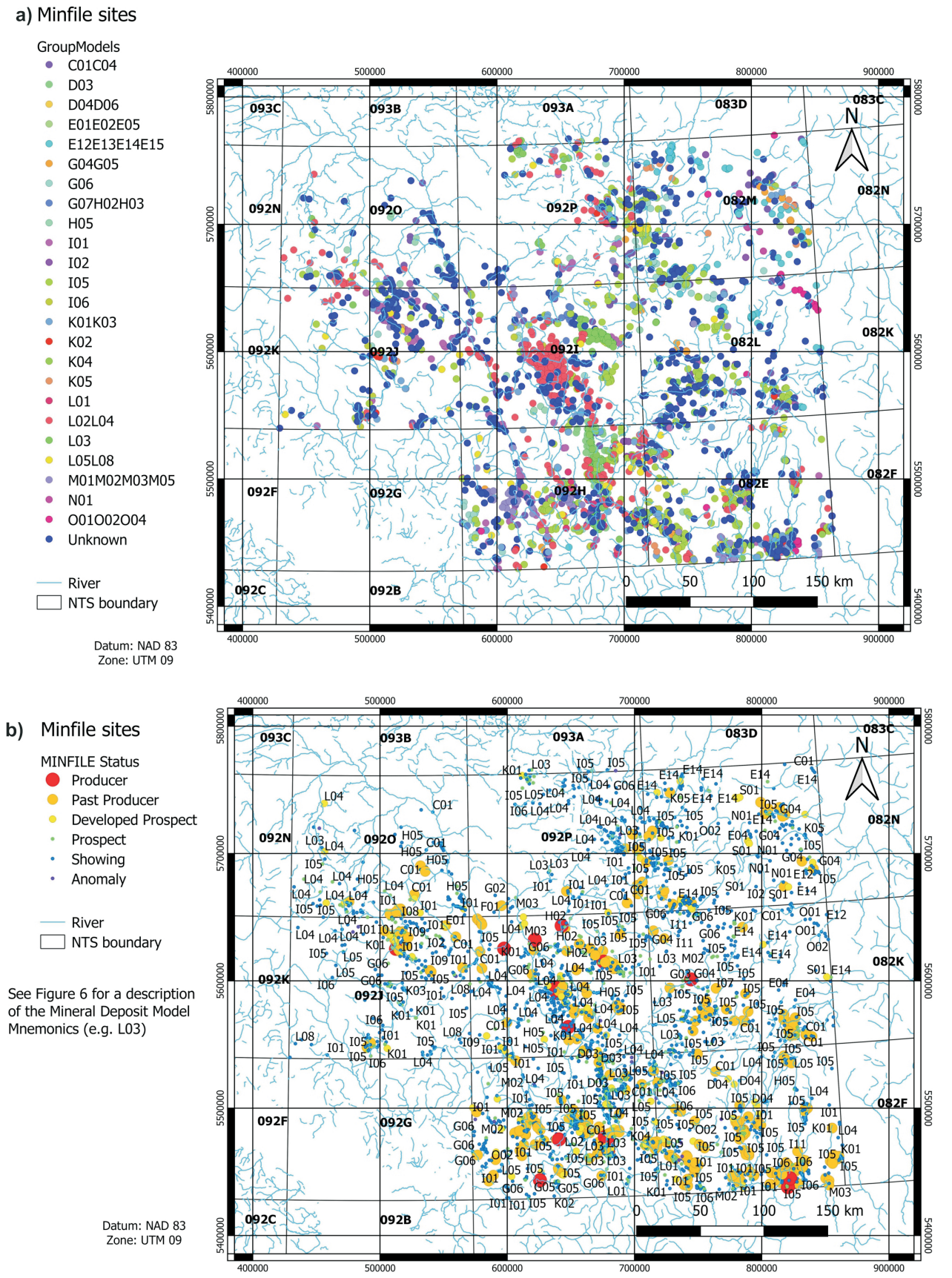

Figure 5. Geographic distribution of **a)** MINFILE sites classified by GroupModel; and **b)** MINFILE sites classified by Status and labelled by BCGS Mineral Deposit Model.

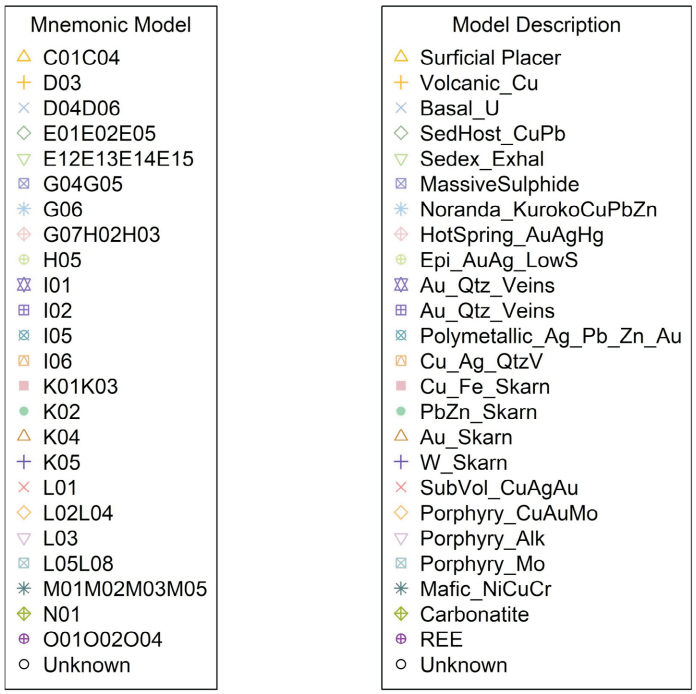

Figure 6. GroupModel classes expressed as BCGS Mineral Deposit Model mnemonics (left), with the respective BCGS Mineral Deposit Models (right).

Table 4. Merged Mineral Deposit Models (GroupModels) tagged at the stream-sediment sites. Note that 100 unknown sites were used with the training set for the application of Random Forest classification/prediction. The remaining 8071 sites were used to classify the 'unknown' GroupModels.

GroupModel	Frequency
C01C04	83
D03	5
E01E02E05	3
E12E13E14E15	22
G04G05	11
G06	27
G07H02H03	6
H05	18
I01	41
I02	1
I06	5
K01K03	23
K02	2
K04	9
K05	6
L01	6
L02L04	61
L03	15
L05L08	13
M01M02M03M05	17
Unknown - test	100
Unknown - train	8071
Total	**8545**

The co-ordinates resulting from a PCA were used to discover patterns and features in the data. The method of PCA used in this study is based on the methodology of Zhou et al. (1983) and Grunsky (2001). The geochemistry of the stream sediments was evaluated using a simultaneous R- and Q-mode extraction of eigenvalues/eigenvectors.

Process Validation – Modelled Investigation of Geochemistry

Using the principal components derived from the clr-transformed geochemical data for stream-sediment sites that were tagged with the GroupModel class (Table 4), a GroupModel was predicted for each site that was classified as Unknown using the method of Random Forests (RF; Breiman, 2001). The Unknown class of data constituted the test set of data, except for 100 analyses that were used as part of the training dataset, as previously explained.

Random forests was previously employed by Harris and Grunsky (2015), Arne et al. (2018b) and Grunsky et al. (2018), and used as part of a remote predictive-mapping strategy (Harris et al., 2008). The method of RF is based on the construction of classification trees (Venables and Ripley, 2002, Chapter 9) in which nodes (splits in classes) are based on continuous variables from which a series of branches in the tree classify correctly (categorical variables) all of the data. A more detailed description of how the Random Forest classification method was used with soil-geochemical data is provided in Harris et al. (2015).

Maps of the posterior probabilities derived from the classification method of random forests can be created using geostatistical methods such as kriging. However, since the posterior probabilities are compositions and sum to 1.0, these values should be log-ratio transformed, followed by subsequent co-kriging, and then back-transformed for subsequent geographic rendering (Pawlowsky-Glahn and Egozcue, 2015; Mueller and Grunsky, 2016). This approach is potentially problematic because, in cases where posterior probabilities are very low or zero, the results from kriging may be unreliable or invalid. It can be argued that the posterior probabilities for each predicted class are independent, since there is no intention, or value, of assessing the variables of probabilities in terms of any interactions. Additionally, maps of the posterior probabilities for each of the classes can be created by posting the sample sites with points and colours. An alternative to this would be to consider the un-normalized (raw) votes as independent and carry out kriging on these estimations. For this study, the posterior probabilities were kriged with the assumption of independence between the estimated classes.

Note that kriged images based on point data have been used for validation purposes to test the sensitivity of various model input parameters and that thematically coded catchment maps will be generated with predictive results for a number of mineral-deposit types using the preferred modelling inputs, once these are finalized.

Results

PCA Process Discovery

A screeplot of the principal components derived from the clr-transformed data is shown in Figure 7. The screeplot shows a steep decay for the first six eigenvalues, after which the curve flattens. The first six principal components can be interpreted as containing the 'structure' of the data that reflect the relationships between the variables (e.g., mineral stoichiometry) and the observations (scores of dominant processes). The remaining eigenvalues (7–35) may represent undersampled geochemical or random processes. Typically, in regional geochemical surveys, principal components associated with mineral deposits are undersampled and the relationships of the elements associated with mineralization do not appear in the dominant principal components (Grunsky et al., 2014).

A full display of PCA biplots is not feasible in this paper, so only the biplots of selected principal components (PC) are shown in order to illustrate the associations between the stream-sediment sites and the elements. Table 5 shows the

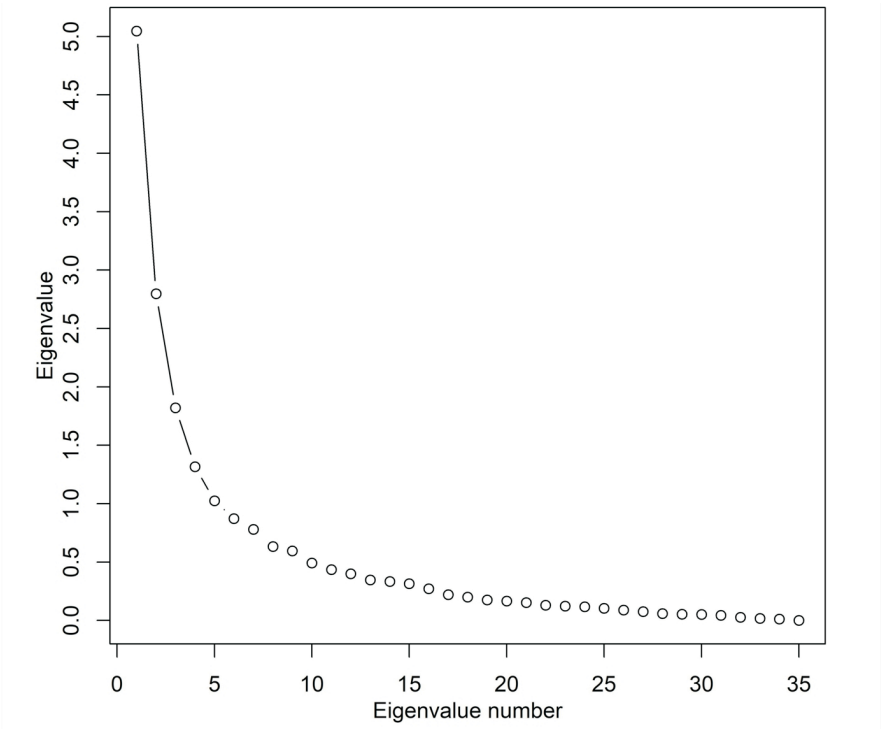

Eigenvalues	PC1	PC2	PC3	PC4	PC5	PC6	PC7	PC8	PC9	PC10	PC11	PC12	PC13	PC14	PC15
λ	5.05	2.8	1.82	1.32	1.02	0.87	0.78	0.63	0.59	0.49	0.43	0.4	0.35	0.33	0.32
λ%	26.1929	14.5228	9.4398	6.8465	5.2905	4.5124	4.0456	3.2676	3.0602	2.5415	2.2303	2.0747	1.8154	1.7116	1.6598
Σλ%	26.1929	40.7158	50.1556	57.0021	62.2925	66.805	70.8506	74.1183	77.1784	79.7199	81.9502	84.0249	85.8402	87.5519	89.2116

Figure 7. Screeplot of the eigenvalues derived from a principal-component analysis (PCA) applied to the clr-transformed data from the QUEST-South stream-sediment geochemistry results.

Table 5. Relative contributions of the elements over the first 15 principal components. Relative values >10 are highlighted in bold.

Element	PC1	PC2	PC3	PC4	PC5	PC6	PC7	PC8	PC9	PC10	PC11	PC12	PC13	PC14	PC15
Au	0.6989	9.2693	0.1610	**86.5505**	0.7772	0.0600	1.7943	0.0188	0.0755	0.0027	0.4066	0.0406	0.0209	0.0055	0.0057
Ag	6.6789	**41.4826**	1.1457	0.2361	0.0384	8.7220	0.1433	2.5385	0.0037	2.1554	6.7573	**13.5810**	2.5598	0.6451	0.2579
Al	0.0073	**19.9318**	0.7834	1.3136	0.2964	3.1666	**17.9160**	0.1333	0.2477	0.0844	**13.2428**	0.6462	0.5518	0.3003	2.6763
As	**52.7714**	9.1233	**14.7048**	0.5437	4.0632	5.2089	0.4267	0.4638	1.1717	4.1879	0.4718	0.0004	0.4169	0.2066	3.5051
Ba	0.9251	5.7988	8.7258	3.6209	4.5142	0.2945	**12.0236**	3.8422	0.7422	2.6072	1.4064	0.7191	**15.0097**	0.0225	1.2733
Bi	**19.2949**	**25.3788**	8.1629	0.0126	2.7926	2.7636	3.2131	0.0355	5.5709	0.1094	6.8646	2.6774	1.4050	5.6101	0.3978
Ca	8.6571	8.0231	**39.4552**	0.3516	0.1194	4.3661	**20.8447**	4.7291	0.0026	0.0279	0.5600	0.0100	1.0093	1.8760	0.1239
Cd	**11.9913**	**37.7998**	1.1252	2.2407	2.0894	**10.6976**	0.8580	**11.7985**	1.2367	2.4223	1.9128	0.1630	1.4068	3.8286	0.8354
Co	**21.8757**	**30.7461**	**12.3658**	0.0009	2.1343	3.8330	0.3574	6.4427	0.2327	2.9409	0.0607	1.0738	0.1751	1.3216	0.8699
Cr	3.9533	**32.2648**	**14.4624**	0.7497	3.5326	1.6345	2.4365	3.5754	**19.9487**	0.0749	0.0344	2.0987	0.0104	0.4468	0.0152
Cu	**28.3649**	0.4362	1.1688	0.3700	6.9193	0.4550	0.0235	0.0691	6.3149	0.0000	5.1011	**18.4051**	0.5214	**14.4846**	2.3262
Fe	1.2387	**26.3040**	**12.2156**	0.4853	6.5318	0.3833	0.2770	7.6755	5.2405	**15.3267**	0.0553	0.1985	1.0379	0.0031	0.0386
Ga	9.5574	**26.7739**	3.5649	1.4437	4.3542	0.0613	**12.6585**	0.0971	0.9433	0.3471	6.0885	0.0241	0.2456	1.5731	0.4626
Hg	7.6828	2.7969	5.5976	2.5895	1.9206	2.7037	**11.9990**	1.2697	8.9787	2.3661	7.1758	**14.7192**	2.8291	4.6620	**14.5259**
K	**28.2095**	**10.9533**	0.3420	0.0167	7.1644	1.2161	1.6222	3.9810	**10.4682**	**20.5831**	1.8238	0.8035	1.5667	0.1013	0.0281
La	**65.9818**	0.3615	0.5050	0.0033	**10.8995**	0.9962	2.9773	1.0602	0.6095	0.4798	0.0142	0.5331	0.3707	2.1423	0.3924
Mg	**17.8416**	**38.9230**	7.0415	0.4319	6.6360	1.4551	1.5168	0.2363	0.8663	0.1638	0.0002	0.4392	0.0376	0.4997	1.5558
Mn	8.2355	0.0945	0.3812	4.9335	8.0692	0.8216	4.1058	1.4504	0.5560	**15.5973**	1.9756	**13.0761**	4.8440	0.4742	**10.5730**
Mo	0.0439	**24.8141**	0.5907	5.8816	0.9833	0.0286	5.7257	0.3953	0.5563	9.6349	**22.2267**	0.0043	5.3417	**13.4736**	0.8498
Na	0.8734	**36.4653**	**12.1305**	1.7574	0.4932	4.3404	2.1695	5.0551	0.8199	0.0628	0.9405	0.1854	**21.6942**	0.3390	0.1006
Ni	**17.1347**	**17.7046**	8.2647	0.4761	9.2980	**10.7745**	6.0195	2.1936	**19.1471**	1.2073	0.1331	0.4499	0.1205	0.2835	0.4157
P	**24.3384**	**10.6489**	2.8629	0.1690	1.9692	1.9944	0.7730	1.3455	2.4417	1.0275	4.5954	0.7438	6.0284	1.4953	0.0372
Pb	5.8067	**27.1246**	0.1257	0.2433	2.4066	7.3107	5.3710	0.2928	1.9793	0.3127	**11.3225**	5.3499	1.1474	1.8773	0.5512
S	6.8137	5.7766	**37.1747**	0.1118	**14.6116**	0.8177	0.0456	**26.4688**	3.8587	0.1187	0.0845	0.0185	0.0707	2.9206	0.0482
Sb	**61.6038**	7.4505	2.9143	0.8911	7.5966	4.5937	0.7771	0.2465	0.4769	1.5758	0.0019	0.1829	0.0369	0.3356	4.0344
Sc	8.4356	**29.2350**	6.3569	0.1566	1.6333	1.0029	4.7795	0.0556	0.0895	0.5047	5.5858	0.3722	0.0039	0.0486	0.4468
Se	**13.2096**	**10.4685**	**20.7614**	3.9385	3.3864	0.4195	0.0148	0.1247	5.5979	0.4276	5.8006	1.3523	0.0379	0.4375	0.9701
Sr	1.4017	9.9012	**46.9785**	0.1692	5.2254	3.6645	**10.3769**	6.2445	0.2397	0.1744	0.2129	0.1055	0.0038	1.5617	2.1919
Th	**68.9774**	0.1632	5.5913	0.3602	3.1495	0.0351	**11.7522**	1.0889	1.4091	0.0655	0.7424	0.0139	0.0239	0.0000	2.9220
Ti	3.8444	**50.5982**	2.2106	0.0038	0.0011	0.4688	8.9841	0.7261	0.0157	0.2574	0.0000	0.6786	1.4654	4.7206	0.7844
Tl	**33.8946**	1.3546	0.0593	1.6900	3.9299	9.2104	7.3387	3.2035	0.6633	**15.7427**	6.1739	0.4171	0.8110	0.5611	0.0018
U	**63.6091**	9.6125	2.9410	1.6616	2.8168	0.6449	1.2336	1.5284	6.6831	1.0701	0.0787	2.4354	1.1198	0.6309	1.8716
V	0.9803	**33.6136**	6.0450	0.2566	7.1988	6.5679	6.8820	0.2465	0.6066	**12.2189**	0.0013	8.1469	0.0896	0.8467	0.6873
W	**25.9920**	8.8420	**11.5808**	0.0601	**20.9871**	**24.9910**	0.0394	2.5198	0.9173	1.3099	0.2506	0.3186	1.1944	0.4243	0.0936
Zn	7.8490	1.3451	1.4823	4.4344	0.2586	**17.4519**	0.0003	4.8889	3.7955	3.3146	0.0004	3.7654	2.2082	2.0354	0.0004

relative contributions of the PCA results. The contribution of variability for each element is shown across the first 15 eigenvectors.

Figure 8a shows a biplot of PC1–PC2. The stream-sediment site scores are coded with their MINFILE GroupModel designation as shown in Figure 6. The components PC1–PC2 account for 40.7% of the variability of the data. The loadings of the elements indicate that chalcophile elements (Sb-As-Cd-Se-S-Hg) are associated with the positive PC1–negative PC2 quadrant. Symbols representing GroupModel I05 (polymetallic veins) occur within this quadrant. A group of siderophile elements (Fe-Cr-Ni-V-Cr-Co) occur within the positive PC1–PC2 quadrant. Stream-sediment sites tagged with mafic base-metal sulphide deposits (M01M02M03M05) occur in this quadrant. The loadings of W-U-Bi-Pb-La-Th-K occur across the PC2 axis and the

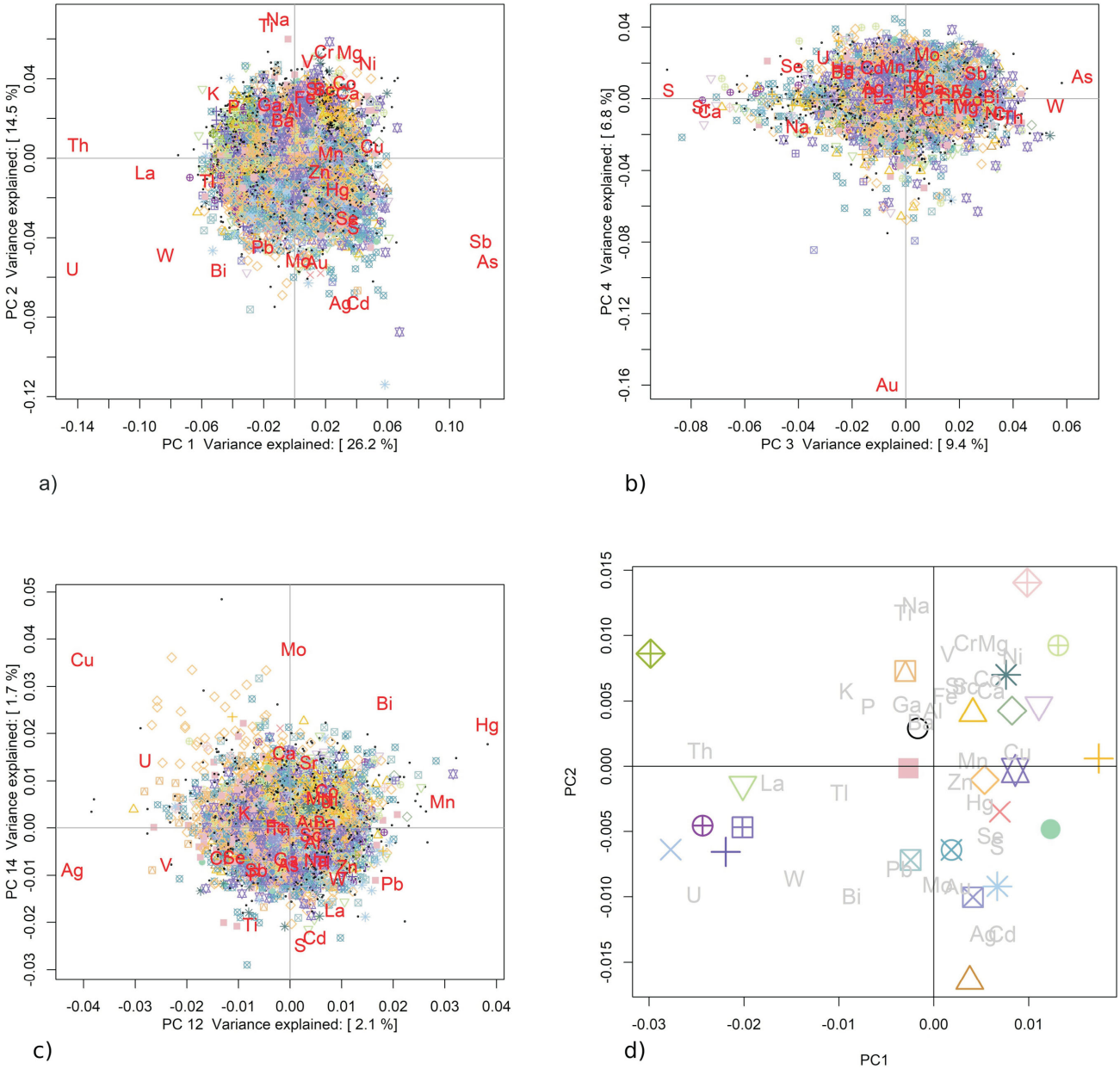

Figure 8. Biplots of **a)** PC1–PC2, showing the relative enrichment of Au along the negative PC2 axis; symbols are coloured/coded according to the legend in Figure 6; components are derived from log-centred transforms to the stream-sediment geochemistry based on a covariance structure; the first PC accounts for 26.2% of the overall variance and the second PC accounts for 14.5% of the overall variance; **b)** PC3-PC4 showing the relative enrichment of Au along the negative PC4 axis; see Figure 6 for the legend of colours and symbols; **c)** PC12-PC14 showing the relative enrichment of Cu along the positive PC14 axis and the negative PC12 axis; sites identified with relative Cu enrichment are associated with L02L04 (porphyry Cu) MINFILE designations; symbols are coloured/coded according to the legend in Figure 6; **d)** PC1-PC2 showing the mean PC1-PC2 values for each of the GroupModel classes; symbols are coloured/coded according to the legend in Figure 6.

negative PC1 axis. The relative associations of these elements likely reflect mineralized environments associated with felsic intrusive rocks. It is worth noting that the L02L04 GroupModel plots throughout the PC1–PC2 biplot. An association of L02L04 deposits is typically not associated with mafic elements and this suggests that not all GroupModel assignments, projected onto a PC1–PC2 biplot, provide insight into the multi-element associations for the different GroupModels.

Lithophile elements dominate the negative PC1–positive PC2 quadrant, including the elements Ba-Al-Ga-P-K-Ti-Na. This region of the biplot shows associations of Cu-Fe skarns (K01K03), Cu-Ag quartz veins (I06) and carbonatite (N01). The GroupModels are clearly distinct from each other, which justifies the attempt to classify the MINFILE-tagged stream-sediment sites with a GroupModel designation.

From Table 5, it is evident that most of the variability of Au is accounted for in PC4 and, for Cu, most of the variability is accounted for in PC1, PC12 and PC14. Figure 8b shows the biplot for PC3–PC4. The relative Au-enrichment trend is shown along the negative PC4 axis. Using the legend for the various MINFILE GroupModels in Figure 6, it can be seen that the relative enrichment in Au is associated with G04G05 (massive sulphides), L05L08 (Mo-rich porphyry), L02L04 (Cu-rich porphyry), L03 (alkalic porphyry), K04 (Au skarn) and I02 (Au veins). Figure 8c shows a biplot of PC12–PC14 that highlights the relative enrichment of Cu, primarily associated with L02L04 (Cu-rich porphyry).

It is difficult to see the compositional differences between the different GroupModel designations in the principal-component biplot. Figure 8d shows the mean values of PC1 and PC2 for each of the GroupModels. The relative enrichment of elements and the corresponding association with the GroupModels is evident in the biplot. Relative enrichment in siderophile elements (Fe-V-Cr-Co-Ni) occurs in the positive PC1–positive PC2 quadrant. Mineral deposits that are associated with this group of elements include mafic Ni-Cu-Cr (M01M02M03M05), sediment-hosted Cu deposits (E01E02E05), surficial placer deposits (C01C04), alkalic porphyry deposits (L03), epithermal Au deposits (H05) and volcanic redbed associated Cu deposits (D03). Elements that are dominantly chalcophile in character, including Cd-Se-Hg-Ag-Au-Mo, occur in the positive PC1–negative PC2 quadrant and are associated with porphyry Cu (L02L04), Vein-hosted Au deposits (I01), subvolcanic Cu-Ag-Au deposits (L01), massive sulphide deposits including Noranda-type deposits (G04G05, G06), polymetallic vein deposits (I05) and Au skarns (K04) occur in this quadrant. Elements that occur in the negative PC1–negative PC2 quadrant are partly chalcophile and lithophile in nature, including Pb-Bi-W-U. Mineral deposits associated with this group include Mo porphyry deposits (L05L08), W skarn deposits (K05), basal U deposits (D04D06), rare-earth element deposits (REE; O01O02O04), quartz vein Au deposits (I02) and sedimentary exhalative deposits (E12E13E14E15).

Kriged images, along with individual point scores for PC4 and PC12, are shown in Figure 9a and b, respectively. Regions of relative Au enrichment (Figure 9a) and relative Cu enrichment (Figure 9b) are clearly shown on these maps. In Figure 9a, PC4 indicates relative Au enrichment associated with negative (blue) values. In Figure 9b, PC12 indicates relative Cu enrichment associated with negative (red) values.

Process Validation – Random Forest GroupModel Prediction

The random forests function 'randomForest' (package randomForest for R; Breiman, 2001) was used to predict a GroupModel classification based on the training set of 474 sites using the distance threshold of 2500 m. One advantage of the random forests process is that a prior selection of variables is not required. The procedure starts with all of the variables (PC1–PC35) and then reduces the number of variables to those that provide the best nodes in the trees that are generated.

Figure 10 shows the significance of the variables derived from the random forests procedure. The significance is measured by the 'Mean Decrease in Gini'. This measure of variable importance is based on the 'node impurity' (i.e., the rate of misclassification). Lower rates of misclassification correspond to higher values of the Gini index. The figure indicates that PC1 is by far the most significant variable, followed by PC6 and PC2. The remaining variables show a monotonic decrease in significance.

Table 6 shows the accuracy of classification in terms of percentage, based on the training set only. The overall classification accuracy is 36.2% when model I05 (polymetallic veins) is excluded from the modelling runs. Several of the GroupModel classes show a classification accuracy of zero. The GroupModel classes that were associated with the most confusion and/or overlap were G04G05 (massive sulphide), K01K03 (Cu-Fe skarn) and L03 (alkalic porphyry Cu deposits). The confusion among these GroupModels is likely due to significant overlap of their geochemical signatures with those of other GroupModels

The random forests procedure estimates posterior probabilities for each GroupModel at each stream-sediment site. The assigned class is selected from the GroupModel with the highest posterior probability. A predictive map of the posterior probabilities can be created for each GroupModel class. Areas of contiguous elevated posterior probabilities for a given class define the 'geospatial coherence' of a

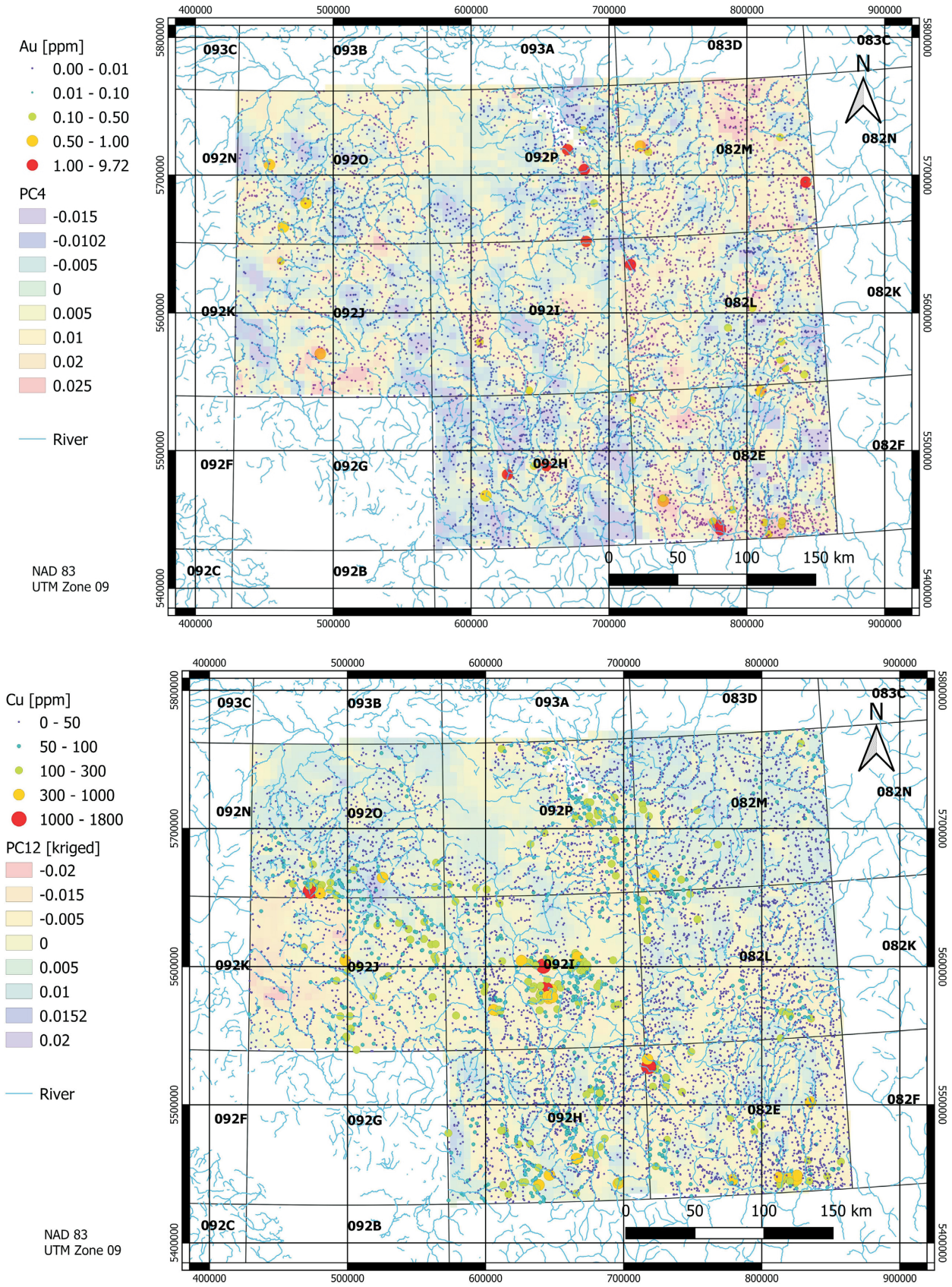

Figure 9. Geographic distribution of **a)** individual sites overlain on a kriged image of PC4, illustrating the relative enrichment of Au at selected sites across the map area; **b)** individual sites overlain on a kriged image of PC12, illustrating the relative enrichment of Cu at selected sites across the map area.

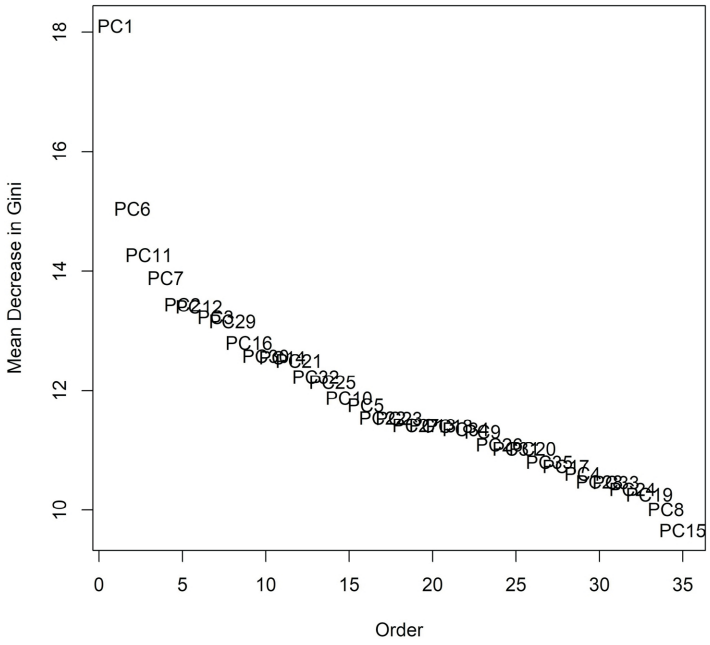

Figure 10. Plot of 'Mean Decrease in Gini' for the principal components used in the application of Random Forest prediction based on the training data [MinDep <2500 m].

GroupModel. It is expected that the maps of posterior probability can show overlap because of compositional overlap between the classes. Also because of compositional overlap, the posterior probabilities for many GroupModels can be very low. However, geospatial coherence in the interpolated image for a given GroupModel increases the potential that the area is associated with that GroupModel. A given stream-sediment site could have nearly equal posterior probabilities for several GroupModels. This increases the confusion and resulting overlap in the classification and, in the cases where there is geospatial coherence for several GroupModels in the same area(s), further investigation is required to determine which GroupModel is most feasible.

Table 6. Accuracy matrix for the GroupModels training set, derived from the application of Random Forest classification.

GroupModel	Accuracy (%)	Class error
C01C04	61.16	0.46
D03	0	16.67
E01E02E05	0	25.00
E12E13E14E15	21.96	3.39
G04G05	8.40	7.63
G06	0.00	3.57
G07H02H03	0.00	14.29
H05	32.14	3.57
I01	26.36	1.75
I02	0	50.00
I06	0	16.67
K01K03	8.36	3.82
K02	0	33.33
K04	20.45	7.95
K05	0	14.29
L01	0	14.29
L02L04	53.69	0.75
L03	6.28	5.86
L05L08	0	7.14
M01M02M03M05	0	5.56
Unknown	65.78	0.34

A map of predictions for the GroupModel class C01C04 (surficial placer Au) deposits is shown in Figure 11. Many more sites were predicted than the actual number of MINFILE sites. The predicted sites and the interpolated image show a north-northwesterly trend and closely follow the stream/river drainage lines on the map.

Figure 12 shows a predictive map of Au skarns (K04). The interpolated map shows elevated values that coincide with the MINFILE sites and the stream-sediment sites that are classed as K04. Several areas have elevated posterior probabilities where there are no known MINFILE sites associated with K04. As explained previously, the posterior probabilities are low (<0.2), but the identified MINFILE sites and assigned random forests class coincide with the elevated kriged image of the posterior probabilities.

Figure 13 shows a predictive map of W skarns (K05). Several sites that are identified as K05 occur in the northeastern part of the area (NTS 082M). A few isolated sites occur in NTS areas 092J, 092I and 082E. The kriged image of the posterior probabilities shows an overall low prediction rate, not exceeding 0.2. Nonetheless, the elevated values in NTS area 082M coincide with the MINFILE sites. Although W was not included in the dataset, the prediction of

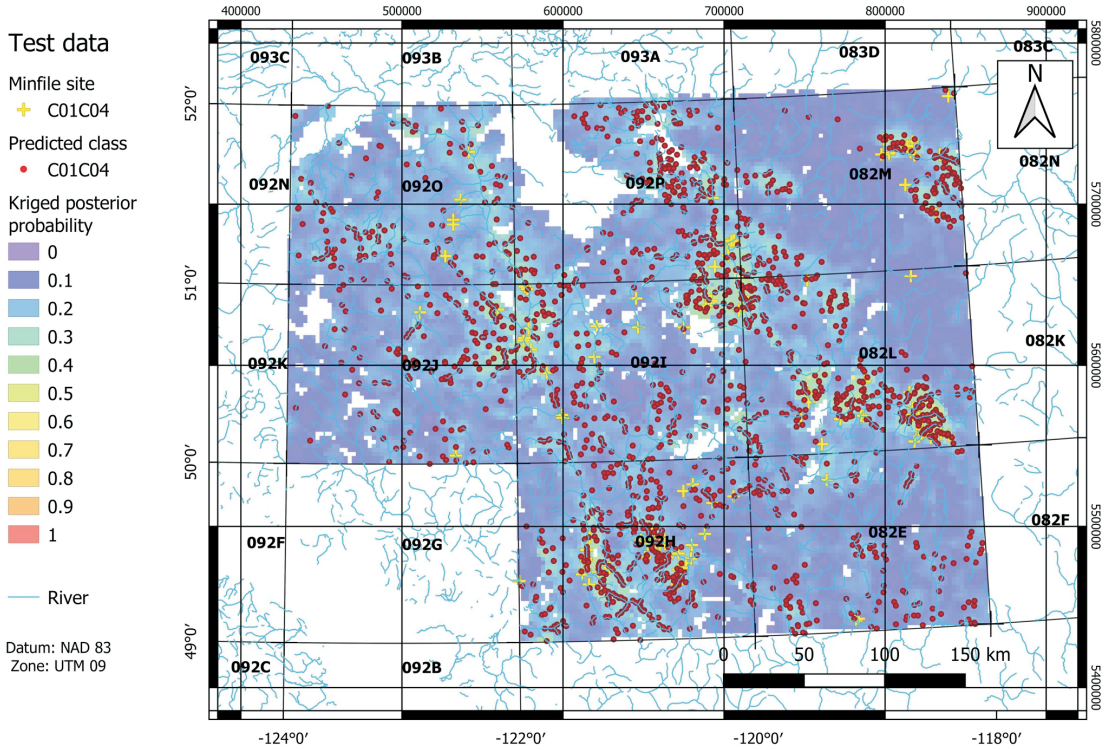

Figure 11. Geographic distribution of individual sites overlain on a kriged image of the posterior probabilities for the GroupModel C01C04 (surficial placer Au) across the map area, based on the test data and a distance threshold of 2500 m. MINFILE sites tagged as C01C04 are shown as yellow crosses. Stream-sediment sites identified as class C01C04 by random forests are shown as red dots. Areas of increased potential for C01C04 deposits are shown by colour shading.

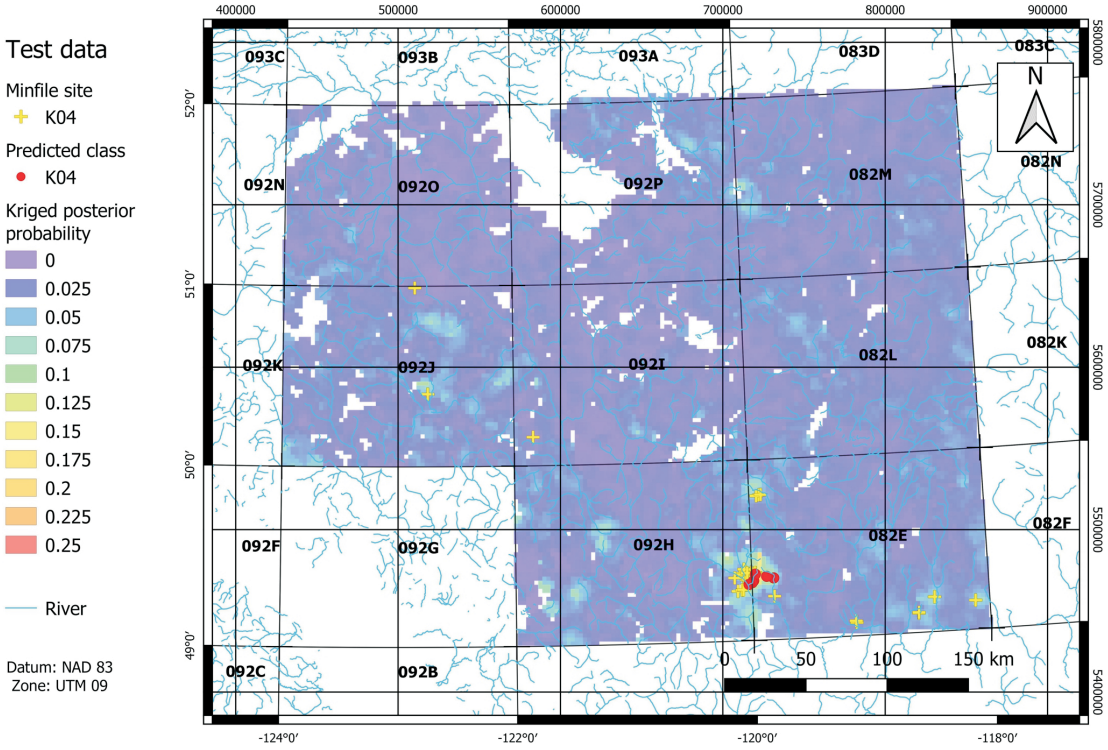

Figure 12. Geographic distribution of individual sites overlain on a kriged image of the posterior probabilities for the GroupModel K04 (Au skarn) across the map area, based on the test data and a distance threshold of 2500 m. MINFILE sites tagged as K04 are shown as yellow crosses. Stream-sediment sites identified as class K04 by random forests are shown as red dots. Areas of increased potential for K04 deposits are shown by colour shading.

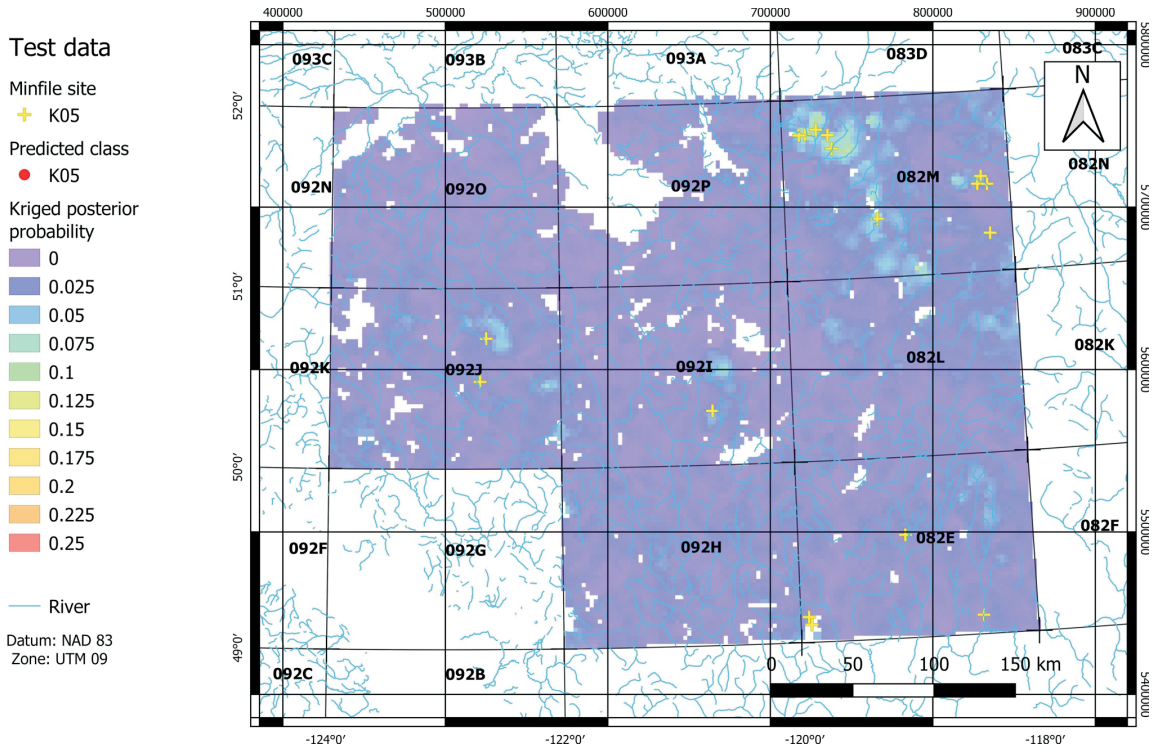

Figure 13. Geographic distribution of individual sites overlain on a kriged image of the posterior probabilities for the GroupModel K05 (W skarn) across the map area, based on the test data and a distance threshold of 2500 m. MINFILE sites tagged as K05 are shown as yellow crosses. Stream-sediment sites identified as class K05 by random forests are shown as red dots. Areas of increased potential for K05 deposits are shown by colour shading.

W skarn deposits demonstrates the unique multi-element character of these types of deposits.

Figure 14 shows a predictive map of the combined porphyry deposit models for Cu, Au and Mo (L02L04). There are clusters of L02L04 sites in the vicinity of Lornex and Highland Valley mines in NTS area 092I. Additional sites that are identified by MINFILE sites and classed as L02L04 by random forests are shown in NTS areas 092H 082E, 092P and 092O. The kriged image of the posterior probabilities coincides with both the MINFILE sites and the predicted classes.

Discussion

The results presented here do not represent the entire range of mineral-deposit types or additional results that were determined by changing the selection of the GroupModels or the distance threshold. For some mineral-deposit types, changing the distance threshold to 1000 and 5000 m yielded different and reasonable predictions. The changes in parameters will be discussed in a forthcoming report.

The predictions for the four GroupModels (C1C04, K04, K05 and L0L04) illustrate the ability to predict existing regions of known mineral-deposit potential, as well as identifying areas that have not been previously recognized as having mineral deposits.

Within the current scope and context of this study, some fundamental assumptions have been made:

1) The geochemical composition of the stream sediment associated with the mineral-deposit model is uniquely distinct. In some cases, this assumption is not warranted. For example, the mineral-deposit model I05 (polymetallic veins) has characteristics that overlap with many other mineral-deposit types, resulting in confusion of prediction. As a result, this model was removed from the GroupModel classes.
2) The stream-sediment samples represent a suitable medium from which the geochemical characteristics of mineral systems can be identified. Not all mineral-deposit types can be best represented in stream sediments. The size fraction and the analytical methods used may not extract unique information to distinguish a mineral deposit or distinguish between different mineral-deposit types. The method of dissolution using aqua regia is useful for sheet silicates and sulphide minerals, but aqua-regia digestion does not dissolve many silicates. Thus, some unique geochemical aspects of specific mineral-deposit types based on silicate mineral assemblages may not be recognized.
3) The MINFILE model identification is accurate. This may not be the case for some types of mineral systems and, as a result, there will be an increase in confusion of prediction. The identification of the BCGS Mineral De-

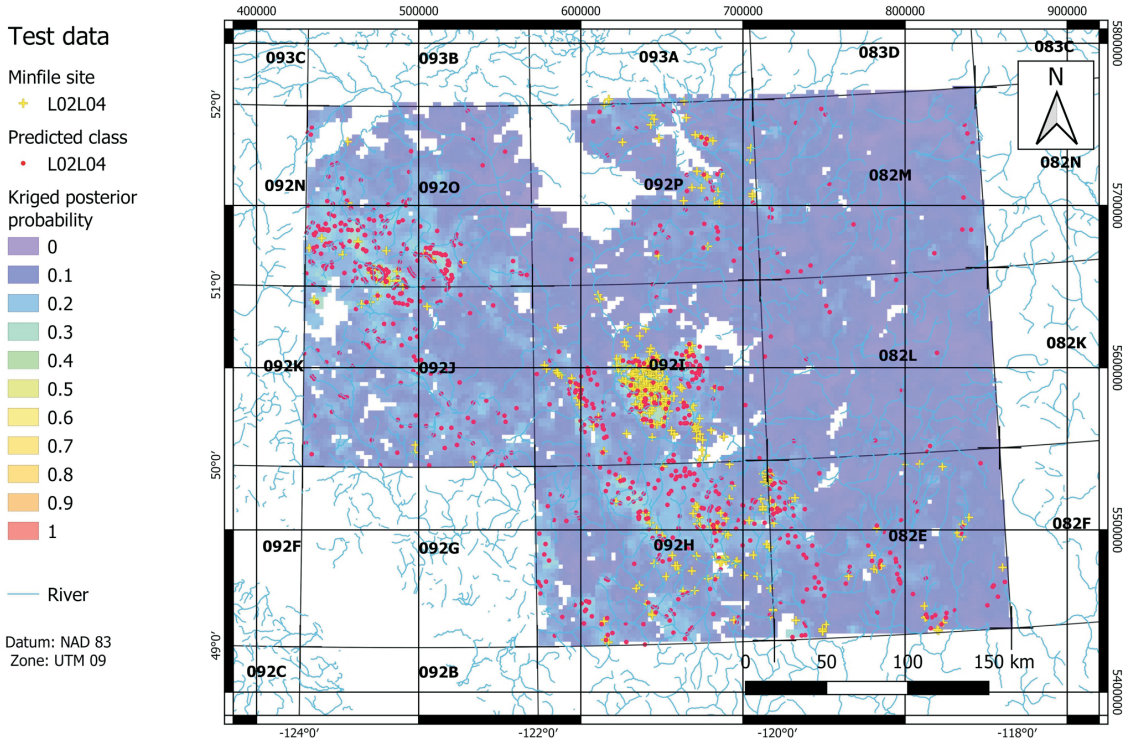

Figure 14. Geographic distribution of individual sites overlain on a kriged image of the posterior probabilities for the GroupModel L02L04 (Cu-Au-Mo porphyry) across the map area, based on the test data and a distance threshold of 2500 m. MINFILE sites tagged as L02L04 are shown as yellow crosses. Stream-sediment sites identified as class L02L04 by random forests are shown as red dots. Areas of increased potential for L02L04 deposits are shown by colour shading.

posit Profiles, as specified in the MINFILE field 'Deposit Type', may be incorrect or inconclusive. This can lead to misclassification errors in the subsequent application of machine-learning prediction methods.

4) The location of a MINFILE site and the associated stream-sediment site may not be within the same catchment area. Thus, the assumption was made that the effect of catchment was not significant. If there is a requirement for the location of a MINFILE site and associated stream-sediment site to be in the same catchment, the number of sites for the training set would be significantly reduced. This requirement may be examined in subsequent work.

Given these assumptions, the results presented here indicate that various types of mineral deposit can be predicted. Although many of the predictions have low values of posterior probability, the geospatial coherence of many of these sites provide evidence that the region is potentially prospective. In cases where isolated sites are identified in regions not previously known to be prospective, these can be considered either as 'new' prospective sites or as representing an overlap with other types of mineral deposit.

Further work is ongoing to provide a comprehensive picture of mineral-deposit potential, based on the BCGS Mineral Deposit Profiles.

Deliverables from this project will include files containing log-centred transformed values of the NAD 83 UTM Zone 10 co-ordinates of the stream sediments, MINFILE attributes, elements, principal-component scores, random forests votes, random forests normalized votes, random forests posterior probabilities and random forests class predictions. The files containing this information will be provided in Esri shapefile format and tab-delimited ASCII format. Kriged images will be provided in 32-bit geoTIFF format.

This paper summarizes the rationale and methodology for the prediction of mineral-deposit types based on the mineral-deposit model framework developed for BC. The use of log-ratio transforms to overcome the problem of closure, and the application of multivariate methods to the stream-sediment geochemistry establish an objective framework for characterizing the data, termed 'process discovery'. The application of a tree-based method (random forest) for predicting potential mineral-deposit sites offers a repeatable, consistent and defensible methodology, termed 'process prediction', that offers promise for the identification of prospective terrains and mineral systems. Together, they will enhance exploration strategies in the province of British Columbia.

Acknowledgments

The authors thank Geoscience BC for funding this project. Y. Cui of the BCGS is thanked for providing a peer review of this paper.

References

Aitchison, J. (1986): The Statistical Analysis of Compositional Data; Chapman and Hall, New York, New York, 416 p.

Arne, D.C. and Bluemel, E.B. (2011): Catchment analysis and interpretation of stream sediment data from QUEST South, British Columbia; Geoscience BC Report 2011-5, 24 p., URL <http://www.geosciencebc.com/reports/gbcr-2011-05/> [November 2019].

Arne, D., Mackie, R. and Pennimpede, C. (2018a): Catchment analysis of re-analyzed regional stream sediment geochemical data from the Yukon; Explore (Newsletter for the Association of Applied Geochemists), no. 179, URL <https://www.appliedgeochemists.org/sites/default/files/documents/Explore%20issues/Explore179-June2018-website.pdf> [November 2019].

Arne, D., Mackie, R., Pennimpede, C., Grunsky, E. and Bodnar, M. (2018b): Integrated assessment of regional stream-sediment geochemistry for metallic deposits in northwestern British Columbia (parts of NTS 093, 094, 103, 104), Canada; Geoscience BC, Report 2018-14, 87 p., URL <http://www.geosciencebc.com/i/project_data/GBCR2018-14/GBCReport2018-14_Report.pdf> [November 2019].

BC Geological Survey (1996): British Columbia mineral deposit profiles; BC Geological Survey, URL <http://cmscontent.nrs.gov.bc.ca/geoscience/PublicationCatalogue/Miscellaneous/BCGS_MP-86.pdf> [November 2019].

BC Geological Survey (2019): MINFILE BC mineral deposits database; BC Ministry of Energy, Mines and Petroleum Resources, URL <http://minfile.ca> [November 2019].

Bonham-Carter, G.F and Goodfellow, W.D. (1986): Background corrections to stream geochemical data using digitized drainage and geological maps: application to Selwyn Basin, Yukon and Northwest Territories; Journal of Geochemical Exploration, v. 25, p. 139–155.

Bonham-Carter, G.F., Rogers, P.J. and Ellwood, D.J. (1987): Catchment basin analysis applied to surficial geochemical data, Cobequid Highlands, Nova Scotia: Journal of Geochemical Exploration, v. 29, p. 259–278.

Breiman, L. (2001): Random Forests; Machine Learning, v. 45, p. 5–32.

Carranza, E.J.M. and Hale, M. (1997): A catchment basin approach to the analysis of reconnaissance geochemical-geological data from Albay Province, Philippines; Journal of Geochemical Exploration, v. 60, p. 157–171.

Comon, P. (1994): Independent component analysis: a new concept? Signal Processing, v. 36, p. 287–314.

Cui, Y. (2010): Regional geochemical survey: validation and refitting of stream sample locations; *in* Geological Fieldwork 2010, BC Ministry of Energy, Mines and Petroleum Resources, BC Geological Survey, Paper 2011-1, p. 169–179, URL <http://cmscontent.nrs.gov.bc.ca/geoscience/PublicationCatalogue/Paper/BCGS_P2011-01-12_Cui.pdf> [November 2019].

Cui, Y., Eckstrand, H. and Lett, R.E. (2009): Regional geochemical survey: delineation of catchment basins for sample sites in British Columbia; *in* Geological Fieldwork 2008, BC Ministry of Energy, Mines and Petroleum Resources, BC Geological Survey, Paper 2009-1, p. 231–238, URL <http://cmscontent.nrs.gov.bc.ca/geoscience/PublicationCatalogue/Paper/BCGS_P2009-01-19_Cui.pdf> [November 2019].

Cui, Y., Miller, D., Schiarizza, P. and Diakow, L.J. (2017): British Columbia digital geology; BC Ministry of Energy, Mines and Petroleum Resources, BC Geological Survey, Open File Report 2017-8, 14 p., URL <http://cmscontent.nrs.gov.bc.ca/geoscience/PublicationCatalogue/OpenFile/BCGS_OF2017-08.pdf> [November 2019].

de Caritat, P. and Grunsky, E.C. (2013): Defining element associations and inferring geological processes from total element concentrations in Australian catchment outlet sediments: multivariate analysis of continental-scale geochemical data; Applied Geochemistry, v. 33, p. 104–126.

de Caritat, P., Main, P.T., Grunsky, E.C. and Mann, A.W. (2016): Recognition of geochemical footprints of mineral systems in the regolith at regional to continental scales; Australian Journal of Earth Sciences, v. 64, p. 1033–1043.

Grunsky, E.C. (2001): A program for computing rq-mode principal components analysis for S-Plus and R; Computers and Geosciences, v. 27, p. 229–235.

Grunsky, E.C. (2010): The interpretation of geochemical survey data; Geochemistry, Exploration, Environment Analysis, v. 10, p. 27–74.

Grunsky, E.C., Drew, L.J. and Sutphin, D.M. (2010): Process recognition in multi-element soil and stream-sediment geochemical data; Applied Geochemistry, v. 24, p. 1602–1616.

Grunsky, E.C., Mueller, U.A. and Corrigan, D. (2014): A study of the lake sediment geochemistry of the Melville Peninsula using multivariate methods: applications for predictive geological mapping; Journal of Geochemical Exploration, v. 141, p. 15–41.

Grunsky, E.C., Drew, L.J. and Smith, D.B. (2018): Analysis of the United States portion of the North American Soil Geochemical Landscapes Project – a compositional framework approach; *in* Handbook on Mathematical Geosciences: Fifty Years of IAMG, Springer, p. 313–346, URL <https://www.springer.com/gp/book/9783319789989> [November 2019].

Harris, J.R., and Grunsky, E.C. (2015): Predictive lithological mapping of Canada's north using Random Forest classification applied to geophysical and geochemical data; Computers & Geosciences, v. 80, p. 9–25.

Harris, J.R., Grunsky, E., Behnia, P. and Corrigan, D. (2015): Data- and knowledge-driven mineral prospectivity maps for Canada's north; Ore Geology Reviews, v. 71, p. 788–803.

Harris, J.R., Schetselaar, E.M., Lynds, T. and deKemp, E.A. (2008). Remote predictive mapping: a strategy for geological mapping of Canada's north; *in* Remote Predictive Mapping: An Aid for Northern Mapping; J.R. Harris (ed.), Geological Survey of Canada, Open File 5643 p. 5–27.

Hron, K., Templ, M. and Filzmoser, P. (2010): Imputation of missing values for compositional data using classical and robust methods; Computational Statistics and Data Analysis, v. 54, no. 12, p. 3095–3107.

Jackaman, W. (2010a): QUEST-South Project sample reanalysis; Geoscience BC, Report 2010-4, 4 p., URL

<http://www.geosciencebc.com/reports/gbcr-2010-04/> [November 2019].

Jackaman, W. (2010b): QUEST-South regional geochemical data, southern British Columbia; Geoscience BC, Report 2010-13, 152 p., URL<http://www.geosciencebc.com/reports/gbcr-2010-13/> [November 2019].

Jackaman, W. (2018): A compilation of quality control data from Geoscience BC RGS initiatives; Geoscience BC, Report 2018-15, 9 p. URL <http://www.geosciencebc.com/projects/2016-018/> [September 2019].

Mueller, U.A. and Grunsky, E.C. (2016): Multivariate spatial analysis of lake sediment geochemical data; Melville Peninsula, Nunavut, Canada; Applied Geochemistry, v. 75, p. 247–262.

Nelson, J.L., Colpron, M. and Israel, S. (2013). The Cordillera of British Columbia, Yukon and Alaska: Tectonic and Metallogeny; *in* Tectonics, Metallogeny, and Discovery: The North American Cordillera and Similar Accretionary Settings, M. Colpron, T. Bissig, B.G. Rusk and J.F.H. Thompson (ed.), Society of Economic Geologists, Special Publication 17, p. 53–109.

Palarea-Albaladejo, J., Martín-Fernández, J.A. and Buccianti, A. (2014). Compositional methods for estimating elemental concentrations below the limit of detection in practice using R; Journal of Geochemical Exploration, v. 141, p. 71–77.

Pawlowsky-Glahn, V. and Egozcue, J.-J. (2015): Spatial analysis of compositional data: a historical review; Journal of Geochemical Exploration, v. 164, p. 28–32.

Pebesma, E.J. (2004): Multivariable geostatistics in S: the gstat package; Computers & Geosciences, v. 30, p. 683–691.

QGIS Development Team (2019): QGIS Geographic Information System; Open Source Geospatial Foundation Project, URL <http://qgis.osgeo.org> [October 2019].

R Core Team (2019): R: a language and environment for statistical computing: R Foundation for Statistical Computing; Vienna, Austria, URL < http://www.r-project.org> [November 2019].

van der Maaten, L.J.P. and Hinton, G.E. (2008): Visualizing data using t-SNE; Journal of Machine Learning Research, v. 9, p. 2579–2605.

Venables, W.N. and Ripley, B.D. (2002): Modern Applied Statistics with S (Fourth Edition); Springer, Berlin, 504 p., URL <http://www.bagualu.net/wordpress/wp-content/uploads/2015/10/Modern_Applied_Statistics_With_S.pdf> [November 2019].

Zhou, D., Chang, T. and Davis, J.C. (1983): Dual extraction of R-Mode and Q-Mode factor solutions; Mathematical Geology, v. 15, p. 581–606.

Atlas of Gold Compositions for British Columbia: Developing a New Tool for the Exploration Community

R.J. Murphy, School of Earth and Environment, University of Leeds, Leeds, United Kingdom, r.j.murphy@leeds.ac.uk

R.J. Chapman, School of Earth and Environment, University of Leeds, Leeds, United Kingdom

J.K. Mortensen, MDN Geosciences Ltd, Salt Spring Island, British Columbia

B. Bluemel, Bonanza Geosciences, Squamish, British Columbia

D.A. Banks, School of Earth and Environment, University of Leeds, Leeds, United Kingdom

Murphy, R.J., Chapman, R.J., Mortensen, J.K., Bluemel, B. and Banks, D.A. (2020): Atlas of gold composition for British Columbia: developing a new tool for the exploration community; *in* Geoscience BC Summary of Activities 2019: Minerals, Geoscience BC, Report 2020-01, p. 77–82.

Introduction

Detrital gold grains can be of great help to mineral exploration campaigns because they are broadly dispersed and create a larger footprint around lode-gold deposits. Erosional products of orebodies provide vectors to mineralization, but these can be obscured by surficial deposits (Averill, 2011). In British Columbia (BC), recent indicator-mineral research has been primarily focused on porphyry-epithermal systems and methodologies based on resistant minerals such as magnetite (Celis et al., 2014; Pisiak et al., 2015), apatite (Bouzari et al., 2010, 2016; Mao et al., 2016) and tourmaline (Chapman et al., 2015). Detrital gold grains are ideal for use as indicator minerals because of their mechanical durability and chemical stability. However, the potential for gold grains recycling into successive fluvial environments diminishes the clear spatial relationship to lode source. In BC, the complex Cordilleran geology provides multiple plausible sources of gold particles; consequently, the discovery of gold particles during routine stream-sampling programs may not be sufficient to confirm a specific mineralization. A methodology has been developed to differentiate gold particles sourced from various styles of mineralization (porphyry, epithermal, skarn and orogenic).

Development of a gold indicator-mineral methodology is advantageous in BC because it benefits both greenfield and brownfield exploration activities. Exploration for porphyry copper-gold deposits in southern and central BC accounts for the majority of greenfield exploration spending, so any new sources of information would be valuable; brownfield exploration in areas of current mining are also important, both in the context of potential expansion and to establish exploration templates related to a known deposit for application elsewhere. In addition to ongoing exploration for porphyry copper-gold deposits in BC, there is also extensive exploration activity targeting orogenic-gold systems. Licence areas may contain detrital gold, but the location and nature of the source may be unclear because of geological and geographic complexity, remoteness of the location or lack of bedrock exposure. In these cases, the ability to establish the geological context of the source mineralization would be of great benefit to explorers.

The compositional variation between gold from different economic placer-locality populations is well known, principally because the silver content of the gold alloy influences the revenue to the miners. Gold-alloy composition is a function of the conditions of metal precipitation (Gammons and Williams-Jones, 1995), which vary according to the style of mineralization. In addition, minerals coeval with gold occur as micro-inclusions in the gold grains and are revealed in polished section. In conjunction, the alloy composition and mineral-inclusion suite of detrital gold particles define a 'microchemical signature' that is consistent with their hypogene source. Therefore, the source mineralogy can be reconstructed even when undiscovered.

Whilst gold may form in several geological environments, the associated mineralogy may provide a strong marker for the nature of the hypogene source. Generic elemental associations have been established for inclusion suites of gold from both alkalic and calcalkalic porphyry environments (e.g., Chapman et al., 2017, 2018) and recent studies have explored the potential to develop trace-element signatures for gold from different environments using laser-ablation inductively coupled plasma–mass spectrometry (Banks et al., 2018; Liu et al., 2019).

This publication is also available, free of charge, as colour digital files in Adobe Acrobat® PDF format from the Geoscience BC website: http://www.geosciencebc.com/updates/summary-of-activities/.

The current project will develop a new, publicly available reference database of gold microchemistry, specifically for mineralization styles encountered in BC, to encourage and assist mineral exploration efforts. The reference database will draw on results of recent projects (3868 gold particles from 68 localities), historic unpublished data and new data from analysis of material in collections at The University of British Columbia (6756 gold particles from 17 placer districts). Gold from porphyry, epithermal, skarn and orogenic systems is represented. The database will be compatible for interrogation using machine-learning techniques and will provide a new targeting tool for exploration companies in BC.

Previous Studies of Gold Composition in the Canadian Cordillera

Previous research has sought to characterize hypogene gold and its associated detrital expression for a variety of deposit styles across the Cordillera. The inclusion suites of gold from calcalkalic porphyry systems in Yukon exhibit a generic Bi-Pb-Te-S signature (Chapman et al., 2018), which is also present but less pronounced in associated epithermal systems. In contrast, detrital gold samples from alkalic porphyry copper-gold deposits in BC exhibit a strong Pd-Hg signature, matching the distinctive Pd-Hg mineralogy reported in late-stage veins (Chapman et al., 2017). Both studies highlighted the variation of gold mineralogy between the main ore stage (generally associated with potassic alteration and present as 5–20 µm blebs, which have exsolved from chalcopyrite or bornite) and later vein mineralization, which commonly contains gold sufficiently massive to be concentrated in placer lags. Thus, the mineralization of the most economically important phase (potassic) may be mineralogically distinct from that which forms the best detrital indicator.

Metamorphic fluids responsible for orogenic mineralization tend to be less chemically complex than their magmatic hydrothermal counterparts and this is reflected in the mineralogy of the inclusion suites observed in gold from orogenic systems (e.g., Chapman and Mortensen, 2016). Nevertheless, the inclusion signature from different episodes of orogenic mineralization may differ substantially even in the same area (e.g., Chapman et al., 2010, 2016), characterized by the relative abundance of base-metal sulphides, and sulpharsenide and telluride minerals. On the other hand, gold-silver alloys from magmatic hydrothermal systems typically contain higher levels of copper than gold from orogenic systems (Morrison et al., 1991, Chapman et al., 2017, 2018), which may be a function of mineralization temperature controlling substitution of copper into the gold-silver lattice (Chudnenko and Palyanova, 2016).

Sample Acquisition

Existing collections of detrital gold particles and hypogene-ore material collected by researchers at The University of British Columbia Mineral Deposit Research Unit (UBC-MDRU) and the University of Leeds are used for this project. The UBC-MDRU collection, curated by J. Knight, provides a key resource; this collection consists of detrital gold particles, polished sections and rock chips collected or donated from 352 localities across BC. Gold samples are also available from published studies describing two previous Geoscience BC funded projects at the University of Leeds relating to the Cariboo gold district (Chapman and Mortensen, 2016) and a regional study of alkalic porphyry copper-gold deposits (Chapman et al., 2017). The sample coverage of the UBC and University of Leeds collections is shown in Figure 1.

Additionally, relevant samples from existing UBC research collections have been made available, consisting of polished blocks of ore material from mines in the Hedley, Rossland, Sheep Creek, Zeballos, and Portland Canal mining districts. Detrital particles collected from drainages of the Kerr-Sulphurets-Mitchell deposit, acquired during recent fieldwork as part of other University of Leeds research, will also be analyzed. The project also benefits from the donation of detrital gold particles and ore-material hand specimens from the CLY prospect on the site of the historic Bunker Hill mine.

In total, samples from 495 localities will be utilized for this project. A summary of the samples available and the current extent of their analysis is presented in Table 1.

Sample Preparation

Gold particles collected from detrital sources or liberated from the crushing and sluicing of hypogene material were mounted in 25 mm diameter resin blocks according to particle size and polished to expose their interiors (Figure 2). Exposing the cores of the particles provides the best opportunity to analyze the primary phase of mineralization and is necessary to identify mineral inclusions.

Analytical Techniques

Scanning Electron Microscope (SEM)

The SEM will be used to locate and identify mineral inclusions, which are identified using both the secondary electron and back-scattered electron functions. The elemental composition of individual inclusions can be determined using the energy dispersive X-ray spectroscopy facility.

Electron Probe Microanalyzer (EPMA)

The EPMA (Figure 3) is used to analyze the alloy composition of each individual gold particle according to the Ag,

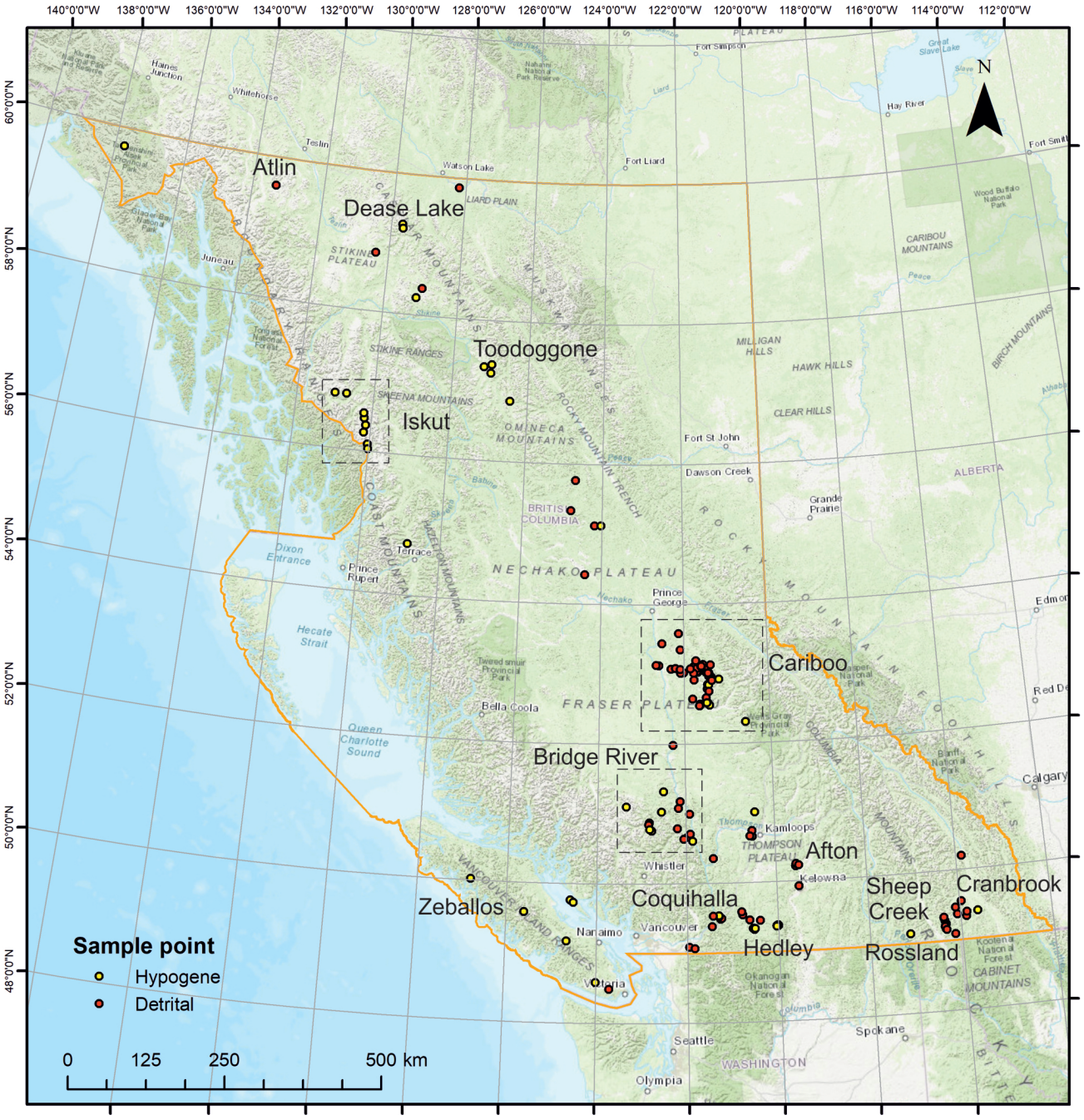

Figure 1. Location of samples from The University of British Columbia and the University of Leeds collections. Key camps and areas have been identified. Base map was created using ArcGIS® software by Esri. ArcGIS® and ArcMap™ are the intellectual property of Esri and are used herein under licence. Copyright © Esri. All rights reserved. For more information about Esri® software, visit https://www.esri.com/en-us/home.

Cu, Hg and Pd contents. Analysis is undertaken using a fully focused beam with a voltage of 20 kV and an intensity of 50 nA. Count times for primary alloy elements (Au and Ag) are 30 s on-peak, and 15 s at high and low off-peak; for trace alloy elements (Cu, Hg and Pd), count times are doubled to improve precision. These settings provide the most efficient compromise between accuracy and analysis time to characterize large numbers of gold particles.

Laser-Ablation Inductively Coupled Plasma–Mass Spectrometry (LA-ICP-MS)

Lastly, LA-ICP-MS is a precise analytical technique that determines elemental concentrations at a parts per billion scale, thus improving the ability to distinguish the minor alloying elements in gold (Banks et al., 2018). However, as it involves the ablation of the sample, it can only be under-

Table 1. Samples analyzed for the project, separated by district; additional usable material, such as hand specimens, polished sections and additional gold grains yet to be mounted, is also detailed.

District	Sample localities	Mounted grains	Analyzed for alloy composition	Analyzed for inclusions	Additional usable material
Alberni	7	1	0	0	17 polished sections
Atlin	3	20	0	0	Unmounted grains; 1 polished section
Cariboo	106	4137	3162	1548	Unmounted grains
Clinton	10	338	213	0	Unmounted grains
Fort Steele	10	34	0	0	None
Golden	2	3	0	0	None
Kamloops	13	363	358	172	3 polished sections; unmounted grains
Lillooet	59	1239	1140	0	4 polished sections; unmounted grains
Nelson	11	17	0	0	26 polished sections; unmounted grains
New Westminster	35	1372	785	0	6 polished sections; unmounted grains
Omineca	8	337	85	65	2 polished sections; unmounted grains
Osoyoos	8	0	0	0	9 polished sections
Portland Canal	12	509	50	0	21 polished sections; unmounted grains
Quesnel	10	349	62	19	Unmounted grains
Similkameen	14	783	681	82	Unmounted grains
Slocan	2	17	17	0	1 polished section
Stikine	75	1320	759	0	12 polished sections; unmounted grains
Trail Creek	3	26	0	0	33 hand specimens
Vancouver	3	147	41	0	Unmounted grains
Vernon	11	31	29	0	Unmounted grains
Victoria	1	48	0	0	Unmounted grains

taken following full characterization by EPMA and SEM. Analysis via LA-ICP-MS will therefore be undertaken on samples where the compositional information collected is insufficient to ascribe a microchemical signature, for example, where minor alloying elements such as Cu, Hg and Pd are below the detection limit of the EPMA.

Integration of Existing Data

Full datasets acquired by Chapman and Mortensen (2016) and Chapman et al. (2017) were made available for the project. These datasets include alloy-composition data using target elements Au, Ag, Cu, Hg and Pd, and recorded mineral inclusions for 3868 gold grains. Furthermore, these datasets are formatted to be compatible with machine-learning techniques and therefore provide the template for the database generated for this project.

Compositional data relating to the UBC gold collection were provided as scanned copies of dot-matrix printouts and required digitizing using optical character-recognition

Figure 2. Gold particles are mounted in circular blocks of resin, which are then polished to reveal the particle interiors for analysis.

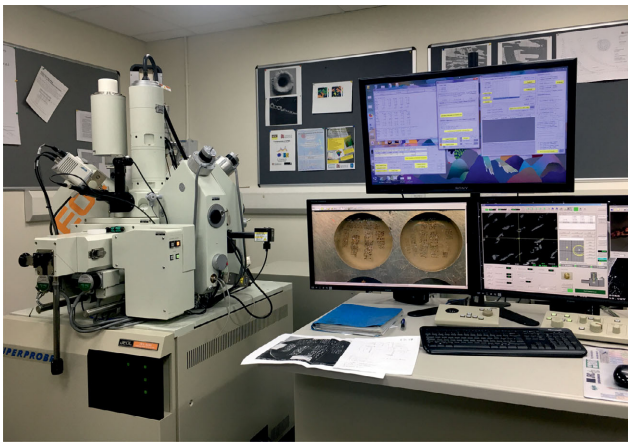

Figure 3. The JEOL Ltd. JXA-8230 electron probe microanalyzer at the University of Leeds.

software. The datasets were then reformatted to be consistent with the existing dataset from the University of Leeds, which describes 5364 gold particles from a total of 148 localities.

Future Work

With the majority of samples now received, analytical work using the SEM and EPMA is underway. Newly generated data will be integrated with the database as it is acquired. Samples that are not yet prepared for use with the instruments will be mounted and polished. Thin sections will be prepared from relevant hand specimens and inspected by reflected-light microscopy; those containing visible gold will be scheduled for analysis.

Conclusion

This project will develop a large, microchemical and mineralogical database of gold grains from a variety of deposit styles encountered in BC. Newly generated data for alloy composition and inclusion mineralogy from a range of locations will be amalgamated with existing datasets. The database will provide a comprehensive reference for exploration companies, allowing the likely source-mineralization styles in their licence area to be determined and therefore being of great help to exploration campaigns at an early stage. The database will be compatible for interrogation using machine-learning techniques and will provide a new targeting tool for exploration companies in BC.

Acknowledgments

This project was funded by Geoscience BC. The authors would like to thank The University of British Columbia and its Mineral Deposit Research Unit for access to relevant sample collections. They also thank W. Howard for the donation of samples and information relating to the CLY prospect at Bunker Hill mine. Lastly, T. Torvela is thanked for her helpful review of this paper.

References

Averill, S.A., (2011): Viable indicator minerals in surficial sediments for two major base metal deposit types: Ni-Cu-PGE and porphyry Cu; Geochemistry, Exploration, Environment, Analysis, v. 11, p. 279–291, URL <https://pubs.geoscienceworld.org/geea/article-abstract/11/4/279/128954> [November 2019].

Banks, D.A., Chapman, R.J. and Spence-Jones, C. (2018): Detrital gold as a deposit-specific indicator mineral by LA-IPS-MS analysis; *in* Geoscience BC Report 2018-21, 49 p., URL <http://cdn.geosciencebc.com/project_data/GBCReport2018-21.pdf> [October 2019].

Bouzari, F., Hart, C.J.R., Barker, S. and Bissig, T. (2010): Porphyry indicator minerals (PIMs): exploration for concealed deposits in south central British Columbia(NTS 092I/06, 093A/12, 093N/01, /14); *in* Geoscience BC Summary of Activities 2009, Geoscience BC, Report 2010-1, p. 25–32, URL <http://cdn.geosciencebc.com/pdf/SummaryofActivities2009/SoA2009_Bouzari.pdf> [October 2019].

Bouzari, F., Hart, C.J.R, Bissig, T. and Barker, S. (2016): Hydrothermal alteration revealed by apatite luminescence and chemistry: a potential indicator mineral for exploring covered porphyry copper deposits; Economic Geology, v. 111, p. 1397–1410, URL <https://pubs.geoscienceworld.org/segweb/economicgeology/article-abstract/111/6/1397/152471> [October 2019].

Celis, M.A., Bouzari, F., Bissig, T., Hart, C.J.R. and Ferbey, T. (2014): Petrographic characteristics of porphyry indicator minerals from alkalic porphyry copper-gold deposits in south-central British Columbia (NTS 092, 093); *in* Geoscience BC Summary of Activities 2013, Geoscience BC, Report 2014-1, p. 53–62, URL <http://www.llbc.leg.bc.ca/public/PubDocs/bcdocs/454425/2013/07_Celis.pdf> [November 2019].

Chapman, R.J. and Mortensen, J.K. (2016) Characterization of gold mineralization in the northern Cariboo Gold District, British Columbia, Canada, through integration of compositional studies of lode and detrital gold with historical placer production: a template for evaluation of orogenic gold districts; Economic Geology, v. 111, no. 6, p. 1321–1345, URL <https://pubs.geoscienceworld.org/segweb/economicgeology/article-abstract/111/6/1321/152454> [October 2019].

Chapman, R.J., Allan, M.M., Mortensen, J.K., Wrighton, T.M. and Grimshaw, M.R. (2018): A new indicator mineral methodology based on a generic Bi-Pb-Te-S mineral inclusion signature in detrital gold from porphyry and low/intermediate sulfidation epithermal environments in Yukon Territory, Canada; Mineralium Deposita, v. 53, no. 6, p. 815–834, URL <https://link.springer.com/article/10.1007/s00126-017-0782-0> [October 2019].

Chapman, R., Mileham, T., Allan, M. and Mortensen, J. (2017) A distinctive Pd-Hg signature in detrital gold derived from alkalic Cu-Au porphyry systems; Ore Geology Reviews, v. 83, p. 84–102, URL <https://www.sciencedirect.com/science/article/pii/S0169136816305005> [October 2019].

Chapman, R.J., Mortensen, J.K., Crawford, E.C. and LeBarge, W., 2010. Microchemical studies of placer and lode gold in the Klondike District, Yukon, Canada: 1. Evidence for a small,

gold-rich, orogenic hydrothermal system in the Bonanza and Eldorado Creek area; Economic Geology, v. 105, no. 8, p. 1369–1392, URL <https://pubs.geoscienceworld.org/segweb/economicgeology/article-abstract/105/8/1369/128235> [October 2019].

Chapman, J.B., Plouffe, A., Jackson, S.E., Ryan, J.J. and Ferbey, T. (2015): Mineral markers of porphyry processes: regional and local signatures of porphyry prospectively; *in* TGI 4 – Intrusion Related Mineralisation Project: New Vectors to Buried Porphyry-Style Mineralisation, N. Rogers (ed.), Geological Survey of Canada, Open File 7843, p. 521–534.

Chudnenko, K.V. and Palyanova, G.A. (2016): Thermodynamic modeling of native formation of Au-Ag-Cu-Hg solid solutions; Applied Geochemistry, v. 66, p. 88–100, URL <https://www.sciencedirect.com/science/article/pii/S0883292715300780> [October 2019].

Gammons, C.H. and Williams-Jones, A.E. (1995): Hydrothermal geochemistry of electrum: thermodynamic constraints; Economic Geology, v. 90, p. 420–432, URL <https://pubs.geoscienceworld.org/segweb/economicgeology/article-abstract/90/2/420/21472> [October 2019].

Lui, H., Beaudoin, G., Makvandi, S. and Jackson, S. (2019): Geochemical signature of native gold from various Au-bearing deposits – implications for mineral exploration; Society for Geology Applied to Mineral Deposits, 15th SGA Biennial Meeting, Glasgow, Scotland, August 27–30, 2019, extended abstract, p. 675–678.

Mao, M., Rukhlov, A.S., Rowins, S.M., Spence, J. and Coogan, L.A. (2016): Apatite trace element compositions: a robust new tool for mineral exploration; Economic Geology, v. 111, p. 1187–1222, URL <https://pubs.geoscienceworld.org/segweb/economicgeology/article-abstract/111/5/1187/152473> [October 2019].

Morrison, G.W., Rose, W.J. and Jaireth, S. (1991): Geological and geochemical controls on the silver content (fineness) of gold in gold-silver deposits; Ore Geology Reviews, v. 6, p. 333–364, URL <http://dx.doi.org/10.1016/0169-1368(91)90009-V> [October 2019].

Pisiak, L.K., Canil, D., Grondahl, C., Plouffe, A., Ferbey, T. and Anderson, R.G. (2015): Magnetite as a porphyry copper indicator mineral in till: a test using the Mount Polley porphyry copper-gold deposit, south-central British Columbia (NTS 093A); in Geoscience BC Summary of Activities 2014, Geoscience BC, Report 2015-1, p. 141–150, URL <http://www.geosciencebc.com/i/pdf/SummaryofActivities2014/SoA2014_Pisiak.pdf> [October 2019].

Mineral Exploration in Central British Columbia's Thick Surficial Deposits: Surficial Mapping to Inform Surface Sediment Data Compilation and Till Sample Reanalysis and Collection in the Central Interior Copper-Gold Research Project Area (Parts of NTS 093A, B, G, J, K, O)

D.A. Sacco, Palmer, Vancouver, British Columbia, david@pecg.ca

W. Jackaman, Noble Exploration Services Ltd., Jordan River, British Columbia

C. McGregor, Palmer, Vancouver, British Columbia

Sacco, D.A., Jackaman, W. and McGregor, C. (2020): Mineral exploration in central British Columbia's thick surficial deposits: surficial mapping to inform surface sediment data compilation and till sample reanalysis and collection in the Central Interior Copper-Gold Research project area (parts of NTS 093A, B, G, J, K, O); *in* Geoscience BC Summary of Activities 2019: Minerals, Geoscience BC, Report 2020-01, p. 83–92.

Introduction

The objective of Geoscience BC's Central Interior Copper-Gold Research (CICGR) project is to investigate the potential for undiscovered mineral deposits buried beneath thick glacial sediments. The CICGR project area occupies a large region in central British Columbia (BC) between the communities of Mackenzie and Williams Lake (Figure 1a). The region has significant mineral potential, however, exploration is hindered by extensive Quaternary sediment units that obscure bedrock. Drift prospecting within a comprehensive glacial framework has proven to provide exploration targets in such terrain (e.g., Levson et al., 1994; Levson, 2001; Plouffe et al., 2001; Sacco et al., 2018). This surficial exploration program is a multiyear initiative targeting specific areas (surficial study areas; Figure 1a, b) within the larger CICGR project area. The program is modelled after Geoscience BC's highly successful **T**argeting **R**esources through **E**xploration and **K**nowledge (TREK; e.g., Jackaman and Sacco, 2014; Jackaman et al., 2014, 2015; Sacco and Jackaman, 2015; Sacco et al., 2018) and Quesnellia Exploration Strategy (QUEST; e.g., Sacco et al., 2010; Ward et al., 2011, 2012, 2013a) surficial exploration programs (Figure 1). The CICGR program will generate high-quality baseline data integral to promoting and supporting successful mineral exploration in this challenging setting. Combined with data from the TREK (Jackaman et al., 2015) and QUEST (Ward et al., 2013a) projects, the results of this study will extend the coverage of directly comparable geochemical and mineralogical data and 1:50 000 scale surficial mapping to a large, nearly continuous portion of central BC.

This publication is also available, free of charge, as colour digital files in Adobe Acrobat® PDF format from the Geoscience BC website: http://www.geosciencebc.com/updates/summary-of-activities/.

The proven methodology applied in this program is designed to generate a geochemical and mineralogical database, and the glacial framework necessary to collect and interpret these data, such that they can be integrated into, and guide private-sector exploration. The scope of the program defines three objectives:

1) 1:50 000 scale surficial geology mapping;
2) comprehensive compilation of historical data and reanalysis of archived till survey samples; and
3) new and infill till geochemical and mineralogical surveys.

The first two tasks (year one) of the program generate 1:50 000 scale surficial base data and accomplish the reconciliation and reanalysis of historical data. The surficial geology will be interpreted from 3-D satellite imagery adhering to established mapping conventions (Deblonde et al., 2017) and be comparable to mapping from the TREK and QUEST projects. These interpretations will be used to derive till sampling suitability (TSS) and drift thickness maps. The TSS maps will identify areas well- and poorly suited to till sampling. The drift thickness maps will identify areas where drift is thin or bedrock is outcropping to guide bedrock mapping and prospecting programs. As some previous sampling programs were less selective of sample medium, the genesis of historical sample materials will be determined from available sample descriptions and the surficial mapping. Archived sample material with incomplete or outdated analytical information will be reanalyzed to provide analytical results compatible and comparable to the current provincial database.

In task three, the results of the surficial mapping and data reconciliation will be used to support the design and execution of subglacial till geochemistry and mineralogy sampling programs. These new data will be combined with the reanalyzed historical data, significantly improving sample

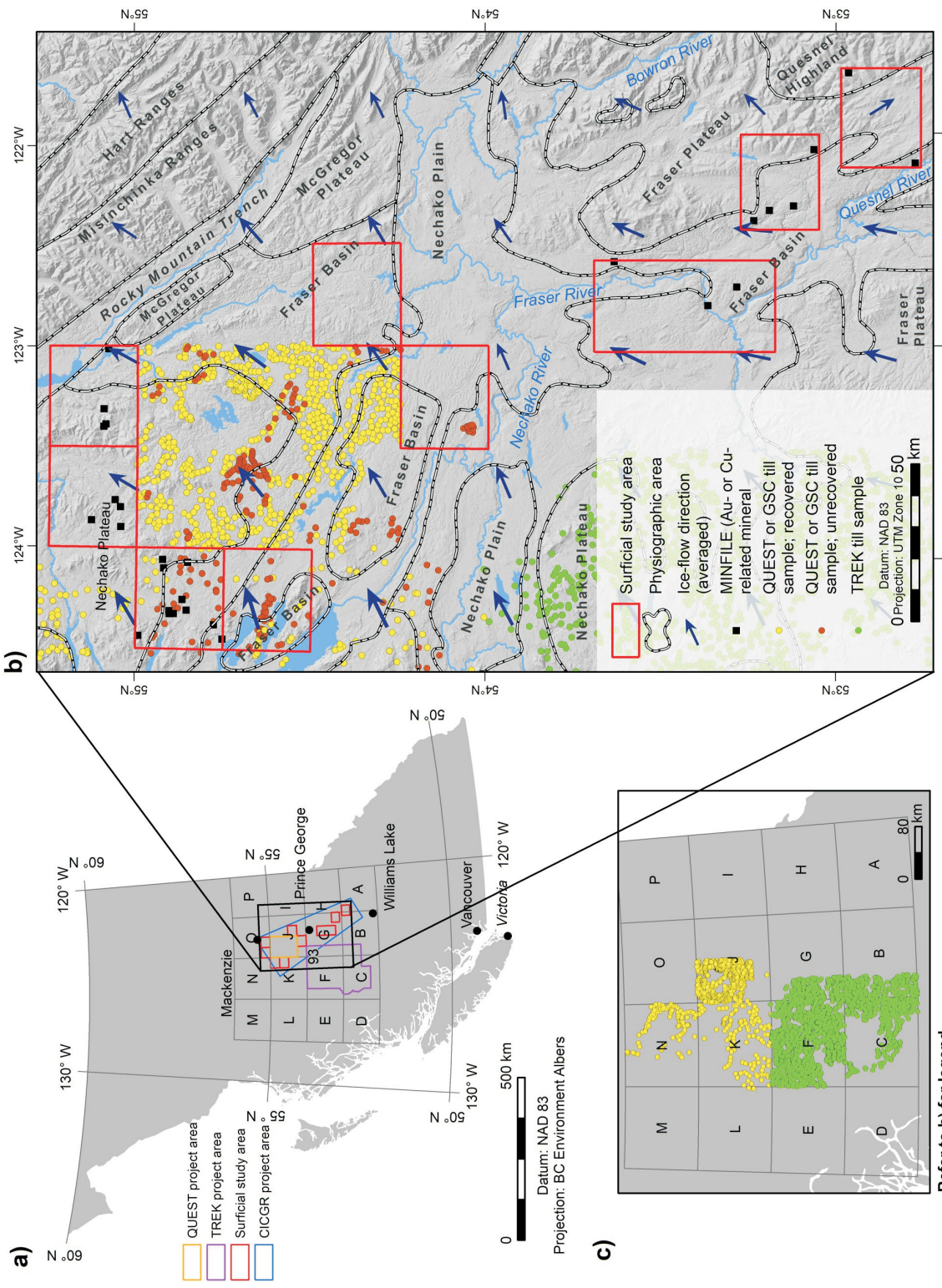

Figure 1. a) Location of Central Interior Copper-Gold Research (CICGR), **T**argeting **R**esources through **E**xploration and **K**nowledge (TREK) and Quesnellia Exploration Strategy (QUEST) project areas. **b)** Surficial study areas; physiographic areas (Holland, 1976; Mathews, 1986); MINFILE occurrences (BC Geological Survey, 2019); locations of historical surface sediment samples proposed for reanalysis from QUEST (Ward et al., 2013a) and Geological Survey of Canada (GSC) programs (Plouffe and Ballantyne, 1993; Plouffe, 1995; Plouffe and Williams, 1998); and TREK till sample locations (Jackaman et al., 2015); **c)** Distribution of recovered historical till samples (yellow symbols) in central British Columbia, which will be reanalyzed to produce data comparable to existing data from the TREK project (green symbols).

site densities across the study area, and reducing the analytical and genetic variability in the dataset, allowing for the generation of lower risk exploration targets.

Project Area and Previous Work

The surficial study areas within the CICGR project area include parts of NTS 093A, B, G, J, K and O and cover approximately 8600 km^2 (Figure 1). There are 30 MINFILE mineral occurrences related to Au or Cu mineralization within the surficial study areas (BC Geological Survey, 2019), although significantly more occur within the larger CICGR project area. The surficial study areas were determined based on three main criteria: 1) prospective geology; 2) avoidance of private land; and 3) applicability of till sampling. For continuity of the till database, the compilation of historical till data and reanalysis of archived samples extends throughout portions of the larger CICGR project area and beyond to include the full extent of previous surveys (Figure 1).

Surficial geology mapping has been conducted at various scales throughout the study area. For example, Fulton (1995) compiled surficial mapping at a scale of 1:5 000 000 for all of Canada, Tipper (1971) mapped much of the project area at a scale of 1:250 000, Plouffe (2000) mapped adjacent areas at a scale of 1:250 000 and Clague's (1998) 1:100 000 scale mapping overlaps a portion of the project area. This and similar mapping provide regional context for the current higher resolution interpretations but lack the detail necessary to inform the sampling program and evaluate the archive data. Several 1:50 000 surficial geology products exist adjacent to and overlapping the study area (e.g., Blaise-Stevens and Clague, 2007), including the terrain mapping completed for the QUEST project (Maynard et al., 2013a–c; Sacco et al., 2013a, b; Ward et al., 2013b). Where applicable, these data will be incorporated into the mapping or used as guidance.

The surficial study areas are within the Interior Plateau physiographic region and consist of parts of the Fraser Basin, Fraser Plateau, Nechako Plain, Nechako Plateau, Rocky Mountain Trench and Quesnel Highland (Holland, 1976; Mathews, 1986). Thick surficial deposits composed dominantly of till, glaciolacustrine and glaciofluvial sediments obscure most bedrock exposures.

The coalescence and subsequent divergence of glaciers in and around the northern part of the CICGR area during the last (Fraser) glaciation resulted in a complex surficial setting that has hindered exploration efforts. During the onset of the last glaciation, ice advancing from source areas north, south and west of the CICGR project area coalesced causing significant variations in ice-flow and sediment transport and altered drainage systems resulting in the development of extensive glacial lakes (Clague, 1988; Plouffe, 1997; Sacco et al., 2017). Till was deposited in most areas throughout glaciation; transport directions varied as the morphology of the ice sheet changed in relation to advance, climax and deglaciation. During deglaciation, ice retreated back to the source areas leaving behind ablating ice masses in topographic lows. The retreating and stagnating ice altered drainage resulting in the deposition of large outwash deposits and the development of glacial Lake Fraser, a dynamic, time-transgressive body of water in which significant amounts of sediment accumulated. These thick sediment units obscure the underlying bedrock and till, which typically provides a basis for exploration, hindering the collection of high-quality surface sediment data. In addition, the complex surficial environment increases the difficulty of interpreting these data. As a result, the CICGR area is underexplored and its mineral resources are largely unknown.

The collection of glacial materials to support prospecting and exploration activities has been evolving in BC since the 1990s. Previous till sampling programs have been conducted in the northwestern part of the project area (Figure 1). The Geological Survey of Canada (GSC) collected till samples during regional mapping campaigns to provide baseline exploration data (e.g., Plouffe and Ballantyne, 1993). The quality of these samples is high in reference to the interpretation of sampling material genesis, however, sampling density is low, there is no mineralogical data and outdated geochemical analytical methods were used. More recently, a till survey was completed in association with surficial mapping as part of Geoscience BC's QUEST project (Ward et al., 2013a). The density of sampling and resolution of surficial mapping are adequate and can be directly compared to that of this project, though these data will be more comparable to newer data with the completion of additional geochemical analyses.

Methods

The methodology for this program was adopted and improved from the previously completed TREK and QUEST projects. Fundamentally, the surficial geology mapping will be used to inform the reanalysis and evaluation of existing surface sediment samples and the planning and execution of the subsequent till sampling program. The till sampling program will include infill sampling in areas where the current density is insufficient and new sampling where no previous sampling has occurred. The new till sampling, combined with the reanalysis of archived samples will culminate in a directly comparable till geochemical and mineralogical dataset for the study area.

Objective 1: Surficial Mapping and Till Sampling Suitability

Objective 1 produces 1:50 000 surficial geology maps and derives till sampling suitability and drift thickness maps (Figure 2); improves the knowledge of the surficial envi-

ronment and implications to till composition; supports design and execution of till geochemical surveys; and supports future exploration efforts.

Surficial geology mapping helps to identify areas where subglacial till, the optimal surface sediment sample media for exploration, occurs at surface and provides the necessary framework to evaluate analytical results from historical and new surface sediment data. The surficial geology is interpreted at a scale of 1:50 000 from 1.5 m resolution satellite imagery converted into pseudo-stereo based on a digital elevation model (Natural Resources Canada, 2015). The imagery has been processed for use in a softcopy photo-interpretation system. The stereo-imagery enables the distinction of subtle patterns in topography and ground vegetation, which are diagnostic in interpreting the thicknesses, material types and landforms in the shallow subsurface, and geomorphological processes that have affected the region, ultimately providing the basis for the collection and interpretation of surface sediment data.

The surficial mapping will follow standardized mapping protocols established by the GSC (Deblonde et al., 2017) with minor refinements to accommodate the project-specific objectives of this assignment (e.g., geomorphological overlays; project-specific surficial map units). These protocols were chosen to maintain consistency with existing regional mapping by the GSC and similar scale mapping conducted by the BC Geological Survey (BCGS). Polygons will be delineated based on surface material and expression, with an emphasis on identifying features that affect till sampling programs such as facies discrimination (e.g., subglacial till versus ablation till), geomorphological processes, which can affect mineralogical or geochemical composition, and important linear and point features (e.g., ice-flow indicators).

The surficial geology mapping will be used to derive till sampling suitability and drift thickness map products. Till sampling suitability will be based on the distribution of subglacial till and the occurrence of postdepositional reworking (e.g., meltwater). All areas will be symbolized based on their suitability for till sampling. A multiclass suitability index will be tailored to the results of the surficial mapping and used to attribute each polygon based on the proportion of subglacial till and consideration of any geomorphological processes that may have affected the material (e.g., reworking by meltwater, slope processes, etc.). In the CICGR area, till sample suitability will be most heavily influenced by the distribution of glacial lake sediments and ablation till. Drift thickness maps will be based on the surface expression of the surficial map units. This product will provide a relative estimation of drift thickness to help determine where bedrock may be accessed at surface or in hand-dug pits, shallow excavations or require drilling.

Objective 2: Compilation of Historical Data and Reanalysis of Archive Samples

Objective 2 assesses historical till datasets to determine analytical deficiencies; identifies and recovers candidate samples from archive storage; and fills analytical data gaps. This will create a high-quality dataset that is comprehensive and directly comparable to the standard of current provincial datasets to support exploration and environmental assessments.

The reanalysis of till samples archived from previous regional geochemical surveys is a cost-effective method of significantly upgrading the utility of the associated geochemical datasets. Many of these projects were completed in the 1990s when sampling protocols were less strict, and a considerable amount of the original results were generated using analytical methods that are now outdated. Reanalysis by modern laboratory techniques and genetic interpretations of the sample medium will significantly upgrade older till geochemical datasets and create information that is directly comparable with new till data.

Approximately 700 till samples that were originally collected in the 1990s as part of a GSC regional till sampling program (Plouffe and Ballantyne, 1993; Plouffe, 1995; Plouffe and Williams, 1998) and approximately 780 samples collected in the late 2000s as part of Geoscience BC's QUEST project (Ward et al., 2013a) are proposed for reanalyses. The sample archives were located in Ottawa (ON) at the GSC's surface materials storage facility. To elevate these datasets to current standards, recommended analytical upgrades for both sample sets include an ultra-trace aqua-regia digestion (0.5 g) inductively coupled plasma–mass spectrometry (ICP-MS) package for 53 elements and for major and minor elements by lithium borate fusion inductively coupled plasma–emission spectrometry (ICP-ES) on the silt- plus clay-sized (<0.063 mm) fraction. In cooperation with the GSC, representative 2 g splits of the silt- plus clay-sized (<0.063 mm) fraction of bulk archive sample material was retrieved from the storage facilities in Ottawa. Due to potential deficiencies of available material, it may not be possible to recover material from all targeted archive samples.

The samples will be delivered to an accredited laboratory for analysis. Prior to this, analytical duplicate and control reference samples will be inserted into the sample sequence to monitor and assess the accuracy and precision of the new analytical results.

The archive samples will be categorized based on sediment genesis in relation to subglacial till. This interpretation is based on the original sample notes, existing or new mapping and ground-truthing during fieldwork. The genetic category for each sample will be included in the final data compilation.

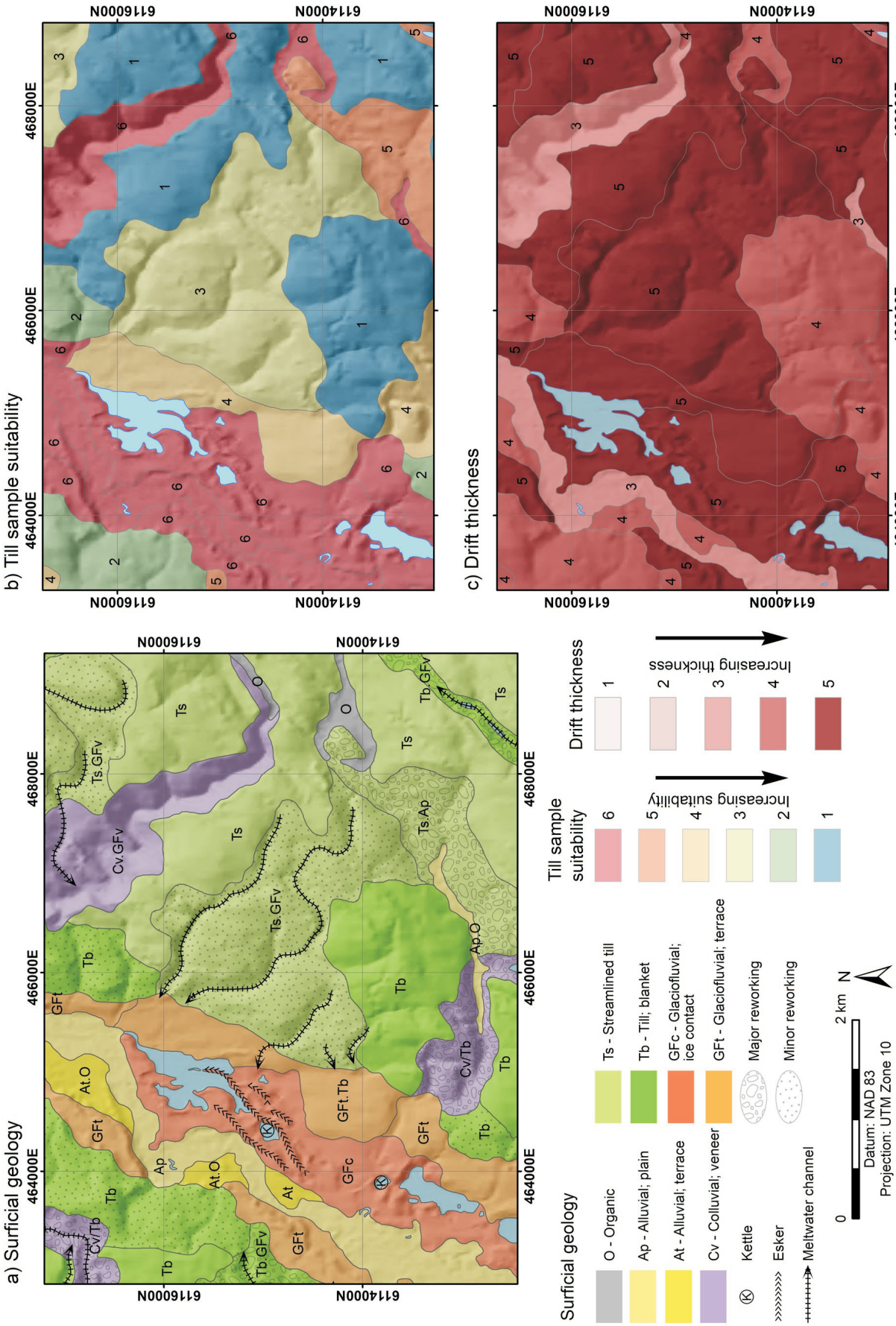

Figure 2. a) Example of surficial geology, **b)** derived till sampling suitability and **c)** drift thickness mapping in the Central Interior Copper-Gold Research project area.

Objective 3: Till Geochemical and Mineralogical Survey

Objective 3 will be conducted during year two of the program, upon the completion of the surficial geology mapping and archive sample compilation. Till geochemical and mineralogical surveys will be conducted to established standards to produce high-quality field and analytical results that are consistent and directly comparable with the existing provincial till geochemical database. Sampling strategies will 1) include new and infill sampling to attain target sample site densities; 2) provide new trace metal and mineral indicator data; 3) create character samples that can be archived for future analytical work; and 4) support exploration and environmental assessment.

Subglacial till is the primary target because it is a first derivative of bedrock (Schilts, 1993), is transported in the direction of ice flow and provides a larger anomaly than the original bedrock source (Levson, 2001). Target sample media must be correctly identified to limit variability within the dataset and ensure contrasts in the dataset (i.e., anomalies) are related to mineralization rather than material genesis. At each potential till sample site, the exposed material will be carefully assessed for texture, structure, density, matrix percentage and clast mode, shape and presence of stria. If the sediment is determined to be subglacial till, the sample observations and site information, including location, the type of exposure, soil development, surficial map unit, topographic position, aspect, slope, drainage and any stratigraphic information will be recorded. At every site, a 1–2 kg subglacial till sample and 50 stones of large pebble to small cobble size will be collected. At approximately every other site, a 10–12 kg bulk subglacial till sample will be collected. Sampling locations will be based on an approximately 2 km, staggered grid aligned with ice flow. Where archive sample density is low, infill sampling will be conducted. Samples will be collected from natural or anthropogenic exposures (>1 m depth), such as roadcuts, borrow pits, hand- and machine-dug soil pits, and river and lake cuts.

The subglacial till samples will be shipped to accredited laboratories where the 1–2 kg samples will be dried, an archive of the original till sample will be generated, and the remaining material will be sieved to produce splits of the silt- plus clay-sized (<0.063 mm) fraction. The splits will be analyzed for minor and trace elements by an ultra-trace aqua-regia digestion (0.5 g) ICP-MS package for 53 elements and by instrumental neutron activation analysis (INAA) for total gold plus 34 elements. Major and minor elements will be determined for till samples by ICP-ES following a lithium metaborate/tetraborate fusion and dilute acid digestion. This analytical package will include loss-on-ignition by weight difference after ignition at 1000ºC, plus total carbon and sulphur by LECO analysis. LECO analysis converts carbon and sulphur forms in a sample into CO_2 and SO_2 by combustion in an induction furnace. The concentrations of CO_2 and SO_2 are measured by infrared absorption and thermal conductivity to determine total concentrations of carbon and sulphur. Quality control for analytical determinations will include the use of field duplicates, analytical duplicates, reference standards and blanks, based on established protocols (Spirito et al., 2011).

Using a combination of gravity tables and heavy liquids, the 10–12 kg bulk till samples will be processed for gold grain concentrates (<2.0 mm) plus heavy and medium mineral concentrates (0.25–2.0 mm) for gold and porphyry copper indicator mineral identification and counts.

The pebble samples will be collected to provide insight on the direction and distance of glacial transport from bedrock source units. Clast lithologies will be grouped into broad categories that reflect the main lithologies of bedrock sources.

Progress and Future Work

During the first year of the program, the imagery from which the surficial geology interpretations are based was acquired and processed for stereo viewing. To date, preliminary interpretations have been completed for approximately 70% of the study area. Additionally, preliminary TSS definitions have been established that will be used to categorize the surficial interpretations (Table 1). Upon completion of the draft mapping, all interpretations will be reviewed by the senior mapper and updates will be made to ensure correctness and consistency across the surficial study areas. An inventory of surficial units will be developed and the preliminary TSS definitions will be updated to ensure applicability to the specific surficial setting of the project area.

Table 2 indicates the historical sample sources and their recovery status. To date, 926 of 1487 targeted samples have been recovered for minor and trace elements by an ultra-trace aqua-regia digestion (0.5 g) ICP-MS package for 53 elements and for major and minor elements by ICP-ES following a lithium metaborate/tetraborate fusion and dilute acid digestion. A compiled database of original analytical data is currently being developed for the historical samples. Upon completion of the mapping, genetic attributions will be added to the database. Recovered archive sample material will be sent to Bureau Veritas Commodities Laboratory (Vancouver, BC) for processing and analysis. The results of these analyses will be compiled and appended to the current database.

The surficial mapping products will be released digitally and as three georeferenced PDF map sets (surficial geology, till sampling suitability and drift thickness). All mapping files will be provided in Esri geodatabase and

Table 1. Proposed till sampling suitability classifications for the Central Interior Copper-Gold Research surficial exploration project.

Till sampling suitability	Description	Implications to exploration
1	All subglacial till	Most surface sediment is composed of till and suitable for sampling; minor amounts of other materials may occur even where not indicated in map unit.
2	Dominantly subglacial till or all subglacial till with minor reworking	Till is the dominant surficial material, or greater than half of the map unit is in situ subglacial till. Most of the map unit is suitable for till sampling.
3	Lesser amounts of subglacial till or dominantly subglacial till with minor reworking	In situ subglacial till comprises less than half of the map unit. Focus on high ground and down-ice from bedrock outcrops to increase the probability of finding till suitable for sampling.
4	Lesser amounts of till with minor reworking or all till with major reworking	Suitable till for sampling likely occurs in only a small proportion of map unit. Dominantly composed of reworked till or other materials. Focus on high ground and down-ice from bedrock outcrops to increase the probability of finding till suitable for sampling.
5	Till is dominant material with major reworking	Map unit dominantly composed of reworked till, which is not suitable for sampling, and other materials. Till suitable for sampling is most likely to occur on high ground, but will be very limited in extent.
6	Minor till with major reworking or no till	Unlikely to locate till suitable for sampling within map unit.

Table 2. Sources and status of archive sample compilation for the Central Interior Copper-Gold Research surficial exploration project.

Report	Year	Recovered	Pending	Archived fraction	NTS map area
Geoscience BC Report 2013-15 (Ward et al., 2013a)	2013	638	143	Unprocessed	093J/03, 05, 06, 10–14
GSC Open File 2593 (Plouffe and Ballantyne, 1993)	1990, 1991	225	63	0.063 mm	093K/01–08, 10–12, 15, 16; 093N/01, 02, 06–11
GSC Open File 3194 (Plouffe, 1995)	1992, 1993, 1994	53	353	0.063 mm/ unprocessed	093K/01–10, 12, 14–16; 093L/01, 08; 093N/02–12, 14–16; 093O/05, 12
GSC Open File 3687 (Plouffe and Williams, 1998)	1997	2	0	0.063 mm	093K/04
Unpublished	1997, 1999	8	2	0.063 mm	093K/O9, 15; 093N/02, 03, 06, 11

Abbreviation: GSC, Geological Survey of Canada

shapefile format, embedded with appropriate GSC symbology codes such that users can easily import and symbolize these data to assist with their own exploration activities. Historical and new geochemical data and mineralogy will be released as digital databases and include all analytical results and quality control data.

Conclusions

The integration of surficial mapping and results of surface sediment samples analyses into a comprehensive dataset contributes to the ongoing development of a province-wide, regional, exploration database. Survey methods conform to strict specifications; compiled information is comprehensive, compatible and reproducible; and the package complements a wide range of other ongoing geoscience initiatives and exploration activities. The project results, combined with data from the earlier **T**argeting **R**esources through **E**xploration and **K**nowledge (TREK) and QUEST projects, extend the coverage of comprehensive geochemical and mineralogical data to a large portion of central British Columbia, and will promote increased awareness in a highly prospective region, assist in the identification of new exploration targets and support follow-up activities.

Acknowledgments

This program was funded by Geoscience BC. The authors would like to thank A. Plouffe from the Geological Survey of Canada for his heroic efforts to recover archive samples from storage in Ottawa and his support in the development of this project. Assistance in archive sample recovery was also provided by R. Lett and T. Ferbey. A special thank you to B. Ward for his thorough review, thoughtful comments and provision of unpublished data.

References

BC Geological Survey (2019): MINFILE BC mineral deposits database; BC Ministry of Energy, Mines and Petroleum Resources, BC Geological Survey, URL <http://minfile.ca/> [September 2019].

Blais-Stevens, A. and Clague, J.J. (2007): Surficial geology, Cottonwood, British Columbia; Geological Survey of Canada, Open File 5270, scale 1:50 000.

Clague, J.J. (1988): Quaternary stratigraphy and history, Quesnel, British Columbia; Géographie physique et Quaternaire, v. 42, p. 279–288.

Clague, J.J. (1998): Surficial geology, Cluculz Lake, British Columbia; Geological Survey of Canada, Open File 3638, scale 1:100 000.

Deblonde, C., Cocking, R.B., Kerr, D.E., Campbell, J.E., Eagles, S., Everett, D., Huntley, D.H., Inglis, E., Parent, M., Plouffe, A., Robertson, L., Smith, I.R. and Weatherston, A. (2017): Surficial data model, version 2.3.0: revisions to the science language of the integrated Geological Survey of Canada data model for surficial geology maps; Geological Survey of Canada, Open File 8236, 60 p.

Fulton, R.J. (1995): Surficial materials of Canada; Geological Survey of Canada, Map 1880A, scale 1:5 000 000.

Holland, S.S. (1976): Landforms of British Columbia: a physiographic outline (second edition); BC Ministry of Energy, Mines and Petroleum Resources, Bulletin 48, 138 p.

Jackaman, W. and Sacco, D. (2014): Geochemical and mineralogical data, TREK project, Interior Plateau, British Columbia; Geoscience BC, Report 2014-10, 13 p., URL <http://www.geosciencebc.com/reports/gbcr-2014-10/> [November 2019].

Jackaman, W., Sacco, D. and Lett, R.E. (2014): Geochemical reanalysis of archived till samples, TREK project, Interior Plateau, central BC (parts of NTS 093C, 093B, 093F & 093K); Geoscience BC, Report 2015-09, 5 p., URL <http://www.geosciencebc.com/reports/gbcr-2015-09/> [November 2019].

Jackaman, W., Sacco, D.A. and Lett, R.E. (2015): Regional geochemical and mineralogical data, TREK project – year 2, Interior Plateau, British Columbia; Geoscience BC, Report 2015-12, 13 p., URL <http://www.geosciencebc.com/reports/gbcr-2015-12/> [November 2019].

Levson, V.M. (2001): Regional till geochemical surveys in the Canadian Cordillera: sample media, methods, and anomaly evaluation; *in* Drift Exploration in Glaciated Terrain, M.B. McClenaghan, P.T. Bobrowsky, G.E.M. Hall and S.J. Cook (ed.), Geological Society, Special Publication No. 185, p. 45–68.

Levson, V.M., Giles, T.R., Cook, S.J. and Jackaman, W. (1994): Till geochemistry of the Fawnie Creek area (93F/03); BC Ministry of Energy, Mines and Petroleum Resources, BC Geological Survey, Open File 1994-18, 40 p., URL <https://www2.gov.bc.ca/gov/content/industry/mineral-exploration-mining/british-columbia-geological-survey/publications/openfiles-1999-1990#1994> [November 2019].

Mathews, W.H. (1986): Physiographic map of the Canadian Cordillera; Geological Survey of Canada, "A" Series Map 1710A, scale 1:5 000 000.

Maynard, D.E., Ward, B.C., Sacco, D.A. and Geertsema, M. (2013a): Terrain map of Bugle Lake map area, British Columbia (NTS 093J/06); Geoscience BC, Map 2013-10-6, scale 1:50 000, URL <http://www.geosciencebc.com/i/project_data/GBC_Report2013-10/GBC_Map2013-10-6.pdf> [November 2019].

Maynard, D.E., Ward, B.C., Sacco, D.A. and Geertsema, M. (2013b): Terrain map of Great Beaver Lake map area, British Columbia (NTS 093J/05); Geoscience BC, Map 2013-10-5, scale 1:50 000, URL <http://www.geosciencebc.com/i/project_data/GBC_Report2013-10/GBC_Map2013-10-5.pdf> [November 2019].

Maynard, D.E., Ward, B.C., Sacco, D.A. and Geertsema, M. (2013c): Terrain map of Weedon Lake map area, British Columbia (NTS 093J/11); Geoscience BC, Map 2013-10-3, scale 1:50 000, URL <http://www.geosciencebc.com/i/project_data/GBC_Report2013-10/GBC_Map2013-10-3.pdf> [November 2019].

Natural Resources Canada (2015): Canadian Digital Elevation Model; Natural Resources Canada, URL <https://open.canada.ca/data/en/dataset/7f245e4d-76c2-4caa-951a-45d1d2051333> [October 2019].

Plouffe, A. (1995): Geochemistry, lithology, mineralogy and visible gold grain content of till in the Manson River and Fort Fraser map areas, central British Columbia (NTS 093K, N); Geological Survey of Canada, Open File 3194, 119 p.

Plouffe, A. (1997): Ice-flow and late-glacial lakes of the Fraser glaciation, central British Columbia; *in* Current Research 1997-A/B, Geological Survey of Canada, p. 133–143.

Plouffe, A. (2000): Quaternary geology of the Fort Fraser and Manson River map-areas, central British Columbia; Geological Survey of Canada, Bulletin 554, 62 p.

Plouffe, A. and Ballantyne, S.B. (1993): Regional till geochemistry, Manson River and Fort Fraser area, British Columbia (NTS 093K, N), silt plus clay and clay size fractions; Geological Survey of Canada, Open File 2593, 224 p.

Plouffe, A. and Williams, S.P. (1998): Regional till geochemistry of the northern sector of Nechako River map area, British Columbia (NTS 093F); Geological Survey of Canada, Open File 3687, scale 1:400 000.

Plouffe, A., Levson, V.M. and Mate, D.J. (2001): Till geochemistry of the Nechako River map area (NTS 93F), central British Columbia; Geological Survey of Canada, Open File 4166, 66 p.

Sacco, D.A. and Jackaman, W. (2015): Targeted geochemical and mineralogical surveys in the TREK project area, central British Columbia (parts of NTS 093B, C, F, G): year two; *in* Geoscience BC Summary of Activities 2014, Geoscience BC, Report 2015-01, p. 1–12, URL <http://cdn.geosciencebc.com/pdf/SummaryofActivities2014/SoA2014_Sacco.pdf> [November 2019].

Sacco, D.A., Lett. R., Jackaman, W. and Elder, B. (2018): Advanced processing of the TREK project geochemical data: identifying and enhancing geochemical anomalies in the TREK project area using sediment transport modeling combined with multimedia and multivariate analysis; Geoscience BC, Report 2018-07, 56 p., URL <http://www.geosciencebc.com/i/project_data/GBCReport2018-07/GBCReport2018-07.pdf> [November 2019].

Sacco, D.A., Ward, B.C., Geertsema, M. and Maynard, D.E. (2013a): Terrain map of Carp Lake map area, British Columbia (NTS 093J/14); Geoscience BC, Map 2013-10-2, scale 1:50 000, URL <http://www.geosciencebc.com/i/project_data/GBC_Report2013-10/GBC_Map2013-10-2.pdf> [November 2019].

Sacco, D.A., Ward, B.C., Geertsema, M. and Maynard, D.E. (2013b): Terrain map of Salmon Lake map area, British Columbia (NTS 093J/13); Geoscience BC, Map 2013-10-1, scale 1:50 000, URL <http://www.geosciencebc.com/i/project_data/GBC_Report2013-10/GBC_Map2013-10-1.pdf> [November 2019].

Sacco, D.A., Ward, B.C., Lian, O.B., Maynard, D.E. and Geertsema, M. (2017): Quaternary geology of part of the McLeod Lake map area (NTS 093J), central British Colum-

bia: lithostratigraphy, glacial history, and chronology; Canadian Journal of Earth Sciences, v. 54, no. 10, p. 1063–1084.

Sacco, D.A., Ward, B.C., Maynard, D., Geertsema, M. and Reichheld, S. (2010): Terrain mapping, glacial history and drift prospecting in the north west corner of McLeod Lake map area (part of NTS 093J), central British Columbia; *in* Geoscience BC Summary of Activities 2009, Geoscience BC, Report 2010-01, p. 33–42, URL <http://cdn.geosciencebc.com/pdf/SummaryofActivities2009/SoA2009_Sacco.pdf> [November 2019].

Shilts, W. (1993): Geological Survey of Canada's contributions to understanding the composition of glacial sediments; Canadian Journal of Earth Sciences, v. 30, p. 333–353.

Spirito, W.A., McClenaghan, M.B., Plouffe, A., McMartin, I., Campbell, J.E., Paulen, R.C. and Hall, G.E.M. (2011): Till sampling and analytical protocols for GEM projects: from field to archive; Geological Survey of Canada, Open File 6850, 83 p.

Tipper, H.W. (1971): Glacial geomorphology and Pleistocene history of central British Columbia; Geological Survey of Canada, Bulletin 196, 103 p.

Ward, B.C., Leybourne, M.I. and Sacco, D.A. (2011): Drift prospecting within the QUEST project area, central British Columbia (NTS 093J): potential for porphyry copper-gold, volcanogenic massive sulphide mineralization and gold-copper veins; *in* Geoscience BC Summary of Activities 2010, Geoscience BC, Report 2011-01, p. 73–96, URL <http://cdn.geosciencebc.com/pdf/SummaryofActivities2010/SoA2010_Ward_etal.pdf> [November 2019].

Ward, B.C., Leybourne, M.I. and Sacco, D.A. (2012): Heavy mineral analysis of till samples within the QUEST project area, central British Columbia (NTS 093J); *in* Geoscience BC Summary of Activities 2011, Geoscience BC, Report 2012-01, p. 59–68, URL <http://cdn.geosciencebc.com/pdf/SummaryofActivities2011/SoA2011_Ward.pdf> [November 2019].

Ward, B.C., Leybourne, M.I., Sacco, D.A., Lett, R.E. and Struik, L.C. (2013a): Drift prospecting for porphyry copper-gold, volcanogenic massive sulphide mineralization and precious and base metal veins within the QUEST project area, central British Columbia (NTS 093J); Geoscience BC, Report 2013-15, 59 p., URL <http://www.geosciencebc.com/reports/gbcr-2013-15/> [November 2019].

Ward, B.C., Maynard, D.E., Sacco, D.A. and Geertsema, M. (2013b): Terrain map of Carrier Lake map area, British Columbia (NTS 93J/12); Geoscience BC, Map 2013-10-4, scale 1:50 000, URL <http://www.geosciencebc.com/i/project_data/GBC_Report2013-10/GBC_Map2013-10-4.pdf> [November 2019].

Real-Time Detection of Bedrock Mineralization and Geological Faults Beneath Glacial Deposits in Central British Columbia using Onsite Soil Gas Carbon Dioxide and Oxygen Analysis by Electronic Gas Sensors (NTS 093A/58, 093G/03)

R.E. Lett, Geochemist, Victoria, British Columbia, raylett@shaw.ca

D.A. Sacco, Palmer, Vancouver, British Columbia

B. Elder, Palmer, Vancouver, British Columbia

W. Jackaman, Noble Exploration Services Ltd., Jordan River, British Columbia

Lett, R.E., Sacco, D.A., Elder, B. and Jackaman, W. (2020): Real-time detection of bedrock mineralization and geological faults beneath glacial deposits in central British Columbia using onsite soil gas carbon dioxide and oxygen analysis by electronic gas sensors (NTS 093A/58, 093G/03); *in* Geoscience BC Summary of Activities 2019: Minerals, Geoscience BC, Report 2020-01, p. 93–100.

Introduction

Geophysical surveys can detect geological faults and related sulphide mineralization, but reliably identifying these features from survey data can be difficult where their signatures are masked by hostrocks with similar properties, or access is hindered by overlying glacial sediments. Faults provide a pathway for the transportation of fluids and gases upward from deeper, crustal rocks to the surface, and thus, fluctuations in soil gas concentrations can be a result of concealed structures and oxidizing sulphide mineralization at depth. Carbon dioxide (CO_2) migration into the soil from depth may also be accompanied by changes in mineral chemistry, such as formation of secondary carbonate minerals. Hence, anomalous soil pH and trace-element values may directly or indirectly reflect increased migration of CO_2 through the soil to the surface (Smee, 1998). Several examples of soil gas anomalies have been reported from the northern hemisphere, associated with a range of mineral deposit styles. Lovell et al. (1979, 1980) reported a decrease in oxygen (O_2) and an increase in CO_2 in the soil gas sampled over Pb-Zn sulphide–mineralized faults beneath thick glacial deposits in Ireland. McCarthy et al. (1986) found elevated CO_2 and CH_4 but decreased O_2 in soil gas sampled at a depth of 0.5 m over the Crandon massive pyrite-sphalerite-galena deposit in Wisconsin, United States. The massive sulphide mineralization was buried beneath up to 65 m of glacial deposits. Duddridge et al. (1991) observed a similar pattern of increase in CO_2 and decrease in O_2 over faults in the soil gas sampled at three glaciated sites in the United Kingdom. Highsmith (2004) proposed a model for the formation of soil gas anomalies and described the use of a field-portable system for measuring CO_2 and O_2 in Arizona, United States.

In Hale's (2010) review of the progress and status of research into the application of soil gas chemistry to mineral exploration, it was identified that past surveys have either measured soil gas CO_2 and O_2 onsite (e.g., Lovell et al., 1980) or collected a soil gas sample for later analysis (e.g., McCarthy et al., 1986). Onsite analysis has the advantage of a real-time measurement, but the commercial instrumentation used for CO_2 and O_2 analysis was historically expensive and difficult to use in remote areas. Previous studies in glaciated areas have also focused on soil gas dispersion from massive sulphides and not from other styles of sulphide mineralization, such as disseminated porphyry Cu-Au deposits.

The availability of small, relatively inexpensive CO_2 and O_2 sensors, such as those distributed by CO2Meter Inc. and Vernier Software and Technology, now provides an opportunity for devising and testing an economical, onsite, real-time analytical system for measuring these gases. The purpose of this study is to develop a cost-effective soil gas measurement system that will aid in the detection of geological faults and mineralization buried beneath surficial cover. This paper describes the development of a compact system able to measure CO_2 and O_2 concentrations in soil gas, and testing of the system in the field by sampling soil gas and soil geochemistry over two drift-covered, fault-controlled, porphyry Cu-Au disseminated sulphide mineral occurrences in central British Columbia (BC; Figure 1).

System Configuration

A system able to generate reliable, real-time geochemical analyses can complement geophysical survey results and aid in bedrock mapping. Ideally, the system should be compact, portable, reliable and relatively economical to be practical for mineral exploration. Several component con-

This publication is also available, free of charge, as colour digital files in Adobe Acrobat® PDF format from the Geoscience BC website: http://www.geosciencebc.com/updates/summary-of-activities/.

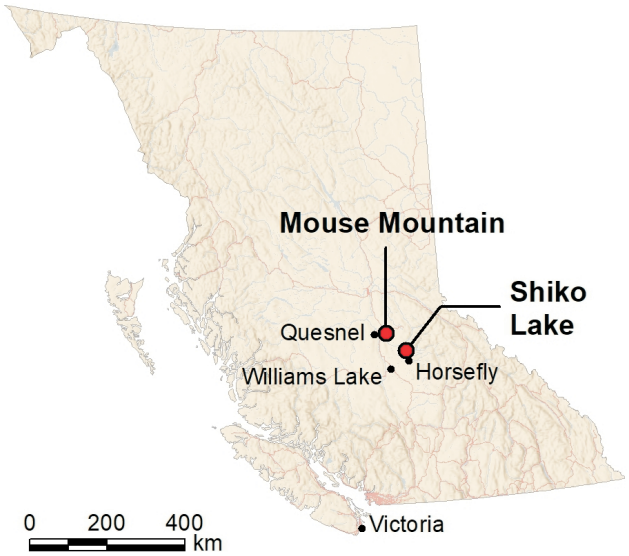

Figure 1. Location of the Mouse Mountain and Shiko Lake study areas in central British Columbia.

figurations were tested before the final system was devised; the final system components, shown in Figure 2, were purchased for roughly $1,100.00 (excluding the computer) and include:

- A CO_2 detector (SprintlRS 5% CO_2 Smart Sensor) and an O_2 detector (Model 25% O_2 UVFLUX MX) distributed by CO2Meter Inc., Ormond Beach, Florida, United States. The sensors, mounted on a circuit board, measure gas concentration, barometric pressure, temperature and relative humidity. Each sensor body has a built-in manifold with two inlet ports for attachment of flexible PVC tubes (CO2Meter Inc. 2015). One inlet port on the CO_2 sensor manifold is connected by a PVC tube to a corresponding inlet port on the O_2 sensor so that the gas can flow continuously through the two sensors. Each sensor circuit board can be linked by USB cable to a computer. The sensors, circuit boards, PVC tube link and USB cables are installed in a waterproof case (Figure 2a).
- A sampling probe constructed from a hollow, 12.7 mm diameter, 1.5 m long steel tube fitted with a retractable, pointed tip and a hammer mounted on the tube axis to drive the tube into the overburden (Figure 2b).
- A 6-volt, battery-powered diaphragm pump designed to continuously draw soil gas through the hollow-steel-tube sampler and PVC tubing from overburden and into the sensors (Figure 2c). The soil gas flow from the hollow-steel-tube soil sampler to the sensors is controlled by two shut-off valves (Figure 2a) that allow alternatively sampling either soil gas, for measuring CO_2 and O_2, or air, for calibrating the sensors with atmospheric CO_2 and O_2. A hydrophobic, 0.26 µm filter between the PVC tubing to the steel-tube sampler protects the sensors from particulate and soil moisture damage (Figure 2a).
- A laptop computer (not pictured) equipped with CO2-Meter Inc. GasLab 2.1 software and connected by USB cables to the CO_2 and O_2 sensor circuit boards. The GasLab 2.1 software measures CO_2 and O_2 concentrations and monitors barometric pressure, temperature and percent relative humidity. The software also displays these variables graphically, and has an option for capturing digital CO_2 and O_2 concentrations for further data analysis.

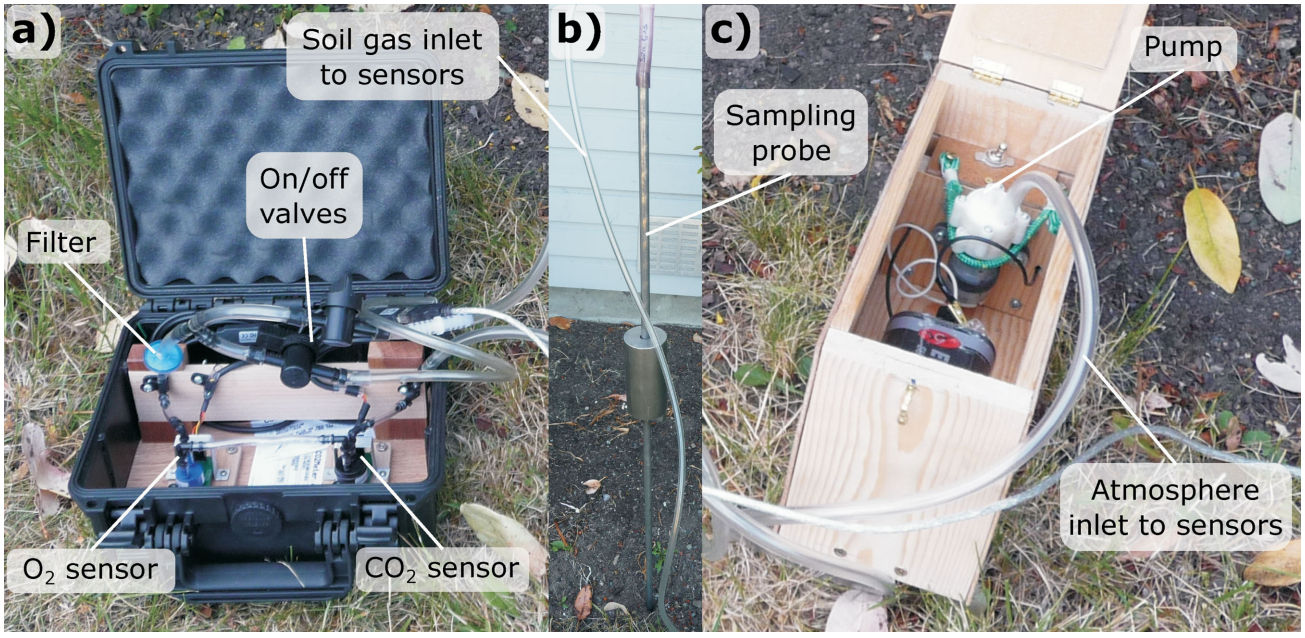

Figure 2. The soil gas sampling and analysis system. Left to right **a)** sensor unit (25 by 22 by 11 cm), **b)** sampling probe (120 by 1.2 cm), **c)** pump and power source (25 by 12 by 16 cm).

System Operation

Ideally, a sample site is level, free of debris and relatively dry, as excessive soil moisture can limit gas mobility. The site location co-ordinates are recorded by GPS, the site photographed, and the soil gas sampling probe, pump and sensor unit assembled. Before sampling soil gas, a small hand pump is attached to the probe with PVC tubing and soil gas pumped to ensure a continuous and stable gas flow through the probe and into the measurement system. The PVC tubing with hydrophobic in-line filter and shut-off valve is attached to an inlet port on the O_2 sensor manifold. A second PVC tube, attached to an inlet port on the CO_2 sensor manifold, is connected to the diaphragm pump.

A solid, 12.7 mm diameter, pointed steel rod is first hammered into the soil to approximately 30 cm depth. The rod is extracted, examined for visible evidence of excess moisture and replaced by the hollow-steel-tube sampler driven farther, to 40–50 cm depth. The hollow steel tube is then carefully withdrawn 1 cm to open the retractable probe tip so that soil gas can flow into the tube. PVC tubing is connected from the sensor unit to the top of the hollow steel tube, the shut-off valve to the sensor unit closed, the valve to the atmosphere line opened and the electric diaphragm pump started.

After connecting the sensors to the laptop computer with the USB cables, the GasLab 2.1 software is opened. Individual sensor settings (sensor model number, computer port) are entered and the CO_2 and O_2 measurement sequence started. The inlet to the atmospheric air PVC tube is positioned 3 m from the system, to avoid possible human CO_2 contamination, and the shut-off valve to the atmosphere opened. Before measuring soil CO_2 and O_2 concentrations, each sensor is calibrated to atmospheric levels (CO_2 = 400 ppm, O_2 = 209 050 ppm); while there are diurnal and seasonal changes in CO_2 and O_2 concentration, the values used for calibration in the software are a reasonable average. Atmospheric CO_2 and O_2 are then measured at 10 second intervals, generally for two minutes, before the shut-off valve to the soil gas sampler is opened and the valve to the atmosphere closed. Measurements of soil CO_2 and O_2 concentrations continue at 10 second intervals for a further two minutes (Figure 3). Profiles of CO_2 and O_2 concentration and temperature show that CO_2 levels typically increase to a plateau and O_2 levels decrease (sections A and B in Figure 3). Finally, the valve to the atmosphere is opened, the valve to the soil gas sampler closed and measurements continued for two more minutes, to complete the measurement sequence (section C in Figure 3). The CO_2 and O_2 concentration, barometric pressure, temperature and relative humidity are captured by the software and recorded as a digital (.csv) text file. A full soil gas sampling and measurement sequence can generally be completed in 20 minutes.

Field Testing

Prior to fieldwork in central BC, the soil gas system was tested locally near Victoria, BC, to identify and resolve any operational issues. Upon satisfactory system testing, two field locations were chosen in central BC based on the inferred occurrence of faults, existence of Cu-Au porphyry disseminated sulphide mineralization and glacial drift: 1) Mouse Mountain (MINFILE 093G 003; BC Geological Survey, 2019) mineral occurrence, 13 km east of Quesnel; and 2) the Shiko Lake property (MINFILE 093A 058), 17 km east of Horsefly (Figure 1). The program was carried out in July and August of 2019. Soil gas and pH measurements and soil samples were collected from each sample site along three transects at Mouse Mountain and two transects at Shiko Lake that cross inferred faults. Sampling

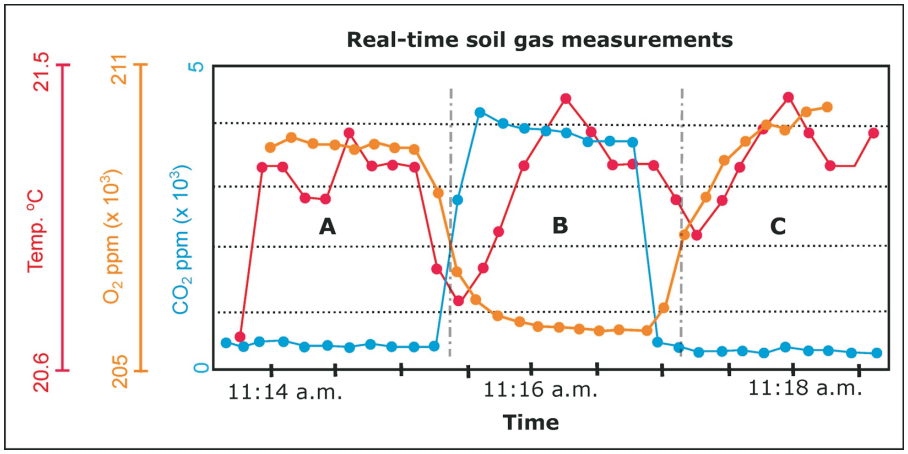

Figure 3. An example of GasLab 2.1 software display from the temporal analysis of soil gas and atmospheric air for CO_2 (blue line), O_2 (tan line) and temperature (red line) at Mouse Mountain site 1101. On the graph, sections A and C are CO_2 measured in atmospheric air flow, and section B is CO_2 measured in soil air. In this example, a total of 32 measurements are made over a period of roughly five minutes.

on a regular grid (e.g., 25 m by 25 m) would have been preferable to detect faults. However, because actual fault locations were uncertain, there were time constraints to sampling and limitations to accessing sites, a more flexible, variable sampling pattern was adopted. Soil samples were sent to Bureau Veritas Minerals Laboratory (Vancouver, BC) for geochemical analysis of trace elements by a modified aqua-regia digestion and a water leach followed by inductively coupled plasma–mass spectrometry. Soil pH, and pH after addition of HCl to allow calculation of the inverse difference hydrogen (IDH) factor (after Smee, 2009) were determined from a subsample in camp. High IDH factor values, representing the inverse of the difference between the acidified and non-acidified H^+ concentrations, are proposed by Smee (2009) to indicate soil where carbonate minerals have been remobilized and precipitated.

At the Mouse Mountain Valentine sulphide-mineralized zone, Cu-Au porphyry–style disseminated chalcopyrite, pyrite and bornite are associated with Jurassic calcalkaline plutons intruded into Upper Triassic to Lower Jurassic Nicola Group sedimentary and volcanic rocks (Figure 4). Sampling was carried out near the Valentine zone, where strongly fractured and faulted fine-grained diorite, monzonite and syenite are in contact with propylitic-, phyllic- and potassic-altered volcanic breccia (Schimann, 2014). The exact location of an inferred northeast-southwest-trending fault (Figure 4) crossing the area south of the Valentine zone is debatable (Jonnes and Logan, 2007). Bedrock is exposed at the Valentine zone, but is concealed in the south under a mantle of till estimated at 2 to 3 m thickness that was deposited during northward ice flow. The south-facing slope below the Valentine zone has been disturbed by logging and has predominantly Brunisolic soils. Soil gas and soil sampling along three transects south from the Valentine zone generated 44 soil gas measurements from 33 sample sites (Figure 4). Soil samples were collected at 29 sites from the Bm horizon beneath the Ae horizon (where present) for geochemical analysis, pH and IDH determinations.

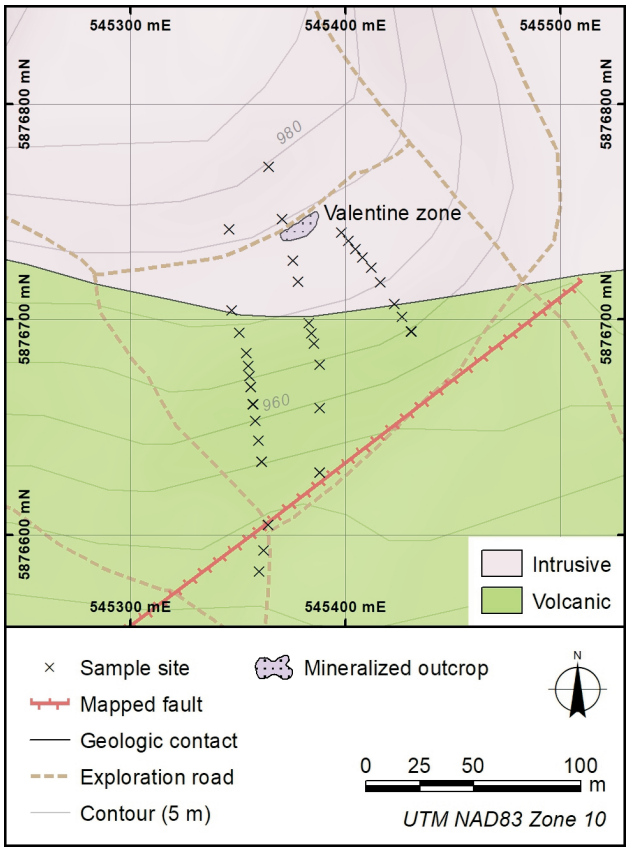

Figure 4. Mouse Mountain study area, sample locations and geology (simplified geology and fault locations from Schimann, 2014).

At Shiko Lake, a diorite-syenite-monzonite stock encloses older, coeval and comagmatic Nicola Group augite basalt, felsic heterolithic breccia, massive to locally laminated tuff, and maroon-coloured, possibly subaerial basaltic flows (Morton, 2003; Lesage, 2011). Hornfelsed, pyrite-bearing siltstone in contact with diorite at the Quarry zone is covered by a mantle of till estimated at 1 to 2 m thick that was deposited during westward ice flow. Mineralization at the Quarry zone consists of copper sulphides and gold in fractures and disseminated in a composite alkalic augite-monzonite-syenite intrusion. Andesite at the East zone is intersected by northeast-striking faults and the bedrock is partially concealed by till. Past mineral exploration and logging have disturbed the land surface. The soil formed at the Quarry and East zones is a Brunisol. Soil gas and soil samples were collected over the Quarry and East zones (Figure 5). Fifteen soil gas measurements were made at the Quarry and East zones from 14 sites, and 14 soil samples were collected for geochemical analysis and pH and IDH determinations.

Soil Gas CO_2 and O_2 Data Processing

In addition to the real-time graphs produced by Gas Lab 2.1 (e.g., Figure 3) that display CO_2 and O_2 variation, the individual CO_2 and O_2 concentrations are also recorded at 10-second intervals throughout the measurement sequence. From these data the mean, standard deviation and percent relative standard deviation (%RSD) are calculated, to estimate mean CO_2 and O_2 values and precision of sensor measurements. The three sets of analyses are used to calculate the statistics representing data recorded for atmospheric air (section A in Figure 3), soil gas (section B in Figure 3) and a second atmospheric air measurement (section C in Figure 3). Comparison of the means in graph sections A and C shows any sensor drift during the measurement sequence, and %RSD values indicate precision of sensor measurement. Table 1 lists mean and %RSD values of CO_2 and O_2 for graph sections A, B and C from Mouse Mountain site 1101, as an example of results from a typical measurement sequence.

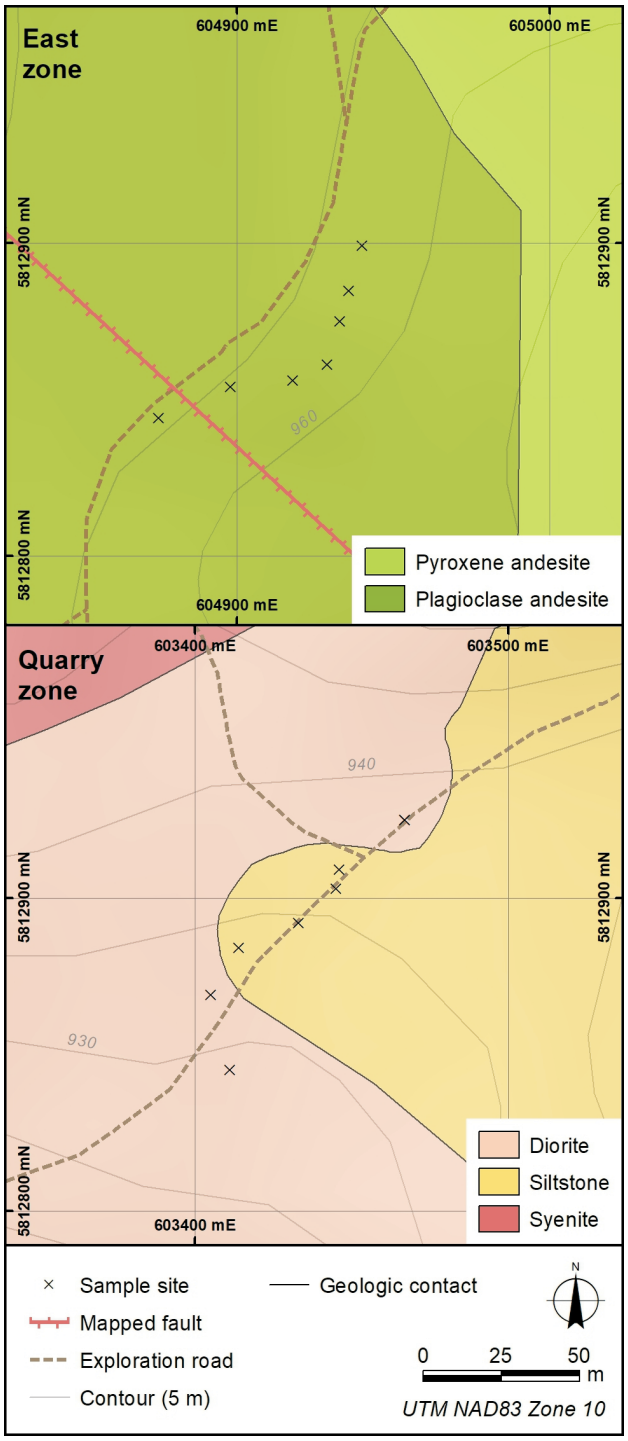

Figure 5. Shiko Lake, Quarry and East zones study areas, sample locations and simplified geology (geology and fault locations from Lesage, 2011).

Net soil gas CO_2 and O_2 values representing the difference between sensor-calibrated atmospheric and soil gas levels are designated ΔCO_2 and ΔO_2, and are calculated using equations 1 and 2. In the equations, the atmospheric [1] and atmospheric [2] values are mean values for the A and C datasets. Equation 3 is the total, net ΔCO_2-O_2 concentration in soil gas, indicating possible CO_2 generation and O_2 depletion by mineral sulphide oxidation reactions.

Table 1. Mean and %RSD (percent relative standard deviation) for CO_2 and O_2 measured at 10-second intervals in atmospheric air (measured twice) and soil gas at Mouse Mountain site 1101.

Source	Atmosphere [1]	Soil gas	Atmosphere [2]
Number of CO_2 measurements	11	9	12
Mean of CO_2 (ppm)	382	3766	328
%RSD	8.7	10.6	14.6
Number of O_2 measurements	11	9	12
Mean of O_2 (ppm)	209357	206660	209913
%RSD	0.04	0.65	0.09
Graph section in Figure 3	**A**	**B**	**C**

$$\Delta CO_2 = \text{Soil gas } CO_2 - [(\text{Atmosphere [1] mean } CO_2 + \text{Atmosphere [2] mean } CO_2)/2] \quad (1)$$

$$\Delta O_2 = \text{Soil gas } O_2 - [(\text{Atmosphere mean [1] } O_2 + \text{Atmosphere [2] mean } O_2)/2] \quad (2)$$

$$\Delta CO_2\text{-}O_2 = \Delta CO_2 + \Delta O_2 \quad (3)$$

Duplicate soil gas CO_2 and O_2 measurements at six sites provide an estimate of combined sampling and analytical precision. At each such field duplicate site, soil gas was sampled twice from two separate holes less than 1 m apart. A coefficient of average variation, CV_{AVG} (%), calculated from six duplicate ΔCO_2 and ΔO_2 values using the equation proposed by Abzalov (2008) gives precision estimates of 18.4% for ΔCO_2, 14.0% for ΔO_2 and 15.9% for ΔCO_2-O_2. These fall in the CV_{AVG} range of 15 to 30% considered by Abzalov (2008) to be an acceptable level of precision.

Results

At Mouse Mountain, the first soil gas ΔCO_2-O_2 concentrations measured over the mapped northeast-southwest fault were found to be less than 2%, suggesting an absence of structural influence on the soil gas concentrations (Figure 6a). Sampling 50 m north of the mapped fault, however, detected ΔCO_2-O_2 levels up to 5%. It is known that the location of the fault is poorly constrained, and the real-time measurements suggested the fault was farther north, thus more closely spaced samples were taken farther north to ensure the structure was not missed by the survey. The highest ΔCO_2-O_2 soil gas level occurs along the westernmost transect. From this peak, ΔCO_2-O_2 levels between 2 and 3.4% extend along a northeast trend across the three transects (Figure 6a). These results suggest the occurrence of a concealed fault or fractures associated with the mineralized bedrock and support the hypothesis that the inferred fault currently mapped in the area is inaccurately sited and more complex than illustrated. Soil IDH factor values up to 866 are also present at sites on the west transect (Figure 6b). Although the sites with elevated IDH on the west transect do not have high soil gas ΔCO_2-O_2, a spatial association between ΔCO_2 and soil pH suggests a possible relationship

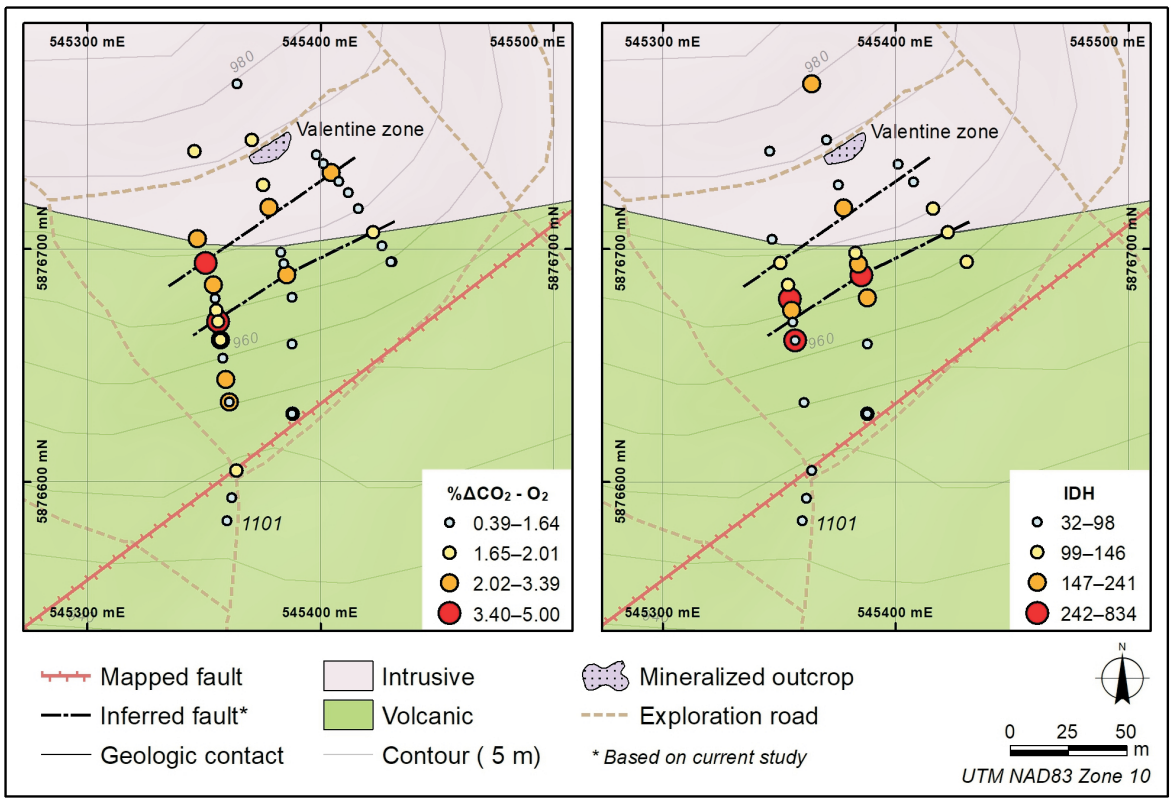

Figure 6. soil gas Δ CO_2-O_2 in percent **(left)** and IDH (inverse difference hydrogen ion) factor **(right)** at Mouse Mountain. Symbols represent values at the median, first quartile, third quartile and third quartile + 1.5 interquartile ranges (simplified bedrock geology from Schimann, 2014).

between higher carbonate in the soil and increased CO_2 flow.

At Shiko Lake Δ CO_2-O_2 soil gas levels and IDH results increase to a peak mid-way along the Quarry zone transect (Figure 7) where bedrock is mapped as a pyrite-bearing hornfelsed siltstone. The peak may reflect CO_2 emanating from weathering pyrite. There is an increase in IDH along the East zone transect (Figure 8) indicating possible weathering of sulphides in bedrock, and the highest Δ CO_2-O_2 soil gas values are close to a mapped northwest-striking fault.

Conclusions and Continued Studies

An economical, compact system has been built for measuring and recording real-time soil gas CO_2 and O_2 concentrations. Sampling soil gas from drift-covered sulphide-mineralized rock at the Mouse Mountain and Shiko Lake Cu-Au porphyry sulphide mineral occurrences revealed that, after calibration to atmospheric levels, the system measures CO_2 and O_2 reliably. Furthermore, the variation in the gas concentrations are spatially coincident with inferred structures or mineralization and, therefore, the system appears to indicate concealed bedrock sulphide and faults.

Soil geochemistry results will be compared to these findings to further refine interpretations and provide additional support to, or refute, the association of CO_2 and O_2 levels and mineralization. A current limitation of this study is that neither the locations of the structures or their relation to mineralization are very well defined, as evidenced by the results at Mouse Mountain. Additional local testing over known structures is planned and, if accomplished, the results will be included in the final report, along with the preliminary testing and geochemical results, to provide additional information from which conclusions on the efficacy of the system can be determined.

The real-time instrumental technique developed by the authors to generate chemical analyses can be used to guide mineral exploration programs and allows for informed adjustments during fieldwork. Carbon dioxide and O_2 in soil gas have been measured onsite in the past to detect geological structure and concealed sulphide mineralization, but the systems used typically needed several cumbersome and relatively expensive instruments. The system developed by the authors and described in this paper is compact, portable, relatively economical and able to detect soil gas CO_2 and O_2 variations that suggest the existence of faults beneath drift-covered bedrock. Carbon dioxide and O_2 fluctuations detected by the system could also be useful for geothermal exploration, earthquake prediction and in agriculture research.

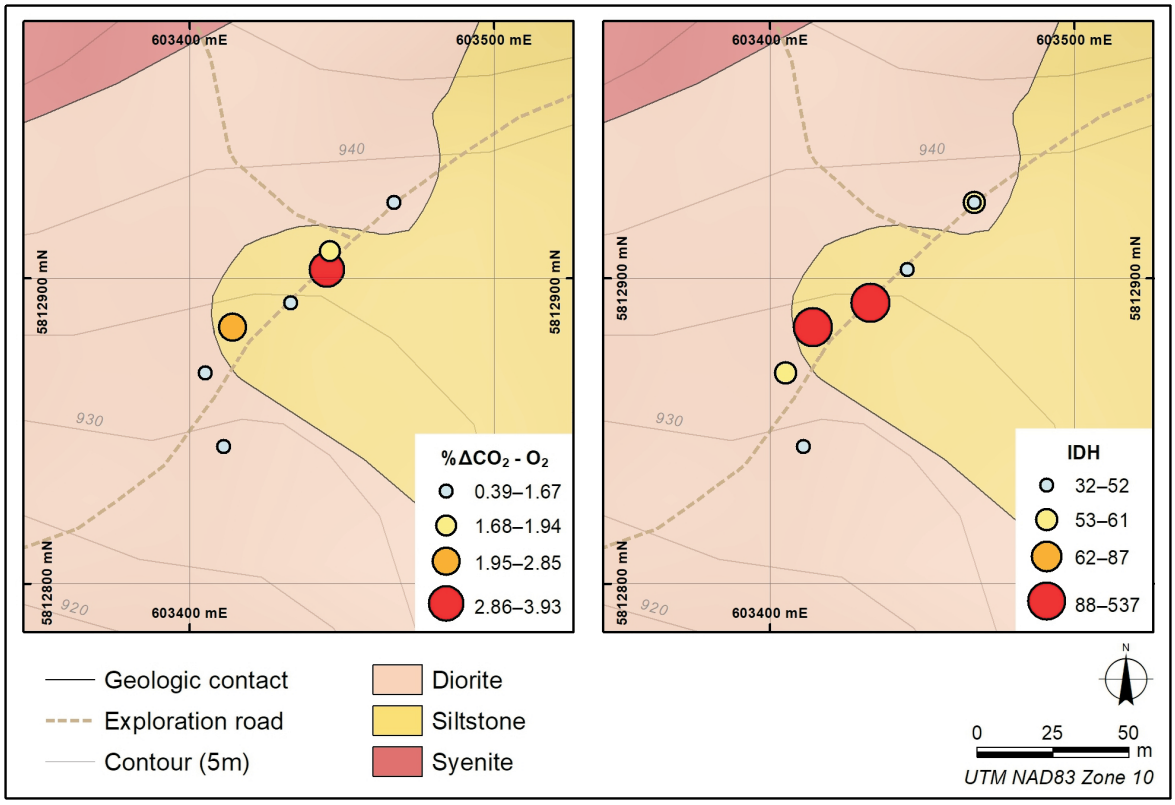

Figure 7. Preliminary soil gas Δ CO_2-O_2 **(left)** and IDH (inverse difference hydrogen ion) measurements **(right)** at the Quarry zone of the Shiko Lake property. Simplified bedrock geology from Lesage (2011).

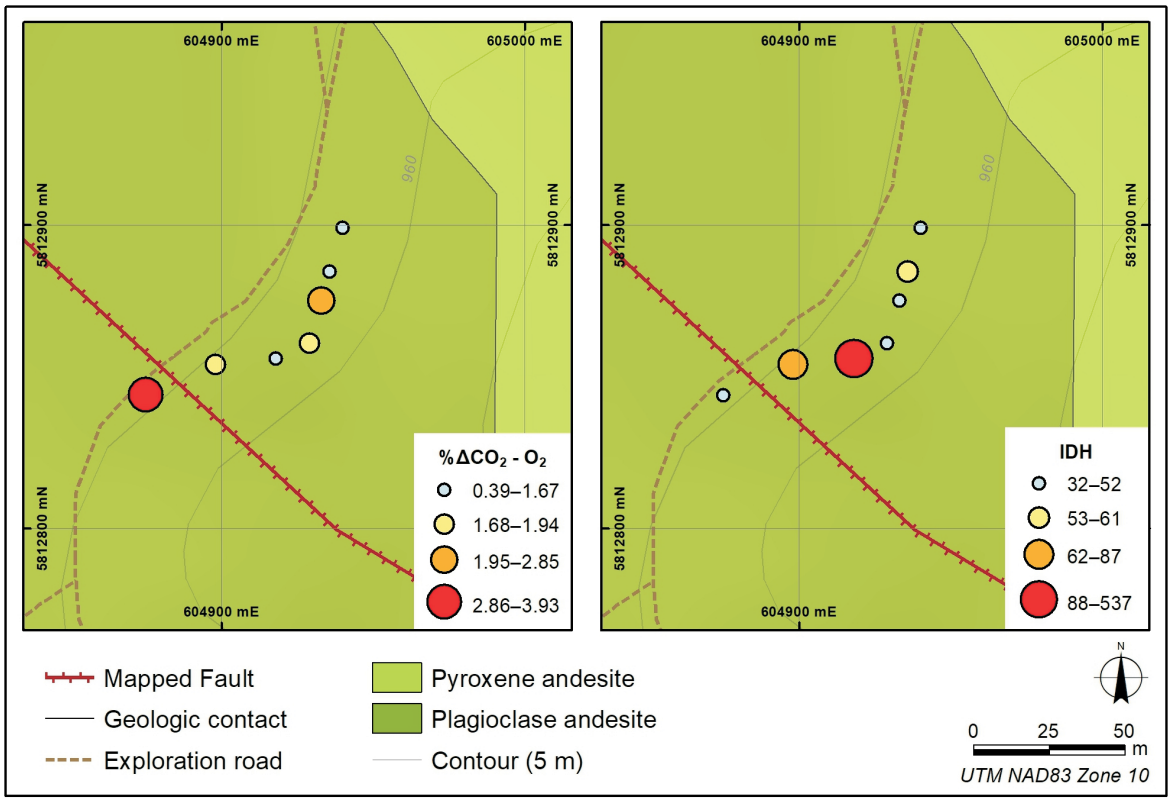

Figure 8. Preliminary soil gas Δ CO_2-O_2 **(left)** and soil IDH (inverse difference hydrogen ion) measurements **(right)** at the East zone of the Shiko Lake property. Simplified bedrock geology from Lesage (2011).

Acknowledgments

Permission from K. Schimann, CanAlaska Uranium Ltd., to access the Mouse Mountain property is appreciated. R. Durfeld, Durfeld Geological Management Ltd. very kindly provided transportation to the Shiko Lake property from Williams Lake, advised on sample transect sites, and helped with the soil gas and soil sampling. His assistance and hospitality during the fieldwork was very much appreciated by the authors. J. Houck, CO2Meter Inc., is thanked for patiently and promptly answering the many questions about the CO_2 and O_2 sensors. S. Cook is especially thanked for a very careful and constructive review of preliminary draft of the paper.

References

Abzalov, M.Z. (2008): Quality control of assay data: A review of procedures for measuring and monitoring precision and accuracy; Exploration and Mining Geology, v. 17, p. 1–14.

BC Geological Survey (2019): MINFILE BC mineral deposits database; BC Ministry of Energy, Mines and Petroleum Resources, URL <https://minfile.ca> [November 2019].

CO2Meter Inc. (2015): GSS sensor user manual; CO2Meter Inc., 51 p., URL <http://www.co2meters.com/Documentation/Manuals/Manual-GSS-Sensors.pdf> [November 2019].

Duddridge, G.A., Grainger, P. and Durrance, E.M. (1991): Fault detection using soil gas geochemistry; Quarterly Journal of Engineering Geology, v. 24, p. 427–435.

Hale, M. (2010): Gas geochemistry and deeply buried mineral deposits: the contribution of the Applied Geochemistry Research Group, Imperial College of Science and Technology, London; Geochemistry: Exploration, Environment, Analysis, v. 10, no. 3, p. 261–267.

Highsmith, P. (2004): Overview of soil gas theory; The Association of Applied Geochemists Quarterly Newsletter Explore, no. 122, p. 1–15, URL <https://www.appliedgeochemists.org/publications/explore-newsletter> [November 2019].

Jonnes, S. and Logan, J.M. (2007): Bedrock geology and mineral potential of Mouse Mountain, central British Columbia; *in* Geological Fieldwork 2006, BC Ministry of Energy, Mines and Petroleum Resources, BC Geological Survey, Paper 2007-1, p. 55–66, URL <http://cmscontent.nrs.gov.bc.ca/geoscience/PublicationCatalogue/Paper/BCGS_P2007-01-06_Jonnes.pdf> [November 2019].

Lesage, G. (2011): Assessment report on the Redgold property, Cariboo Mining Division, BC, NTS: 093A06W; BC Ministry of Energy, Mines and Petroleum Resources, Assessment Report Indexing System (ARIS), ARIS Report 32975, 755 p., URL <https://aris.empr.gov.bc.ca/ArisReports/32975.PDF> [November 2019].

Lovell, J.S., Hale, M. and Webb, J.S. (1979): Soil air disequilibrium as a guide to concealed mineralization at Keel, Eire; *in* Prospecting in Areas of Glaciated Terrain, 1979: papers presented at a symposium organized by the Irish Association for Economic Geology and held in Dublin, Ireland, 26–29 August, 1979, The Institute of Mining and Metallurgy, London, p. 45–50.

Lovell, J.S., Hale, M. and Webb, J.S. (1980): Vapour geochemistry in mineral exploration; The Mining Magazine, September 1980, p. 229–239.

McCarthy, J.H., Lambe, R.N. and Dietrich, J.A. (1986): A case study of soil gases as an exploration guide in glaciated terrain: Crandon massive sulfide deposit, Wisconsin; Economic Geology, v. 81, p. 408–420.

Morton, J.W. (2003): Prospecting and a geological reconnaissance on the Redgold property, Cariboo Mining Division, BC; BC Ministry of Energy, Mines and Petroleum Resources, Assessment Report Indexing System (ARIS), ARIS Report 27046, URL <https://aris.empr.gov.bc.ca/ArisReports/27046.PDF> [November 2019].

Schimann, K. (2014): Geology and geochemistry at the QM property, NTS: 93G 01, BC; BC Ministry of Energy, Mines and Petroleum Resources, Assessment Report Indexing System (ARIS), ARIS Report 35262, 28 p.

Smee, B.W. (1998): A new theory to explain the formation of soil geochemical response over deeply covered gold mineralization in arid environments; Journal of Geochemical Exploration, v. 61, p. 149–172.

Smee, B.W. (2003): Theory behind the use of soil pH measurements as an inexpensive guide to buried mineralization, with examples; The Association of Applied Geochemists Quarterly Newsletter Explore, no. 118, p. 1–18, URL <https://www.appliedgeochemists.org/publications/explore-newsletter> [November 2019].

Smee, B.W. (2009): Soil micro-layer, airborne particles and pH: the Govett connection; *in* Proceedings of the 24th International Applied Geochemistry Symposium, June 1–4, 2009, Fredericton, New Brunswick, D.R. Lentz, K.G. Thorne and K.-L. Beal (ed.), v. 1, p. 91–95.

Geochemical Investigation of Halogens in Spruce Treetops and Integration with Existing Multi-Element Data from the Blackwater Region and TREK Project Area, Central British Columbia (NTS 093C, F)

C.E. Dunn, Colin Dunn Consulting Inc., North Saanich, British Columbia, colindunn@biogeochemistry.ca

D.R. Heberlein, Heberlein Geoconsulting, North Vancouver, British Columbia

Dunn, C.E. and Heberlein, D.R. (2020): Geochemical investigation of halogens in spruce treetops and integration with existing multi-element data from the Blackwater region and TREK project area, central British Columbia (NTS 093C, F); *in* Geoscience BC Summary of Activities 2019: Minerals, Geoscience BC, Report 2020-01, p. 101–108.

Introduction

In 2015, Geoscience BC funded a helicopter-supported spruce-treetop sampling program at 1.5 km spacing on an offset grid, followed by multi-element analysis of twigs and needles, in the Blackwater region and TREK project area (Jackaman and Sacco, 2016) of central British Columbia (BC; Figure 1). The survey area has a thick vegetation cover, few lakes and a limited road network such that other surface geochemical-exploration methods would be very time-consuming and expensive.

Jackaman and Sacco (2016) published results from the analysis of 421 milled spruce-twig samples (dry tissues; locations shown in Figure 2); the needles from these same samples were also analyzed, but were first reduced to ash to concentrate elements prior to multi-element analysis by inductively coupled plasma–mass spectrometry (ICP-MS) with an aqua-regia digestion. Surplus needle ash was available for further analytical work and, since the analysis method for detecting halogens in similar materials was being developed under another project (Heberlein et al., 2017a, b), the opportunity was taken to use these archived samples to further develop the analytical methodology and add another layer of data to the original datasets. The purpose of the sample reanalysis was to examine the distribution patterns of halogens at a regional scale of sampling to determine if these volatile elements might identify geologically meaningful patterns and provide confirmation of some subtle element enrichments identified in the original survey datasets.

Fluorine is the most reactive element in the periodic table, forming compounds with every element except the noble gases He, Ne and Ar. It is also the most electronegative element. The remaining halogen elements (i.e., Cl, Br and I) are also highly reactive but less so than F. All four halogens

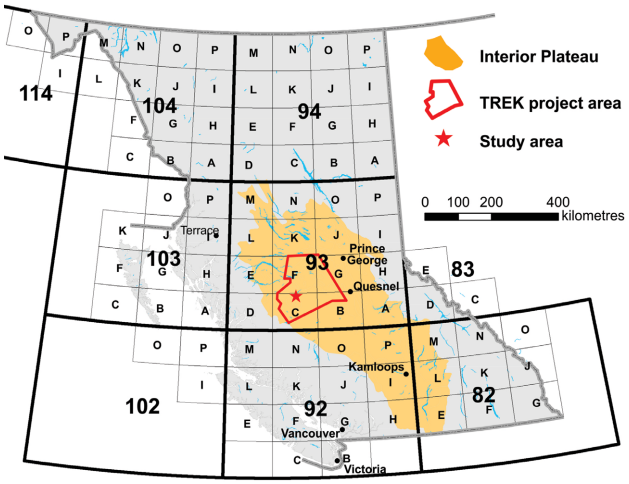

Figure 1. Biogeochemical survey area, Interior Plateau, central British Columbia.

are particularly enriched in differentiated magmas; the hydrothermal fluids and volatile compounds derived from them play an important role in the mobilization and transport of metals in ore-forming systems. In the primary environment, they reside in a variety of hydrous minerals including micas, amphiboles, scapolite, topaz and apatite. Elevated halogen concentrations are also documented in high-salinity liquid phases and daughter minerals in fluid inclusions in igneous and hydrothermal minerals (Kendrick et al., 2012; Kendrick and Burnard, 2013). On exhumation and weathering at the earth's surface, the host minerals break down either mechanically or chemically and release the halogens into the surficial environment. Being highly soluble in water, they are rapidly transported through drainage systems to the ocean as anions.

In mineral exploration, there are case histories that demonstrate positive responses of all these elements to zones of concealed mineralization (Billings and Williams, 1967; Al Ajely et al., 1985; Lavery, 1985; Ridgway, 1989, 1991; Ridgway et al., 1990; Trofimov and Rychkov, 2004). However, other than some Geoscience BC research projects carried out in recent years (Dunn et al., 2007; Bissig et al.,

This publication is also available, free of charge, as colour digital files in Adobe Acrobat® PDF format from the Geoscience BC website: http://www.geosciencebc.com/updates/summary-of-activities/.

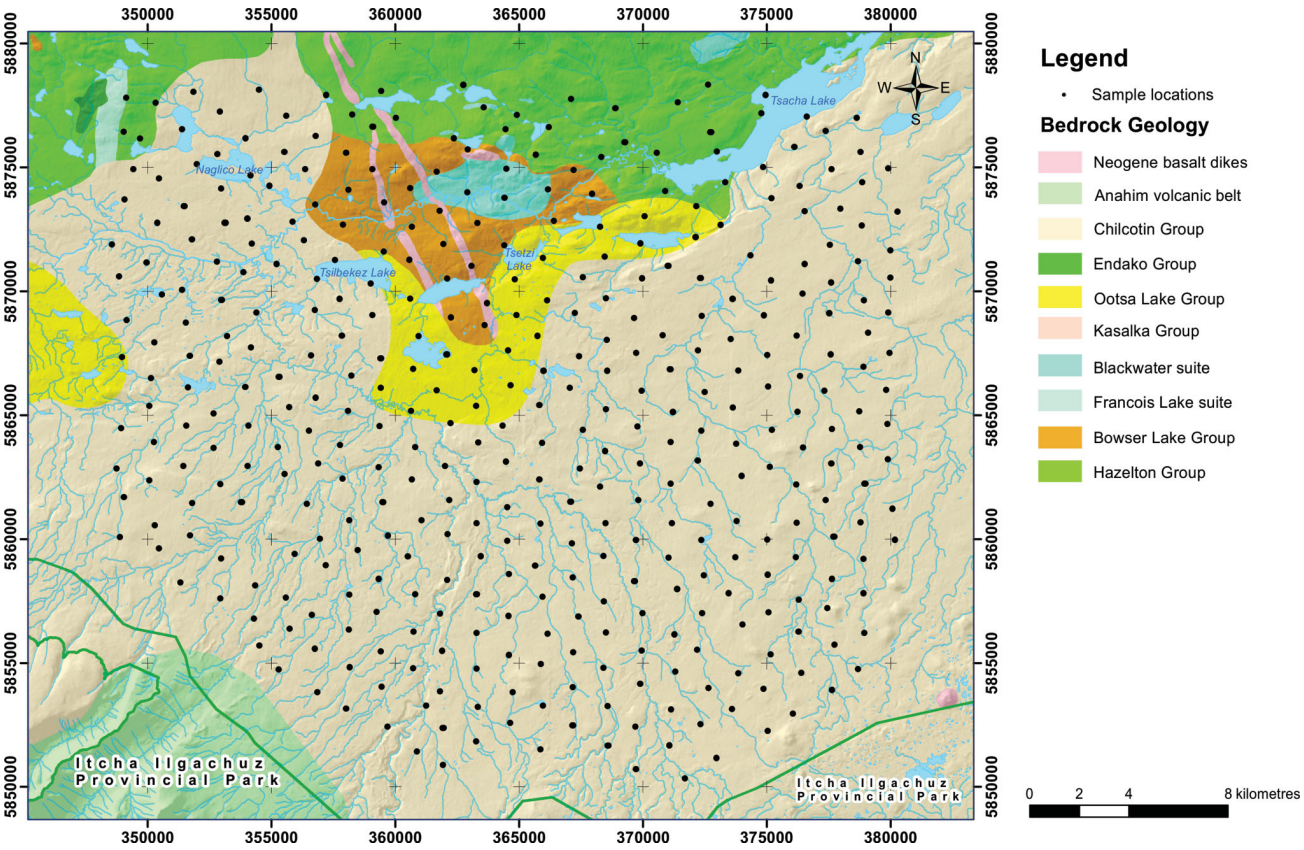

Figure 2. Geology of survey area with treetop sample sites; the green lines indicate park boundaries. Geological units after Angen et al. (2017).

2013; Heberlein et al., 2013; Heberlein and Dunn 2017a, b; Heberlein et al., 2017a, b) and a trial study on a limited dataset, using ashed Douglas-fir needles (Dunn and Thompson, 2009), these methods have seen little or no application to the exploration for minerals in the extensively covered terrains of BC or elsewhere.

A good example of a large geochemical footprint of F surrounding a volcanogenic massive-sulphide ore deposit is at Crandon (Wisconsin), where the halo extends approximately 320 m into the footwall rocks and at least 220 m from the ore. Other base-metal deposits also exhibit F haloes: in Arizona, for example, the United Verde deposit has a F enrichment in footwall rocks of at least 650 m from the ore and distinct F haloes are present around smaller deposits in New South Wales (Lavery, 1985). Similarly, Church and Barakso (1990) reported in a study of about 1700 rock samples in the Buck Creek area of BC:

> *"Fluorine is ubiquitous in the rocks of the map area and rarely falls below 100 ppm. At the Equity mine fluorine is depleted over the ore zone. A weak discontinuous halo rising above 1000 ppm fluorine can be interpreted as surrounding the deposit."*

With these examples in mind, ALS-Geochemistry analytical laboratory (North Vancouver, BC) has further developed analytical methods enabling scientists to investigate the halogen responses in surface media near base-metal and gold mineralization in BC (Dunn et al., 2007; Heberlein and Dunn, 2017a, b; Heberlein et al., 2017a, b) with a certain measure of success. The last of these studies resulted in ALS developing their HAL-01 and HAL-01a methods and marketing them at a lower cost than had previously been possible. However, further analytical refinement of the methods was still required and is presented in this summary.

Relevance to the Exploration Community

This study is designed to provide the mineral-exploration community with additional layers of geochemical data from the analysis of tree tissues that could contribute to the identification of zones of metal enrichment possibly deriving from deep-seated or covered mineralization and/or could reveal structural elements and rock types likely to provide a focus for exploration efforts. This is based on the rationale that the halogen elements are commonly instrumental in the emplacement of metal deposits and generate broader haloes of enrichment than the metals themselves. Refinement of the analytical methodology leads to more accurate and precise data, and potential lowering of costs,

thus making these methods more attractive and practical to the exploration community.

Survey Area

The following description is taken largely from Jackaman and Sacco (2016), in which the authors describe the survey area as characterized by gentle, north-facing slopes that are blanketed with glacial drift and dissected by streams that flow into the lowland. Interspersed throughout the 1000 km^2 survey area are stands of lodgepole pine (*Pinus contorta*), white spruce (*Picea glauca*) and Engelmann spruce (*Picea engelmannii*). A hybrid species of white and Engelmann spruce (known as Interior spruce) is also common in the central Interior. Fortunately, from several previous studies, the lead author was able to determine that these spruce species have very similar chemical characteristics. Wetland features and sedge-grass meadows are common. There is evidence of beetle-killed pine, recent forest fires and regeneration from previous forest fires. Few access roads extend into the survey area, but forest service roads are located to the north and east.

The survey area is underlain by Hazelton Group and Ootsa Lake Group rocks, and Chilcotin Group volcanic rocks. Several developed prospects that contain Au, Ag, Zn, Pb and Cu mineralization are located in the region. The Blackwater-Davidson intermediate-sulphidation epithermal Au-Ag deposit (NTS 093F/02; MINFILE 093F 037, BC Geological Survey, 2019) is located 15 km northeast of the survey area and the 3Ts polymetallic Ag-Pb-Zn±Au deposit (NTS 093F/03; MINFILE 093F 068) is situated on the northern survey boundary. Previous work at the 3Ts deposit established a positive response of halogens to concealed mineralization (Dunn et al., 2007). No recorded mineral occurrences exist within the survey area south of the West Road (Blackwater) River and lack of outcrop has resulted in interpretation (from airborne geophysics) of the underlying bedrock in most of the survey area as being Chilcotin Group volcanic rocks (Figure 2).

Sample Collection and Analysis

Sampling and Sample Preparation

Details of the sampling program are given in Jackaman and Sacco (2016), in which it is stated that:

> *"Field survey methods, sample preparation and analysis protocols guiding the 2015 biogeochemical survey were based on previous field surveys, orientation investigations and detailed research (Dunn, 1995, 2007). During a six-day period in June 2015, a 1000 km^2 area was surveyed using predetermined flight-lines along an offset grid with 1500 m spacing between sample sites. A total of 421 side-branch samples, comprising 1 kg of twigs, needles and cones, were systematically collected near the tops of 399 healthy spruce trees (Figure 3). The target spruce trees were healthy, 80–100 years old, 20–25 m tall and commonly extended 2–3 m above a lower canopy of lodgepole pine, which typically showed effects of the mountain pine beetle infestation. A recent forest fire in the northern part of the survey area and several immature patches of forest regeneration limited the availability of spruce for a small number of the predetermined sites.*
>
> *Navigation along the predetermined flight lines and the recording of sample site location co-ordinates were completed using tablet based mapping and GPS computer programs."*

Figure 3. Spruce-treetop sample collection in central British Columbia, showing sampler secured to the helicopter with a safety harness and lanyard. Photo courtesy of E. Banner.

After oven drying at 60°C, the needles were removed from the twigs and a 50 g split of dry needles (which were the only tree tissues used in the current study for determining the halogen contents) was reduced to ash at 475°C, generating 2–3 g of ash. A 0.25 g aliquot of the ash was analyzed for 53 elements plus rare-earth elements by ICP-MS following aqua-regia digestion. Consequently, plenty of ash remained for refinement of methods used for halogen analysis; all the original packets of ash were therefore obtained from W. Jackaman and sent to ALS for further method development, after which all 421 samples were analyzed for F, Br, I and Cl.

Method Description

The information on which this section is based has been provided by ALS.

'Super Trace F, Cl, Br, I' is a recently developed method, which ALS describes as the ME-HAL01a method, that has proven to be suitable for ashed vegetation. After reducing vegetation to ash at 475°C for 24 hours, samples are leached with hot de-ionized water (90°C) and analyzed by a combination of ion chromatography and ICP-MS.

Method precision was determined using ashed vegetation reference materials. The aliquot weight was optimized (0.5 g) to improve recovery and precision for all halogen elements. Table 1 shows concentrations of halogens obtained from 0.25 and 0.5 g aliquots of VEG-V4a (balsam fir-needle ash) and VEG-V8a (spruce-needle ash). It demonstrates very good precision and shows that there are higher F recoveries from the 0.50 g than from the 0.25 g samples.

A comparison of F results obtained by the Super Trace method and traditional ion-selective electrode analysis indicates that the Super Trace method (0.50 g) consistently recovers about 50% of the total F (the water-soluble component) yet is suitable for exploration targeting. Work is ongoing on the percentage recoveries of Br, Cl and I.

Multi-Element Analysis and Reanalysis of Selected Samples

The original multi-element datasets included a comprehensive suite of control samples and repeat analyses for defining the analytical quality. These results are detailed in Jackaman and Sacco (2016), who noted that some elements (e.g., Au and Ga in ashed needles) exhibited slightly elevated values along sample sequences. The concentrations of these elements were generally very low and may reflect detection-level artifacts related to sample weights and/or heterogeneity (J. Sader, pers. comm., 2016). Of concern was a trend of elevated Au values in the western part of the survey area. Investigation of the original data established that this sequence was confined to one particular test-tube rack of samples, indicating that a slight difference in the digestion procedure might have been the cause. As a follow-up to this problem, the original analytical laboratory, Bureau Veritas Minerals (Vancouver, BC), has been asked to reanalyze the ash samples in question to assess the reproducibility of the anomalous results. A total of 22 samples were sent to the laboratory, including two control samples. Results can be summarized as follows:

- After storage of ash in packets for four years, the data for most elements were very reproducible, confirming that the ash samples retain their integrity over time.
- The Au, As and Sb data did not reproduce well, largely due to the very low concentrations of these elements in the samples (As and Sb have therefore been omitted from comparisons of trends with the halogen data); however, given the low levels, the Au values nevertheless appear to be reproducible for all samples except the problem samples, which returned values below the lower detection limit and, consequently, the original analytical values for Au in this short sequence of samples have been replaced by the new results (of relevance is that the results from some of the reanalyzed samples requested by W. Jackaman were very similar to the latest results, thereby confirming that the original values for Au in a short sequence of samples were suspect and should not be relied upon).
- Other elements that showed a good correlation on reanalysis, but were lower after four years, were Li and Sc, whereas the opposite occurred for Mo (higher after four years).
- The Sb values were higher on the reanalysis and the Te values lower, which suggests that these data should be treated with caution.
- Since analytical precision for this study is of more relevance than analytical accuracy, the original dataset is

Table 1. Average (n = 3) concentrations obtained for ashed vegetation samples leached with de-ionized hot water. Abbreviations: DL, detection limit; RSD, relative standard deviation; wt, weight.

Sample	Sample wt	I (ppm)		Br (ppm)		F (ppm)		Cl (ppm)	
Detection limit		0.002		0.02		0.05		0.1	
		mean	%RSD	mean	%RSD	mean	%RSD	mean	%RSD
VEG-V4a	0.25 g	3.85	8.1	67.37	4.8	<DL	<DL	7043	1.85
VEG-V4a	0.50 g	3.99	6	73.5	1.3	14.45	1	6817	0.61
VEG-V8a	0.25 g	0.099	4.8	66.3	1.1	<DL	<DL	4700	4.99
VEG-V8a	0.50 g	0.108	2.8	70.7	1.1	9.76	3.7	4390	0.79

therefore considered sound for the purpose of examining element-distribution patterns; however, the linear trend of Au values identified in the original dataset (sequential samples) was determined an analytical artifact and those values have therefore been replaced by the new (lower) values to eliminate the false anomaly (a few other samples with elevated Au values in the northwestern part of the sample grid returned slightly lower values on repeat analysis, but very similar relative concentrations).

Halogen Results

Data Quality

Experimentation was undertaken to refine the analytical methodology for the four halogens; details of the methodology are described above.

The reproducibility achieved for field duplicate pairs is summarized in Table 2 and shows that, on average, the relative standard deviation for each of the halogens is about 20%, which is a reasonable level for reconnaissance samples.

Two vegetation ash samples were inserted by ALS as controls (VEG-V8a in Table 3 and Figure 4 and VEG-V4a in Table 4 and Figure 5) as well as control blanks and soil control OREAS-25a. The precision on all these controls was very good and somewhat better than that on the blind control (CDV-1a in Table 5 and Figure 6) because the latter

Table 2. Halogen relative standard deviations (RSD) for 20 field duplicate pairs.

	Average %RSD (n = 20 pairs)			
Analyte	Br	Cl	F	I
Average RSD	19.8%	20.3%	16.8%	17.9%

Table 3. Halogen averages, standard deviations (Std dev.) and relative standard deviations (RSD) for control vegetation ash sample VEG-V8a.

Control VEG-V8a (n = 12)				
Average (ppm)	0.14	53.87	12.77	3888
Std dev.	0.01	2.65	0.53	417
%RSD	6.1	4.9	4.2	10.7

Table 4. Halogen averages, standard deviations (Std dev.) and relative standard deviations (RSD) for control vegetation ash sample

Control VEG-V4a (n = 5)				
Average (ppm)	4.3	57	17	5838
Std dev.	0.15	3.17	0.72	665
%RSD	3.5	5.6	4.2	11.4

Table 5. Halogen averages, standard deviations (Std dev.) and relative standard deviations (RSD) for blind control vegetation ash sample CDV-1a.

Control CDV-1a (n = 24)				
Average (ppm)	0.11	94.48	8.14	395
Std dev.	0.01	3.57	5.91	23
%RSD	9.2	3.8	72.7	5.7

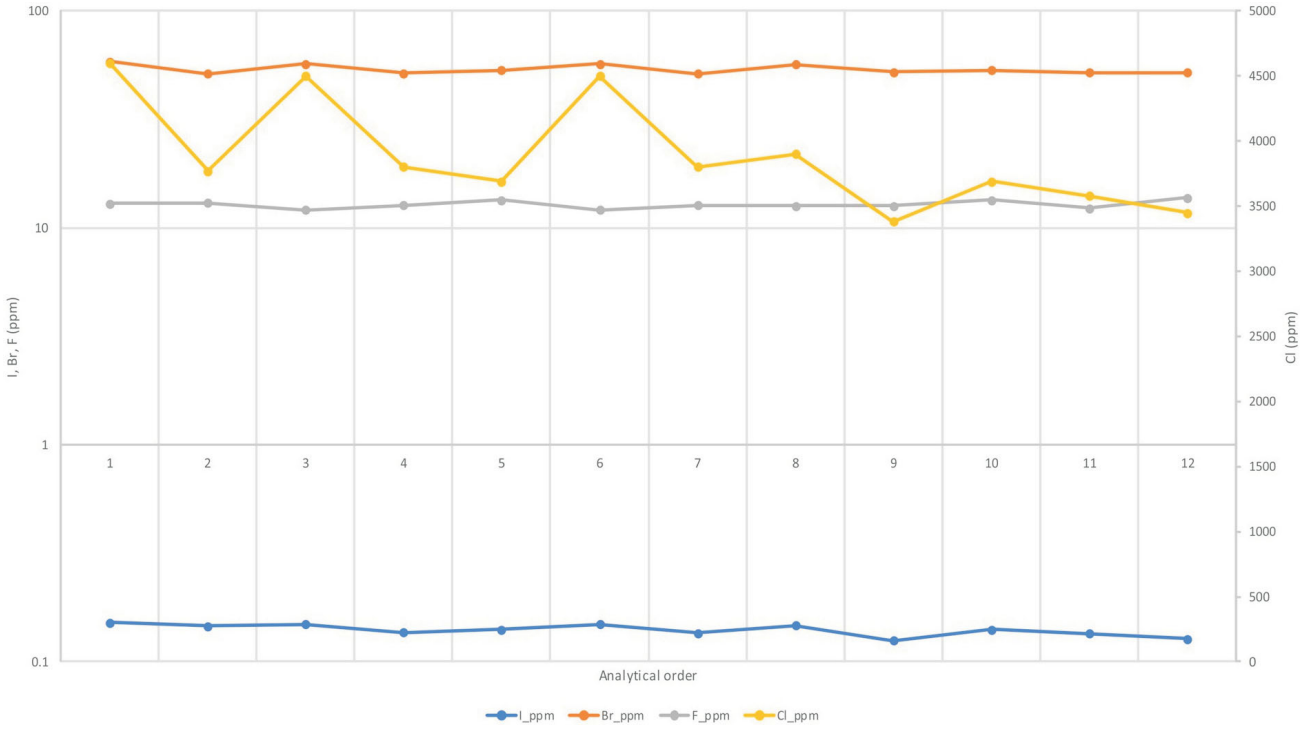

Figure 4. Chart of data summarized in Table 3 for control vegetation ash sample VEG-V8a.

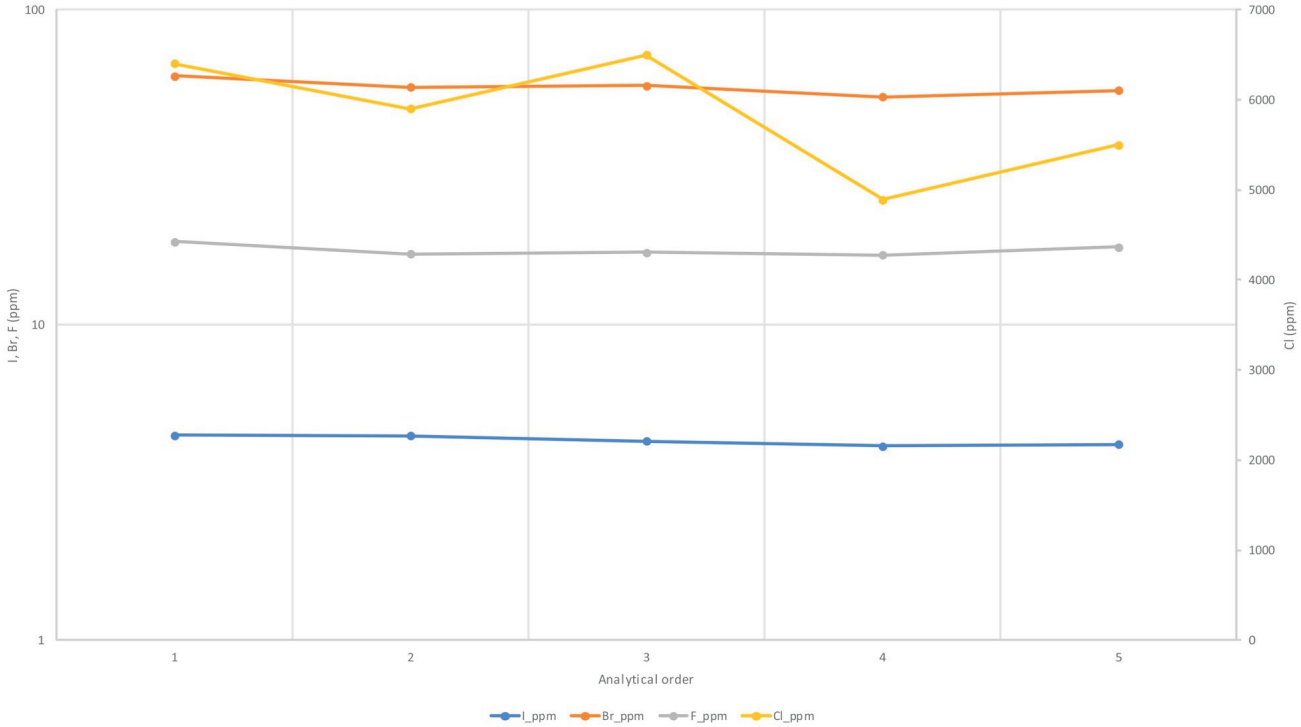

Figure 5. Chart of data summarized in Table 4 for control vegetation ash sample VEG-V4a.

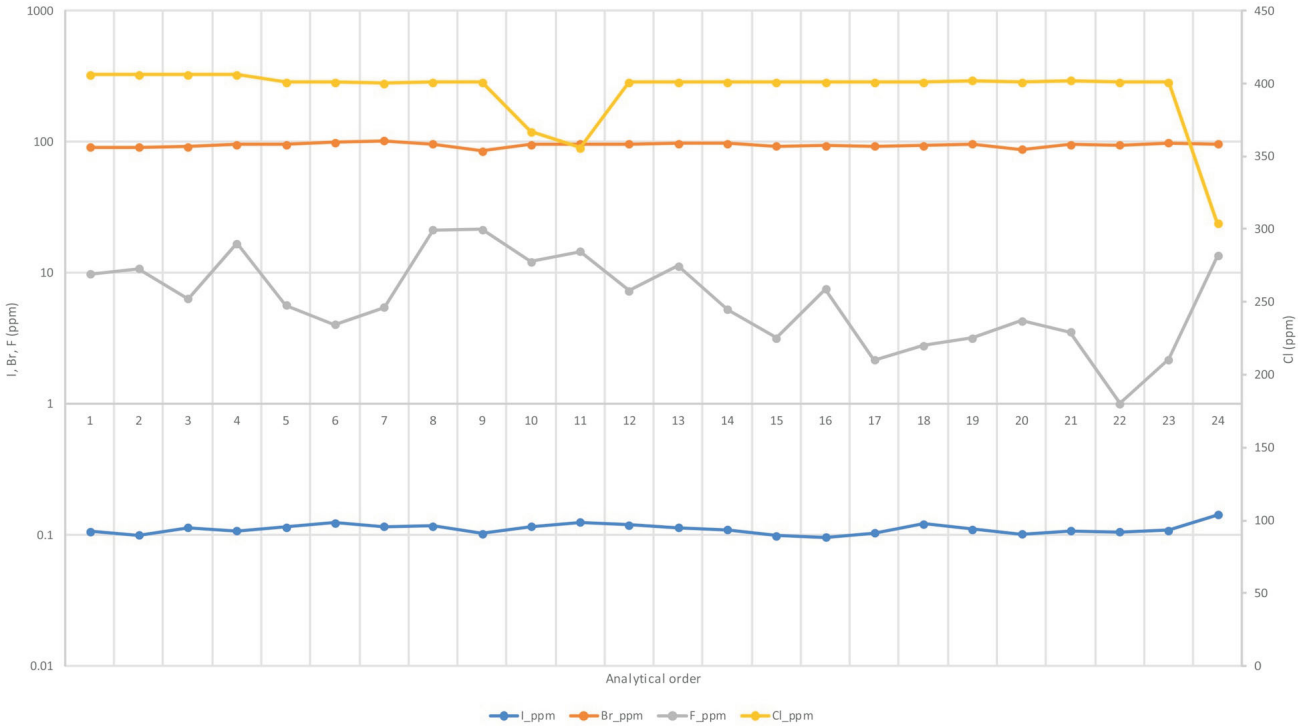

Figure 6. Chart of data summarized in Table 5 for blind control vegetation ash sample CDV-1a.

proved to have, in particular, lower concentrations of F than either the survey samples or laboratory controls.

Survey Results

A preliminary plot of F concentrations (levelled to dry weight) is shown in Figure 7. Several areas of relative enrichment are apparent, notably the pronounced southwest trend in the northern half of the survey area. This trend follows the northern edge of the Chilcotin Group and coincides with a linear chain of lakes and an aeromagnetic break, suggesting that it could be reflecting a major structure. The other anomalies south of the trend all lie within Chilcotin Group basalts and could either indicate eruptive centres for the basalts or, more intriguingly, potential hydrothermal alteration in the underlying units exposed in windows through the basalt cover.

The relationships of these anomalous zones will be compared to new plots that will be prepared from the multi-element data provided by Jackaman and Sacco (2016), and with existing geophysical and Quaternary maps.

Acknowledgments

The authors thank ALS-Geochemistry (Vancouver) for their substantial in-kind contribution, in the form of their ongoing development of the analytical method to achieve low detection levels and high analytical precision, as well as their discounted rates applied to analytical work undertaken; in particular, they thank A. Asfaw, E. Armstrong, A. Stolze and management at ALS. They are also grateful to W. Jackaman, for providing the samples used for this work, and to R. Lett, for his constructive comments on the draft of this summary.

References

Al Ajely, K.O., Andrews, M.J. and Fuge, R. (1985): Biogeochemical dispersion patterns associated with porphyry-style mineralization in the Coed Y Brenin forest, North Wales; *in* Prospecting in Areas of Glaciated Terrain 1984, 6th Symposium, Institute of Mining and Metallurgy, London, United Kingdom, v. 6, p. 1–10.

Angen, J.J., Rahimi, M., Hart, C.J.R., Westberg, E., Logan, J.M. and Kim, R. (2017): Bedrock geology, TREK project area, northern Interior Plateau, central British Columbia; Geoscience BC Map 2017-06-01 and MDRU Map 12-2017, scale 1:250 000, URL <http://www.geosciencebc.com/i/

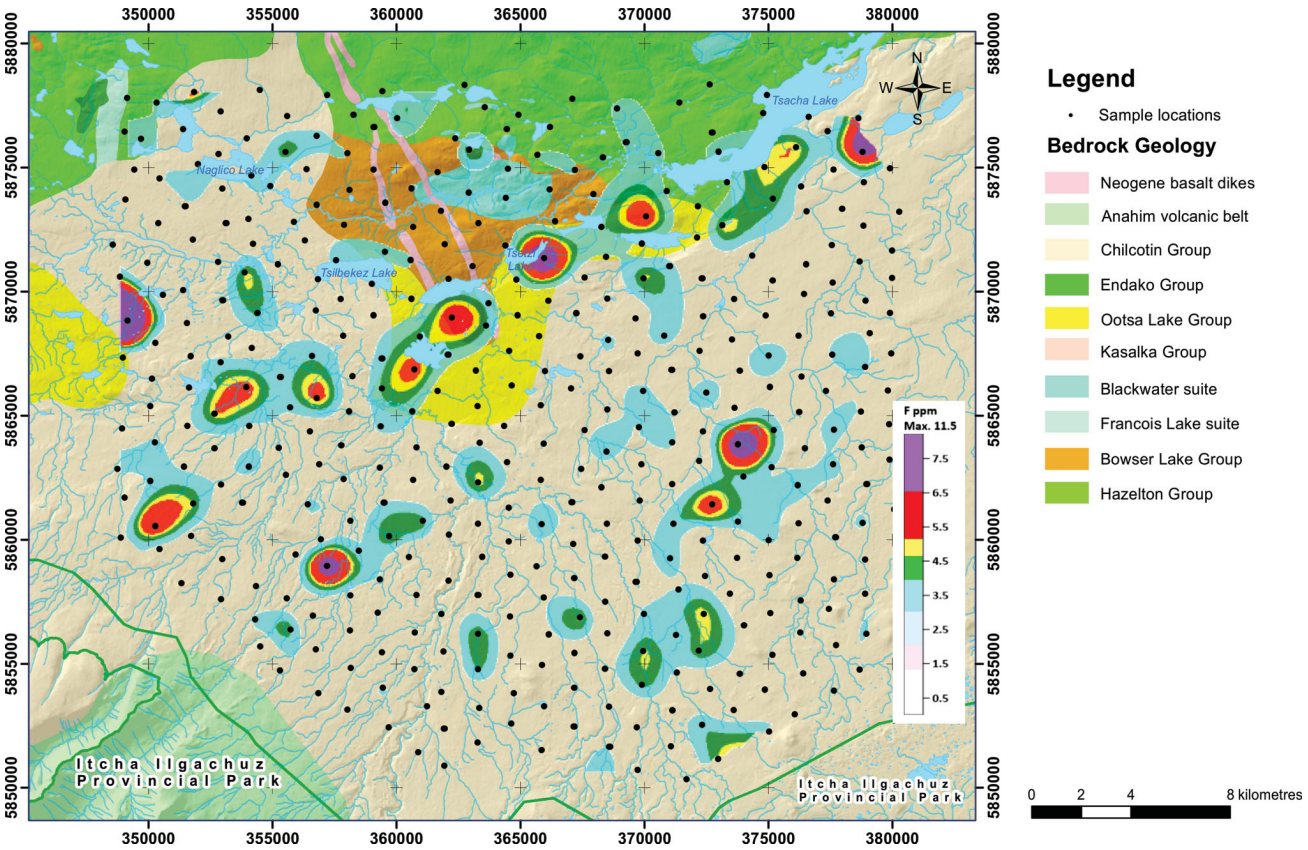

Figure 7. Fluorine in spruce-treetop needles from central British Columbia, based on concentrations in ash levelled to dry-weight basis. Geological units after Angen et al. (2017).

project_data/GBCReport2017-06/GBCMap2017-06-01.pdf>[November, 2019]

BC Geological Survey (2019): MINFILE BC mineral deposits database; BC Ministry of Energy, Mines and Petroleum Resources, BC Geological Survey, URL <http://minfile.ca> [September 2019].

Billings, G.K. and Williams, H.H. (1967): Distribution of chlorine in terrestrial rocks: a discussion. Geochimica et Cosmochimica Acta, v. 31, p. 22–47.

Bissig, T., Heberlein, D.R. and Dunn, C.E. (2013): Geochemical techniques for detection of blind porphyry copper-gold mineralization under basalt cover, Woodjam property, south-central British Columbia (NTS 093A/03, 06); Geoscience BC, Report 2013-17, 53 p., URL <http://www.geoscience bc.com/reports/gbcr-2013-17/> [September 2019].

Church, B.N. and Barakso, J.J. (1990): Geology, lithogeochemistry and mineralization in the Buck Creek area, British Columbia; BC Ministry of Energy, Mines and Petroleum Resources, Geological Survey Branch, Paper 1990-2, 85 p., URL <http://cmscontent.nrs.gov.bc.ca/geoscience/PublicationCatalogue/Paper/BCGS_P1990-02.pdf> [September 2019].

Dunn, C.E. (1995): Mineral exploration beneath temperate forests: the information supplied by trees; Exploration Mining Journal, v. 4, no. 3, p. 197–204.

Dunn, C.E. (2007): Biogeochemistry in Mineral Exploration; Handbook of Exploration and Environmental Geochemistry (M. Hale, ser. ed.), v. 9, Elsevier, Amsterdam, 462 p.

Dunn, C.E. and Thompson, R.I. (2009): Investigations of base metal and gold biogeochemical anomalies in the Mabel Lake area, southern British Columbia (NTS 82L09 and 10); Geological Survey of Canada, Open File 6147, 59 p., CD-ROM, URL <https://doi.org/10.4095/248086> [September 2019].

Dunn, C.E., Cook, S.J. and Hall, G.E.M. (2007): Halogens in surface exploration geochemistry: evaluation and development of methods for detecting buried mineral deposits; Geoscience BC Report 2007-10, 74 p., URL <http://www.geosciencebc.com/reports/gbcr-2007-10/> [September 2019].

Heberlein, D.R. and Dunn, C.E. (2017a). Preliminary results of a geochemical investigation of halogen and other volatile compounds related to mineralization, part 1: Lara volcanogenic massive-sulphide deposit, Vancouver Island (NTS 092B/13); *in* Geoscience BC Summary of Activities 2016, Geoscience BC, Report 2017-01, p. 141–150, URL <http://www.geosciencebc.com/i/pdf/SummaryofActivities2016/SoA2016_Heberlein-Lara.pdf> [September 2019].

Heberlein, D.R. and Dunn, C.E. (2017b). Preliminary results of a geochemical investigation of halogen and other volatile compounds related to mineralization, part 2: Mount Washington epithermal gold prospect, Vancouver Island (NTS 092F/14); *in* Geoscience BC Summary of Activities 2016, Geoscience BC, Report 2017-01, p. 151–158, URL <http://www.geosciencebc.com/i/pdf/SummaryofActivities2016/SoA2016_Heberlein-MtWashington.pdf> [September 2019].

Heberlein, D.R., Dunn, C E. and Macfarlane, W. (2013): Use of organic media in the geochemical detection of blind porphyry copper-gold mineralization in the Woodjam property area, south-central British Columbia (NTS 093A/03, /06); *in* Geoscience BC Summary of Activities 2012, Geoscience BC, Report 2013-1, p. 47–62, URL <http://www.geoscience bc.com/reports/gbcr-2013-20/> [September 2019].

Heberlein, D.R., Dunn, C.E. and Rice, S. (2017a). Halogens and other volatile compounds in surface sample media as indicators of mineralization, part 1: Lara VMS deposit, Vancouver Island (NTS 092B13); Geoscience BC Report 2017-11, 42 p., CD, URL <http://www.geosciencebc.com/i/project_data/GBCReport2017-11/GBCR2017-11_Lara_Rpt.pdf> [September 2019].

Heberlein, D.R., Dunn, C E. and Rice, S. (2017b). Halogens and other volatile compounds in surface sample media as indicators of mineralization, part 2: Mount Washington epithermal Au-Cu-Ag prospect, Vancouver Island (NTS 092F/14); Geoscience BC Report 2017-12, 61 p., CD, URL <http://www.geosciencebc.com/i/project_data/GBCReport2017-12/GBCR2017-12_MW_Rpt.pdf> [November 2019].

Jackaman, W. and Sacco, D.A. (2016): Reconnaissance biogeochemical survey using spruce-tops in the West Road (Blackwater) River area, Fraser Plateau, British Columbia; Geoscience BC, Report 2016-05, URL <http://www.geosciencebc.com/reports/gbcr-2016-05/> [September 2019].

Kendrick, M.A. and Burnard, P. (2013): Noble gases and halogens in fluid inclusions: a journey through the Earth's crust; *in* The Noble Gases as Chemical Tracers, Advances in Isotope Geochemistry, Springer-Verlag, Berlin-Heidelberg, Germany, p. 319–369.

Kendrick, M.A., Woodhead, J.D. and Kamenetsky, V.S. (2012): Tracking halogens through the subduction cycle; Geology, v. 40, no. 12, p. 1075–1078.

Lavery, N.G. (1985): The use of fluorine as a pathfinder for volcanic-hosted massive sulfide ore deposits; Journal of Geochemical Exploration, v. 23, p. 35–60.

Ridgway, J. (1989): Ammonium geochemistry in the search for hydrothermal gold mineralization: final report to the Overseas Development Administration; British Geological Survey, Technical Report WC/89/13 (open file).

Ridgway, J. (1991): Ammonium geochemistry in the search for hydrothermal gold deposits (II): final report to the Overseas Development Administration, November, 1991; British Geological Survey, Technical Report WC/91/41, 8 p., URL <www.bgs.ac.uk/research/international/dfid-kar/WC91041_col.pdf> [October 2016].

Ridgway, J., Appleton, J.D. and Levinson, A.A. (1990): Ammonium geochemistry in mineral exploration – a comparison of results from the American cordilleras and the southwest Pacific; Applied Geochemistry, v. 5, p. 475–489, URL <http://www.sciencedirect.com/science/article/pii/088329279090022W> [October 2016].

Trofimov, N.N. and Rychkov A.I. (2004): Iodine and bromine: geochemical indicators of deep ore deposits (translated by E. Erlich and M.-M. Coates); Colorado Mountain Publishing House, Denver, Colorado, 205 p.

Advancing the Utility of the British Columbia Regional Geochemical Survey Database Using Indicator Minerals Derived from a Regional Bulk Stream-Sediment Survey, Boundary District, South-Central British Columbia (NTS 082E)

W. Jackaman, Noble Exploration Services Ltd., Jordan River, British Columbia, wjackaman@shaw.ca

R.E. Lett, Victoria, British Columbia

Jackaman, W. and Lett, R.E. (2020): Advancing the utility of the British Columbia Regional Geochemical Survey database using indicator minerals derived from a regional bulk stream-sediment survey, Boundary District, south-central British Columbia (NTS 082E); *in* Geoscience BC Summary of Activities 2019: Minerals, Geoscience BC, Report 2020-01, p. 109–114.

Introduction

Government-funded, reconnaissance-scale regional geochemical surveys (RGS) have been routinely conducted in British Columbia (BC) since 1976 (McCurdy et al., 2014). During this time, silt-sediment samples have been collected from more than 55 000 sites distributed throughout the province. The BC Geological Survey, the Geological Survey of Canada and Geoscience BC continue to support the development of the RGS database. New field surveys have been conducted and most available archived materials have been included in sample-reanalysis initiatives. The resulting RGS database has evolved into a comprehensive collection of field information plus accompanying multi-element analytical data. It continues to be recognized as an important resource for supporting mineral-exploration activities.

Although RGS coverage is extensive and the resulting database has great utility, there remain opportunities to collect samples in regions not previously surveyed and, more notably, in areas that have a limited number of existing sample sites. In many of these areas, deficiencies exist due to survey parameters established by the Geological Survey of Canada (GSC) that specified average densities to be one sample site every 13 km^2 (Friske and Hornbrook, 1991). The targeting of first- and second-order drainages at this scale has resulted in the partial coverage of some previously surveyed areas. In addition, using conventional silt sampling at the outlets of larger drainage basins potentially misrepresents the geochemical information generated due to the influence of sediment dilution and greater lithological variations within the stream catchment (Fletcher, 1997; Heberlein, 2013).

To examine how to resolve these gaps in the RGS database, a modified RGS sampling strategy that integrates the collection of bulk stream-sediment samples and derived mineralogical information, plus trace-metal data, has been included as part of a new regional stream-sediment survey conducted in the Boundary District in south-central BC (Figure 1).

Project Objectives

Indicator minerals derived from bulk sediments collected at the outlets of large drainage basins can effectively detect potential mineral deposits at far greater distances upstream than conventional silt sampling (McClenaghan, 2005). Extending the length of detectable mineral-dispersion trains enables the use of significantly fewer, strategically located bulk-sediment sample sites. Processing bulk-sediment material captures gold and sulphide mineral grains, plus potential oxide- and silicate-mineral indicators. Interpreting the abundance of these mineral grains and their morphological characteristics provides information about potential economic mineralization associated with precious- and base-metal deposit types that may exist upstream from a sample site in a drainage basin.

Collecting bulk sediments at a density of one site per 100 km^2 is routinely used as part of the Geological Survey of Canada's (GSC) current National Geochemical Reconnaissance (NGR) program and has been successful in detecting a variety of ore-deposit types (McCurdy et al., 2014). In BC, indicator-mineral methods are included as part of regional till surveys (Jackaman and Sacco, 2014) but are not yet fully integrated into regional stream-sediment programs.

Conducting a bulk-sediment sampling program in an area that was previously covered by a government-funded RGS program will demonstrate that this method can improve existing geochemical coverage; can add valuable mineralogical information to the existing RGS database; can enable relatively larger areas to be effectively assessed for mineral deposits; and is complementary to other exploration initiatives. In addition, this survey strategy targets considerably fewer sample sites, allowing for significant cost savings when compared to conventional infill methods that require

This publication is also available, free of charge, as colour digital files in Adobe Acrobat® PDF format from the Geoscience BC website: http://www.geosciencebc.com/updates/summary-of-activities/.

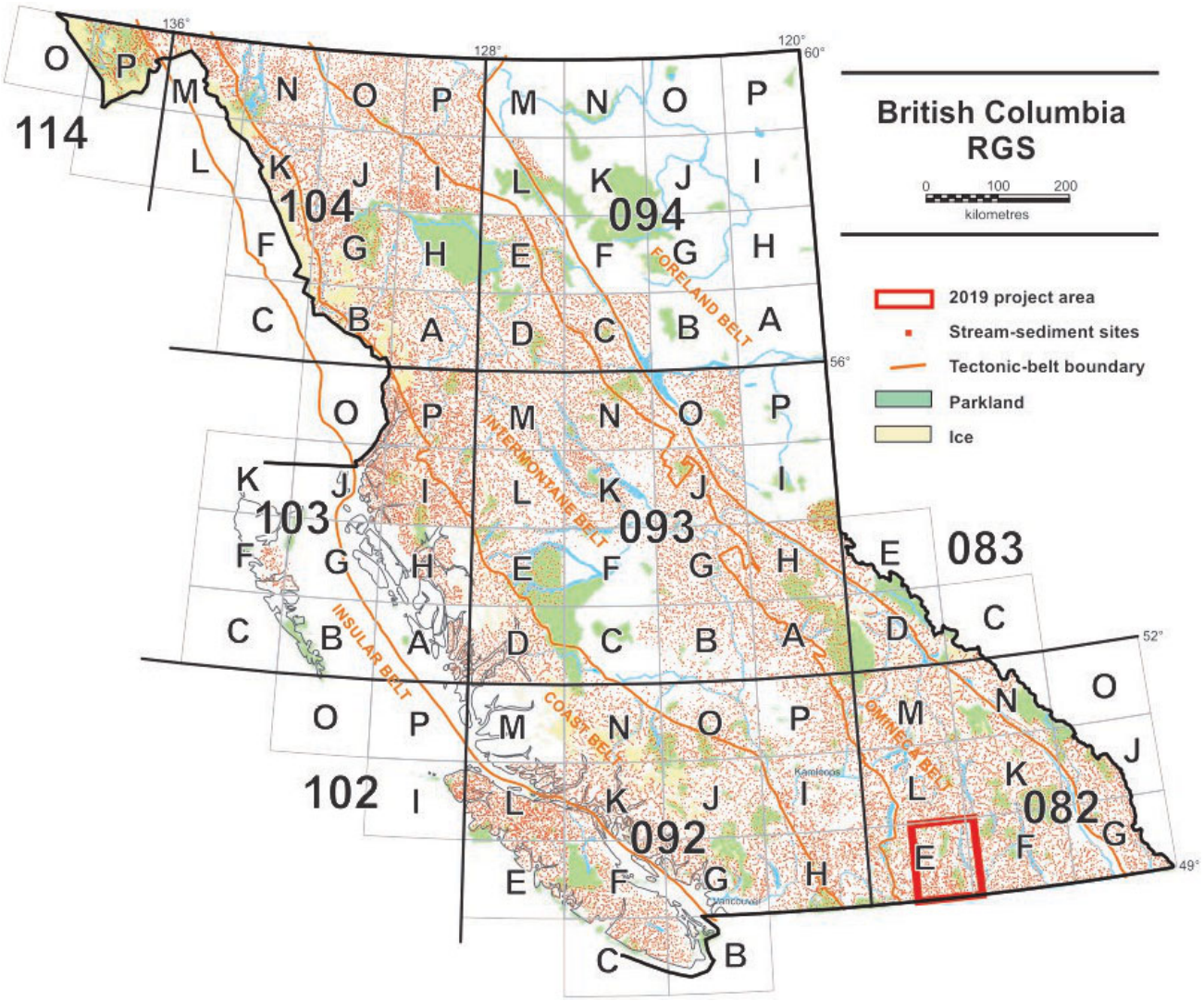

Figure 1. Location of the study area in the Boundary District, south-central BC.

greater sample-site densities and, more commonly, helicopter support.

Project Location

The project area is focused on the east half of NTS area 082E and covers approximately 10 000 km^2 (Figure 2). It is in the Columbia Mountain physiographic region. The west edge of the survey area includes part of the Okanagan Highland and extends east through the Monashee Mountains, past Lower Arrow Lake and into the Selkirk Mountains (Holland, 1976). Mountain peaks up to 2000 m in elevation are common and are drained by the Kettle and Granby rivers.

This region was targeted for this study for a number of reasons: 1) historical Au and Ag (plus Cu, Pb and Zn) mining camps hosted within a prospective geological setting continue to support an active exploration community; 2) other locally focused geoscience initiatives are ongoing, including an extensive geological mapping and mineral-evaluation program (Höy, 2019) funded by Geoscience BC; 3) the area offers ample opportunities to access sites using a well-developed highway and forest-service-road infrastructure; 4) the mountainous terrain that contains abundant, well-defined stream drainages suitable for regional geochemical stream-sediment surveys is typical of many areas in BC; and 5) a previous government-funded RGS program was completed in the area in the mid-1970s.

Previous RGS Programs

In 1976, reconnaissance-scale stream-sediment and water regional geochemical surveys were conducted by the GSC (Matysek et al., 1991). Within the study area, more than 1000 conventional silt-sediment samples were collected at an average sample-site density of approximately one site every 8 km^2. First- and second-order drainages would generally have been targeted, although many larger drainages (>10 km^2) would also have been sampled. These samples

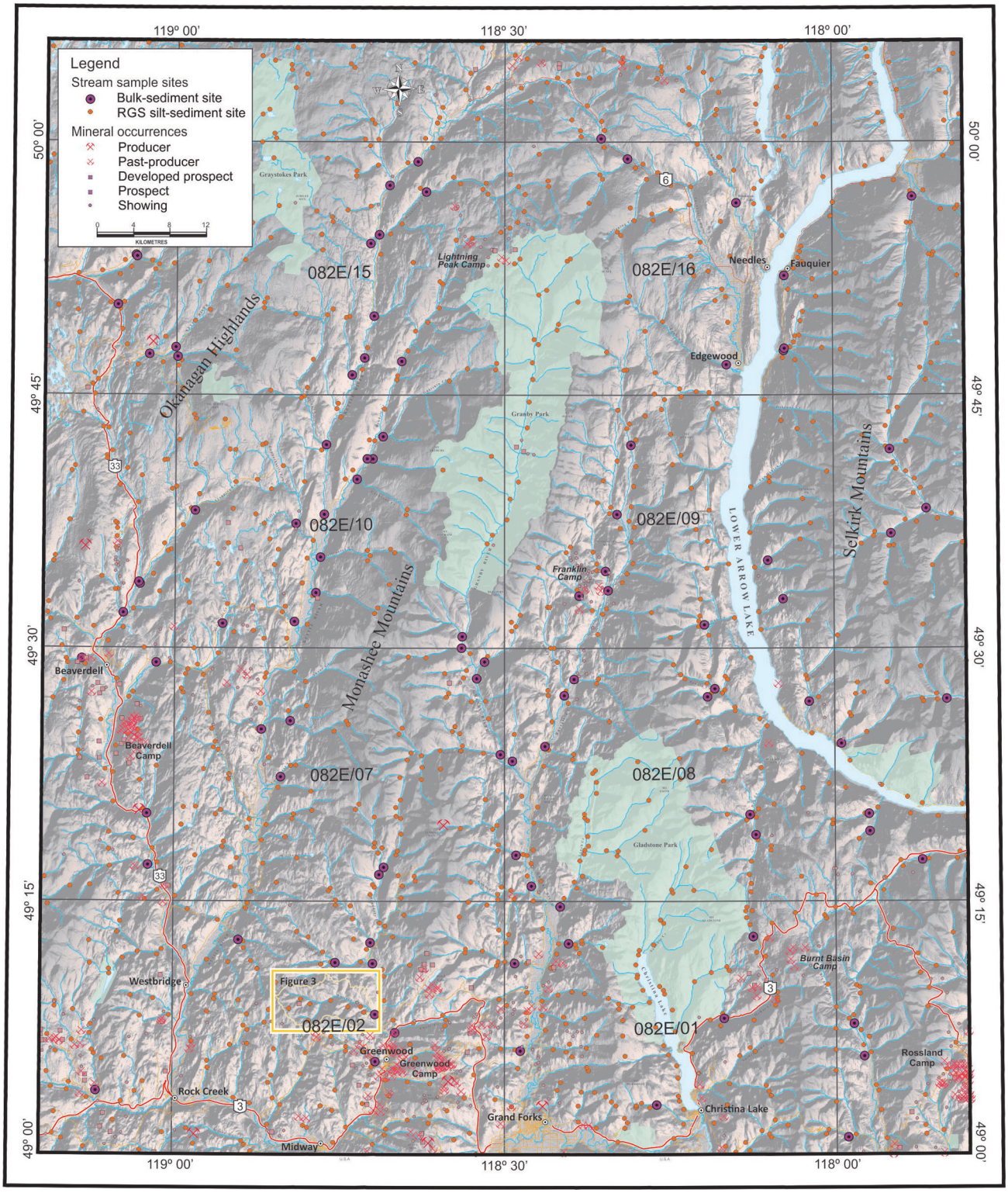

Figure 2. Distribution of MINFILE occurrences, previous RGS silt-sediment sample sites and new bulk-sediment sites in the study area, Boundary District, south-central BC. Digital elevation model from Natural Resources Canada (2015).

weighed from 1 to 2 kg and consisted of recently deposited, fine-grained sediments collected within the active stream channel.

Using the Wallace Creek drainage basin as an example, Figure 3 illustrates a typical distribution of silt-sediment samples collected during the 1976 RGS program. As part of the current study, a single bulk-sediment sample was collected at the main stem outlet. Six of the sites are at the outlets of small first- or second-order tributaries that have an average basin area of 2.5 km^2, and three sites located on the main stem of Wallace Creek drain areas of 20, 31 and 38 km^2. Coordinates for the RGS sites were acquired from Han and Rukhlov (2017). Originally digitized from 1:250 000 scale maps, location information collected during early RGS programs is inaccurate when mapped at a greater scale and results in sites being detached from the intended stream channel. To correct this situation, site locations were moved to the closest stream channel. The PEN Zn-Ag-Pb-Cu prospect (NTS 082E/02; MINFILE 082ESE118; BC Geological Survey, 2019) and CM Cu showing (NTS 082E/02; MINFILE 082ESE196) are located in the drainage, and underlying geology is from Höy (2019).

Sample pulps from these surveys were saved and stored at the GSC facilities in Ottawa. Starting in 1990, the samples were recovered from storage and reanalyzed by instrumental neutron activation analysis (INAA; Jackaman et al., 1991). In 2009, Geoscience BC funded the reanalysis of these pulps by inductively coupled plasma–mass spectrometry (ICP-MS; Jackaman, 2010).

Project Methods

Sample collection, sample processing and analytical methods are based on protocols developed by the GSC's NGR program. Accredited laboratories with previous experience of NGR requirements have been selected for sample preparation and analysis. These guidelines ensure that portions of collected materials can be incorporated into existing GSC and BC Geological Survey (BCGS) archives, and survey results can be included as part of the provincial and national geochemical databases.

During the late summer of 2019, 98 bulk sediment samples, 104 conventional silt samples and 98 pebble samples were collected at 98 stream sites draining areas that averaged 35 km^2. The smallest drainage sampled was 15 km^2 and the largest was more than 80 km^2. The average stream-channel width was 8 m and channel-bed composition ranged from gravels to cobbles in the larger valleys, with boulders in steeper drainages at higher elevations. Although efforts

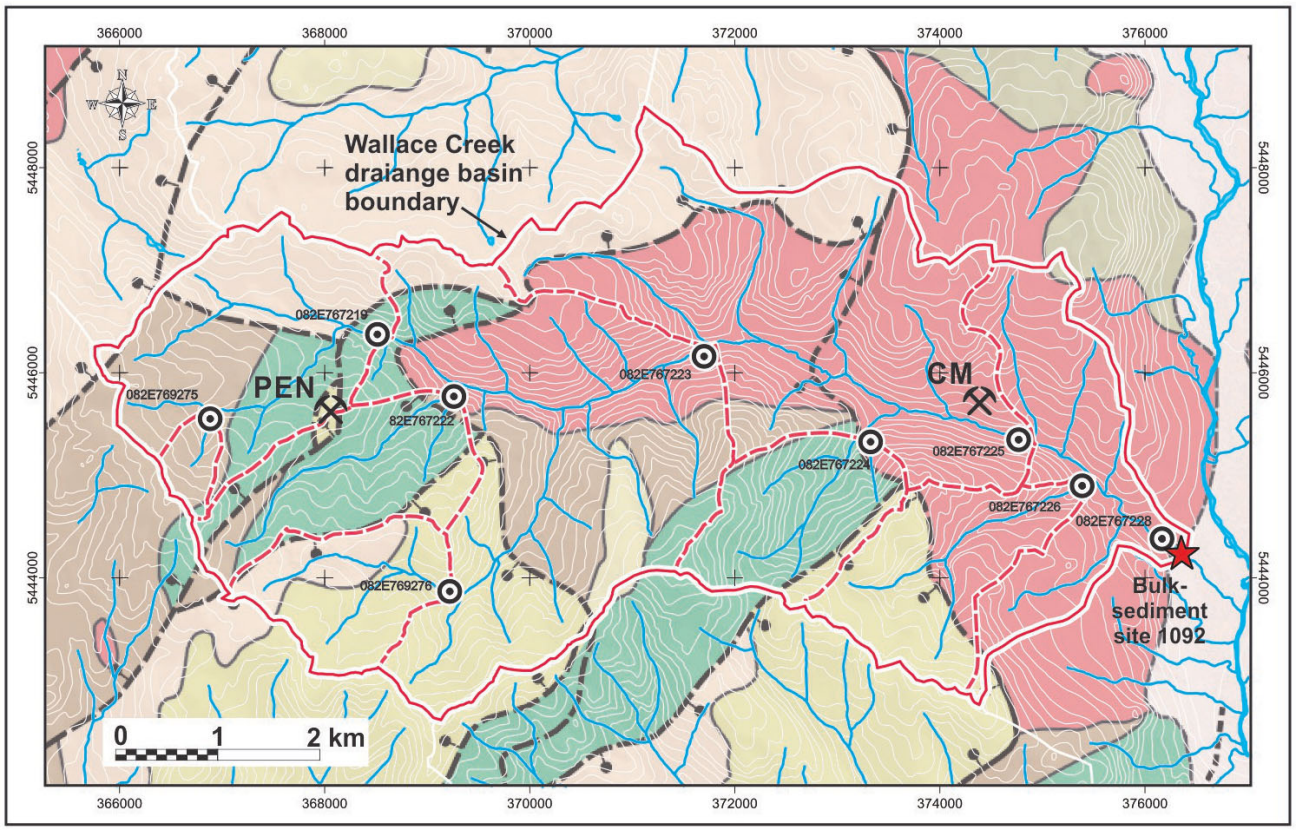

Figure 3. Typical distribution of the previous RGS silt-sediment sample sites and their relationship to a bulk-sediment sample collected at the main stem outlet of Wallace Creek. Mineralization: PEN Zn-Ag-Pb-Cu prospect, CM Cu showing.

were made to collect samples from predetermined sites, restrictions related to road quality and access to private land resulted in the collection of some samples from alternate locations.

At each site, a 12–15 kg bulk sample of sediment was collected from a single 50–75 cm deep, hand-dug pit located at the upstream end of mid-channel or side-channel bars or from mid-channel boulder traps (Figure 4). The material was obtained by wet-sieving coarse-grained sands and gravel using a US Sieve Series 10-mesh (2 mm) sieve and capturing the less than 10 mesh size grains in a 20 litre plastic pail lined with a polyethylene sample bag. Conventional silt samples were also collected from the active stream channel. An approximately 2 kg sample of fine-grained material was recovered and placed in a synthetic cloth bag. In addition, 50 large pebbles acquired from the oversized material during the sieving process were placed in a synthetic cloth bag. Standard field observations, photographs and location co-ordinates were recorded. Samples were sealed immediately after collection and carefully transported to ensure that their integrity would not be compromised.

Before processing of the bulk-sediment samples by Overburden Drilling Management Limited (Nepean, Ontario), a 500 g character sample is collected from each sample for archiving. The bulk-sediment samples will then be progressively reduced by a range of processing techniques to concentrate gold and base-metal indicators. Potential oxide and silicate indicators of massive-sulphide deposits will be visually identified, counted and hand-picked.

Stream-sediment samples are being air-dried at temperatures below 40°C. After drying, samples will be sieved through a minus 80 mesh (177 µm) screen. Control reference and duplicate samples will be inserted randomly into each batch of 20 samples.

Processed sediment pulps and a minus 80 mesh sample recovered from the bulk samples will be analyzed by Bureau Veritas Commodities Laboratory (Vancouver, BC) for minor and trace elements by ICP-MS following aqua-regia digestion (53 elements). Total gold determinations plus 35 elements by INAA will be provided by Maxxam Analytics, a Bureau Veritas Group company. Loss-on-ignition (LOI) will also be determined.

Pebble samples will be sorted and catalogued to provide information on the lithology of bedrock sources found upstream from the sample site.

Summary

Incorporating bulk stream-sediment sampling into government-funded regional geochemical surveys has been identified for effectively maintaining strict design requirements and program objectives while reducing overall collection costs. There are numerous opportunities to apply this survey technique in BC, including regions where RGS programs have not been conducted and areas where nominal sample-site densities may have undervalued mineral assessments or inadvertently misrepresented geochemical results.

Guided by NGR specifications, older RGS programs typically collected conventional silt-sediment samples at an average sample-site density of one site every 13 km^2. Although first- and second-order drainages were targeted, larger drainages were also sampled. Widely spaced sample sites leave large areas unrepresented. The geochemical results from samples collected at the outlet of large drainages could also be adversely affected by dilution of anomalous sediment and by complex bedrock and surficial geology that may limit the extent of element dispersal.

Figure 4. Examples of representative bulk-sediment sample sites located on **a)** the upstream end of a mid-channel bar, and **b)** a mid-channel boulder trap.

This project has been designed to demonstrate the application of this method in the ongoing development of the BC RGS database. It is expected that acquiring indicator minerals from a relatively small number of strategically located sample sites will improve overall geochemical coverage and enhance the detection and interpretation of mineral dispersion. Applying this technique to other regions of the province can further the utility of the existing RGS database as an exploration tool for the discovery of hidden mineralization, and be accomplished economically.

Results of this study are scheduled to be released in late spring 2020.

Acknowledgments

This program was funded by Geoscience BC. Commendable assistance with the field program by J. Constandinou was very much appreciated. The manuscript benefited considerably from comments provided by N. Nunn and T. Höy.

References

BC Geological Survey (2019): MINFILE BC mineral deposits database: BC Ministry of Energy, Mines and Petroleum Resources, BC Geological Survey, URL <http://www.minfile.ca> [November 2019].

Fletcher, W.K. (1997): Stream sediment geochemistry in today's exploration world; *in* Proceedings of Exploration 97: Fourth Decennial International Conference on Mineral Exploration, A.G. Gubins (ed.), Prospectors and Developers Association of Canada, p. 249–260.

Friske, P.W.B. and Hornbrook, E.H.W. (1991): Canada's National Geochemical Reconnaissance programme; Transactions of the Institution of Mining and Metallurgy, sec. B, v. 100, p. 47–56.

Han, T. and Rukhlov, A.S. (2017): Regional Geochemical Survey (RGS) data update and release using the newly developed RGS database; BC Ministry of Energy, Mines and Petroleum Resources, BC Geological Survey, GeoFile 2017-11, 7 p., URL <http://cmscontent.nrs.gov.bc.ca/geoscience/PublicationCatalogue/GeoFile/BCGS_GF2017-11.pdf> [November 2019].

Heberlein, D.R. (2013): Catchment basin analysis and weighted sums modeling: enhanced interpretation of RGS data using examples from map sheets NTS 105M, 105O and part of 105P; Yukon Geological Survey, Open File 2013-16, 18 p. and 116 maps, URL <http://data.geology.gov.yk.ca/Reference/68175> [November 2019].

Holland, S.S. (1976): Landforms of British Columbia: a physiographic outline; BC Ministry of Energy, Mines and Petroleum Resources, BC Geological Survey, Bulletin 48, 136 p., <http://cmscontent.nrs.gov.bc.ca/geoscience/PublicationCatalogue/Bulletin/BCGS_B048.pdf> [November 2019].

Höy, T. (2019): Geology of the Penticton map sheet (NTS 082E east half); Geoscience BC, Map 2019-04, scale 1:150 000, URL <http://cdn.geosciencebc.com/project_data/GBCR2019-04/GBCMap2019-04.pdf> [November 2019].

Jackaman, W. (2010): QUEST-South Project sample reanalysis; Geoscience BC, Report 2010-4, 4 p., URL <http://www.geosciencebc.com/reports/gbcr-2010-04/> [November 2019].

Jackaman, W. and Sacco, D. (2014): Geochemical and mineralogical data, TREK Project, Interior Plateau, British Columbia; Geoscience BC, Report 2014-10, 13 p., URL <http://www.geosciencebc.com/reports/gbcr-2014-10/> [November 2019].

Jackaman, W., Matysek, P.F. and Cook, S.J. (1991): The Regional Geochemical Survey program: summary of activities; *in* Geological Fieldwork 1991, BC Ministry of Energy, Mines and Petroleum Resources, BC Geological Survey, Paper 1992-1, p. 307–318, URL <https://www2.gov.bc.ca/gov/content/industry/mineral-exploration-mining/british-columbia-geological-survey/publications/papers-1999-1980#1992> [November 2019].

Matysek, P.F., Jackaman, W., Gravel, J.L., Sibbick, S.J. and Feulgen, S. (1991): British Columbia regional geochemical survey, Penticton (NTS 82E), stream sediment and water geochemical data; BC Ministry of Energy, Mines and Petroleum Resources, BC Geological Survey, Regional Geochemical Survey, Open File 29 / Geological Survey of Canada, Open File 2354, 21 p., URL <https://geochem.nrcan.gc.ca/cdogs/content/pub/pub00446_e.htm> [November 2019].

McClenaghan, M.B. (2005): Indicator mineral methods in mineral exploration; Geochemistry: Exploration, Environment, Analysis, v. 5, p. 233–245, <https://pubs.geoscienceworld.org/geea/article-abstract/5/3/233/22635/Indicator-mineral-methods-in-mineral-exploration?redirectedFrom=fulltext> [November 2019].

McCurdy, M.W., Spirito, W.A., Grunsky, E.C., Day, S.J.A., McNeil, R.J. and Coker, W.B. (2014): The evolution of the Geological Survey of Canada's regional reconnaissance geochemical drainage sediment and water surveys; Explore, no. 163, p. 1, 3–4, 6–10.

Natural Resources Canada 2015: Canadian Digital Elevation Model; Natural Resources Canada, URL <https://open.canada.ca/data/en/dataset/7f245e4d-76c2-4caa-951a-45d1d2051333> [November 2019].

Porphyry Vectoring within Advanced Argillic-Altered Rocks of British Columbia

F. Bouzari, Mineral Deposit Research Unit, The University of British Columbia, Vancouver, British Columbia, fbouzari@eoas.ubc.ca

R.G. Lee, Mineral Deposit Research Unit, The University of British Columbia, Vancouver, British Columbia

C.J.R. Hart, Mineral Deposit Research Unit, The University of British Columbia, Vancouver, British Columbia

B.I. van Straaten, British Columbia Geological Survey, Victoria, British Columbia

Bouzari, F., Lee, R.G., Hart, C.J.R. and van Straaten, B.I. (2020): Porphyry vectoring within advanced argillic-altered rocks of British Columbia; *in* Geoscience BC Summary of Activities 2019: Minerals, Geoscience BC, Report 2020-01, p. 115–130.

Introduction

Porphyry copper deposits commonly form vertical bodies of mineralized rock and alteration zones that vary depending on depth, fluid composition and hostrock. In many calcalkalic-type porphyry deposits, a large blanket of advanced argillic-altered rocks that are characterized by abundant quartz and clay minerals form a cap above the main porphyry intrusion. However, the location of the porphyry system beneath this lithocap is rarely apparent and new tools are required to inform exploration decision-making in these geological situations.

The application of alteration studies has played a key role in the discovery of several porphyry deposits, and recent research at The University of British Columbia's Mineral Deposit Research Unit (MDRU) has identified the distal alteration-footprint characteristics of the porphyry system (e.g., Halley et al., 2015; Lesher et al., 2017), and the use of resistate minerals for alteration studies (e.g., Bouzari et al., 2016). However, most of these studies focused on the broader alteration footprints of the porphyry system and did not examine the advanced argillic alteration above these systems.

Advanced argillic alteration has been preserved at several British Columbia (BC) localities (Table 1). Studies in the Toodoggone district (Bouzari et al., 2019), the Bonanza volcanic field in northern Vancouver Island (Panteleyev and Koyanagi, 1994), Limonite Creek in central BC (Deyell et al., 2000) and several other locations in BC have recognized linkages to porphyry-type mineralization at depth. Identifying the textural, mineralogical and geochemical trends within these advanced argillic-alteration zones will guide BC explorers in better identifying porphyry copper potential and provide tools that point toward mineralization.

Table 1. Localities with advanced argillic alteration in British Columbia (after Panteleyev, 1992).

Property	Advanced argillic alteration	High-sulphidation-type sulphide	Porphyry-type alteration or veins
Sutlahine River area:			
Thorn, Daisy, Ink, Camp Creek	X	X	X
Kay, Lin, Lin 1-8	X	X	
Iskut River Area:			
Johnny Mountain/REG/Quartz Rise	X	X	
Treaty Glacier	X		
Dease Lake area:			
Tanzilla-McBride	X		X
Toodoggone River area:			
Alunite Ridge	X	X	X
Quartz Lake	X		
Brenda	X	X	
Black Gossan	X		X
Silver Pond	X		
Baker	X		X
Central BC:			
Equity Silver mine	X		
Limonite Creek	X		X
Taseko River/Mount McClure area:			
Empress	X		
Taylor-Windfall	X	X	
Vancouver Island:			
Hushamu	X	X	X
Macintosh, Pemberton Hills	X		
Red Dog	X		
Wanokana	X		
Island Copper mine	X		X
Kyuquot Sound (Easy Inlet)	X		
Southern BC:			
Riverside	X		
Pyro	X		

This publication is also available, free of charge, as colour digital files in Adobe Acrobat® PDF format from the Geoscience BC website: http://www.geosciencebc.com/updates/summary-of-activities/.

Tops of Porphyry Systems

Advanced argillic alteration in upper parts of porphyry copper systems are known as 'lithocaps' because they cap porphyry deposits, have a blanket-like geometry with areal extents of >10 km^2 and reach a thickness of up to 1 km. Therefore, advanced argillic-alteration zones can form the largest near-surface footprint of porphyry copper systems. Indeed, two or more porphyry copper deposits may underlie some large, coalesced advanced argillic zones (Sillitoe, 2010) and advanced argillic-alteration zones themselves may host high-sulphidation epithermal-type gold mineralization in those locations where they are preserved from erosion.

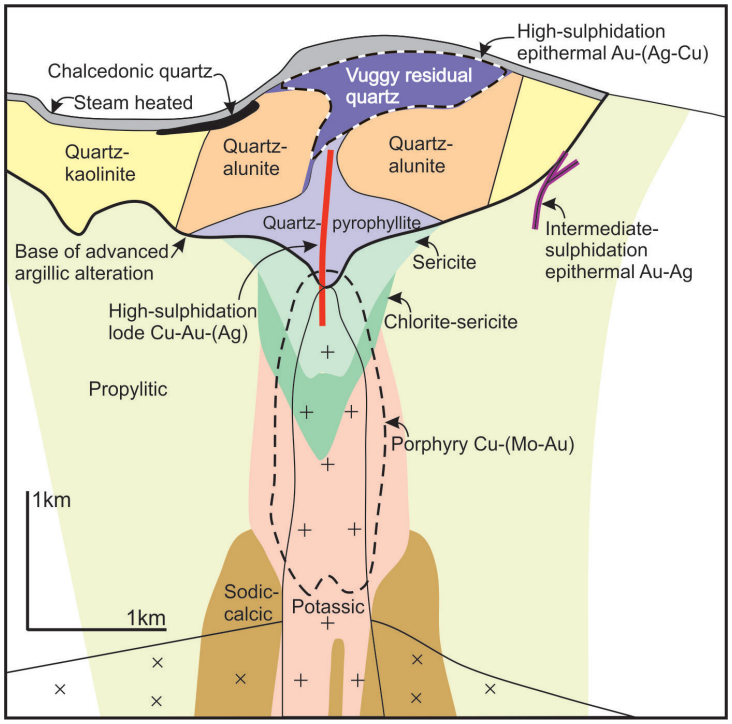

Figure 1. Schematic cross-section showing the main components of advanced argillic alteration above a zone of porphyry mineralization in the study area (after Sillitoe, 2010).

The advanced argillic zones tend to be vertically zoned, from quartz-pyrophyllite locally with andalusite and diaspore at depth to predominantly quartz-alunite and residual quartz with a vuggy appearance at shallower levels. Laterally, kaolinite predominates with topaz and zunyite, and locally fluorite in F-rich systems (Figure 1). In the shallowest zones that form within the paleo–water table, subhorizontal, tabular bodies of massive opaline or chalcedonic silicification, up to 10 m or so thick, are deposited, while steam-heated alteration is characterized by fine-grained, powdery cristobalite, alunite and kaolinite in the overlying vadose zones (Sillitoe, 1993, 2000).

The development of advanced argillic alteration is attributed to two hydrothermal stages (e.g., Simmons et al., 2005):

1) an early stage of intense acid leaching of the wallrocks, which results from magmatic vapours that cool to <300 °C and condense into groundwaters that are acidified by dissociation of potent acids such as HCl or H_2SO_4 (Hedenquist and Taran, 2013)
2) a second stage, which develops from weakly acidic fluid that deposits the bulk of the sulphide minerals and precious metals with euhedral quartz precipitate (Stoffregen, 1987; Heinrich et al., 2004; Heinrich, 2007)

Vectoring in Advanced Argillic Alteration

The recognition of mineralogical patterns within areas of advanced argillic alteration provides a fundamental opportunity to identify the presence of high-sulphidation epithermal-gold and potential underlying porphyry mineralization. Minerals such as diaspore and andalusite with pyrophyllite occur at the roots of advanced argillic alteration above the porphyry system, whereas zones of residual quartz, quartz-alunite and quartz-kaolinite occur laterally in more permeable hostrocks at higher levels.

Mineral exploration in advanced argillic zones is traditionally difficult for several reasons. These alteration zones can cover large areas (>10 km) and not only are the mineralogical changes cryptic but they could be affected by the hostrock composition or obliterated by subsequent supergene weathering effects. Advanced argillic alteration is well developed in hostrocks with low acid-buffering capacity, whereas rocks with high acid-buffering capacity produce weaker advanced argillic alteration and may not develop the typical mineral zoning. As a result, alunite may not form in some areas. Alunite composition itself has been used as a vector toward mineralization (e.g., Chang et al., 2011), but other studies (e.g., Deyell and Dipple, 2005) have shown that alunite chemistry is influenced by hostrocks, may vary between fluid pulses and does not necessarily reflect proximity to mineralization. Moreover, in these environments, alunite can form in at least three types of zones: 1) in the high-sulphidation alteration zone above the pyrophyllite zone; 2) in the steam-heated alteration zone near the surface; and 3) within the overprinting supergene alteration zone. Therefore, distinguishing each of the alunite types, using techniques such as texture and composition, is of significant importance in exploration.

The most abundant mineral within advanced argillic-alteration zones is quartz. Most quartz is residual after intense acid leaching and has a vuggy texture; it can also occur with low-pH stable alunite or kaolinite. Quartz can form during the early barren alteration phase and can be deposited dur-

ing the later gold-mineralization stages. Textures and cathodoluminescence characteristics of the quartz have been used to identify the ore-stage quartz (T. Bissig, pers. comm., 2016).

Clay minerals, such as illite, kaolinite, dickite and montmorillonite are widespread in advanced argillic alteration. The distribution of clay minerals and, more importantly, their crystallinity are useful tools to use as vectors toward rocks affected by higher temperature alteration. However, advanced argillic-alteration zones typically contain abundant, fine-grained disseminated pyrite. Oxidation of pyrite during the supergene processes also generates acids and abundant clays (mostly kaolinite), and can obliterate the hypogene mineralogy. Therefore, distinction of supergene clay and identifying the remnants of hypogene advanced argillic alteration is important in areas affected by supergene oxidation.

Geological Setting

Advanced argillic-alteration zones occur in several locations in BC, commonly within the districts that are highly prospective to host porphyry-type copper mineralization (Table 1). They occur throughout BC but cover larger areas in northern BC and Vancouver Island. Some of these areas have been evaluated to host epithermal-type gold mineralization, but evidence for underlying porphyry-type copper mineralization has been shown to occur in several locations such as in the Toodoggone and Sutlahine River areas and on Vancouver Island (Table 1). Moreover, these highly-altered areas could also be considered to have resource potential for kaolinite and silica (Shearer et al., 2004).

In this study, three areas in northern BC with notable advanced argillic-alteration zones are evaluated: Tanzilla, Alunite Ridge and Kemess North (Figure 2).

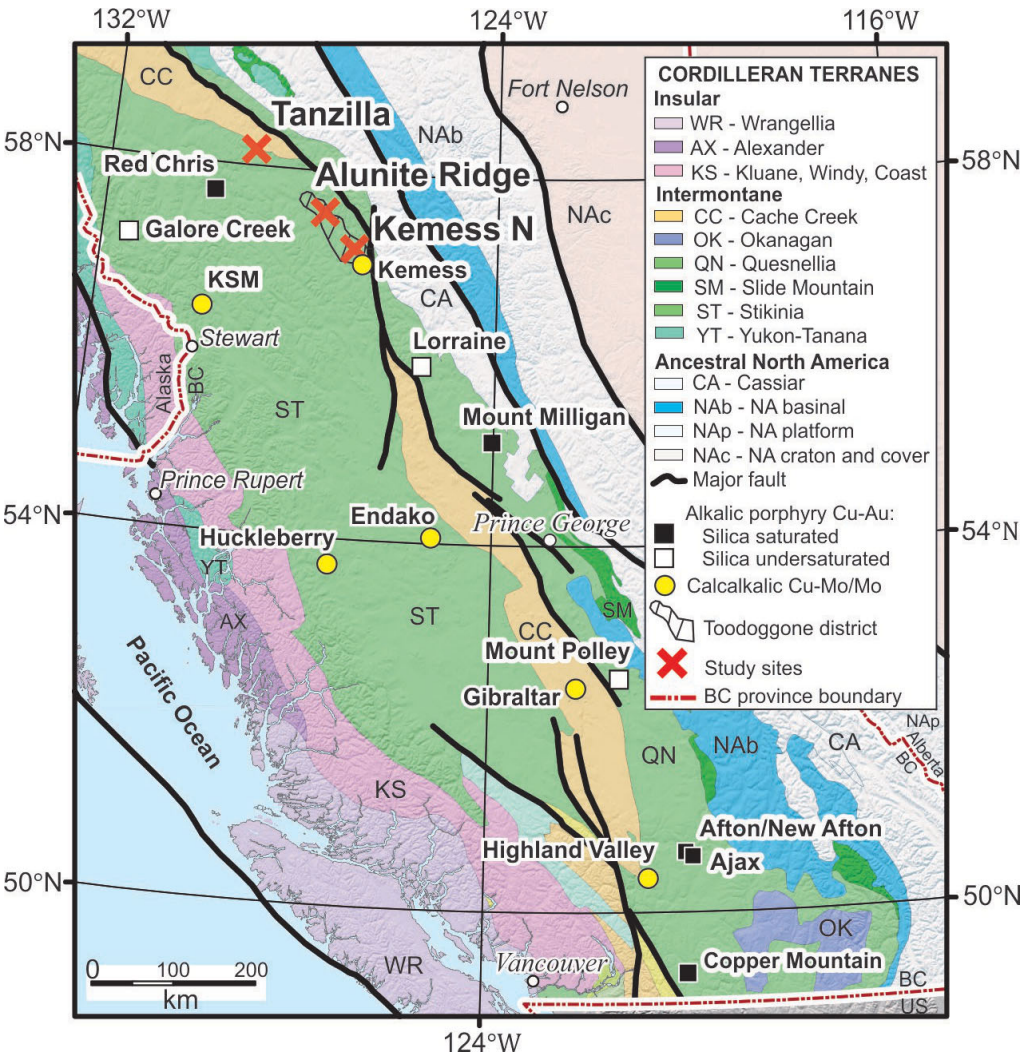

Figure 2. Cordilleran terranes of British Columbia showing the location of the study areas (after Bissig and Cooke, 2014).

Tanzilla

The Tanzilla property is within the Intermontane belt, near the northeastern margin of the Stikine terrane (Figure 2), a Late Triassic–Early Jurassic volcanic island-arc complex that was accreted to ancestral North America during the Middle Jurassic (Nelson and Mihalynuk, 1993). The property is underlain by a volcanic succession about 4.5 km thick assigned to the Horn Mountain Formation (late Early to Middle Jurassic; van Straaten and Nelson, 2016) in the upper part of the Hazelton Group (Figure 3). The lower part of the Horn Mountain Formation includes massive green augite-plagioclase-phyric volcanic breccia (not exposed in the study area), whereas the middle part is mainly maroon volcanic breccias, autobreccias and flows, and includes minor laminated felsic tuffs to bedded lapillistone. The upper parts of the Horn Mountain Formation consist of a felsic volcanic unit of mainly aphanitic and plagioclase-phyric clasts capped by a mafic volcanic unit of augite-plagioclase–phyric volcanic breccias and flows (van Straaten and Gibson, 2017). These units are unconformably overlain by sedimentary rocks of the Bowser Lake Group. To the north, folded Takwahoni Formation siliciclastic rocks (Early Jurassic) deposited in the Whitehorse trough are in the hangingwall of the Kehlechoa thrust fault. The Late Jurassic Snowdrift Creek pluton (160.43 ±0.16 Ma; van Straaten and Gibson, 2017) cuts the Horn Mountain strata and the Kehlechoa thrust fault. Moderate to intense pervasive biotite alteration is reported from several hundred metres up to one kilometre from the margin of the Snowdrift Creek pluton (van Straaten and Gibson, 2017).

The Horn Mountain Formation hosts areally extensive advanced argillic alteration at the Tanzilla-McBride property for at least 17 km along strike (van Straaten and Gibson, 2017; van Straaten and Bouzari, 2018). At Tanzilla, the advanced argillic-alteration zone is at least 5 by 2 km and overlies porphyry-style alteration at depth, which is characterized by quartz-sericite-pyrite to potassic alteration with anomalous copper and molybdenum centred around a 173 Ma plagioclase porphyry body (van Straaten and Nelson, 2016; van Straaten and Gibson, 2017).

Recent work at Tanzilla includes geophysical surveys, diamond drilling, mapping and a shortwave-infrared (SWIR) alteration-mineral study (Luckman et al., 2013; Barresi et al., 2014; van Straaten and Gibson, 2017; van Straaten and Bouzari, 2018).

Alunite Ridge

Alunite Ridge is located within the Toodoggone district in the Stikine terrane of northeastern BC (Figure 2). The Toodoggone district hosts a number of preserved Early Jurassic high- and low-sulphidation epithermal-type deposits (e.g., Alunite Ridge, Brenda, Shasta, Lawyers) with advanced argillic-alteration zones (Diakow et al., 1993; Bouzari et al., 2019). These deposits are hosted by a thick (>2 km) succession of Early Jurassic subaerial andesitic and dacitic volcanic rocks of the Toodoggone Formation (lower part of the Hazelton Group; Diakow et al., 1993). These and underlying strata were probably covered by thick successions (>4 km) of Jurassic and Cretaceous Bowser and Sustut basin clastic strata that protected and facili-

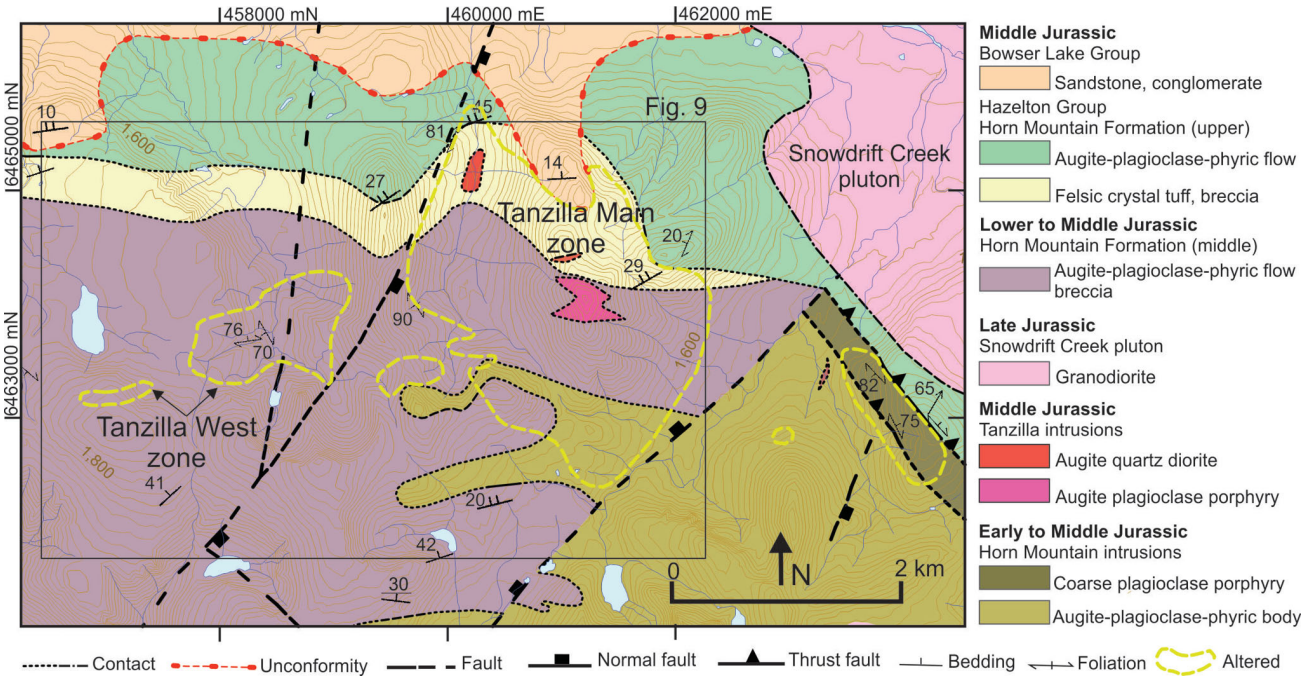

Figure 3. Geology of the Tanzilla study area (after van Straaten et al., 2017).

tated the preservation of the epithermal deposits during subsequent, post-Late Cretaceous uplift.

The Alunite Ridge area near Quartz Lake hosts several mineral occurrences, including Quartz Lake, Alunite Ridge, North Ridge and Sickle Creek. The Alunite Ridge and North Ridge occurrences form two northeast-trending ridges and the Quartz Lake occurrences are in the intervening valley. The underlying geology consists of lower Toodoggone Formation andesitic lava flows, tuffs, breccia and epiclastic rocks that are intruded by small dikes and stocks of monzonite (Figure 4). The Jock Creek monzonitic pluton forms a large body to the south and east.

Zones of intense alteration are northwest-trending and about 200 m wide. Gold mineralization occurs in a 10–15 m wide zone (Duuring et al., 2009) of silicified rock with quartz-alunite alteration, locally with vuggy textures and zones of buff-grey intense diaspore alteration (Bouzari et al., 2019). These are surrounded by quartz-sericite alteration, which locally contains pyrophyllite in zones that transition to the quartz-alunite alteration. Banded quartz veins with calcite and K-feldspar host low-sulphidation–type chalcopyrite-sphalerite-galena-pyrite mineralization and typically occur 100–300 m from the advanced argillic-altered zone at Alunite Ridge. Similar types of veins and mineralization, locally with amethystine quartz, occur at the base of the valley near Quartz Lake. Postmineralization monzonite dikes cut the alteration. A small granodiorite body at the Sofia prospect in the Toodoggone River valley is about 3 km northeast of Alunite Ridge, at an elevation of 1050 m asl (i.e., 700 m lower than Alunite Ridge). The granodiorite at Sofia hosts quartz-magnetite veins with K-feldspar alteration and traces of chalcopyrite, which are typical of deeper level porphyry mineralization (Bouzari et al., 2019).

Kemess North

The Kemess North porphyry mineralization is located about 6.5 km north of the main Kemess deposit (Kemess South) in the southern part of the Toodoggone district (Figure 2). Hostrocks at Kemess North include Upper Triassic Takla Group andesite/basaltic volcanic rocks locally overlain by Lower Jurassic Toodoggone Formation dacitic fragmental volcanic rocks (Figure 5). Toodoggone Formation volcaniclastic rocks crop out as prominent north-trending ridges or as isolated, fault-bounded blocks within Takla Group basalt. Several Early Jurassic stocks or dikes of quartz monzonite to quartz rhyolite composition of the Black Lake intrusive suite have intruded the volcanic succession. The area is dominated by horst-and-graben–style

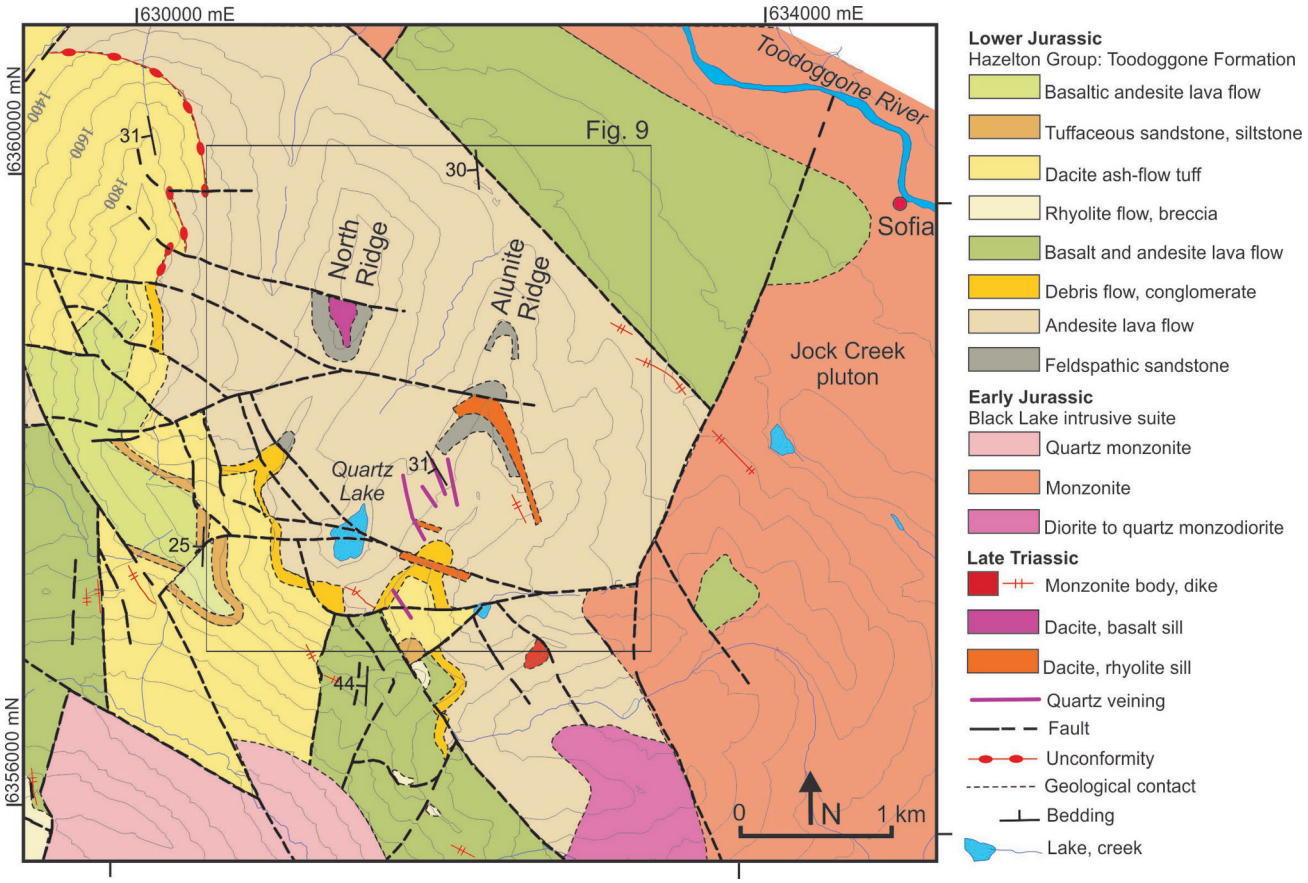

Figure 4. Geology of the Alunite Ridge study area (after Diakow et al., 2006).

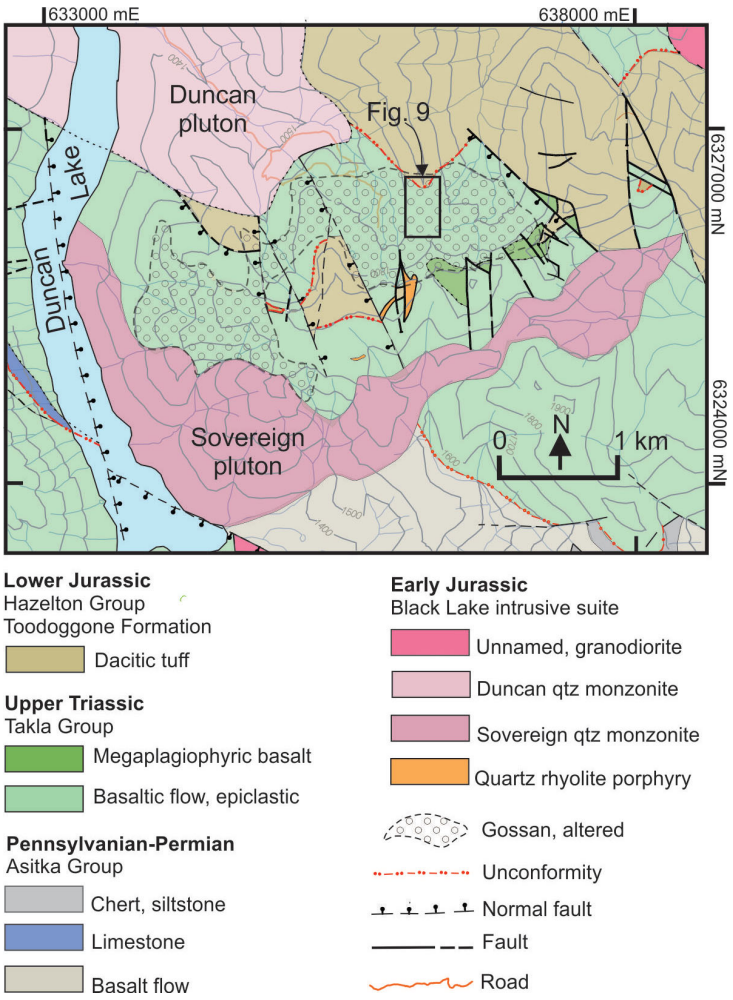

Figure 5. Geology of the Kemess North study area (after Diakow., 2001).

normal faulting, south-dipping thrust faulting and southwest-dipping dip-slip faulting (SRK Consulting Inc., 2016).

Porphyry-type veins and sulphide mineralization are centred around a quartz diorite body (ca. 202 Ma). The east-trending, south-dipping mineralization seems to have formed along faults. Associated phyllic-type alteration is characterized by very fine-grained quartz sericite-chlorite-pyrite alteration. The upper 80 m of the alteration is characterized by a zone of sulphate (anhydrite) leach and distinct depletion in calcium content of the rock (SRK Consulting Inc., 2016). At depth, the K-silicate alteration is characterized by quartz-magnetite stringers with decrease in the pyrite to chalcopyrite ratio. Early-stage veins include magnetite stringer veins and later quartz-magnetite-pyrite+chalcopyrite+molybdenite veins within the K-silicate alteration zone. The Main-stage quartz-pyrite+chalcopyrite± molybdenite veins occur with phyllic (sericite-quartz) alteration and yielded a Re-Os molybdenite age of 201.8 ±1.2 Ma (McKinley, 2006). These veins are cut by late-stage pyrite-chalcopyrite and anhydrite±pyrite±chalcopyrite veins, and postmineralization anhydrite and carbonate-zeolite veins (McKinley, 2006).

Fieldwork, Sampling and Analytical Work

Fieldwork was carried out during June and July 2019 at Tanzilla, Alunite Ridge and Kemess North. Access to the Tanzilla area was by helicopter from Dease Lake, and to Alunite Ridge by helicopter from a seasonable base at the Kemess mine. Access to the Kemess North area was by road from Kemess mine.

At Tanzilla, advanced alteration was mapped and sampled across a 3.5 km north–south profile and a 4 km east–west profile. A total of 54 samples were collected from surface outcrops. Drillhole TZ15-01 (Barresi and Luckman, 2016), which tested mineralization below the Main Ridge to the depth of 840 m (–60°) was examined, and 20 core samples were collected to characterize mineralization at depth. At Alunite Ridge, the footprint of alteration was mapped and sampled along three northeast-trending profiles with a total length of approximately 5 km in an area of 2 by 2 km. In to-

tal, 63 samples from surface outcrops ranging in elevation from 1908 to 1560 m asl and ten samples from drillhole SG-04-18 (SRK Consulting Inc., 2016) to a depth of 227 m below surface (1642 m asl) were collected. At Kemess North, advanced argillic alteration zone was mapped and sampled along a north-south profile of approximately 0.5 km. In total, 18 samples were collected from surface outcrops. Drillholes KN-01-12 and KN-02-09 (SRK Consulting Inc., 2016), which tested mineralization below the advanced argillic alteration to a depth of ~500 m below surface, were examined, and 44 core samples were collected to characterize alteration and mineralization at depth. In addition, from six other holes drilled into the advanced argillic-alteration zone, six samples were collected at a depth of approximately 150 m below surface to further compare with the samples from the surface outcrops.

To further characterize alteration assemblages, all samples were analyzed at MDRU using the tabletop version of the Terraspec® by Analytical Spectral Devices (ASD) Inc., with full-range visible and near-infrared (VNIR) and shortwave-infrared (SWIR) wavelengths for the range of 350–2500 nm. A sheet of Mylar™ was used as a standard, and this sheet was scanned at the start and end of every sampling day. Calibration with the white reflectance disk was completed at the start of every sampling day and re-calibrated every hour. The spectrum input was left at 100, and the white reference was set at 200. Spectra were visually inspected during collection, and where spectra were weak or absent, additional locations on the sample were scanned. Samples were processed with The Spectral Geologist (Commonwealth Scientific and Industrial Research Organisation, 2019) software for measuring spectral features such as wavelength position and crystallinity. Mineral identification and spectra quality assessment (e.g., noise and molecular water contamination) were performed using the SpecWin (Instrument Systems, 2019) software using the SpecMIN™ (Spectral Evolution, 2019) reference library.

All samples were cut into rock slabs and photographed for more detailed description. All samples are being processed for whole-rock geochemical analysis and selected samples for thin-section preparation. The results of these analyses will be provided in a subsequent publication.

Field Observations

Tanzilla

At Tanzilla, advanced argillic alteration covers an area of 5 by 2 km at the western margin of the Snowdrift Creek pluton (Figure 3; van Straaten and Nelson, 2016). The main Tanzilla hill alteration occurs in an area of 2 by 2 km (Figures 3, 6a, b), referred to here as the 'Main zone', but similar types of alteration zones occur 2–3 km to the west, referred to here as the 'West zone'. The hostrocks to the Tanzilla alteration are augite-plagioclase-phyric volcanic rocks with altered mafic minerals (Figure 6c), locally tuff and volcanic breccia (Figure 6d) of the Horn Mountain Formation. Coarse hornblende-plagioclase porphyry (Figure 6e) and feldspar porphyry dikes, with fresh texture or weak alteration, cut the strongly altered volcanic rocks. These porphyry dikes are interpreted as part of Snowdrift Creek pluton (van Straaten and Gibson, 2017).

The Tanzilla area is characterized by a large (>2 km) pale green quartz-green sericite-chlorite-pyrite alteration zone (Figure 6f) that grades to a quartz-white sericite-pyrite assemblage (Figure 6g) toward the zones of advanced argillic alteration. Coarse sericite or muscovite occurs locally within this assemblage. In the Main zone, copper oxides occur with narrow jarosite-goethite veinlets. In more central locations and commonly at higher elevations, the alteration is characterized by highly silicified rock (Figure 6h), with remnants of sericite, pyrite and locally with abundant clays typical of advanced argillic alteration. The latter alteration is developed along structures and locally contains narrow zones of high sulphidation-type pyrite-grey sulphide mineralization. Bladed calcite, coated by quartz and sulphides, now mostly leached, occurs within the silicified rocks of the Main zone (Figure 6k), which suggests a boiling environment at shallow levels.

Alteration outside of the quartz-green sericite-chlorite-pyrite is dominantly darker green chlorite-sericite-pyrite (Figure 6d, i) and more distal patchy chlorite-epidote alteration occurs within the volcanic rocks (Figure 6j).

Porphyry-type alteration occurs in a diorite body at approximately 780 m in drillhole TZ15-01 (Barresi and Luckman, 2016), with K-silicate alteration and weak sulphide mineralization cutting the chlorite-sericite–altered volcanic rock. A similar type of alteration occurs in a coarse-grained pinkish monzodiorite(?) body, approximately 50 m wide, cut by quartz-magnetite-(trace sulphide) veins, about 1.8 km south of the Main zone (Figure 6b, l). Remnants of pervasive, fine-grained biotite alteration at depth in the drillhole, largely replaced by chlorite and sericite, point to an earlier, larger porphyry-related potassic alteration. Thus, the K-silicate–altered monzodiorite and diorite may represent shallower and probably younger manifestations of such an intrusive body at depth in the area, which generated the advanced argillic alteration at the shallowest level.

Alunite Ridge

Advanced argillic alteration at Alunite Ridge occurs for over 2 km along a northeast-trending ridge. Similar types of alteration occur in the North Ridge occurrence approximately 1 km to the northwest (Figure 4). Field observations indicate that the central part of the Alunite Ridge (Figure 7a) is characterized by an alteration zone of strong sili-

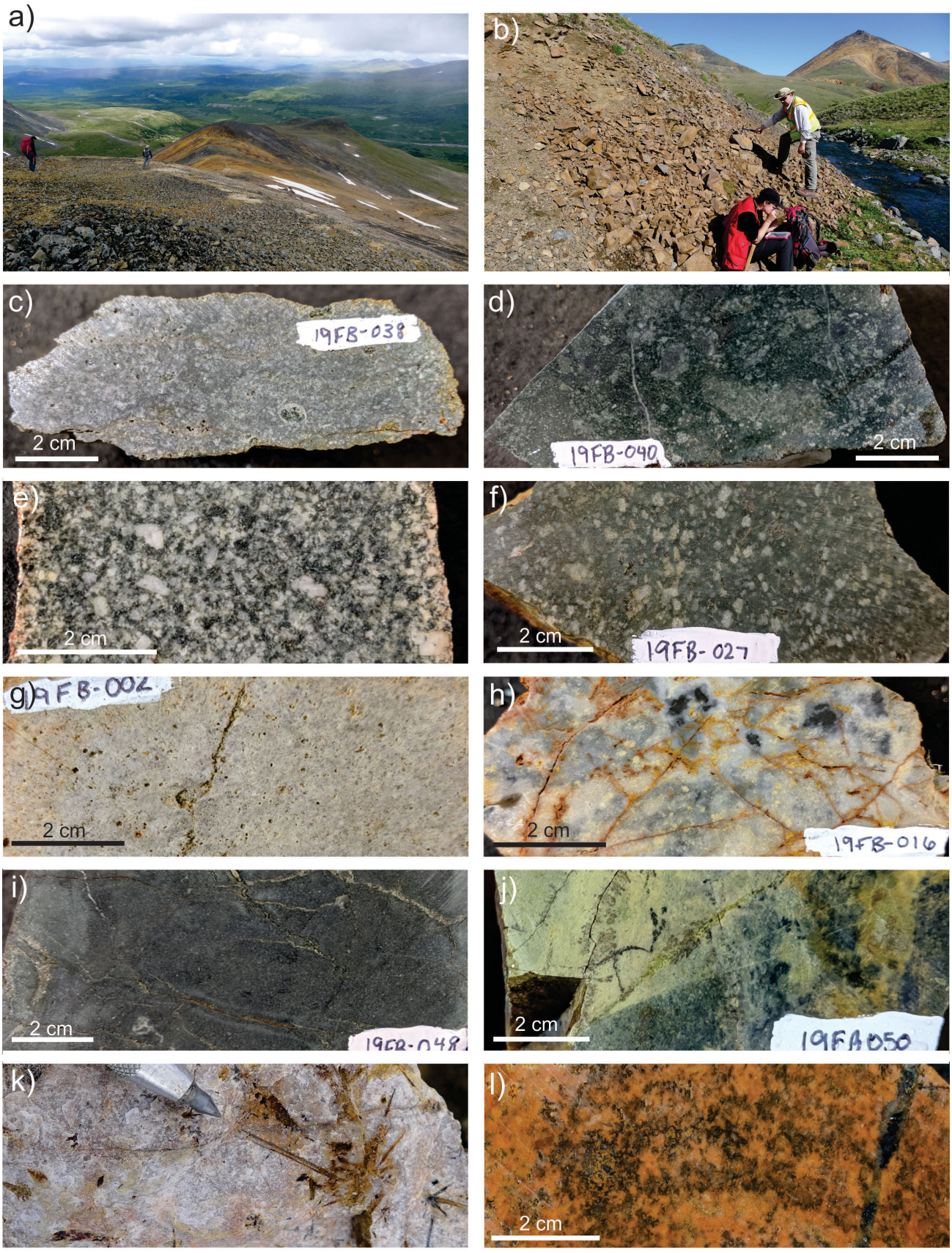
a)
b)
c)
19FB-038
2 cm
d)
19FB-040
2 cm
e)
2 cm
f)
2 cm
19FB-027
g)
2 cm
h)
2 cm
19FB-016
i)
2 cm
j)
2 cm
k)
l)
2 cm

Figure 6. Hostrock and alteration samples from the Tanzilla study area: **a)** looking north to the Tanzilla northern ridge characterized by limonite-stained volcanic outcrops and, in the foreground, an outcrop of weakly altered hornblende-plagioclase porphyry dike; **b)** looking north to the Tanzilla Main zone (in the background), the outcrop in the foreground is a small body of monzodiorite with pervasive biotite and K-feldspar alteration cut by quartz-magnetite-(chalcopyrite) veinlets; **c)** sample of the main hostrock at Tanzilla, which is a plagioclase-phyric volcanic rock with altered mafic minerals; **d)** volcanic breccia with chlorite alteration; **e)** coarse-grained hornblende-plagioclase porphyry with weak chlorite alteration; **f)** sample of pale green quartz-green sericite-chlorite-pyrite altered rock; **g)** sample of quartz-white sericite-pyrite altered rock; **h)** sample showing strong silicification and silica flooding with remnants of sericite alteration; **i)** sample of dark green chlorite-sericite-pyrite alteration; **j)** sample of chlorite-epidote alteration; **k)** silicified bladed calcite, coated by sulphides, now mostly leached; **l)** pinkish monzodiorite(?) cut by quartz-magnetite-(trace sulphide) veins.

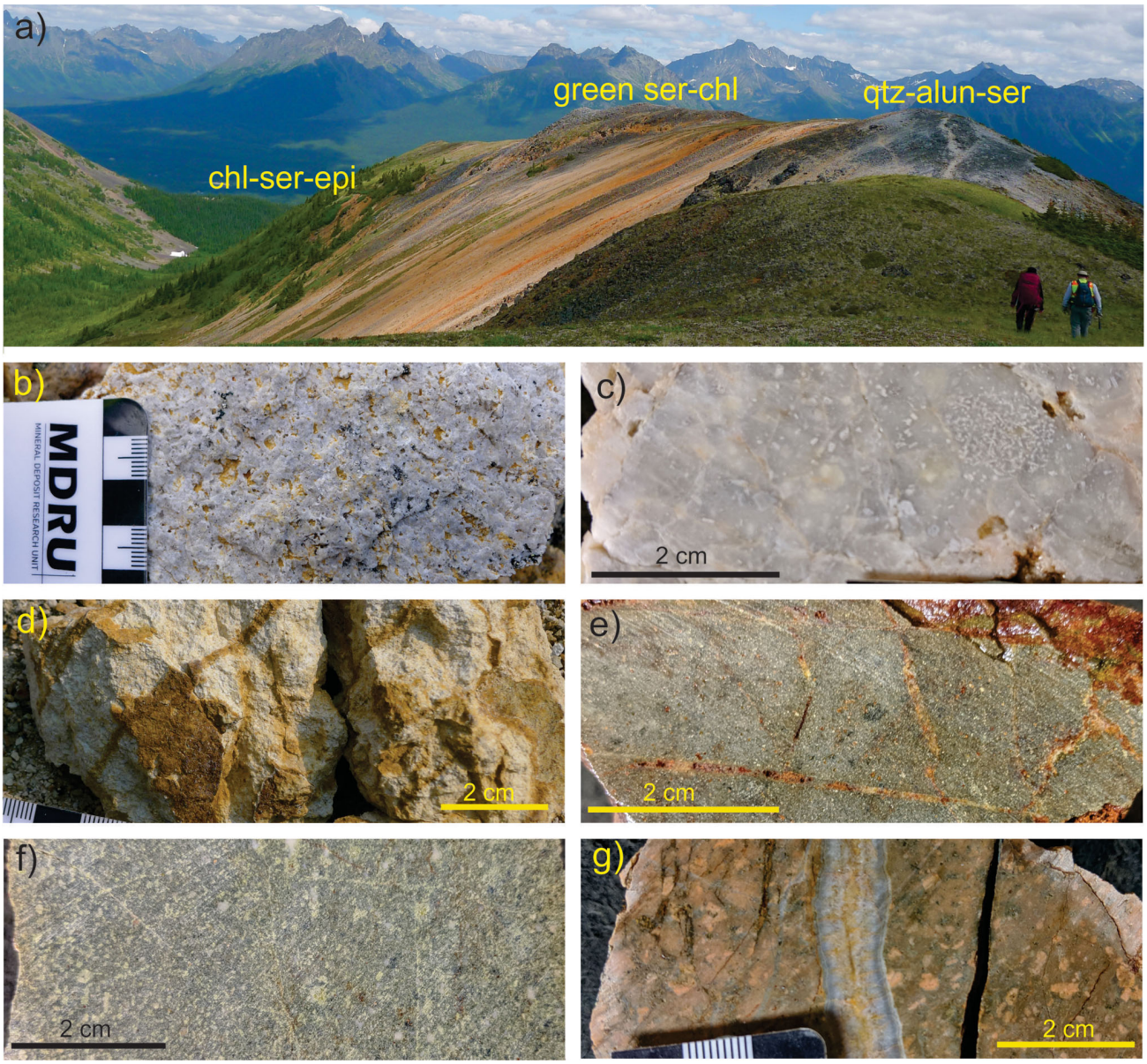

Figure 7. Hostrock and alteration samples from the Alunite Ridge study area: **a)** looking northeast to the Alunite Ridge, showing a grey silicified rock-alunite-sericite (qtz-alun-ser)–rich zone followed by limonite-stained green sericite-chlorite (green ser-chl) alteration and chlorite-sericite-epidote (chl-ser-epi) alteration occurring more distally; **b)** sample of strongly silicified rock displaying vuggy texture; **c)** host volcanic rock with remnants of plagioclase phenocrysts overprinted by silicification, alunite and white sericite alteration; **d)** clay alteration with stockwork of oxidized sulphide veinlets; **e)** pale green sericite-chlorite alteration with disseminated and thin veinlets of pyrite largely oxidized to jarosite; **f)** chlorite-sericite-epidote alteration; **g)** banded quartz and carbonate vein cuts pervasive pink K-feldspar–altered plagioclase porphyry.

cification, locally displaying vuggy texture (Figure 7b). Alunite and white sericite (Figure 7c) occur locally in this zone with clay (Figure 7d). This zone is surrounded by an alteration zone of pale green sericite- chlorite with disseminated and thin veinlets of pyrite largely oxidized to jarosite (Figure 7e). Locally, coarser grained sericite occurs and veins are typically thin quartz veinlets, locally with barite. This alteration gradually transitions to the north and east at lower elevations (e.g., below 1700 m asl) to darker green alteration of chlorite-sericite and locally epidote occurs more distally (Figure 7f). Green sericite-chlorite and chlorite-sericite alteration zones in the southern parts of the Alunite Ridge are cut by breccia as well as banded quartz and carbonate veins, locally with pervasive pink K-feldspar (Figure 7g) characterizing a low-sulphidation-type alteration overprint.

Kemess North

Advanced argillic to phyllic alteration at Kemess North is largely hosted by basaltic plagioclase-phyric volcanic rocks of the Takla Group, which are in fault contact with dacitic tuff of the Toodoggone Formation of the Hazelton Group. The strongly altered rocks form a large orange gossan over an area of 3 by 1 km (Figure 5). During the fieldwork, samples were recovered from along an approximately 0.5 m section of a north-trending ridge above the hypogene mineralization (Figure 8a). The alteration zone exposed on the surface is distinctly zoned from south to north. In the southern parts of the ridge, alteration is charac-

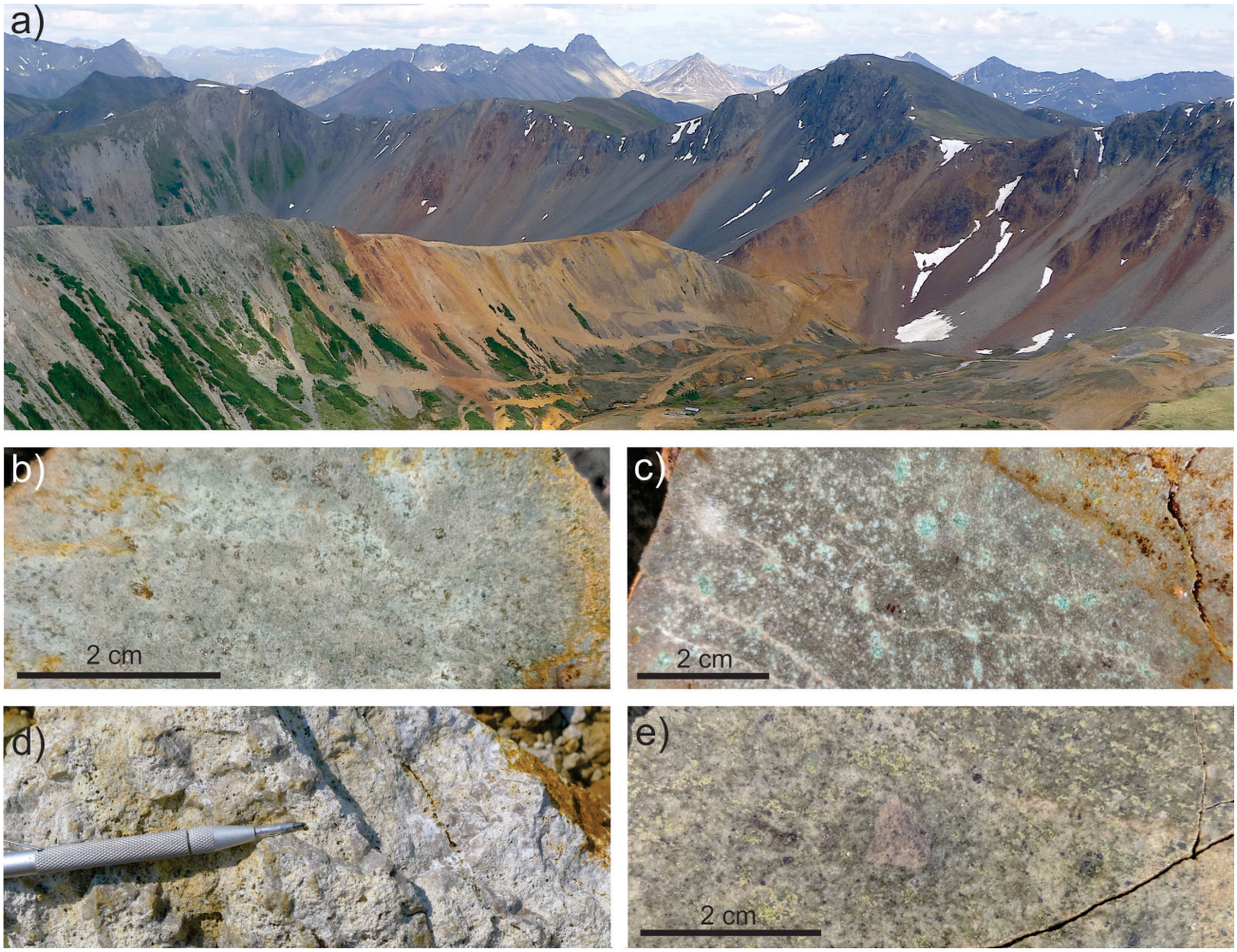

Figure 8. Hostrock and alteration samples from the Kemess North study area: **a)** looking southeast to the Kemess North ridge, showing strongly altered Takla Group volcanic rocks with orange gossan colouration; **b)** pale green altered rock characterized by a green sericite-chlorite-pyrite assemblage; **c)** green-grey sericite-pyrite assemblage; **d)** grey-white sericite-clay-pyrite with strong pervasive silicification and quartz veining; **e)** chlorite-epidote altered volcanic rock of the Toodoggone Formation.

terized by green sericite-chlorite-pyrite, which appears as a pale greenish rock (Figure 8b). This gradually transitions northward to a green-grey sericite-pyrite assemblage (Figure 8c) and then to a grey-white sericite-clay-pyrite typically with pervasive silicification and quartz veins (Figure 8d). The latter is in fault contact with the chlorite-epidote–altered volcanic rocks of the Toodoggone Formation to the north (Figure 8e). Pyrite is abundant (>2%) occurring as dissemination and stockwork veining with quartz. Sulphides are oxidized along fractures producing the rusty outcrops. Locally, minor copper oxides occur, which suggests that hypogene chalcopyrite is leached, but abundant pyrite remains preserved and is only coated by jarosite.

Similar alteration zones occur at depth as indicated in the drillholes. The alteration zone beneath the advanced argillic-alteration zone is quartz-green sericite-(magnetite-hematite) with disseminated pyrite and chalcopyrite. The chlorite content increases with depth and the alteration assemblage becomes darker green. Granular quartz veins with chalcopyrite, pyrite and magnetite (cp > py) occur within the green sericite-chlorite alteration zone. Zones of white sericite with abundant pyrite locally cut and overprint the green sericite-chlorite alteration, indicating that white sericite-pyrite alteration is well developed at shallow levels and overprints the sericite-chlorite alteration at depth. The K-silicate alteration is characterized by pink K-feldspar, typically along fractures with quartz, and variable amounts of pyrite and chalcopyrite occur below the sericite-chlorite zone. Epidote is locally present with K-feldspar, which indicates that the K-silicate alteration transitions toward propylitic-type alteration. It is apparent that both K-silicate and sericite-chlorite alteration zones host copper and gold mineralization at Kemess North.

SWIR Results

Alteration assemblages were further characterized by evaluating SWIR mineralogy. Results of samples collected from surface outcrops are shown in Figure 9, and those for samples collected from drillholes will be discussed in a future publication.

White micas (muscovite or illite) are a typical alteration phase at all the studied sites (Figure 9a). At Tanzilla, muscovite is dominant in the Main zone and locally in bodies of altered rocks in the West zone. White mica alteration at Alunite Ridge and Kemess North is characterized dominantly by illite. Muscovite occurs only in the southern part of the North Ridge. Pyrophyllite occurs in the Main zone at Tanzilla and within the quartz-alunite alteration zone at Alunite Ridge (Figure 9a).

The composition of the white mica (Figure 9b) is described as paragonitic (Na-rich), muscovite/illite (K-rich) and phengitic (Mg-Fe-rich). At Tanzilla, both K-rich muscovite/illite and paragonite are abundant, whereas phengitic micas occur locally. At Alunite Ridge, K-rich illite is abundant, especially with the quartz-alunite-white sericite–altered rock, whereas phengitic illite is more abundant with the pale green sericite-chlorite alteration. At Kemess North, paragonitic illite occurs in the south, whereas K-rich illite occurs to the north, thus correlating more closely with the white-sericite alteration. The occurrence of K-rich white mica is attributed to fluids with lower pH relative to the fluids responsible for the formation of the phengitic micas.

The sericite crystallinity index, calculated from the ratio of 2200 and 1900 nm wavelength depths, shows that white micas at the Tanzilla Main zone are strongly crystalline (>2.0), whereas farther south and at the West zone they are less crystalline (<1.5; Figure 9c). At Alunite Ridge, the crystallinity varies from moderate (ca. 1–1.5) to poor (<1). The latter seems to be more common distally within the sericite-chlorite and chlorite-epidote alteration zones. At Kemess North, white mica crystallinity increases from south (ca. 1) to north (>2). The more highly crystalline sericite occurs with the white-grey sericite alteration (Figure 9c).

Chlorite was identified in most rock samples and displays a wide range of compositions, from Mg rich to Fe-Mg rich (Figure 9d). No obvious trends in chlorite composition with alteration type is recognized. However, locally there is a correlation between the occurrence of phengitic mica and that of Fe-Mg chlorite. More petrography work is planned to study chlorite occurrence, and its relationship to alteration and hostrock types.

Clay minerals are not typical at Tanzilla, whereas dickite and kaolinite occur at Alunite Ridge with the alunite-white sericite zone and, at Kemess North, with the grey-white sericite alteration zone (Figure 9e). The SWIR analyses also identified topaz occurring locally with pyrophyllite or alunite at the Tanzilla Main zone (Figure 9f).

Conclusions and Further Work

Field and SWIR data show that advanced argillic alteration in the studied sites is distinctly zoned. The central parts of the advanced argillic-alteration zone are typically characterized by strong silicification, both as quartz flooding and veining. Alunite, pyrophyllite and topaz locally occur with the silicified rock. Vuggy textures occur, but are not widespread. Sericite and clay minerals also occur. Collectively, they form an alteration assemblage of quartz-white to grey sericite-(clay). Clay minerals include both kaolinite and dickite, and there is a reverse correlation between abundance of clay minerals and abundance of coarse, especially strongly crystalline sericite. This is interpreted as a fluid-temperature control characterizing vertical zonation of the alteration profile. Clay-rich alteration assemblages, espe-

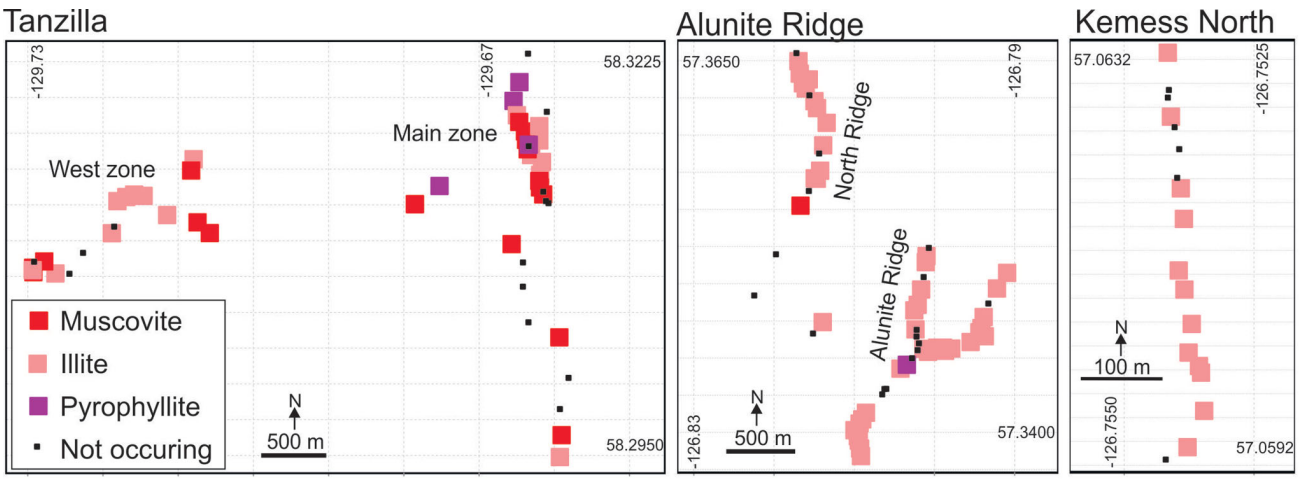

a) White mica and pyrophyllite

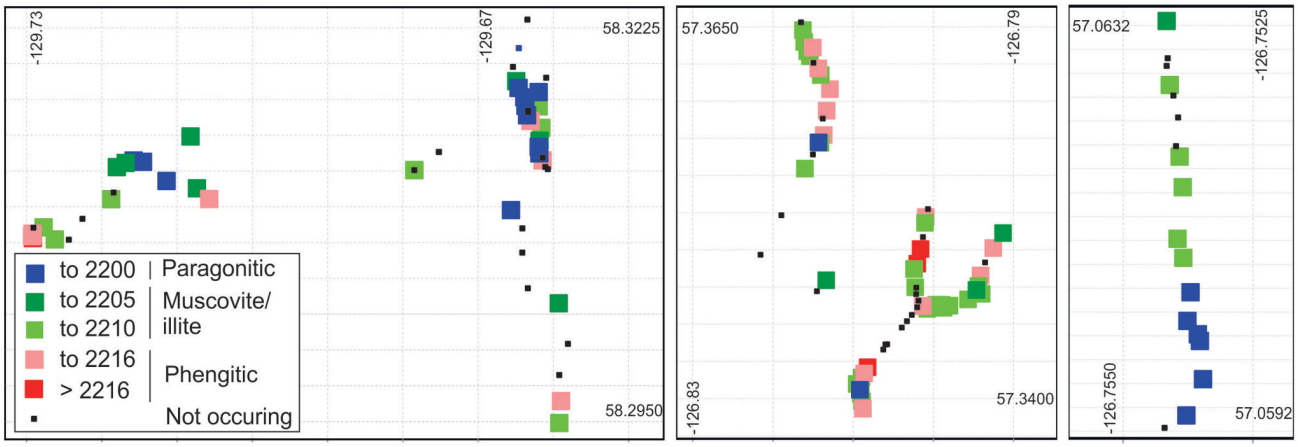

b) White mica, 2200 nm wavelength

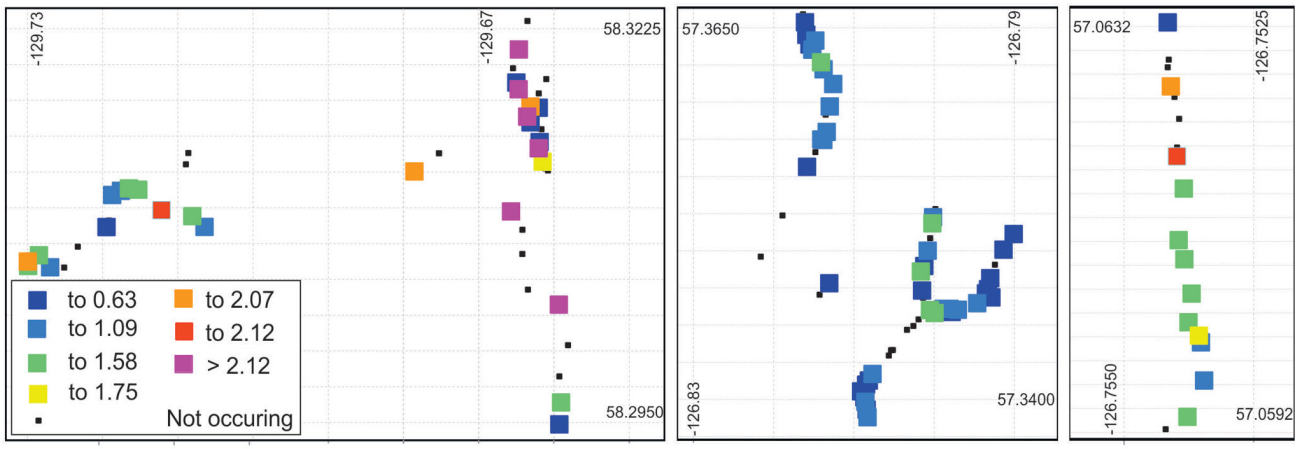

c) White mica, crystallinity index

Figure 9 [this page and the next]. Diagrams showing mineral phases and compositions identified by shortwave-infrared analyses at the Tanzilla, Alunite Ridge and Kemess North study areas: **a)** distribution of white mica and pyrophyllite; **b)** composition of white micas; **c)** crystallinity of white micas; **d)** distribution and composition of chlorite; **e)** distribution of clay minerals; **f)** distribution of alunite and topaz. Small black squares represent mineral of interest not occurring in the sample location.

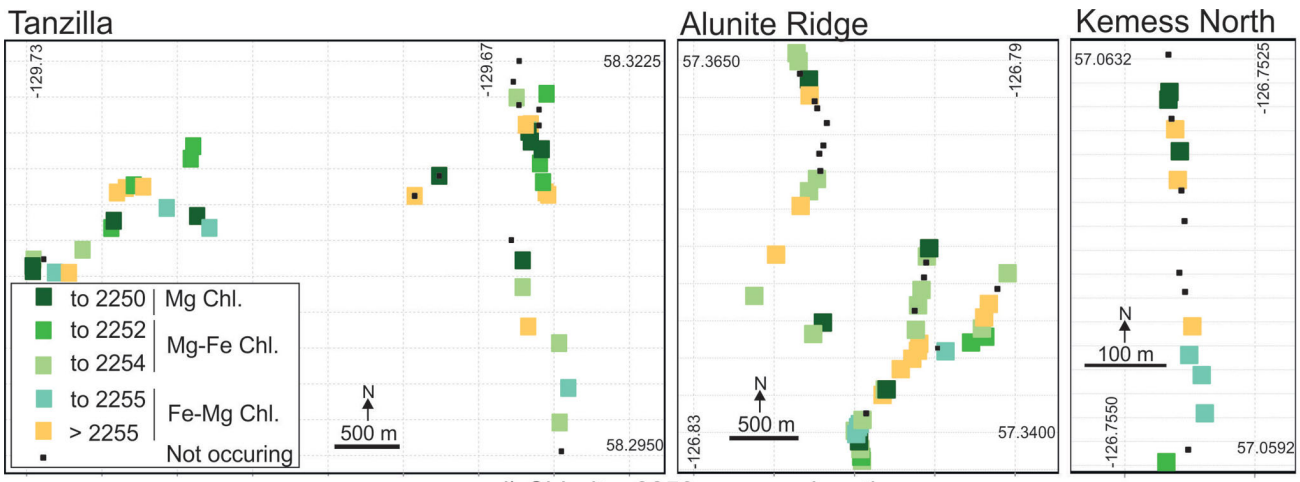

d) Chlorite, 2250 nm wavelength

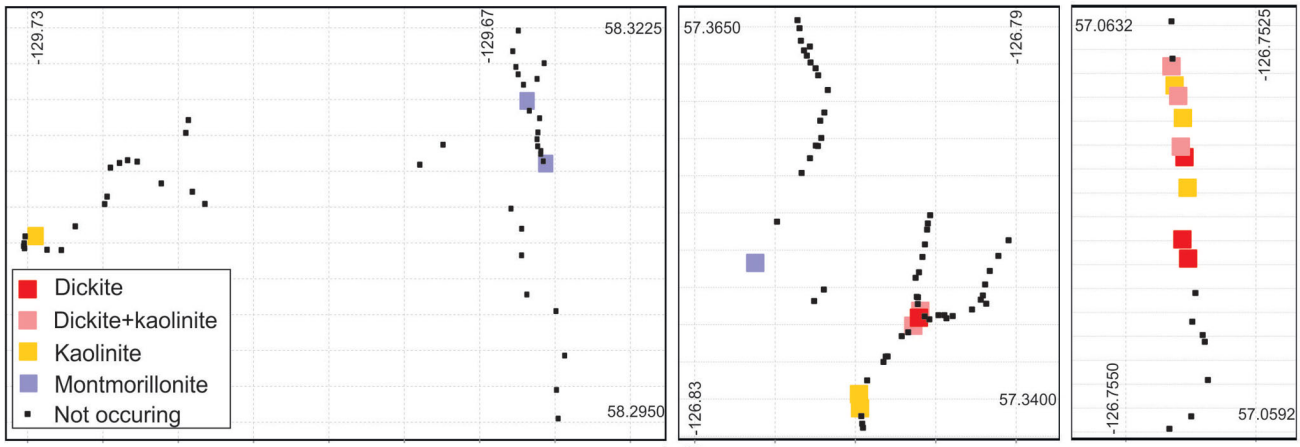

e) Clays

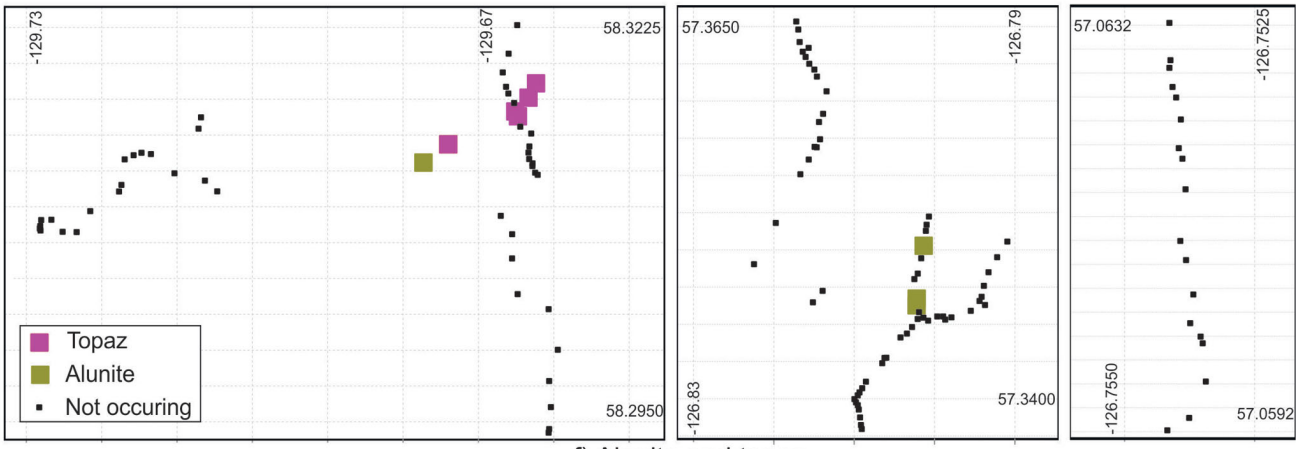

f) Alunite and topaz

cially kaolinite, are less abundant than those consisting of sericite and chlorite. This is interpreted as a hostrock-effect control by the dominantly mafic character of the volcanic rocks of the Takla or Hazelton groups, which buffered the fluids.

Alteration outside of the quartz-white to grey sericite-(clay) zone is characterized by a pale greenish rock containing assemblages of quartz-green sericite-chlorite. The sericite is typically K-rich and reflects the acidic environment of formation. The size of this alteration varies laterally from a few hundred metres to over two kilometres. The crystallinity of the sericite increases toward and within the quartz-white to grey sericite-(clay) zone, but the chlorite compositions do not show distinct-scale variations. More distally, the proportion of the chlorite increases to form green chlorite-sericite alteration and chlorite-epidote-(sericite) more distally.

These field observations and the SWIR mineral identifications provide a framework to further characterize the mineralogical and chemical compositions of zoned, advanced argillic-alteration systems. Samples collected from drillholes will further characterize vertical zonation. Detailed petrography, X-ray diffraction and scanning electron microscope work is planned for mineral characterization. Chemical analyses and measuring physical rock properties (e.g., rock density and magnetic susceptibility) will further characterize each alteration zone. Cathodoluminescence studies are planned to characterize quartz from various alteration stages or zones. Together, these data will be used to establish a field and laboratory toolkit for exploration.

Acknowledgments

Geoscience BC is thanked for its financial contribution in support of this project. Kaizen Discovery Inc. gave permission to visit the Tanzilla property and sample drillcore. Centerra Gold provided access to Kemess North and drillcore, as well as accommodation at the Kemess mine. The authors thank R. Billingsley for giving them permission to visit the Alunite Ridge property. Field assistance was provided by Z. Boileau and F. Bhanji helped draft the maps. They also thank H. Leal-Mejía of the Mineral Deposit Research Unit of The University of British Columbia for his review and comments on this paper.

References

Barresi, T. and Luckman, N. (2016): Diamond drilling report on the Tanzilla property, northwestern British Columbia; BC Ministry of Energy, Mines and Petroleum Resources, Assessment Report 36431, 45 p., URL <https://aris.empr.gov.bc.ca/ArisReports/36431.PDF> [December 2019].

Barresi, T., Bradford, J. and Luckman, N. (2014): 2014 Diamond drilling report on the Tanzilla property, northwestern British Columbia; BC Ministry of Energy, Mines and Petroleum Resources, Assessment Report 35471, 46 p., URL <https://aris.empr.gov.bc.ca/ARISReports/35471.PDF> [May 2019].

Bissig, T. and Cooke, D.R. (2014): Introduction to the special issue devoted to alkalic porphyry Cu-Au and epithermal Au deposits; Economic Geology, v. 109, p. 819–825.

Bouzari, F., Bissig, T., Hart, C.J.R. and Leal-Mejía, H. (2019): An exploration framework for porphyry to epithermal transitions in the Toodoggone mineral district (94E); Geoscience BC Report 2019-08, MDRU Publication 424, 101 p., URL <http://www.geosciencebc.com/wp-content/uploads/2019/11/Geoscience-BC-Report-2019-08.pdf> [October 2019].

Bouzari, F., Hart, J.R.C., Bissig, T. and Shaun, B. (2016): Hydrothermal alteration revealed by apatite luminescence and chemistry: a potential indicator mineral for exploring covered porphyry copper deposits; Economic Geology, v. 111. p. 1397–1410.

Chang, Z., Hedenquist, J.W., White, N.C., Cooke, D.R., Roach, M., Deyell, C.L. and Cuison, A.L. (2011): Exploration tools for linked porphyry and epithermal deposits: example from the Mankayan intrusion-centered Cu-Au district, Luzon, Philippines; Economic Geology, v. 106, p. 1365–1398.

Commonwealth Scientific and Industrial Research Organisation (2019): The Spectral Geologist (TSG™): the industry standard tool for the mineralogical analysis VIS/NIR/SWIR/MIR and TIR reflectance spectra, release 8.0.5.1, Commonwealth Scientific and Industrial Research Organisation, software application, URL <https://research.csiro.au/thespectralgeologist/> [November 2019].

Deyell, C.L. and Dipple, G.M. (2005): Equilibrium mineral–fluid calculations and their application to the solid solution between alunite and natroalunite in the El Indio–Pascua belt of Chile and Argentina; Chemical Geology, v. 215, p. 219–234.

Deyell, C.L., Thompson, J.F.H., Friedman, R.M. and Groat, L.A. (2000): Age and origin of advanced argillic alteration zones and related exotic limonite deposits in the Limonite Creek area, central British Columbia; Canadian Journal of Earth Sciences, v. 37, p. 1093–1107.

Diakow, L.J. (2001): Geology of the southern Toodoggone River and northern McConnell Creek map areas, north-central British Columbia (parts of NTS 94E/2, 94D/15 and 94D16); BC Ministry of Energy, Mines and Petroleum Resources, BC Geological Survey, Geoscience Map 2001-1, scale 1:50 000, URL <http://cmscontent.nrs.gov.bc.ca/geoscience/PublicationCatalogue/GeoscienceMap/BCGS_GM2001-01.pdf> [May 2019].

Diakow, L.J., Nixon, G.T., Rhodes. R. and van Bui, P. (2006): Geology of the central Toodoggone River map area, north-central British Columbia (parts of NTS 94E/2, 6, 7, 10 and 11); BC Ministry of Energy, Mines and Petroleum Resources, Open file map 2006-6, scale 1:50 000, URL <http://cmscontent.nrs.gov.bc.ca/geoscience/PublicationCatalogue/GeoscienceMap/BCGS_GM2006-06.pdf> [May 2019].

Diakow, L.J., Panteleyev, A. and Schroeter, T.G. (1993): Geology of the early Jurassic Toodoggone Formation and gold-silver deposits in the Toodoggone river map area, northern British Columbia; BC Ministry of Energy, Mines and Petroleum Resources, Bulletin 86, 72 p., URL <http://cmscontent.nrs.gov.bc.ca/geoscience/PublicationCatalogue/Bulletin/BCGS_B086.pdf> [May 2019].

Duuring, P., Rowins, S.M., McKinley, B.S.M., Dickinson, J.M., Diakow, L.J., Kim, Y.-S. and Creaser, R.A. (2009): Examining potential genetic links between Jurassic porphyry Cu-

Au±Mo and epithermal Au±Ag mineralization in the Toodoggone district of North-Central British Columbia, Canada; Mineralium Deposita, v. 44, p. 463–496.

Halley, S.W., Dilles, J.H. and Tosdal, R.M. (2015): Footprints: hydrothermal alteration and geochemical dispersion around porphyry copper deposits, Society of Economic Geologists, Newsletter, no. 100.

Hedenquist, J.W. and Taran, Y.A. (2013): Modeling the formation of advanced argillic lithocaps: volcanic vapor condensation above porphyry intrusions; Economic Geology, v. 108, p. 1523–1540.

Heinrich, C.A. (2007): Fluid-fluid interactions in magmatic-hydrothermal ore formation; Reviews in Mineralogy and Geochemistry, v. 65, p. 363–387.

Heinrich, C.A., Driesner, T., Stefánsson, A. and Seward, T.M. (2004): Magmatic vapor contraction and the transport of gold from the porphyry environment to epithermal ore deposits; Geology, v. 32, p. 761–764.

Instrument Systems (2019): SpecWin spectral software; Instrument Systems, software for spectrometer operation, URL <http://www.instrumentsystems.com/products/spectral-software/specwin-pro/> [November 2019].

Lesher, M., Hannington, M., Galley, A., Ansdell, K., Astic, T, Banerjee, N., Beauchamp, S., Beaudoin, G., Bertelli, M., Bérubé, C., Beyer, S., Blacklock, N., Byrne, K., Cheng, L.-Z., Chouinard, R., Chouteau, M., Clark, J., D'Angelo, M., Darijani, M., Devine, M. et al. (2017): Integrated multi-parameter exploration footprints of the Canadian Malartic disseminated Au, McArthur River–Millennium unconformity U, and Highland Valley porphyry Cu deposits: preliminary results from the NSERC-CMIC Mineral Exploration Footprints Research Institute; *in* Proceedings of Exploration 17: Sixth Decennial International Conference on Mineral Exploration, V. Tschirhart and M.D. Thomas (ed.), p. 325–347, URL <https://www.semanticscholar.org/paper/Integrated-Multi-Parameter-Exploration-Footprints-%2C-Lesher-D'Angelo/414a5bd2152876577f69dd53b7276a8441a612f0> [October 2019].

Luckman, N., Celiz, M.A.D., Wetherup, S. and Walcott, P. (2013): Induced polarization, terraspec and structural surveys on the Tanzilla property; BC Ministry of Energy, Mines and Petroleum Resources, Assessment Report 34 550, 24 p., URL <https://aris.empr.gov.bc.ca/ArisReports/34550.PDF> [May 2019].

McKinley, B.S.M. (2006): Geological characteristics and genesis of the Kemess North porphyry Au–Cu–Mo deposit, Toodoggone district, north-central British Columbia, Canada; M.Sc. thesis, University of British Columbia, 136 p., URL <https://open.library.ubc.ca/cIRcle/collections/ubctheses/24/items/1.0052897> [May 2019].

Nelson, J. and Mihalynuk, M. (1993): Cache Creek ocean: closure or enclosure?; Geology, v. 21, p. 173–176.

Panteleyev, A. (1992): Copper-gold-silver deposits transitional between subvolcanic porphyry and epithermal environments; *in* Geological Fieldwork 1991, BC Ministry of Energy, Mines and Petroleum Resources, BC Geological Survey, Paper 1992-1, p. 229–234, URL <https://www2.gov.bc.ca/gov/content/industry/mineral-exploration-mining/british-columbia-geological-survey/publications/fieldwork> [May 2019].

Panteleyev, A. and Koyanagi, V.M. (1994): Advanced argillic alteration in Bonanza volcanic rocks, northern Vancouver Island – lithologic and permeability controls; *in* Geological 1993, BC Ministry of Energy, Mines and Petroleum Resources, BC Geological Survey, Paper 1994-1, p. 101–110, URL <https://www2.gov.bc.ca/gov/content/industry/mineral-exploration-mining/british-columbia-geological-survey/publications/fieldwork> [May 2019].

Shearer, J.T. (2004): Kaolin and silica resources in advanced argillic (acid sulphate) alteration zones, northern Vancouver Island, British Columbia, Canada; in Industrial Minerals with Emphasis on Western North America, G.J. Simandl, N.J. McMillan and N. Robinson (ed.), BC Ministry of Energy, Mines and Petroleum Resources, Paper 2004-02, p. 31–32, URL <http://cmscontent.nrs.gov.bc.ca/geoscience/PublicationCatalogue/Paper/BCGS_P2004-02-06_Shearer.pdf> [May 2019].

Sillitoe, R.H. (1993). Epithermal models: genetic types, geometrical controls and shallow features; *in* Mineral Deposit Modelling, R.V. Kirkham, W.D. Sinclair, R.J. Thorpe and J.M. Duke (ed.), Geological Association of Canada, Special Paper 40, p. 403-417.

Sillitoe, R.H. (2000): Gold-rich porphyry deposits: descriptive and genetic models and their role in exploration and discovery; *in* Gold in 2000, S.G. Hagemann and P.E. Brown (ed.), Reviews in Economic Geology, v. 13, p. 315–345.

Sillitoe, R.H. (2010): Porphyry copper systems; Economic Geology, v. 105, p. 3–41.

Simmons, S.F., White, N.C. and John, D. (2005): Geological characteristics of epithermal precious and base metal deposits; *in* Economic Geology One Hundreth Anniversary Volume 1905–2005, J.W. Hedenquist, J.F.H. Thompson, R.J. Goldfarb and J.P. Richards (ed.), Economic Geology, p. 485–522.

Spectral Evolution (2019): SpecMIN™: reference mineral spectral library; Spectral International, Inc., URL <https://spectralevolution.com/products/software/mining-software/> [November 2019].

SRK Consulting Inc. (2016): Technical report for the Kemess underground project and Kemess East resource estimate, British Columbia, Canada; prepared for AuRico Metals Inc., 409 p., URL <https://www.centerragold.com/cg-raw/cg/KemessUG_Updated_Technical-Report_2CA046-004_20160506_FNL.pdf> [May 2019].

Stoffregen, R.E. (1987): Genesis of acid-sulfate alteration and Au-Cu-Ag mineralization at Summitville, Colorado; Economic Geology, v. 82, p. 1575–1591.

van Straaten, B.I. and Bouzari, F. (2018): The Middle Jurassic Tanzilla-McBride hydrothermal system: one of the largest lithocaps in BC?; Mineral Exploration RoundUp, Vancouver, BC, January 22–25, 2018, poster presentation.

van Straaten, B.I. and Gibson, R. (2017): Late Early to Middle Jurassic Hazelton Group volcanism and mineral occurrences in the McBride-Tanzilla area, northwest British Columbia; *in* Geological Fieldwork 2016, BC Ministry of Energy, Mines and Petroleum Resources, BC Geological Survey, Paper 2017-1, p. 83–115, URL <http://cmscontent.nrs.gov.bc.ca/geoscience/PublicationCatalogue/Paper/BCGS_P2017-01-06_vanStraaten.pdf> [May 2019].

van Straaten, B.I. and Nelson, J.L. (2016): Syncollisional late Early to early Late Jurassic volcanism, plutonism, and porphyry-style alteration on the northeastern margin of Stikinia; *in* Geological Fieldwork 2015, BC Ministry of Energy, Mines and Petroleum Resources, BC Geological Survey, Paper 2016–1, p. 113–143, URL <http://cmscontent.nrs.gov.bc.ca/geoscience/PublicationCatalogue/Paper/BCGS_P2016-01-07_vanStraaten.pdf> [May 2019].

van Straaten, B.I., Gibson, R. and Nelson, J. (2017): Preliminary bedrock geology of the Tanzilla and McBride area, British Columbia; BC Ministry of Energy, Mines and Petroleum Resources, BC Geological Survey, Open File 2017-9, scale 1:50 000, URL <http://cmscontent.nrs.gov.bc.ca/geoscience/PublicationCatalogue/OpenFile/BCGS_OF2017-09.pdf> [May 2019].

Producing Clean Coal from British Columbia Coalfields Using the Water-Based Roben Jig Process: Application to an Industrial Setting

M.L. Mackay, Trillium Geoscience Ltd., Vancouver, British Columbia, mmackay@trilliumgeoscience.com

L. Giroux, Natural Resources Canada, CanmetENERGY, Ottawa, Ontario

R.L. Leeder, Leeder Consulting Inc., Surrey, British Columbia

H. Dexter, GWIL Industries–Birtley Coal & Minerals Testing Division, Calgary, Alberta

J. Halko, Teck Coal Ltd., Calgary, Alberta

M. Holuszko, The University of British Columbia, Vancouver, British Columbia

D. Thomas, CWA Engineers, Vancouver, British Columbia

Mackay, M.L., Giroux, L., Leeder, R.L., Dexter, H., Halko, J., Holuszko, M. and Thomas, D. (2020): Producing clean coal from British Columbia coalfields using the water-based Roben Jig process: application to an industrial setting; *in* Geoscience BC Summary of Activities 2019: Minerals, Geoscience BC, Report 2020-01, p. 131–136.

Introduction

There are a number of coalfields in British Columbia (BC): several thermal coalfields and two major metallurgical coalfields, the Kootenay and Peace River (Figure 1). Metallurgical coals are destined mainly for use in commercial coke ovens to produce coke for use in blast furnaces in steelworks.

One of the main challenges after finding and identifying coal seams is evaluating the quality of the coal resource during the exploration stage. Understanding coal quality can be a complex process and is key to a sound economic evaluation of the resource. During the exploration phase of coal-mine development, evaluation of metallurgical-coal quality is often done using samples collected from drill-core, since the bulk of the coal deposit is generally deep underground.

Coal samples collected during exploration are prepared by screening and then lab-scale or pilot-scale washing that simulates the coal behaviour in commercial coking coal-wash plants. The coarser sized coal is processed using mixtures of organic liquids and the finer fraction is cleaned by a process called froth flotation. The quality of the coal produced by these smaller scale washing methods is critical to understand the market potential of the coal. These processes must produce the same quality coal as a commercial plant.

On the lab scale, the float-and-sink procedure (Figure 2) is used to separate coal from dirt, rock and mineral matter using a density separation, the same process used in commercial plants. The lower density solutions tend to float mainly the coal. During the float-and-sink process, the coal sample is separated at relative densities (specific gravities, sg) between roughly 1.40 and 1.80 using tanks of organic mixtures made from white spirit (1.40 sg), perchloroethylene (PCE; 1.60 sg) and methylene bromide (1.80 sg; ASTM D4371-06(2012)). This produces clean-coal samples at the target ash, sulphur and calorific content typical of what would be produced in a commercial coal-washing plant.

Commercial plants separate the coal into size fractions that are processed in equipment that separates the coal from waste (rock, dirt and minerals) using differences in density—coal being less dense than the waste. The equipment uses water-magnetite mixtures of controlled density in cyclones and

Figure 1. Location of coalfields in southeastern British Columbia from which the coal samples used in this study originated.

This publication is also available, free of charge, as colour digital files in Adobe Acrobat® PDF format from the Geoscience BC website: http://www.geosciencebc.com/updates/summary-of-activities/.

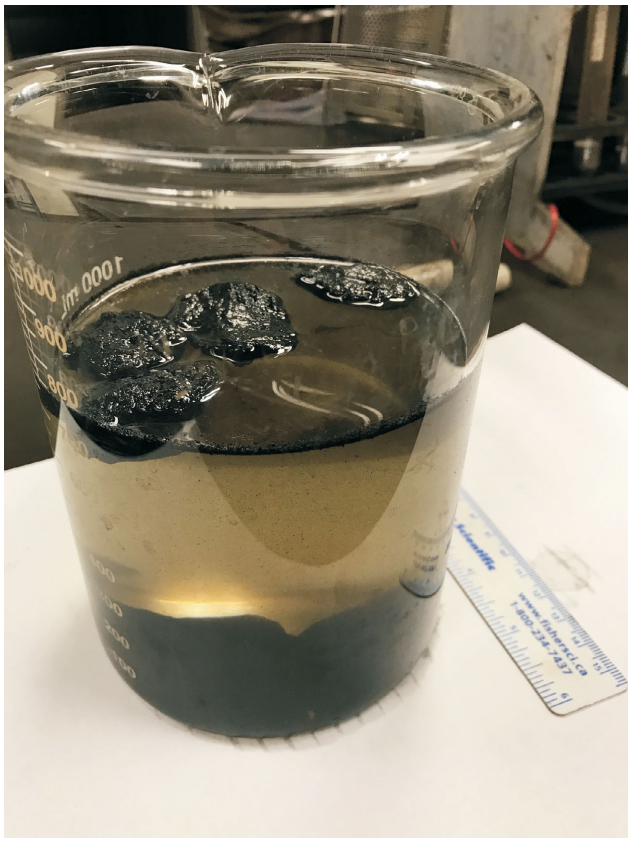

Figure 2. Coal particles floating in perchloroethylene.

baths, centrifugal force for coal-water mixtures in cyclones, and relative settling rates of the coal particles of differing densities in water to isolate/separate the 'clean' coal in jigs and settling tanks. The finest sizes are treated by water-based froth flotation, which can 'float' the coal from the waste. Exploration samples are treated/cleaned in a similar fashion.

Project economics are based on the results of the float-and-sink testing, which produces information on the yield of clean coal as well as the quality of the cleaned coal and resulting coke quality. The coking characteristics for a metallurgical coal deposit are critical in evaluating project economics (i.e., expected price for the clean coal). It is important to ensure that coal/coking properties are correctly assessed from drillcore samples to properly evaluate project economics.

Background

Historically, the major concern in the handling and use of organic liquids such as perchloroethylene (PCE) was the safety risks associated with human exposure. Perchloroethylene is a known carcinogen and poses a safety hazard for laboratory operators, so it must be handled carefully. Figure 3 shows a laboratory technician working in a specially designed fume hood wearing personal protective equipment, including a respirator mask.

Figure 3. Operator working with organic liquids in a specially designed fume hood.

In addition to the health issues, there have been increasing concerns about the impact these solvents have on the quality of coking coal. It has been the experience of the authors and their colleagues that cleaned drillcore coal samples often had lower caking/coking properties than bulk or production coal samples, an observation that goes back many decades. A number of investigations looked at how PCE and other organic solvents may impact the coking quality of coal samples, including Australian and American work (DuBroff et al., 1985; Campbell, 2010; Iveson and Galvin, 2010, 2012). These studies found that there were different impacts depending on the quality characteristics of the coal being assessed. Coals similar to the western Canadian coking coals (higher inert, lower thermal rheological coals) appeared to have been negatively impacted.

Based on these observations, the Canadian Carbonization Research Association (CCRA) undertook a preliminary program to investigate the impact of the organic solvents used in float-and-sink procedures on the coal and coke properties of a higher inert, low-fluidity, western Canadian coal sample (Holuszko et al., 2017). This study looked at the effects of PCE on coal rheology and coke quality. It was found that an 80% decrease (relative to the control sample) in Gieseler maximum fluidity occurred in the perchloroethylene-treated coal immediately following treatment. The coke resulting from the treated sample showed a 16-point decrease in coke strength after reaction (CSR) relative to the control sample. These two coal- and coke-quality parameters are key when evaluating coal resources and reserves. The ramifications of using the wrong numbers for these parameters when determining the characteristics of product for sale are severe and could result in unwarranted project abandonment or false overvaluing of the property.

After the initial study outlined above, the CCRA also completed an exploratory study that examined an alternative to organic liquids by washing coal samples in a jig. A lab-

scale Roben Jig (Figures 4, 5) was used to clean several coals using only water, and the resulting quality characteristics of the clean coal and its coke were compared to those of coal that was processed using the traditional process of washing with organic chemicals. It was found that it was possible to produce a clean-coal product with quality properties very similar to those obtained using the organic liquids (Mackay et al., 2019). The Roben Jig–cleaned coals had the same/similar results for coal-quality parameters and better results for coal-rheology parameters. These findings are important because they demonstrate that the Roben Jig can be used to produce clean-coal composites similar to those obtained from traditional float-and-sink methods.

Objectives

The studies completed on the Roben Jig to date have verified the jig as a tool to help evaluate coal deposits with respect to coal and coke quality at the exploration phase. They have shown that traditional organic liquids (perchloroethylene, white spirits and methylene bromide) can negatively affect coal rheology and coke strength, resulting in an undervaluation of exploration samples (Mackay et al., 2019). Tasks completed include the development of a jig methodology; a comparison of coal and coke quality when using the jig versus organic liquids; the identification, characterization and mitigation of misplaced particles; and a comparison of jig-washed coal to an industrial process plant (using the same raw coal). Three clean-coal samples will be available for carbonization from three different washing processes: industrial wash plant, organic liquids (bulk wash) and Roben Jig (bulk jigging).

The gold standard for proving the effectiveness of the Roben Jig in cleaning coal is to compare it to an industrial setting. This was initiated in 2018 when clean coal washed through the jig was compared with coal washed through an industrial processing plant (Mackay et al., 2019). Work in 2019 has focused on creating clean-coal composites for charging in a pilot-scale coke oven (350 kg capacity). Previous work used only a small carbonization oven—the sole-heated oven (12 kg capacity). This small oven produces only enough coke to measure the CSR/CRI (coke strength after reaction / coke reactivity index). The pilot-scale carbonization oven will yield enough coke to measure up to four additional coke-strength drum indices (ASTM, JIS, Micum/Irsid) in addition to CSR/CRI.

The current research will aim to answer the following questions:

1) Since misplaced particles occur throughout the segregated coal column, how do the high-ash particles (fragments of minerals and rock) affect the coke-strength

Figure 4. Roben Jig equipment used in this study.

Figure 5. Inverted Roben Jig with coal slice to be removed.

drum indices measured on coke produced in a pilot-scale coke oven?

2) How do the coke samples made from clean coal derived from organic liquids washability, Roben Jig and industrial processing plant compare with respect to all relevant coke characteristics?
3) What is the best methodology and expected cost to do 'bulk jigging'—the process where the Roben Jig is used to create 400 kg of clean coal for charging in the pilot-scale coke oven?

The research group also aims to draft a standard operating procedure for operating the Roben Jig for the purpose of producing small-mass clean-coal samples in British Columbia.

The success of this project is beneficial to the coal industry for the following reasons:

- It eliminates the potential negative effects of perchloroethylene and other organic liquids on small-mass exploration coal- and coke-quality parameters.
- It reduces the exposure of lab technicians/operators to carcinogenic organic liquids.

Experimental Washing Methodology

The research group devised two Roben Jig methodologies that could yield products with lower ash content while minimizing misplaced coal and rock particles. These methodologies were compared to the original coal-washing methodologies from the Phase 1 research (Mackay et al., 2018). The clean coals from all processes were then compared to the product from an industrial coal-washing plant. The method for the industrial coal-washing plant is detailed in Mackay et al. (2019).

The coarse coal particles in each sample (greater than 0.50 mm) were washed during this study in several different ways:

- Raw coal was washed in an industrial coal-washing plant.
- Raw coal was segregated into one coarse fraction (12.5 × 0.5 mm) and washed in organic liquids using the float-and-sink method and following the ASTM D4371-06(2012) standard (Phase 1 Method: Float-and-Sink, One Coarse Fraction), as described in Mackay et al., 2018.
- Once initial washability was completed using organic liquids, targeting a specific ash %, one specific gravity was chosen to 'bulk wash' the remainder of the raw coal to create a clean-coal composite. This methodology is described below.
- Raw coal was segregated into one coarse fraction (12.5 × 0.5 mm) and washed in the Roben Jig (Mackay et al., 2018, Phase 1 Method: Roben Jig, One Coarse Fraction).
- A new method called 'Bulk Jigging' was developed for this phase of research and will be explained in detail below.

Common to all methodologies, the fine coal (particle sizes of less than 0.5 mm) was washed using the froth-flotation method (ASTM D5114-90(2010)). The clean coal resulting from this method was recombined with the coarser coal (greater than 0.5 mm) when creating clean-coal composite samples.

Bulk Washing in Organic Liquids

In this phase of work, the results of the 'Phase 1 Method: Float-and-Sink, One Coarse Fraction' (Mackay et al., 2018) were reviewed, a target ash % was chosen for the clean sample, and a 'cut point' (the specific gravity at which all clean coal that floated at that specific gravity and all lower specific gravities would be combined to create the clean-coal composite) was then selected. For instance, in a washability table that listed masses and ash values for the coal that floated at specific gravities of 1.30, 1.40, 1.50 and 1.60, depending on the target ash %, one may choose a cut-point of 1.50 sg. The remainder of the raw coal would then be floated in a large bath of 1.50 sg liquid instead of undergoing several flotations at specific gravities of 1.30 to 1.80.

Bulk Jigging

The intent of Bulk Jigging is similar to that of Bulk Washing in Organic Liquids. Knowing that all coal below a certain relative density will have ash % values desired for the clean-coal composite, the process of cleaning the coal can be sped up by eliminating some of the detail in the washing process (i.e., finding a 'cut point' in the jig column).

First, a trial is carried out by jigging 15 kg of raw coal and removing 12–18 slices from the jig column. The ashes are analyzed for each slice and reviewed with the corresponding apparent relative densities. The obvious rock (>1.90 ARD) and obvious clean coal (<1.35 ARD) zones are identified and measured. For instance, once the column is inverted, the rock would be located in approximately the top 15 cm of the jig column and the clean coal would be in the bottom 30 cm. Next, the higher ash coal zone is identified—this zone is always the area between the obvious rock and cleanest coal. More batches of raw coal are jigged and the thickness of the slices is increased because the boundaries between obvious clean coal, higher ash coal and rock are roughly known. For each batch, slices with similar ARD values are grouped together into buckets. Once the bulk jigging is complete, the ash % of each bucket is analyzed. A specific ash % is targeted and the buckets with ashes allowing for this ash % are chosen to be added to the clean-coal sample.

Analysis

Clean-Coal Analysis

Each clean-coal composite will be analyzed at GWIL Industries–Birtley Coal & Minerals Testing Division (Calgary, AB) for yield (percent), proximate analysis, free swelling index (FSI), specific gravity (sg), total sulphur, Hardgrove Grindability Index (HGI), calorific value (kcal/kg), mercury, ultimate analysis, mineral analyses of the ash, phosphorus in coal (calculated, percent), Gieseler maximum fluidity, Ruhr dilatation, ash fusion (oxidizing and reducing), chlorine, fluorine, alkali-extraction–light-transmittance test, Sapozhnikov X and Y indices, and caking index (G). Petrographic analysis of the coal and coke will be carried out at both CanmetENERGY (Ottawa, ON) and David E. Pearson & Associates (Victoria, BC).

Carbonization

Clean-coal samples from this study, once generated, will be sent to CanmetENERGY in Ottawa. Upon reception, coals will be air dried in open air in the laboratory for 12 hours for the sole-heated oven charges and 24 hours in the case of the larger samples that will be coked in the Carbolite oven. The coal samples will then be homogenized prior to preparing charges for coking in CanmetENERGY's 12 kg capacity sole-heated oven and its 340 kg capacity Carbolite pilot coke oven.

A description of the features and operating conditions for carbonization of coal in the sole-heated oven (ASTM D2014-97(2010)), including the preparation of coke samples from coals in this project for measurement of coke strength after reaction (CSR) and coke reactivity (CRI) following a procedure developed at CanmetENERGY (MacPhee et al., 2013), is provided in Mackay et al. (2019), as is a description of the Carbolite pilot oven.

Results

After this part of the project began on April 1, 2019, the team had the opportunity to obtain raw and clean coal from a single-seam plant run, which is a relatively rare event. Due to the timing of the single-seam plant run, the time schedule of GWIL Industries–Birtley Coal & Minerals Testing Division, and the time needed to jig a large volume of raw coal (close to 1 ton of raw coal), the project does not yet have any clean coal or carbonization results. It is expected that carbonization of the three clean-coal samples will begin prior to December 31, 2019. A final report for the project is expected to be released in early 2020.

Acknowledgments

The project members thank the peer reviewer, E. Gravel (P.Geo.), Independent Consultant. Thanks also go to Geoscience BC, the Canadian Carbonization Research Association, Teck Resources Ltd. and GWIL Industries–Birtley Coal & Minerals Testing Division for their financial and in-kind contributions that made the project possible.

References

Campbell, M. (2010): Options for sink/float analysis – economic and technical review; *in* Proceedings of 37th Symposium on the Geology of the Sydney Basin, Pokolbin, Australia, May 2010.

DuBroff, W., Kaegi, D.D., Knoerzer, J.J. and Spearin, E.Y. (1985): Solvent pretreatment of coal to improve coke strength; United States Patent and Trademark Office, patent number 4528069, URL <http://patft.uspto.gov/netacgi/nph-Parser?Sect1=PTO2&Sect2=HITOFF&p=1&u=%2Fnetahtml%2FPTO%2Fsearch-bool.html&r=3&f=G&l=50&co1=AND&d=PTXT&s1=4528069&OS=4528069&RS=4528069> [November 2017].

Holuszko, M.E., Leeder, R., Mackay, M., Giroux, L., MacPhee, J.A., Ng, K.W. and Dexter, H. (2017): Effects of organic liquids on coking properties of a higher-inert western Canadian coal; Fuel Processing Technology, v. 155, p. 225–231, URL <https://doi.org/10.1016/j.fuproc.2016.06.021> [November 2019].

Iveson, S. and Galvin, K.P. (2010): Influence of organic liquids on coal carbonisation properties; Australian Coal Association Research Program (ACARP), Brisbane, Australia, Project C17051.

Iveson, S. and Galvin, K.P. (2012): The effect of perchloroethylene on coking properties; Fuel, v. 95, p. 504–513, URL <https://doi.org/10.1016/j.fuel.2011.10.009> [November 2012].

Mackay, M.L., Giroux, L., Leeder, R.L., Dexter, H., Halko, J., Holuszko, M., and Thomas, D. (2019): Producing clean coal from western Canadian coal fields using the water-based Roben Jig process; *in* Geoscience BC Summary of Activities 2018: Minerals and Mining, Geoscience BC, Report 2019-01, p. 87-100, URL <http://cdn.geosciencebc.com/pdf/SummaryofActivities2018/MM/2017-013_SoA2018_MM_Mackay.pdf> [November 2019].

Mackay, M.L., Leeder, R.L., Giroux, L., Dexter, H., Holuszko, M., Halko, J., Howey, C. and Thomas, D. (2018): Producing clean coal from western Canadian coal fields using the water-based Roben Jig process; *in* Geoscience BC Summary of Activities 2017, Geoscience BC, Report 2018-01, p. 69–86, URL <http://cdn.geosciencebc.com/pdf/SummaryofActivities2017/MM/SoA2017_MM_Mackay.pdf> [November 2019].

MacPhee, J.A., Giroux, L., Ng, K.W., Todoschuk, T., Conejeros, M. and Kolijn, C. (2013): Small-scale determination of metallurgical coke; Fuel, v. 114, p. 229–234, URL <https://doi.org/10.1016/j.fuel.2012.08.036> [November 2019].

ASTM Standard Methods

ASTM D2014-97(2010): Standard test method for expansion or contraction of coal by the sole-heated oven; ASTM International, West Conshohocken, PA, 2010.

ASTM D4371-06(2012): Standard test method for determining the washability characteristics of coal; ASTM International, West Conshohocken, PA, 2012, URL <http://www.astm.org/cgi-bin/resolver.cgi?D4371-06(2012)> [November 2019].

ASTM D5114-90(2010): Standard test method for laboratory froth flotation of coal in a mechanical cell; ASTM International, West Conshohocken, PA, 2010.

Assessment of the Carbon Mineralization Potential of British Columbia by Quantifying the Response of Physical Properties to the Alteration of Ultramafic Rocks (NTS 092H/08, 10, 093K/13, 14, 094C/05, 104I, 104N)

J.A. Cutts, Bradshaw Research Initiative for Minerals and Mining, The University of British Columbia, Vancouver, British Columbia, jcutts@eoas.ubc.ca

G.M. Dipple, Bradshaw Research Initiative for Minerals and Mining, The University of British Columbia, Vancouver, British Columbia

C.J.R. Hart, Mineral Deposits Research Unit, The University of British Columbia, Vancouver, British Columbia

D. Milidragovic, British Columbia Geological Survey, Ministry of Energy, Mines and Petroleum Resources, Victoria, British Columbia

Cutts, J.A., Dipple, G.M., Hart, C.J.R. and Milidragovic, D. (2020): Assessment of the carbon mineralization potential of British Columbia by quantifying the response of physical properties to the alteration of ultramafic rocks (NTS 092H/08, 10, 093K/13, 14, 094C/05, 104I/01–16, 104N/01–16); *in* Geoscience BC Summary of Activities 2019: Minerals, Geoscience BC, Report 2020-01, p. 137–144.

Introduction

British Columbia (BC) contains large volumes of ultramafic rocks (Figure 1) and these have been, and continue to be, of economic interest due to the common occurrence of Ni±Fe-Cu-PGE mineralization (e.g., Nixon et al., 2015; Britten, 2017). However, resource extraction typically produces large volumes of solid waste and contributes significant carbon dioxide (CO_2) emissions, presenting both an environmental and—given BC's and Canada's carbon tax—an economic challenge. Recent research has demonstrated the potential of ultramafic rocks and their serpentinized products to react with and sequester CO_2 (e.g., Hansen et al., 2005; Keleman and Matter, 2008; Wilson et al., 2009). As such, BC's carbon offset scheme provides companies mining ultramafic rocks with significant economic incentive for reacting mine tailings with either atmospheric or emission-related CO_2. The alteration of ultramafic rocks (Figure 2) can be broadly divided into two main stages: 1) serpentinization, which involves the hydration of Mg-rich silicate minerals, and 2) carbonation, which involves the reaction of serpentinization-related minerals with CO_2 and the formation of Mg-carbonate and -silicate minerals and quartz into a rock termed listwanite (e.g., Kelemen and Hirth, 2012; Power et al., 2013). Strongly serpentinized rocks represent the primary target for carbon sequestration, which occurs through naturally occurring carbonation reactions (e.g., Hansen et al., 2005).

Ultramafic rocks in BC are mainly exposed along a province-wide south-southeast-trending belt (Figure 1). The first-order distribution of these rocks is known and, locally mapped in detail; however, this is not true for all occurrences in the province and, more importantly, the degree of serpentinization and carbonation in all cases is poorly constrained. As such, the potential of these rocks for carbon sequestration remains uncertain. Due to the time investment required to map, sample, and analyze the geochemistry of every occurrence in detail, it is of great interest to develop remote sensing techniques that can identify and quantify the degree to which the ultramafic rocks are serpentinized or carbonated and, thus, their potential to be used as carbon sinks.

The serpentinization of ultramafic rocks (reaction 1 (R1) in Figure 2) mainly involves the hydration and breakdown of the constituents olivine [$(Mg,Fe)_2SiO_4$] and orthopyroxene [$(Mg,Fe)SiO_3$] (e.g., Toft et al., 1990). During serpentinization, Mg^{2+} (and to a lesser extent Fe^{2+}) is incorporated into serpentine-group minerals [$(Mg, Fe)_3(Si_2O_5)(OH)_4$] and brucite [$(Mg,Fe)(OH)_2$], while some Fe^{2+} is oxidized to Fe^{3+} and incorporated into magnetite (Fe_3O_4; Kelemen and Hirth, 2012). Locally, Fe^{2+} may be reduced to Fe^0 and incorporated into awaruite (Ni_3Fe or Ni_2Fe; e.g., Britten, 2017). The hydration process is associated with 25–50% volume increase (Schwarzenbach, 2016) and, in doing so, the rocks may incorporate as much as 15–16 wt. % H_2O (Komor et al., 1985). Brucite has been shown to be highly reactive with CO_2—even at room temperature—and, thus, is the primary targeted mineral for low-cost carbon sequestration (e.g., Vanderzee et al., 2018, 2019); serpentine-group minerals are far less reactive (e.g., Daval et al., 2013). The highest brucite contents are predicted to result from the serpentinization of the most olivine-rich (Si-poor) ultramafic rocks and should be associated with high degrees of hydration. Due to the net volume increase associated with the ser-

This publication is also available, free of charge, as colour digital files in Adobe Acrobat® PDF format from the Geoscience BC website: http://www.geosciencebc.com/updates/summary-of-activities/.

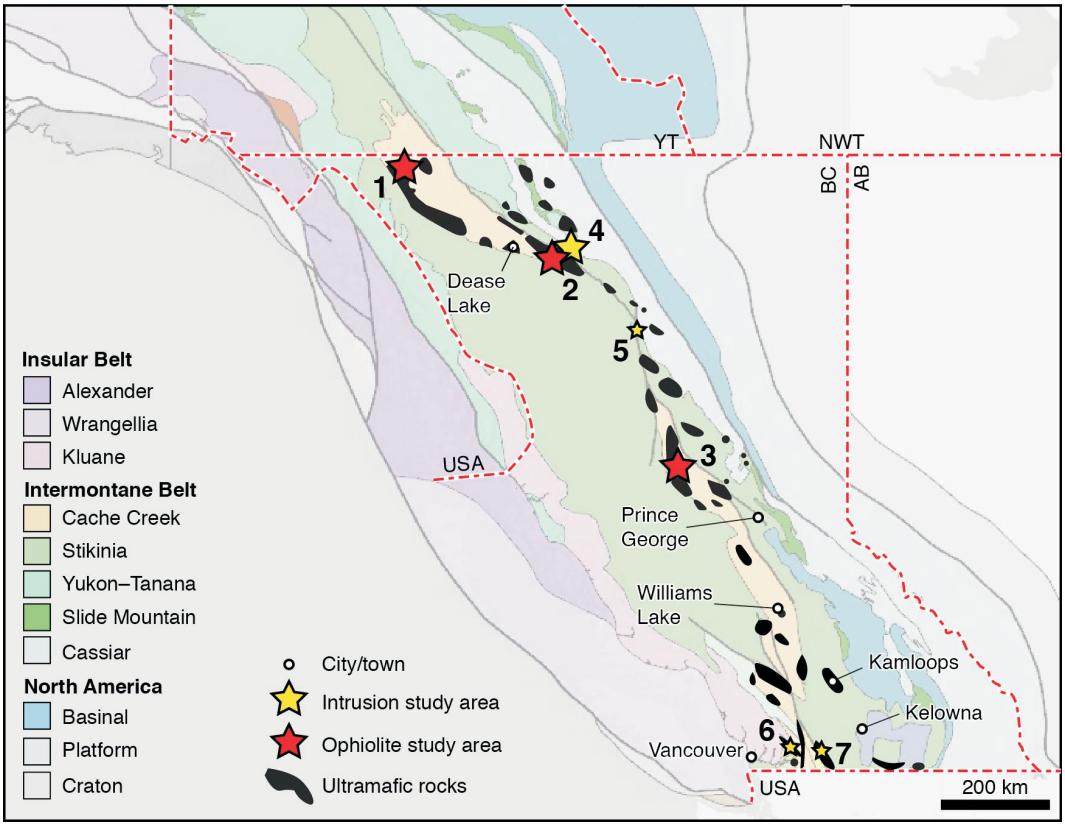

Figure 1. Tectonostratigraphic map of British Columbia showing the distribution of ultramafic rocks and the study areas of interest for this research. Ophiolite-hosted ultramafic study areas include Atlin (1), King Mountain (2) and Decar (3), while intrusion-hosted ultramafic study areas include Turnagain (4), Polaris (5), Giant Mascot (6) and Tulameen (7). Study sites 1–4 (large stars) will serve as the primary study sites for developing petrological and physical rock property models, whereas study sites 5–7 (small stars) will serve as secondary study sites. (Map modified from Cui et al., 2017).

pentinization reactions and due to the production of magnetite, brucite-rich rocks should be distinguished from less serpentinized rocks by being less dense and more magnetic (Toft et al., 1990). The progressive carbonation of serpentinized ultramafic rocks (Figure 2) is subdivided into three stages: reaction 2 (R2) involves the formation of (ferro-)magnesite [$(Mg,Fe)CO_3$] and the continued formation of serpentine-group minerals at the expense of olivine or brucite; reaction 3 (R3) involves the breakdown of serpentine-group minerals and magnetite and the reduction of Fe^{3+} to Fe^{2+} to form (ferro-)magnesite and talc-minnesotaite [$(Mg,Fe)_3Si_4O_{10}(OH_2)$]; and reaction 4 (R4) involves the formation of magnesite and quartz (SiO_2) at the expense of talc-minnesotaite (Forbes, 1971; Hansen et al., 2005). The first two stages of carbonation are associated with a net loss of H_2O and gain of CO_2, whereas during the final stage, H_2O is no longer present and thus, it is associated with only a gain of CO_2. The latter two reactions should result in rocks that are denser and less magnetic.

The response of various physical rock properties of ultramafic rocks, such as magnetic susceptibility and density, to serpentinization and carbonation have been investigated previously (e.g., Toft et al., 1990; Hansen, 2005; Hansen et al., 2005); however, quantitative estimates of these relationships have not been systematically tested in multiple ultramafic rock localities, or have been focused on the carbonation process only. The serpentinization process is particularly important as it results in the formation of the primary carbon sequestration targets, serpentinites. Still, characterization of the carbonation process is important to identify rocks that are not suitable for sequestration purposes. This research aims to identify and quantify the relationship between the alteration of ultramafic rocks and physical rock properties in four key localities in BC (Figure 1) for which detailed mapping and geochemical studies have already been completed. A key question that will be addressed is whether or not these relationships are uniform or vary among the localities. The relationships established between alteration and physical rock properties from these study areas will then be used to inform geophysical inversions that will be used to build 3-D models for carbon sequestration in each site, and will be applied to the other ultramafic rock occurrences (see Figure 1) to establish a carbon sequestration potential index for BC. This paper presents preliminary results for initial work conducted from July 2019 to September 2019.

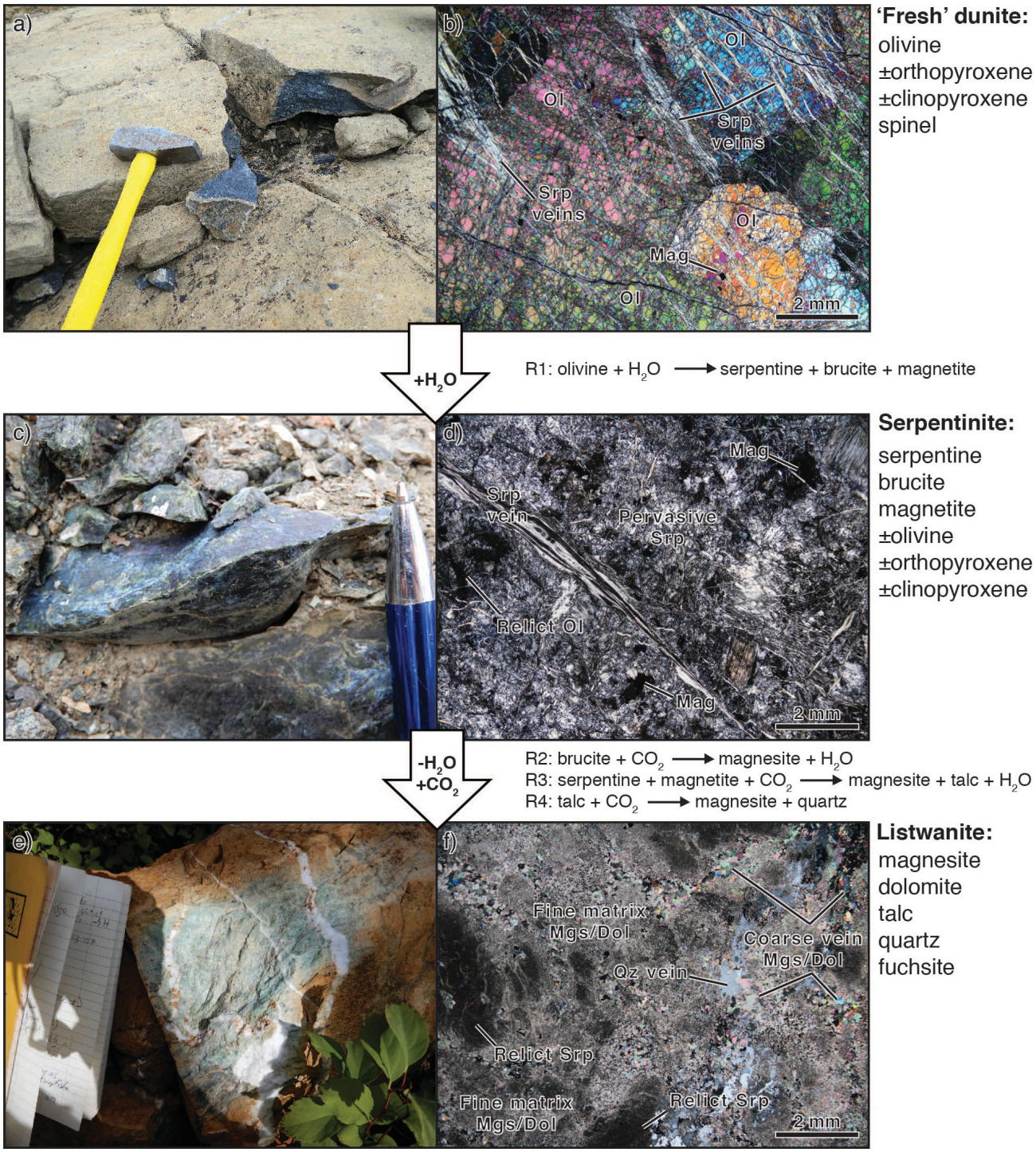

Figure 2. Photographs (a, c, e) and photomicrographs taken in crossed-polarized light (b, d, f) of representative samples from the Decar area. **a, b)** Relatively fresh (~30% serpentine) dunite that comprises coarse olivine (Ol), disseminated magnetite (Mag) and trace spinel, all of which are cut by veinlets of serpentine (Srp). **c, d)** Serpentinite (90–100% serpentine) showing a pervasively serpentinized matrix with globular to blebby magnetite (Mag) and preserved relict olivine (Ol), all of which are crosscut by a vein of serpentine (Srp). **e, f)** Listwanite that comprises magnesite (Mgs), dolomite (Dol), quartz (Qz), fuchsite and talc (fuchsite and talc not shown in the photomicrograph). R1, 2, 3 and 4 are reactions (see text for more details).

Study Localities

The ultramafic rocks of interest occur in two main associations: as ophiolite massifs (e.g., Schiarizza and MacIntyre, 1999; Zagorevski et al., 2017), or as intrusive complexes (e.g., Nixon et al., 2015). The four main localities selected for this study are the Decar, Atlin and King Mountain areas, which are ophiolitic ultramafic massifs, and the Turnagain Alaskan-type intrusion. Three additional intrusions (Polaris, Giant Mascot, Tulameen) may be investigated; however, these are secondary study sites. The Decar area is one of the main localities of ongoing research (e.g., Vanderzee et al., 2018, 2019) at the Bradshaw Research Initiative for Minerals and Mining (BRIMM) at the Department of Earth, Ocean and Atmospheric Sciences (EOAS), University of British Columbia (UBC), and is in collaboration with the Mineral Deposits Research Unit (MDRU) at UBC, FPX Nickel, and the British Columbia Geological Survey (BCGS). The area has been mapped in detail and the geochemistry of the rocks has been studied by the BCGS (Milidragovic et al., 2018; Milidragovic, 2019; Milidragovic and Grundy, 2019) and FPX Nickel (e.g., Britten, 2017); however, these studies were focused on regional-scale correlations among all rock types, or were focused only on the highly serpentinized and mineralized rocks. Two weeks of additional fieldwork in summer 2019 by researchers at BRIMM resulted in a comprehensive sample suite spanning the full range of serpentinized and carbonated ultramafic rock types, and these will complement the existing samples and datasets (Table 1).

The ultramafic rocks in and immediately surrounding the town of Atlin have been the subject of several graduate student theses at EOAS (e.g., Hansen, 2005) and the surrounding area has been one of the main foci of the Geological Survey of Canada's (GSC) Geo-mapping for Energy and Minerals, Phase 2 (GEM-2) research program (e.g., Zagorevski et al., 2017). The Atlin area ultramafic rocks are subdivided into two main areas: 1) the Atlin ophiolite (e.g., Hansen et al., 2005; Zagorevski et al., 2017), and 2) the Nahlin ophiolite (e.g., McGoldrick et al., 2017, 2018; Zagorevski et al., 2017). The extensive sample suites and whole-rock geochemistry results from the EOAS theses and from GEM-2 have been made available for this study (Table 1). The King Mountain area has not been sampled as extensively as the other two ophiolitic areas; however, it was studied as part of GEM-2 and the sample suite and whole-rock geochemistry results have been made available for this study (Table 1). Additionally, the King Mountain area was at one point considered by FPX Nickel as a target for Fe-Ni exploration (e.g., Letain locality in Britten, 2017).

The Turnagain Alaskan-type mafic-ultramafic intrusion (e.g., Nixon et al., 2015) has been the subject of several graduate theses at UBC (e.g., Scheel, 2007; Jackson-Brown, 2017) and has been extensively studied by Giga Metals Corp. as one of the largest undeveloped Ni-Cu-PGE deposits in the province. BRIMM has recently entered into a research partnership with Giga Metals; the number and

Table 1. Summary of the localities of interest for this study, and the status of progress into the whole-rock chemical analyses and physical property measurements. For sample suites with finished datasets, the numbers in columns indicate the number of samples analyzed; 'In progress' refers to sample suites for which analyses have begun but are not yet complete; 'TBD' (to be determined) refers to sample suites for which analyses have not yet begun.

Locality	Ophiolite	Locality details	Source	Whole-rock chemistry	CO_2 content	Magnetic Susceptibility[1]	Density[1]
Atlin Area	Atlin	Atlin (town)	Hansen (2005)	160	160	116	In progress
		Atlin (town)	Zagorevski (2018)	26	TBD	In progress	In progress
		Mount Barham	Zagorevski (2018)	12	TBD	In progress	In progress
		Sentinal Peak	Zagorevski (2018)	7	TBD	In progress	In progress
		Union Mountain	Zagorevski (2018)	22	TBD	In progress	In progress
	Nahlin	Menatutuline Peak	Zagorevski (2018)	58	TBD	In progress	In progress
		Mount Nimbus	Zagorevski (2018)	5	TBD	In progress	In progress
		Mount O'Keefe/Focus	Zagorevski (2016, 2018)	5	TBD	In progress	In progress
		Nahlin Mountain	Zagorevski (2018)	7	TBD	In progress	In progress
		Peridotite Peak	Zagorevski (2018)	7	TBD	In progress	In progress
Decar Area	Decar	Baptiste deposit	BRIMM	In progress	TBD	17	In progress
			Milidragovic and Grundy (2019)	1	TBD	9	In progress
			FPX Nickel	18	18	8	In progress
		Van deposit	BRIMM	In progress	TBD	6	In progress
			Milidragovic and Grundy (2019)	6	TBD	17	In progress
		Mount Sydney-Williams	BRIMM	In progress	TBD	20	In progress
			Milidragovic and Grundy (2019)	3	TBD	5	In progress
		Other	BRIMM	In progress	TBD	23	In progress
			Milidragovic and Grundy (2019)	2	TBD	22	In progress
King Mountain Area	Unnamed	King Mountain	Zagorevski (2016, 2018)	26	TBD	In progress	In progress
Turnagain Intrusion	-	-	Jackson-Brown (2017)	17	-	-	-
Polaris Intrusion	-	-	-	-	-	-	-
Giant Mascot Intrusion	-	-	-	-	-	-	-
Tullameen Intrusion	-	-	-	-	-	-	-

[1]Measured on hand samples at UBC

nature of the samples that will be made available for study are, as yet, uncertain.

Methods

Whole-Rock Geochemistry

Whole-rock major-element geochemistry—compiled from the literature and from newly collected samples—will be used to characterize and calculate the composition and mineralogy of the protolith and the extent of alteration of the samples (Table 1). Specifically, the calculated olivine/pyroxene content of the protolith will be used to predict the brucite potential, and the H_2O and CO_2 contents of the rocks will be important to determine the degree to which the samples have been serpentinized and carbonated, respectively. Major-element chemistry results have been or currently are being determined by X-ray fluorescence (XRF) at various commercial laboratories, including Activation Laboratories (Ancaster, Ontario) and ALS Geochemistry (North Vancouver, British Columbia).

Physical Properties

The main physical properties of interest are magnetic susceptibility and density. Magnetic susceptibility was measured using a ZH Instruments SM30 instrument, and sample thickness and demagnetization corrections were applied. Measurements were done in the field primarily on flat, weathered surfaces, whereas measurements done in the lab were done on flat (cut), fresh surfaces; this approach was used to characterize the effects of surface weathering and because fresh surfaces in the field are rare. To capture the intra-sample heterogeneity, each plotted magnetic susceptibility value represents 5–10 individual measurements from various parts of the sample or outcrop; for weathered surfaces, the highest measurements were averaged, whereas for fresh surfaces an average of all measurements was used. This approach was taken because magnetite tends to break down during the weathering of ultramafic rocks and, thus, the highest values should reflect the least altered rock. Sample masses for density determination were measured using an A&D Company Ltd. EJ-6100 balance. Density was calculated using Archimedes principal, which uses the dry and wet masses of the samples and applying equation (1)

$$\rho_s = \rho_w\left[\frac{m_{dry}}{m_{dry}-m_{wet}}\right] \quad , \qquad (1)$$

where ρ_s = density of the sample in g/cm^3, ρ_w = density of water, m_{dry} = mass in air in grams, and m_{wet} = mass in water in grams. This equation is simplified by using a density for water of 1 g/cm^3, which is true at temperatures of 25°C and pressures of 1 bar. To assess the accuracy of our magnetic susceptibility and density measurements, and to provide additional information on the porosity, permeability and electrical conductivity of the sampled ultramafic rocks, a selection of samples will be sent to the Paleomagnetism and Petrophysics Laboratory (PPL) at GSC–Pacific in Sidney, BC. All measurements will be done on a 2.5 cm diameter core of unweathered material using a Sapphire Instruments SI2B instrument to measure magnetic susceptibility, a specially built Jolly balance to determine density, and a Solartron 1260 Frequency Response Analyzer and Gamry Reference 600+ Potentiostat to measure electrical impedance (resistance/conductivity or energy loss in a circuit; Enkin, 2017).

Preliminary Results

Hansen et al. (2005) used a limited set of samples (~20) from a relatively restricted area in the Atlin ophiolite to establish a semiquantitative relationship between the carbonation of serpentinite and magnetic susceptibility. To further explore this relationship, additional samples from the same ophiolite (Hansen, 2005), for which there are corresponding whole-rock geochemistry data, were analyzed for their magnetic susceptibility; density measurements are ongoing. The volatile components of the whole-rock geochemistry (H_2O and CO_2) for the samples and their corresponding magnetic susceptibility are consistent with what is predicted on the basis of the observed mineral assemblages and the reactions that they reflect (Figure 3). As the degree of serpentinization increases, as indicated by increasing H_2O contents up to 13–15 wt. %, so too does the magnetic susceptibility of the rocks; this is consistent with increased production of magnetite during reaction 1 (R1; Figures 2, 3). Pure serpentine-group minerals and brucite can accommodate up to 13 wt. % and 31 wt. % H_2O, respectively (e.g., Komor et al., 1985), thus the observed volatile compositions in the analyzed rocks (with CO_2 <1 wt. %) are consistent with variable mixtures of olivine, serpentine and brucite. Due to a lack of unhydrated samples from the Atlin ophiolite, the response of magnetic susceptibility to low degrees of serpentinization (H_2O <8 wt. %) has yet to be investigated (Figure 3); this will be addressed in future work.

Reaction 2 involves a net loss of H_2O and gain of CO_2 from the system. For samples that have undergone mild carbonation (<5 wt. % CO_2), there is no appreciable decrease in magnetic susceptibility relative to uncarbonated samples (Figure 3), implying that magnetite has not been consumed. Whether or not brucite is still present at this stage is as yet uncertain. Further carbonation of the samples (R3: >5 wt. % CO_2) results in a marked decrease in magnetic susceptibility (Figure 3), which is consistent with magnetite breakdown, the reduction of Fe^{3+} to Fe^{2+}, and the formation of (ferro-)magnesite and talc-minnesotaite. Samples that have undergone the final stage of carbonation (R4) have the lowest associated magnetic susceptibility (Figure 3), consistent with complete breakdown of magnetite.

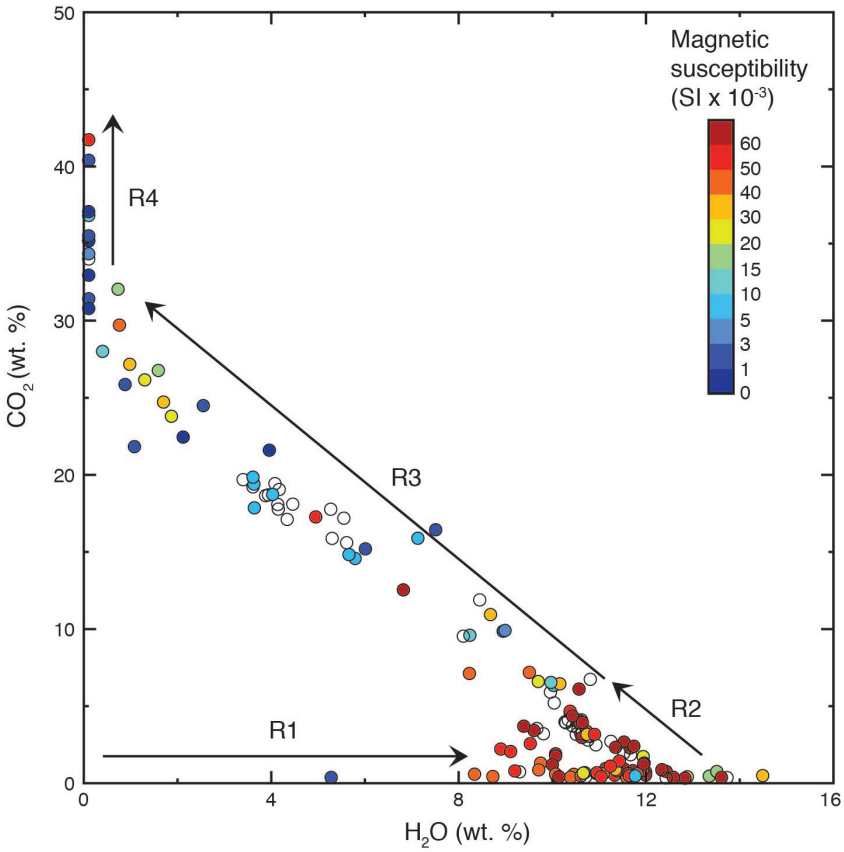

Figure 3. CO_2 and H_2O (loss on ignition – CO_2) concentrations in wt. % of ultramafic samples from the immediate vicinity of the town of Atlin, with colours assigned based on their corresponding magnetic susceptibility; white circles represent samples for which there is no corresponding magnetic susceptibility measurement. Reactions 1 to 4 (R1–R4) refer to the mineral reactions occurring during serpentinization and carbonation that are described in the main text and Figure 2. High degrees of serpentinization, as indicated by H_2O concentrations of 10–14 wt. %, are associated with the highest magnetic susceptibility and likely reflect the formation of magnetite during R1. The initial stage of carbonation (R2) does not result in an appreciable decrease in magnetic susceptibility but may cause the breakdown of brucite (Daval et al., 2013), the main target mineral for carbon sequestration (Vanderzee et al., 2018, 2019). Subsequent carbonation reactions (R3 and R4) result in an overall drop in magnetic susceptibility due to the breakdown of magnetite.

The relationships between H_2O, CO_2 and magnetic susceptibility deduced from the Atlin area samples will serve as a framework to compare results from other ultramafic rock localities. Analysis of the magnetic susceptibility of the Decar area samples (Figure 4) demonstrates—as predicted—that the highest values obtained from weathered surfaces in the field are typically lower than those obtained from the fresh surfaces in the lab (Figure 4a). This first-order observation will be further explored through detailed physical property analysis at the PPL at GSC–Pacific in Sidney. The density of the Decar area samples has been constrained, and shows a broadly negative correlation between density and magnetic susceptibility (Figure 4b), reflecting the net volume–increasing reactions and magnetite production associated with serpentinization; this is consistent with the predicted mineral reactions and with observations made on other, similar, peridotite bodies (e.g., Toft et al., 1990). Once received, the whole-rock chemical analyses of the samples from the Decar area will enable further testing of the established physical property trends.

Conclusions and Future Work

Preliminary analysis of the magnetic susceptibility of a suite of samples from the Atlin ophiolite are consistent with the observed mineral assemblages and the inferred reactions. The observed trends will be used as a framework for future analyses of samples from the Atlin, Decar and King Mountain ophiolites, and the Turnagain Alaskan-type intrusion. Magnetic susceptibility and density measurements of the Decar area samples indicate a negative correlation between the two physical properties; serpentinization is associated with an increase in magnetic susceptibility and decrease in density, whereas carbonation is associated with the opposite trend. These relationships will be further tested using samples from other localities, and these will form the basis for interpreting airborne geophysical sur-

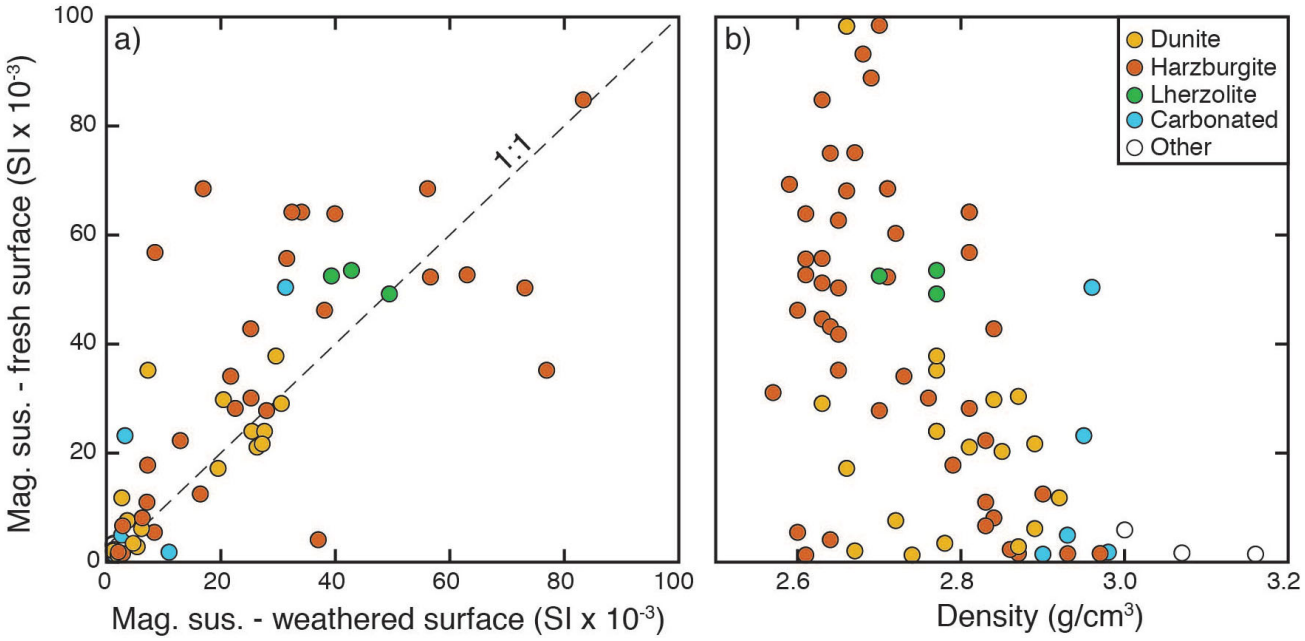

Figure 4. a) Comparison of magnetic susceptibility (Mag. sus.) measurements taken from the weathered surface in the field and on fresh surfaces in the lab for Decar area samples. Field measurements (n = 5–10 per sample) were done on the weathered surface and the plotted value reflects the average of the highest values, whereas lab measurements were done on the fresh surface and the value reflects the average of five measurements. In general, the two datasets fall close to a 1:1 correlation line; however, values tend to be higher for measurements on the fresh surfaces. This discrepancy reflects the propensity for magnetite to break down during weathering. **b)** Comparison of magnetic susceptibility and specific gravity of samples from the Decar area, coloured by rock type as determined using a CIPW normalization scheme. The samples show a broadly negative correlation, with carbonated and non-ultramafic samples ('Other') distinctly less magnetic and denser than the variably serpentinized samples.

veys to evaluate the extent of serpentine and carbonate alteration of ultramafic rocks.

Acknowledgments

In addition to Geoscience BC, the authors thank FPX Nickel Corp., Giga Metals Corp., and the Natural Sciences and Engineering Research Council for financial support of this project. The authors also thank A. Zagorevski at the Geological Survey of Canada–Central Division for providing access to samples from the northern BC ophiolites, which were collected as part of the Geo-mapping for Energy and Minerals, Phase 2 research program. This paper benefited from a constructive review by S. Peacock from The University of British Columbia.

References

Britten, R. (2017): Regional metallogeny and genesis of a new deposit type—disseminated awaruite (Ni_3Fe) mineralization hosted in the Cache Creek Terrane; Economic Geology, v. 112, p. 517–500.

Cui, Y., Miller, D., Schiarizza, P. and Diakow, L.J. (2017): British Columbia digital geology; BC Ministry of Energy, Mines and Petroleum Resources, BC Geological Survey, Open File 2017-8, 9 p. Data version 2018-04-05.

Daval, D., Hellmann, R., Martinez, I., Gangloff, S. and Guyot, F. (2013): Lizardite serpentine dissolution kinetics as a function of pH and temperature, including effects of elevated pCO_2; Chemical Geology, v. 351, p. 245–256.

Enkin, R.J. (2017): Physical property measurements at the Geological Survey of Canada Paleomagnetism and Petrophysics laboratory; Explorations 2017 Petrophysics Workshop, p. 02-1–02-16.

Forbes, W.C. (1971): Iron content of talc in the system $Mg_3Si_4O_{10}(OH)_2$-$Fe_3Si_4O_{10}(OH)_2$; Journal of Geology, v. 79, p. 63–74.

Hansen, L. (2005): Geologic setting of listwanite, Atlin, B.C.: implications for carbon dioxide sequestration and lode-gold mineralization; M.Sc. thesis, The University of British Columbia, Vancouver, BC, 192 p.

Hansen, L.D., Dipple, G.M., Gordon, T.M. and Kellett, D.A. (2005): Carbonated serpentinite (listwanite) at Atlin, British Columbia: a geological analogue to carbon dioxide sequestration; Vancouver Island, Canada; Canadian Mineralogist, v. 43, p. 225–239.

Jackson-Brown, S. (2017): Origin of Cu-PGE-rich sulfide mineralization in the DJ/DB zone of the Turnagain Alaskan-type intrusion, British Columbia; M.Sc. thesis, The University of British Columbia, Vancouver, BC, 272 p.

Kelemen, P.B. and Hirth, G. (2012): Reaction-driven cracking during retrograde metamorphism: olivine hydration and carbonation; Earth and Planetary Science Letters, v. 345–348, p. 81–89.

Kelemen, P.B. and Matter, J. (2008): In situ carbonation of peridotite for CO_2 storage; Proceedings from the National Academy of Science, v. 105, no. 45, p. 17295–17300.

Komor, S.C., Elthon, D. and Casey, J.F. (1985): Serpentinization of cumulate ultramafic rocks from the North Arm Mountain massif of the Bay of Islands ophiolite; Geochimica et Cosmochimica Acta, v. 49, p. 2331–2338.

McGoldrick, S., Canil, D. and Zagorevski, A. (2018): Contrasting thermal and melting histories for segments of mantle lithosphere in the Nahlin ophiolite, British Columbia, Canada; Contributions to Mineralogy and Petrology, v. 173, p. 25–42.

McGoldrick, S., Zagorevski, A. and Canil, D. (2017): Geochemistry of the volcanic and plutonic rocks from the Nahlin ophiolite with implications for a Permo-Triassic arc in the Cache Creek terrane, northwestern British Columbia; Canadian Journal of Earth Sciences, v. 54, p. 1214–1227.

Milidragovic, D. (2019): Geology of the Cache Creek terrane north of Trembleur Lake, parts of NTS 93K/14; BC Ministry of Energy, Mines and Petroleum Resources, BC Geological Survey, Open File 2019-06, 1:50 000 scale.

Milidragovic, D. and Grundy, R. (2019): Geochemistry and petrology of rocks in the Decar area, central British Columbia: Petrologically constrained subdivision of the Cache Creek complex; *in* Geological Fieldwork 2018, BC Ministry of Energy, Mines and Petroleum Resources, BC Geological Survey, Paper 2019-1, p. 55–77.

Milidragovic, D., Grundy, R. and Schiarizza, P. (2018): Geology of the Decar area north of Trembleur Lake; NTS 93K/14; *in* Geological Fieldwork 2017, BC Ministry of Energy, Mines and Petroleum Resources, BC Geological Survey, Paper 2018-1, p. 129–142.

Nixon, G.T., Manor, M.J., Jackson-Brown, S., Scoates, J.S. and Ames, D.E. (2015): Magmatic Ni-Cu-PGE sulphide deposits at convergent margins; *in* Targeted Geoscience Initiative 4: Canadian Nickel-Copper-Platinum Group Elements-Chromium Ore Systems—Fertility, Pathfinders, New and Revised Models, D.E. Ames and M.G. Houlé (ed.), Geological Survey of Canada, Open File 7856, p. 17–34.

Power, I.M., Wilson, S.A. and Dipple, G.M. (2013): Serpentinite carbonation for CO_2 sequestration; Elements, v. 9, p. 115–121.

Scheel, E.J. (2007): Age and origin of the Turnagain Alaskan-type intrusion and associated Ni-sulphide mineralization, north-central British Columbia, Canada; M.Sc. thesis, The University of British Columbia, Vancouver, BC, 201 p.

Schiarizza, P. and MacIntyre, D. (1999): Geology of the Babine Lake–Takla Lake area, central British Columbia (93K/11, 12, 13, 14; 93N/3, 4, 5, 6); *in* Geological Fieldwork 1998, BC Ministry of Energy, Mines and Petroleum Resources, BC Geological Survey, Paper 1999-1, p. 33–68.

Schwarzenbach, E.M. (2016): Serpentinization and the formation of fluid pathways; Geology, v. 44, no. 2, p. 175–176.

Toft, P.B., Arkani-Hamed, J. and Haggerty, S.E. (1990): The effects of serpentinization on density and magnetic susceptibility: a petrological model; Physics of the Earth and Planetary Interiors, v. 65, p. 137–157.

Vanderzee, S.S.S., Dipple, G.M. and Bradshaw, P.M.D. (2019): Targeting highly reactive labile magnesium in ultramafic tailings for greenhouse-gas offsets and potential tailings stabilization at the Baptiste deposit, central British Columbia (NTS 093K/13, 14); *in* Geoscience BC Summary of Activities 2018: Minerals and Mining, Geoscience BC, Report 2019-01, p. 109–118, URL <http://cdn.geosciencebc.com/pdf/SummaryofActivities2018/MM/Schol_SoA2018_MM_Vanderzee.pdf> [November 2019].

Vanderzee, S.S.S., Power, I.M., Dipple, G.M. and Bradshaw, P.M.D. (2018): Carbon mineralization in ultramafic tailings, central British Columbia: a prospect for stabilizing mine waste and reducing greenhouse gas emissions; *in* Geoscience BC Summary of Activities 2017: Minerals and Mining, Geoscience BC, Report 2018-01, p. 109–112, URL <http://cdn.geosciencebc.com/pdf/SummaryofActivities2017/MM/SoA2017_MM_Vanderzee.pdf> [November 2019].

Wilson, S.A., Dipple, G.M., Power, I.M., Thom, J.M., Anderson, R.G., Raudsepp, M., Gabites, J.E. and Southam, G. (2009): Carbon dioxide fixation within mine wastes of ultramafic-mafic-hosted ore deposits: Examples from the Clinton Creek and Cassiar chrysotile deposits, Canada; Economic Geology, v. 104, p. 95–112.

Zagorevksi, A. (2016): Geochemical data of the northern Cache Creek and Stikine terranes and their overlap assemblages, British Columbia and Yukon; Geological Survey of Canada, Open File 8039, 13 p.

Zagorevksi, A. (2018): Geochemical data of the northern Cache Creek, Slide Mountain, and Stikine terranes and their overlap assemblages, British Columbia and Yukon; Geological Survey of Canada, Open File 8395, 12 p.

Zagorevski, A., Bédard, J.H., Bogatu, A., Coleman, M., Golding, M. and Joyce, N. (2017): Stikinia bedrock report of activities, British Columbia and Yukon: GEM2 Cordillera; Geological Survey of Canada, Open File 8329, 13 p.

Logging SEDAR: A Better Access Road to New Mineral-Occurrence Records in British Columbia

N.D. Barlow, Purple Rock Inc., Victoria, British Columbia, nicole@purplerock.ca

J.R. Barlow, Purple Rock Inc., Victoria, British Columbia

J.G. McArthur, Kildalton Enterprises Inc., Victoria, British Columbia

Barlow, N.D., Barlow, J.R. and McArthur, J.G. (2020): Logging SEDAR: a better access road to new mineral-occurrence records in British Columbia; *in* Geoscience BC Summary of Activities 2019: Minerals, Geoscience BC, Report 2020-01, p. 145–150.

Background

National Instrument 43-101 Regulation

In 2007, the Canadian Securities Administrators (CSA) and its provincial member organizations (Figure 1) began to require technical reports conforming to National Instrument (NI) 43-101, the *Standards of Disclosure for Mineral Projects*. These technical, geoscientific reports must be prepared by 'qualified professionals' (QP) and filed by companies listed on a Canadian stock exchange, regardless of where in the world the exploration occurs. These reports include data and an interpretation of the geoscience research that contributed to any exploration results they disclose. Along with numerous other financial disclosures, they are posted to the System for Electronic Document Analysis and Retrieval (SEDAR) website (Alberta Securities Commission, 2019), which is managed by the CSA.

Project Rationale

Even though designed to protect investors (Canadian Securities Administrators, 2011), NI 43-101 technical reports contain exploration data that may be of interest from a geoscience perspective and, in many cases, these reports contain millions of dollars of geoscience research. Mineral claim holders may have copies of all NI 43-101 reports for their claim but they may also be interested in comparing results with nearby exploration projects and even more distant projects believed to share similar deposit features. Mineral exploration by machine learning or artificial intelligence, for example, requires high-quality raw data to train its neural networks. This is the sort of data available in NI 43-101 reports.

SEDAR, unfortunately, provides no online method to spatially locate a NI 43-101 technical report. Moreover, such a feature is not considered to be a necessary addition by the CSA or its users in the finance industry, nor does SEDAR track other information useful to geoscientists, such as work types or related mineral occurrences.

British Columbia (BC) has an extensive public geoscience database, contained in database systems managed by the BC Geological Survey (BCGS). These include MINFILE, MapPlace 2, ARIS, Property File and COALFILE (BC Geological Survey, 2019a–d; BC Ministry of Energy, Mines and Petroleum Resources, 2019a; Figure 1). Primary data from the mineral exploration industry is collected in ARIS (the assessment report indexing system pertaining to assessment reports submitted by companies and individuals to maintain mineral tenure rights), Property File (geoscience archives that were voluntarily submitted to, or collected by, the BC Geological Survey) and COALFILE (coal assessment reports). These data are aggregated in MINFILE (a provincial-scale database of mineral occurrences, describing the regional and local geological setting as well as the exploration and mining history) and are displayed on MapPlace 2. The NI 43-101 technical reports are thought to be a major source of primary geoscience data that is not automatically included or integrated into the public geoscience database. As previously noted, companies submit assessment reports to the BC Mineral Tenures Branch to keep mineral titles in good standing. These reports might disclose the same information as that contained in an NI 43-101 report for investors. Some mineral-title holders choose to not file assessment reports (and pay cash in lieu), but they are obliged to file NI 43-101 reports if they are public companies. See Table 1 for a comparison of NI 43-101 reports and assessment reports.

Phase 1

To improve the availability of SEDAR data for BC, Geoscience BC approved Phase 1 of this project in 2016. The initial objective was to gain access to all of the BC-related NI 43-101 technical reports for analysis and gain permission to publish metadata derived from the reports. The provinces and territories have jurisdiction over securities, so each has its own securities regulator, but they co-ordinate policy and harmonize regulations as the Canadian Securities Administrators—the federal government is not di-

This publication is also available, free of charge, as colour digital files in Adobe Acrobat® PDF format from the Geoscience BC website: http://www.geosciencebc.com/updates/summary-of-activities/.

rectly involved. Phase 1 required several years of discussion and negotiations to obtain the approvals from the provincial securities commissions, CSA and CSA's IT Systems Office for feasibility.

In 2018, Phase 1 was completed successfully: reports were released to Geoscience BC and the project team for metadata capture and data mining in order to update the MINFILE database. Phase 1 was not presented in any prior *Summary of Activities* volume because there was no research to report.

Phase 2 of the project, the current phase, aims to focus on capturing the geoscience data contained in these otherwise difficult-to-access reports.

Method

The SEDAR website has no project-location index, so the CSA provided a complete collection of all NI 43-101 reports (approximately 11 000 reports and amendments, but excluding the many other report types they collect through their regulation of Canadian public companies). Some early reports contained scanned pages without text recognition, so the authors used OCRmyPDF (Barlow, 2019), a free open-source tool developed by the second author, to insert optical character recognition (OCR) as needed. The authors used Poppler (Poppler Development Team, 2019), a free open-source PDF-to-text extraction tool, to obtain the complete text of all reports (1.7 million pages) and inserted the text into an SQLite (Hipp, 2018) database with a full-text search schema. The resulting database was 6.3 GB.

Several search queries were used to identify reports pertaining to BC mineral properties and exclude those that were not in BC. 'British Columbia' or 'BC' were not suitable keywords, given the large number of mining companies based in Vancouver with exploration projects in other parts of Canada or the world. MINFILE numbers or NTS

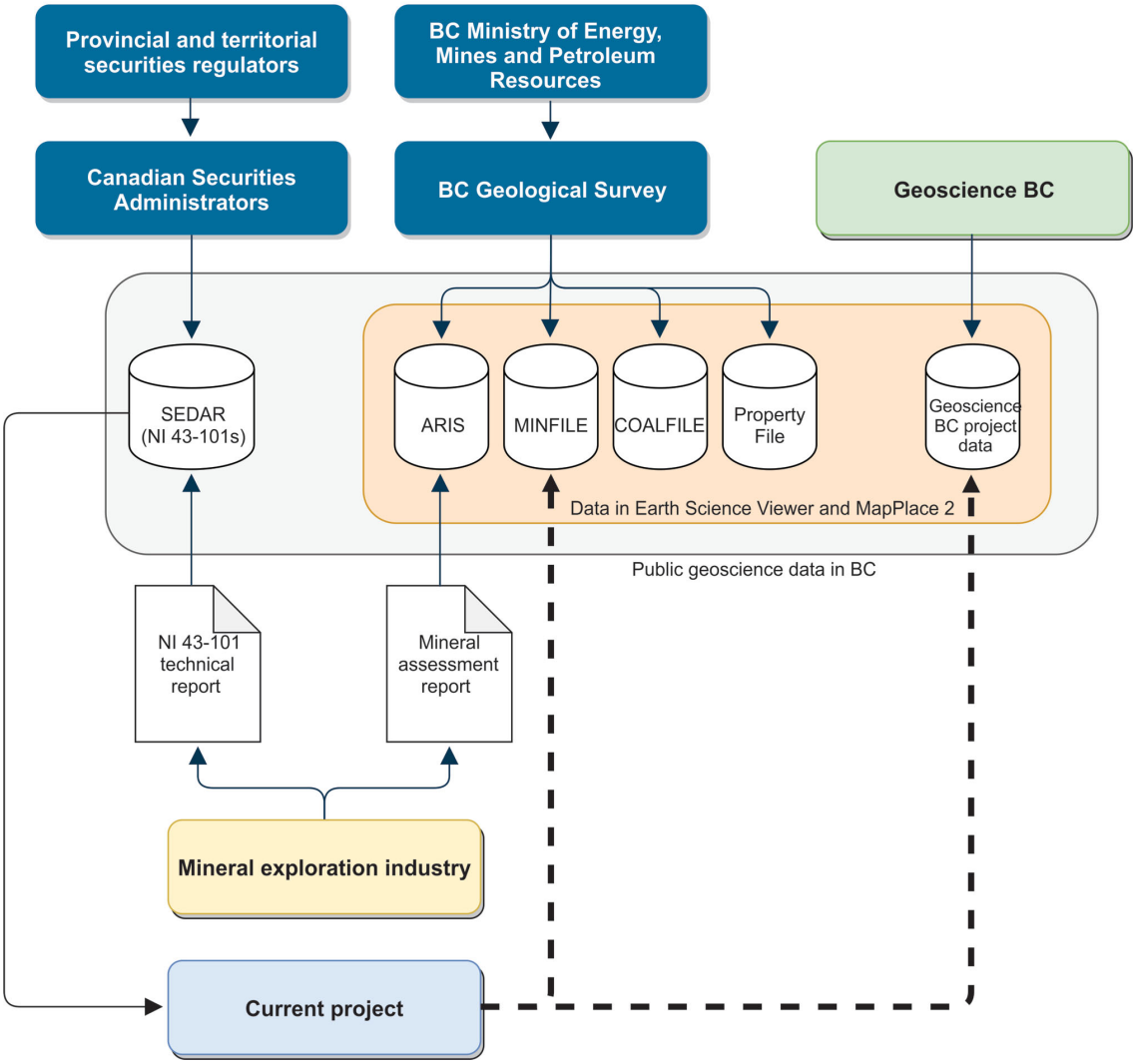

Figure 1. Schematic diagram of the sources and providers of public geoscience data in British Columbia. Abbreviation: NI, national instrument.

Table 1. Comparison between National Instrument (NI) 43-101 technical reports and mineral assessment reports. Abbreviations: BCSC, British Columbia Securities Commission; CSA, Canadian Securities Administrators.

	NI 43-101 reports	Assessment reports
Submitted to	CSA's provincial member organization (i.e., BCSC)	BC Mineral Titles Branch
Submitted by	Public companies	Mineral tenure owners
Prepared by	A qualified professional independent of the property owner	P.Geo. or P.Eng., may be affiliated with property owner
Reviewed and approved by	CSA's provincial member organization (i.e., BCSC)	BC Geological Survey
Hosted by	www.sedar.com	www.aris.empr.gov.bc.ca
Intended audience	Investors	Mining industry
When filed	Generally, when information that may change the value of a publicly traded company's stock is disclosed	Annual report of mineral exploration on mineral tenures
When published	Upon approval	Held confidential for one year
Total number for BC	870	37 412

map numbers covering BC were reliable indicators of a report being in BC. Latitudes and longitudes were less reliable—for several years, latitude and longitude were not required on a report's cover sheet and errors in co-ordinates were more common than one might expect, especially when given in degrees-minutes-seconds. Occasional novel formatting of degree symbols also contributed to false positives. Finally, a list of place names that are unique to BC within Canada was derived from the Canadian Geographical Names Data Base (Natural Resources Canada, 2016), and these were matched to reports. Geospatial data embedded in PDFs were not checked for because this feature is not commonly used.

A GeoPackage file (Open Geospatial Consortium, 2019) was generated that specified the co-ordinates of all locatable reports, and QGIS (QGIS Development Team, 2019) was used to review and correct the point locations. Reports that gave bounding boxes or polygons were collapsed to the centroid for consistency (Figure 2).

Having narrowed the list of reports to those likely related to BC mineral properties (approximately 870 reports), a spreadsheet was generated consisting of the report's identifier (internal to SEDAR's database and not easily visible to the public), the metadata that could be extracted using scripts, and the contents of the first page (because most other metadata can be pulled from here). A manual review of the reports and organization of the metadata was then completed. Where available, the total expenditure was recorded to give a sense of the scope of a report. The types of work performed were also recorded to help users locate work types of interest to them, such as drilling and geochemistry. See Table 2 for a list of metadata fields that will be captured.

Work is in progress to review the NI 43-101 reports for updates to the MINFILE database (whether new occurrences or updates to existing occurrences).

Discussion

Contents of NI 43-101 Reports

The authors are not aware of any previous effort to analyze or summarize the contents of NI 43-101 reports in existence, including those pertaining to BC projects. As a general observation, an NI 43-101 report encompasses a wider project area and usually involves several MINFILE occurrences, as defined by the BC Geological Survey. Projects typically involve multiple mineral land titles. Out of 870 reports, 147 reported total property expenditures directly (a total is only reported if it was given in the report; no attempt was made to calculate or estimate it). The property expenditures reported in the 147 reports amounted to $67 million in exploration activity, or approximately $500 000 per report. This figure is surprisingly low considering the levels of exploration activity between 2007 and 2018 ($5.0 billion; BC Ministry of Energy, Mines and Petroleum Resources, 2019). It can safely be assumed that using only those reports that disclosed total expenditures is only a partial reflection of the true total.

The CSA and securities regulators caution that the content of all NI 43-101 technical reports is the responsibility of the company filing the report; although CSA checks that submitted reports conform to NI 43-101 standards, the reports are not 'audited' for scientific accuracy. As with other sources of industry-derived public geoscience data, they may contain errors and, as such, are distributed without warranty.

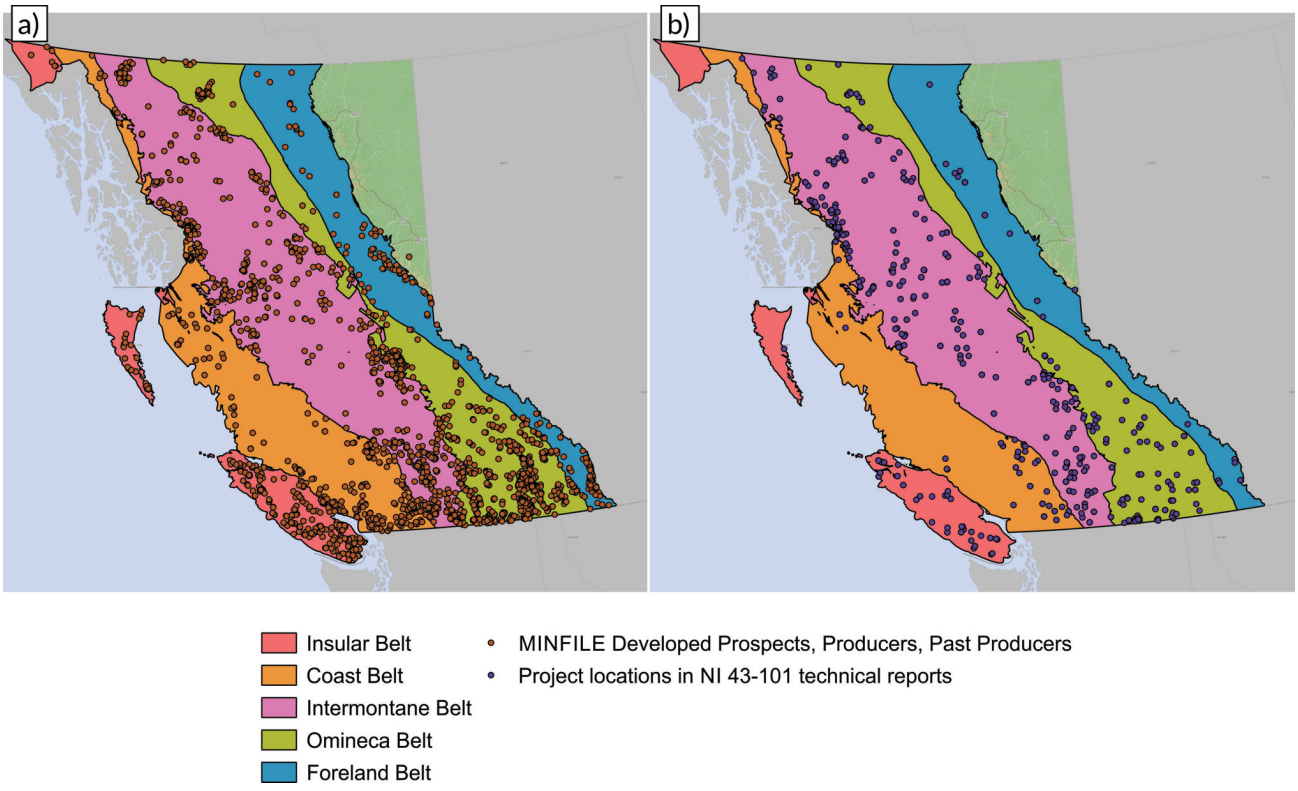

Figure 2. Locations of **a)** MINFILE occurrences labelled 'Developed Prospect', 'Producer' or 'Past Producer'; and **b)** National Instrument (NI) 43-101 reports relating to BC. Base map from DataBC (2019), morphogeological belts from Cui et al. (2017) and MINFILE locations from BC Geological Survey (2019c).

Future Work

Following completion of the metadata index, the intent is to update all MINFILE occurrences referenced in the NI 43-101 reports, to ensure that NI 43-101 research is integrated into the public geoscience database. A geospatial layer will also be available on Geoscience BC's Earth Science Viewer and the BC Geological Survey's MapPlace 2.

Once the MINFILE portion of Phase 2 is completed, the authors will comment on the value and findings of the project in *Summary of Activities* 2020.

Table 2. Metadata fields captured from National Instrument (NI) 43-101 reports relating to BC.

Metadata fields
SEDAR Number
Title
Date
Project name
Primary company
Secondary company
Latitude
Longitude
Related MINFILE number(s)
NTS map sheet(s)
Total expenditures
Work types

Acknowledgments

The authors acknowledge B. Madu (formerly Geoscience BC), whose support and championing of this project at its conceptual stage made it possible; N.C. Carter (retired consulting geologist) for his support for the project and thorough and thoughtful review of this paper; C. Pellett and B. Clift (Geoscience BC); R. Cosman, M. Hurn and N. Varga (Canadian Securities Administrators); and A. Hickin, L. Jones and S. Meredith-Jones (BC Geological Survey). The authors also acknowledge supporting work done by the Purple Rock team, including K. Flower, A. Campbell and M. Shuert.

References

Alberta Securities Commission (2019): SEDAR system of electronic document analysis and retrieval; Canadian Securities Administrators, URL <http://sedar.com> [November 2019].

Barlow, J.R. (2019): OCRmyPDF; GitHub, URL <https://github.com/jbarlow83/OCRmyPDF> [November 2019].

BC Geological Survey (2019a): COALFILE BC coal data and reports; BC Ministry of Energy, Mines and Petroleum Resources, BC Geological Survey, URL <http://webmap.em.gov.bc.ca/mapplace/coal/search.asp> [November 2019].

BC Geological Survey (2019b): MapPlace GIS internet mapping system; BC Ministry of Energy, Mines and Petroleum Re-

sources, BC Geological Survey, URL <http://www.mapplace.ca> [November 2019].

BC Geological Survey (2019c): MINFILE BC mineral deposits database; BC Ministry of Energy, Mines and Petroleum Resources, BC Geological Survey, URL <http://minfile.ca> [November 2019].

BC Geological Survey (2019d): Property File digital document database; BC Ministry of Energy, Mines and Petroleum Resources, BC Geological Survey, URL <http://propertyfile.gov.bc.ca> [November 2019].

BC Ministry of Energy, Mines and Petroleum Resources (2019a): Assessment Report Indexing System (ARIS); BC Ministry of Energy, Mines and Petroleum Resources, BC Geological Survey, URL <https://aris.empr.gov.bc.ca/> [October 2019].

BC Ministry of Energy, Mines and Petroleum Resources (2019b): Exploration spending; BC Ministry of Energy, Mines and Petroleum Resources, URL <https://www2.gov.bc.ca/gov/content?id=DB9E37B6D3274CFDA8C9E1DFE4E4B708> [November 2019].

Canadian Securities Administrators (2011): Rules and policies; Chapter 5 *in* National Instrument 43-101: Standards of Disclosure for Mineral Projects, Canadian Securities Administrators, URL <https://mrmr.cim.org/media/1017/national-instrument-43-101.pdf> [November 2019].

Cui, Y., Miller, D., Schiarizza, P. and Diakow, L.J., (2017): British Columbia digital geology; BC Ministry of Energy, Mines and Petroleum Resources, BC Geological Survey, Open File 2017-8, 9 p., data version 2018-04-05, URL <https://www2.gov.bc.ca/gov/content/industry/mineral-exploration-mining/british-columbia-geological-survey/geology/bcdigitalgeology> [November 2019].

DataBC (2019): BC Base Map Service – BC Albers; BC Ministry of Citizen Services, DataBC, URL <https://catalogue.data.gov.bc.ca/dataset/bc-base-map-service-bc-albers> [November 2019].

Hipp, R. (2018): SQLite [Computer software]; SQLite Development Team, URL <https://www.sqlite.org/> [November 2019].

Natural Resources Canada (2016): Canadian Geographical Names Data Base; Natural Resources Canada, URL <https://www.nrcan.gc.ca/earth-sciences/geography/geographical-names-board-canada/about-canadian-geographical-names-database/9180> [November 2019].

Open Geospatial Consortium (2019): GeoPackage open format for geospatial information; Open Geospatial Consortium, URL <https://www.geopackage.org/> [November 2019].

Poppler Development Team (2019): Poppler, version 0.83.0; Freedesktop.org, URL <https://poppler.freedesktop.org/> [November 2019].

QGIS Development Team (2019): QGIS Geographic Information System; Open Source Geospatial Foundation Project, URL <http://qgis.osgeo.org> [October 2019]

Digitizing British Columbia's Geological Heritage

A. Randell, Below BC Geological Association, Vancouver, British Columbia, andy@stratageodata.com

A. Whistler, Below BC Geological Association, Vancouver, British Columbia

J. Moffat, Below BC Geological Association, Vancouver, British Columbia

Randell, A., Whistler, A. and Moffat, J. (2020): Digitizing British Columbia's geological heritage; *in* Geoscience BC Summary of Activities 2019: Minerals, Geoscience BC, Report 2020-01, p. 151–154.

Introduction

The province of British Columbia (BC) has a rich mining history with many communities built around exploration, mining and prospecting activities. Today, mining and mineral exploration continue to play a key role in the provincial economy, providing jobs and resources such as coal, metals and minerals. These resources are essential for many modern technologies as well as for generating and storing renewable power. Despite this, many British Columbians remain disconnected from the integral part mining plays in their day-to-day lives. Many organizations and events exist within BC to bridge this gap between citizens and the mining industry. The Below BC Geological Association, or Below BC, is a nonprofit Earth science outreach organization, whose goal is to connect BC citizens with the local geology as well as to provide education about a variety of topics, including the history of mining. This summer, Below BC has collaborated with Geoscience BC, mining and mineral exploration companies, professional geologists, prospectors, rockhounds, and municipal and provincial government agencies to launch its latest endeavour, the BC Geological Heritage Project.

Currently in its early stages, the project consists of an online, interactive museum and database of geological samples—rocks, core, fossils and minerals—from all areas of BC (Figure 1). The goal is to centralize and increase accessibility to geological data, while preserving the samples and heritage pieces. The digital museum, or Rock Library, will be complemented by virtual geotours, or field trips, providing 360° views and insight into the geology at key locations across BC. The digital museum and virtual geotours will integrate high-quality interactive images with scientific studies, chemical data, maps, multimedia and social history to form a user-friendly resource for geologists and non-geologists alike. The BC Geological Heritage Project will increase accessibility to rock collections and geological data from BC, making research simpler and eliminating the necessity to travel, thus contributing to the reduction in carbon emissions. In addition, the process of digitally recording samples and locations preserves and archives BC's geological history, protecting it from loss, destruction or redevelopment.

The digital museum and database will be accessible to a wide range of audiences for research, education, outreach and general inquiry. The creators and participants of the project hope that it will serve as a valuable and unique resource to professional geologists in their projects and studies, while engaging other audiences to give the Earth sciences context, delivering facts in an understandable manner and ultimately improving the overall Earth science literacy of British Columbians.

Figure 1. Over 700 rock, mineral and fossil specimens from British Columbia were digitally documented this summer by the Below BC Geological Association to increase accessibility to, and preserve and promote, BC's geology and geological heritage. This specimen of molybdenum and pyrite in a quartz vein comes from the Davidson deposit, at Hudson Bay Mountain, near Smithers, British Columbia (specimen courtesy of D. Ethier).

This publication is also available, free of charge, as colour digital files in Adobe Acrobat® PDF format from the Geoscience BC website: http://www.geosciencebc.com/updates/summary-of-activities/.

Earth Science Literacy

One of the primary goals of the BC Geological Heritage Project is to engage a variety of audiences—professional geologists in industry and academia, university students, educators, kindergarten to grade 12 students, communities and policy makers—to improve the overall Earth science literacy of BC residents. In 2010, the United States National Science Foundation created the Earth Science Literacy Principles, a guide comprising nine 'Big Ideas', to help geologists and educators effectively communicate Earth science (Earth Science Literacy Initiative, 2019). The guide defines an Earth science literate person as an individual who

> *"...understands the fundamental concepts of Earth's many systems, knows how to find and assess scientifically credible information about Earth, communicates about Earth science in a meaningful way, and is able to make informed and responsible decisions regarding Earth and its resources."*

'Big Idea' 7 from the Earth Science Literacy Principles focuses on humankind's dependence on Earth's natural resources and is most relevant to the framework of the BC Geological Heritage Project. Improving the Earth science literacy of British Columbians using this project and similar initiatives can improve attitudes toward exploration and mining, provide insight and greater appreciation for the past and present roles of mining within the province, promote stewardship and sustainable practices, and allow BC to continue to be a global leader in the mining and mineral-exploration industry. In addition, engaging new audiences could encourage youth to pursue education in the field of Earth sciences, potentially halting the declining enrollment numbers in Earth Science programs in Canadian universities (Johnston et al., 2018).

The Digital Rock Museum and Database

The digital museum, the first of its kind, uses high-resolution interactive images that provide a full 360° perspective of a geological sample (Figure 2). The clarity of the high-quality images is remarkable; the photos are aesthetic and precise, revealing mineral cleavage, mineral habit, texture, mineralization and alteration in detail (Figure 3). Individual specimens will have their own detailed rock descriptions, complete with age and location. Available complementary data and resources will also be added (e.g., thin-section images, scientific studies, chemical data, maps, press releases, figures and diagrams, as well as videos).

Rock suites curated from private collections, museums, mining and exploration companies, local exploration groups, and government organizations have been documented and will be added to the Below BC server. Already, over 100 rock, mineral and fossil specimens from the Association for Mineral Exploration, the Pacific Museum of Earth of The University of British Columbia, the BC Ministry of Energy, Mines and Petroleum Resources, and the Smithers Exploration Group are available; already, these have been used by academics, geological researchers, schools and the public.

Virtual Geotours

Virtual field trips created for the BC Geological Heritage Project will highlight important geological locations throughout the province by providing the audience with a 360° perspective. This technique documents and digitally preserves landscapes, outcrops, viewpoints, exploration sites and museum displays in case they are destroyed or redeveloped. The virtual field trips share these locations with a wider audience, which otherwise would be unable to visit the various sites.

To produce the virtual field trips, an ultra-wide–angle THETA camera from Ricoh Company Ltd. and robotic camera mount by GigaPan Systems are used to capture, respectively, outward 360° images and detailed panoramic images. The outward 360° image can be taken instantaneously and allows the observer to be virtually placed at the scene. The panoramic images from the GigaPan comprise hundreds of images, taken fully zoomed into the subject, which are then stitched together. The final product is a highly detailed panoramic image that allows small details, such as a boulder in the distance, to be preserved (Figure 4). As was the case for the samples in the digital library, additional material and data can be integrated with the virtual field trips to provide the reader more information (e.g., scientific studies, chemical data, maps, satellite imagery, press releases, figures and diagrams, as well as videos).

Digitizing and Preserving Geological Specimens

The project organizers required the collaboration of individuals, companies, museums and government agencies to photograph and digitize the geological samples, which will be preserved and shared on the digital museum platform and database. These collaborations will allow Below BC to access a variety of rock suites, which represent the diverse geology of BC. In the summer of 2019, Below BC organized two trips, phase 1 through southern BC and phase 2 through northwestern BC, to collect material not only for the digital museum and database but also for the virtual field trips (Table 1). Over the span of two months, the organization was able to collect historical data, virtual geotours and panoramas, while also digitizing over 700 rock, mineral and fossil specimens.

Conclusion and Future Work

Geologists possess a fundamental understanding of the Earth and its systems; they have the responsibility and privilege of sharing that knowledge with people of all back-

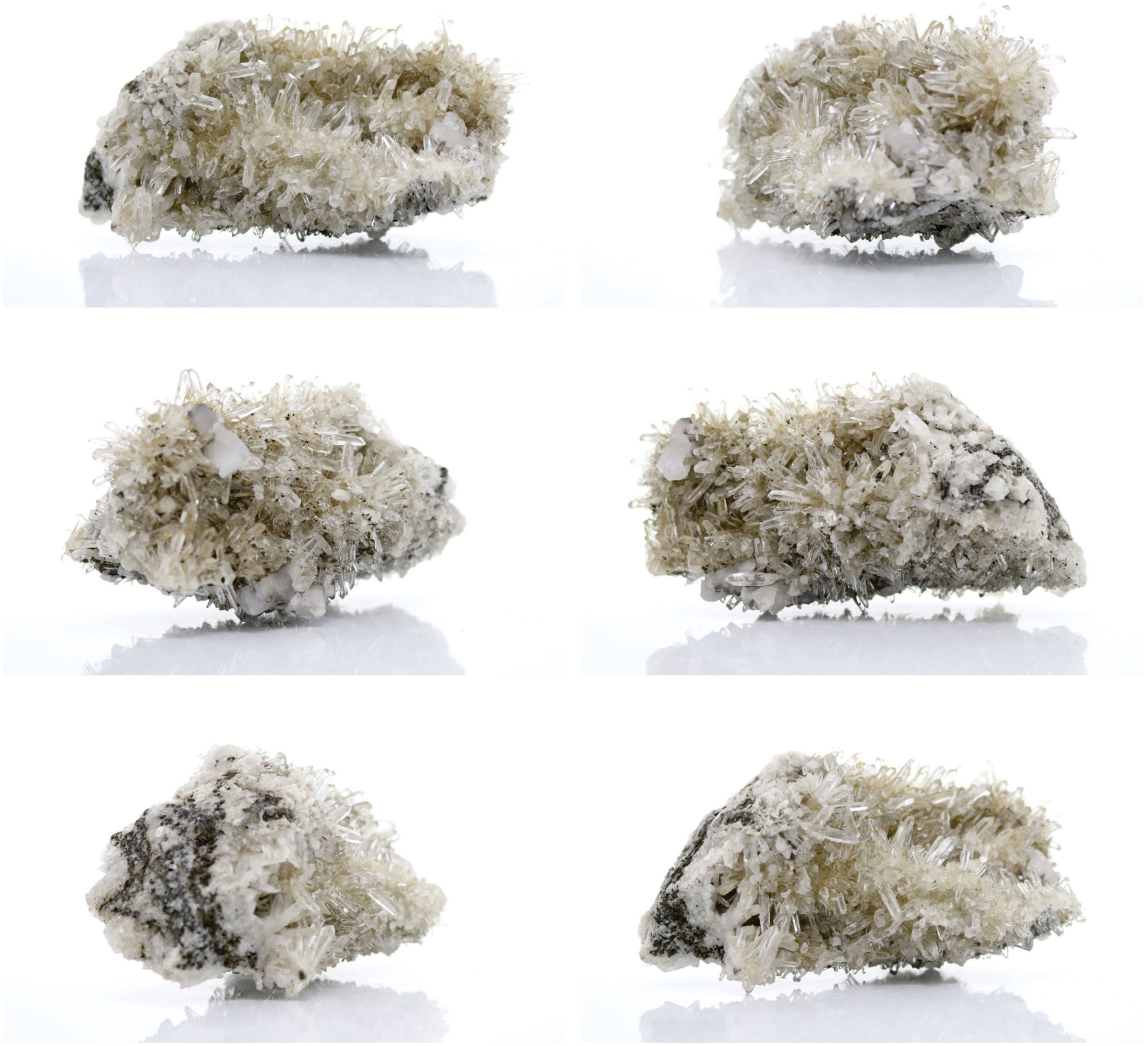

Figure 2. Multiple photographs of a single specimen are taken from different angles and stitched together to produce an interactive, high-quality, rotating 360° image that can be accessed in the Digital Rock Library created by the Below BC Geological Association. This specimen of quartz-calcite crystals comes from the Bluebell Mine in Riondel, BC (specimen courtesy of P. Ransom at the Kimberly Underground Mining Railway).

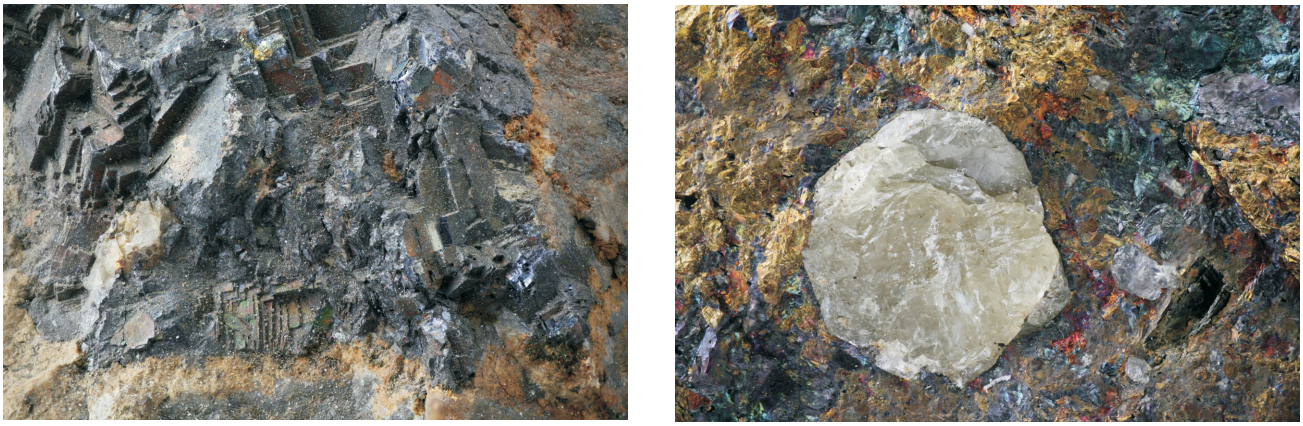

Figure 3. A series of macroscopic images are taken at different locations (focal depth) on the sample and are focus stacked to produce high-resolution images. **(Left)** Massive sphalerite vein. **(Right)** High-grade vein material from the Granisle mine, Babine Lake, British Columbia (specimens courtesy of the Smithers Exploration Group).

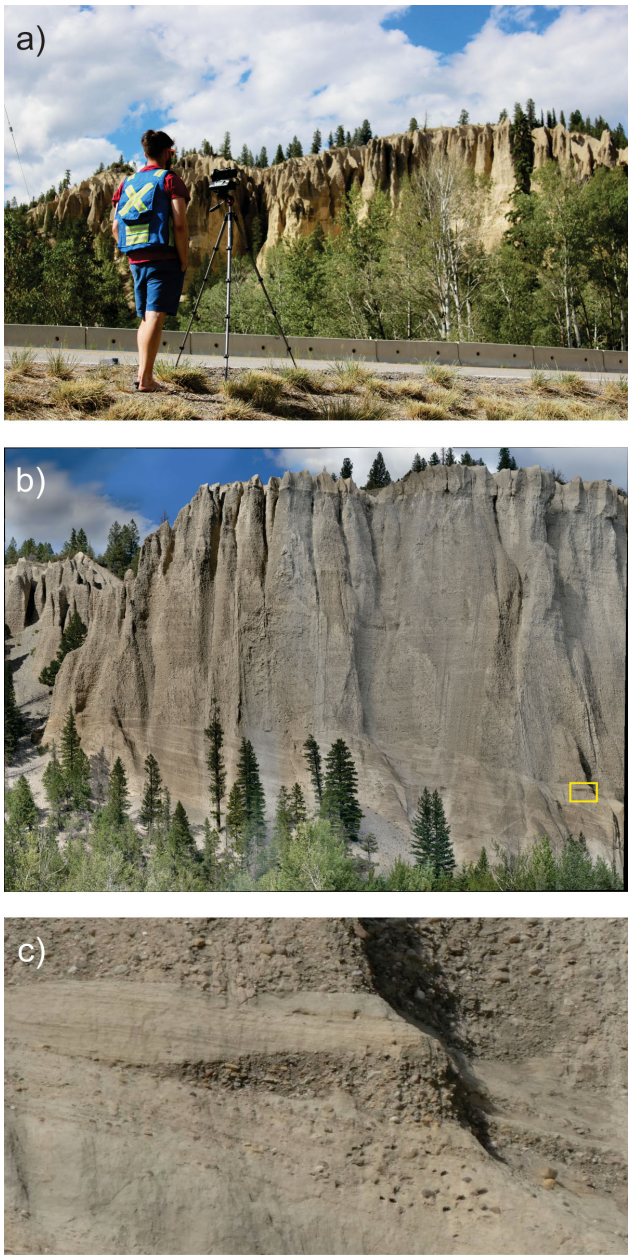

Figure 4. Examples of **a)** cameraman with the robotic panohead by GigaPan Systems taking pictures of the Hoodoos near Fairmont Hot Springs, British Columbia; **b)** photograph taken from a distance of 1 km (location of (c) indicated by box with yellow outline); **c)** details of individual rocks in the layers picked up by the camera; resolution can be increased, but even at this medium resolution, data can be captured about sorting, roundness and distribution of the pebbles that are otherwise lost in the first 'distal' image.

Table 1. Sites visited on phase 1 and phase 2 trips across southern and northwestern BC, respectively.

Location	Rotating 360° sample images
Hedley Museum	14
Princeton Museum	13
Oliver Museum	16
Greenwood Museum	13
Rossland Museum	34
(Kaslo) Kootenay Star Mining Museum	14
Kimberley Heritage Museum	11
Sandon Museum	10
East Kootenay Chamber of Mines	22
Kimberley Underground Mining Railway	22
Ministry of Energy, Mines and Petroleum Resources (Cranbrook)	21
D. Pighin (private collector)	6
Revelstoke Museum	7
Silvery Slocan mine (New Denver)	14
Cranbrook History Centre	11
Nelson Chamber of Mines	22
Margaux Resources Ltd.	31
Crystal Lake Mining	63
Stewart Museum	27
Decade Resources (private collector)	15
Drifter Ventures Ltd. (private collector)	18
D. Ethier (private collector)	19
Lakes District Museum	20
Quesnel and District Museum	23
Museum of Cariboo Chilcotin	19
Barkerville Historic Town	5
Smithers Exploration Group	275

grounds and education levels to improve Earth science literacy, which is especially essential in a location such as BC where geology is ubiquitous. The BC Geological Heritage Project gives geologists, communities, governments, and mining and exploration companies the opportunity to collaborate on a unique initiative, through which geological samples and sites are digitally archived, preserved and promoted through the digital museum and database, and virtual tours. The project allows past and present geological information to be centralized, making the information more widely accessible. This project allows fusion of an old and evolving industry integral to this province's history with modern technology. In the future, Below BC plans to continue building its database of specimens with additional trips to Vancouver Island and northeastern BC. Below BC will continue to work with the Smithers Exploration Group to catalogue their collection and improve the quality of both groups' websites.

Acknowledgments

The authors thank D. Wilkie for his review of the draft manuscript of this paper.

References

Earth Science Literacy Initiative (2019): Earth Science Literacy Principles; United States National Science Foundation, URL <www.earthscienceliteracy.org/es_literacy_6may10_.pdf> [September 2019].

Johnston, S.T., Schröder-Adams, C., Branfireun, B., Mayer, B. and Venditti, J. (2018): S. 19-08; External Review Report, Department of Earth Sciences, Simon Fraser University, 34 p., URL <https://docushare.sfu.ca/dsweb/Services/Document-1548322> [September 2019].

Progress Report on the Smithers Exploration Group's Rock Room (Northwestern British Columbia)

A. Ledwon, Smithers Exploration Group, Smithers, British Columbia, rockroom@smithersexplorationgroup.com

C. Ogryzlo, Smithers Exploration Group, Smithers, British Columbia

Ledwon, A. and Ogryzlo, C. (2020): Progress report on the Smithers Exploration Group's Rock Room (northwestern British Columbia); *in* Geoscience BC Summary of Activities 2019: Minerals, Geoscience BC, Report 2020-01, p. 155–158.

Introduction

When the Smithers Exploration Group (SEG) was founded back in the early 1970s, no one could have foreseen its successful growth and community involvement over the decades. From co-creating the School of Exploration and Mining with Northwest Community College (now Coast Mountain College) to organizing a myriad of public education projects, SEG has played an active role in the community of Smithers, northwestern British Columbia (BC), and in BC as a whole through its advocacy for the mining and exploration industry. During this time, SEG had amassed an extensive rock collection that, through a grant and some very hard work, was sorted into what is now the SEG Rock Room. Located in Smithers, the collection has attracted much attention at recent conferences, and has become the focus of many hopes and plans for the future. Thanks to a Geoscience BC grant, SEG has been able to move forward with several of these projects in 2019.

Project Updates

Completion of Collection

A large donation (four pallet loads) of samples from the BC Ministry of Energy, Mines and Petroleum Resources in Prince George is allowing SEG to fill in some specific gaps in the collection. Shipments from private collections have also arrived, mainly from geologists who explored the region during the 1970s, 1980s and 1990s for the provincial and federal governments. A temporary storage and sorting area (Figure 1) has been set up near the main Rock Room as local and visiting geologists work together to pick out the best samples to be used both in the collection and for future teaching programs.

Rock Room Improvements

The main improvement to the Rock Room in 2019 has been the changeover to daylight bulbs. Being able to study and photograph hand samples under natural lights helps keep colour analyses accurate and assists in preventing eye strain. Also, SEG updated and posted its emergency response plan and upgraded the first-aid materials in the office.

Presentations to KEG and MEG

In April of 2019, SEG presented an introduction to the Rock Room at the annual conference of the Kamloops Exploration Group (KEG) in Kamloops, BC. Audience members responded enthusiastically to the potential of the Rock Room and many questions ensued, particularly on how ge-

Figure 1. Storage and sorting area for rock donations from the BC Ministry of Energy, Mines and Petroleum Resources and private collectors. Many of these rocks will be used as teaching samples as they arrived with little but a name, and sometimes not even that.

This publication is also available, free of charge, as colour digital files in Adobe Acrobat® PDF format from the Geoscience BC website: http://www.geosciencebc.com/updates/summary-of-activities/.

ologists and prospectors could share and/or donate parts of their own collections. Access to the Rock Room was also of key interest, as was the potential to view the collection samples digitally.

The Smithers Exploration Group has reached out to the Vancouver Mining Exploration Group (MEG) in hopes of presenting a talk toward the end of 2019.

Training for Regional Rockhounds

Teaching rocks have become a common theme in the Rock Room as donations have arrived from across the province. Ideally, SEG wants to ensure as many of these samples end up in use as possible; as such, plans are underway to create both an introductory course (late fall 2019) for amateur rockhounds and an advanced prospecting course (late spring 2020) for those with experience in the industry. Local geologists will make up most of the pool of instructors and visiting geologists have helped develop regional field trips that will supplement the classroom work.

AME Roundup Poster and Prospectors' Tent Presentations

Applications for a table in the Prospectors' Tent and a poster for the annual Roundup conference of the Association for Mineral Exploration (AME; Figure 2) have been submitted. At that event, SEG hopes to have a selection of relevant hand samples available to match the showcases of individual prospectors. Additionally, SEG will display educational posters and other materials to encourage the use of the Rock Room.

SEG Rock Talk Workshop

In February 2020, SEG will host its annual Rock Talk in Smithers, BC. A full-day educational workshop is planned for the day prior to the conference and will revolve around a hands-on presentation in the Rock Room.

3D Photography Project and Online Interactive Map

The Smithers Exploration Group is excited to be working with another Geoscience BC grant recipient, the Below BC Geological Association (Below BC; Figure 3). Over 400 samples from the Rock Room have been photographed and added to Below BC's online three-dimensional (3D) catalogue. Over the next few months, an interactive digital map will be created, also in conjunction with Below BC, allowing the public access to photos, locations and other information on most items in the collection.

Educational Poster Development

During the preparations for Rock Talk 2019 (Figure 4), several draft educational posters were created and used in conjunction with numerous hand samples from the rock collection. These posters were digitized and are in the process of being printed for use in future educational programs, outreach activities and workshops. Participants greatly enjoyed the three-dimensional, hands-on aspect of the informational posters, accompanied as they were with actual associated rock specimens.

Figure 2. Local and visiting geologists planning field trips and posters for the Association for Mineral Exploration Roundup. From left to right: P. Ogryzlo, T. Richards and T. L'Orsa.

Figure 3. Below BC photographers J. Moffat and A. Whistler discussing rocks in the Smithers Exploration Group office with T. Richards (far right) and D. MacIntyre (back to camera).

Figure 4. Rock Talk 2019 participants exploring hand samples and associated educational posters.

Acknowledgments

The Smithers Exploration Group would like to thank J. Nelson, H. Tremblay, H. Smit and T. Richards for their ongoing support and championing of the Rock Room project. Many others have been instrumental in bringing the Rock Room to its current state and SEG thanks them all.

Invertebrate Response to Mine Reclamation (South-Central British Columbia): The Effects of Reclamation Age on Arthropod Assemblages

C.A. Gervan[1], **Department of Natural Resource Science, Thompson Rivers University, Kamloops, British Columbia, chantallegervan@hotmail.com**

W.C. Gardner, Department of Natural Resource Science, Thompson Rivers University, Kamloops, British Columbia

E.M. Bottos, Department of Biological Sciences, Thompson Rivers University, Kamloops, British Columbia

J.D. Van Hamme, Department of Biological Sciences, Thompson Rivers University, Kamloops, British Columbia

R.J. Higgins, Department of Biological Sciences, Thompson Rivers University, Kamloops, British Columbia

L.H. Fraser, Department of Natural Resource Science, Thompson Rivers University, Kamloops, British Columbia

Gervan, C.A., Gardner, W.C., Bottos, E.M., Van Hamme, J.D., Higgins, R.J. and Fraser, L.H. (2020): Invertebrate response to mine reclamation (south-central British Columbia): the effects of reclamation age on arthropod assemblages; *in* Geoscience BC Summary of Activities 2019: Minerals, Geoscience BC, Report 2020-01, p. 159–166.

Introduction

In Canada, regulations state that planning for mine closure must occur before mining companies begin production (Mining Association of Canada, 2019). Mine closure entails ecosystem reclamation: returning the land that has been altered by mining back to a functioning, self-sustaining ecosystem. More specifically, mine reclamation in British Columbia (BC) addresses terrestrial areas, water bodies and cultural resources (Government of British Columbia, 2019). Ecosystem reclamation research is required to reduce knowledge gaps and further understand the recovery trajectory of reclaimed sites to optimize reclamation practices.

Postmining landscapes undergo succession as it relates to flora and fauna (such as invertebrates). Currently, researchers call attention to the lack of information regarding the outcomes of mine reclamation (Bacher et al., 2018), especially addressing invertebrate-community recovery. Biotic diversity is identified as an important factor in achieving a functioning ecosystem. Biodiversity is defined as the variety of life in a given area with regard to genetic variance, trophic levels and taxonomy (Gaston and Spicer, 2004); it therefore follows that biodiversity can be used as a measure of ecological health.

Invertebrates comprise a significant portion of taxonomic biodiversity and provide essential ecosystem services (McGeoch et al., 2011). More specifically, arthropods play a fundamental role in ecological succession and soil formation in reclaimed areas as they contribute to nutrient turnover, decomposition, litter breakup, herbivory and pollination; they also act as dispersal agents (fungi and propagule) and are food resources for wildlife (Majer et al., 2002). Alternatively, invertebrates can play negatively perceived ecological roles, such as those of vectors for disease or pests in the context of agriculture and forestry. Recovery of species-rich invertebrate assemblages in reclaimed areas, particularly species correlated with ecosystem functions, is encouraged (Majer et al., 2002).

Invertebrates are sensitive to environmental change (Buchori et al., 2018). Their mobility allows them to relocate in response to environmental change and, despite their short generational times, they can produce large numbers of offspring, making them a good indicator of environmental change (Samways et al., 2010). Likewise, invertebrates provide a good study focus for measuring species richness (i.e., average species diversity within a site referred to as 'alpha diversity') and drawing comparisons between assemblage compositions found on different landscapes or treated mine-waste–contaminated sites (Gerlach et al., 2013). However, because of complexities associated with the taxonomic identification of invertebrates, they have not historically been used as a means of monitoring or assessing reclamation strategies. Recent progress in molecular identification techniques (deoxyribonucleic acid or DNA metabarcoding) has helped to overcome challenges in taxonomic identification of invertebrates. In this study, the

[1]*The lead author is a 2019 Geoscience BC Scholarship recipient.*

This publication is also available, free of charge, as colour digital files in Adobe Acrobat® PDF format from the Geoscience BC website: http://www.geosciencebc.com/updates/summary-of-activities/.

methods of assessing invertebrate-assemblage response to mine reclamation using DNA metabarcoding to identify invertebrates are examined.

Objectives

The aim of this study is to address research questions established on the basis of using parallel sequencing of invertebrate-community DNA metabarcodes as a new tool for examining reclamation trajectory. The first step entails assessing whether changes can be identified in invertebrate assemblages with different reclamation ages as a result of ongoing succession characterized by changes in biotic assemblages. Secondly, taxa will be examined to establish whether any display the effects of specific experimental factors (amendment, age).

Methodology

In 2017, four mines were sampled in BC: the Teck Resource Highland Valley Copper mine, the New Gold Inc. New Afton mine, the Imperial Metals Corporation Mount Polley mine and the Avino Silver & Gold Mines Ltd. Bralorne Gold mine (Figure 1). At each mine, two reclamation treatments were sampled: sites reclaimed within eight years ('new') and sites that were reclaimed more than eighteen years ago ('old'). A grassland 'control' site was also sampled at the Highland Valley Copper mine site. In this paper, only data from the 'new' and 'old' Highland Valley Copper and New Afton sites, as well as the 'control' site, are examined. Site descriptions, including the year of reclamation, reclaimed materials and the methods used to conduct reclamation of the sampled areas, are presented in Table 1.

Vegetation data and invertebrate samples were collected from the Highland Valley Copper and New Afton sites. Vegetation was measured using canopy cover by species in 0.5 by 0.5 m quadrats. Invertebrate samples were collected using two types of traps: pitfall traps (Figure 2) and Malaise traps (Figure 3). Pitfall traps were used to collect primarily ground-dwelling invertebrates (Bassett and Fraser, 2015). At each site, a 100 m transect was laid out and pitfall traps were placed every 10 m. Pitfall traps were constructed using a 450 g container (Solo® cup) placed so that its top is level with the surface of the ground. The pitfall traps were filled with ethanol and a plastic plate, held up by nails, was placed over them to reduce the amount of ethanol evaporation. Malaise traps are tent-like structures, with bottles of ethanol attached to them and used to collect primarily flying invertebrates (Thomas, 2016). One Malaise trap was placed at each site. The invertebrate traps were left on site for five days once over the summer and samples recovered from them were stored at –20 °C until laboratory processing.

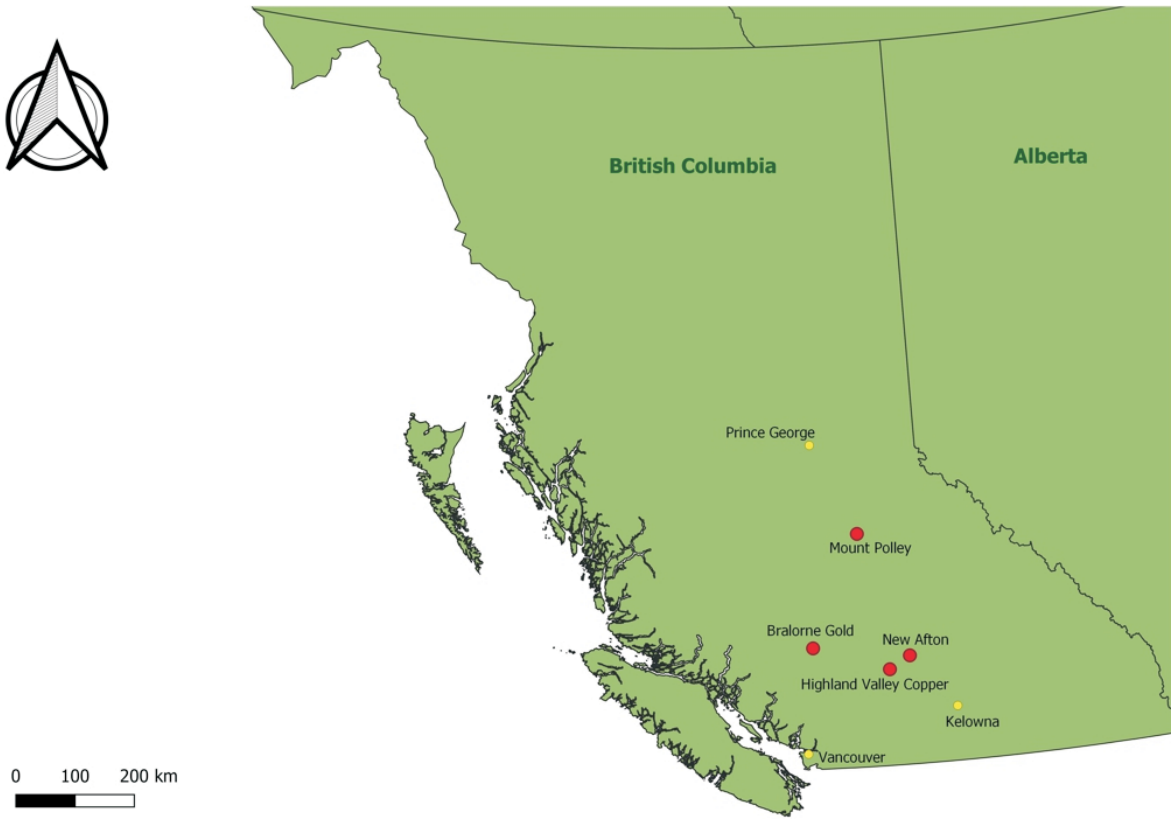

Figure 1. Location of mines in the study area sampled in July and August of 2017 and 2018, including Highland Valley Copper and New Afton, where vegetation and invertebrate data were collected for this paper.

In 2018, the New Afton and Highland Valley Copper sites were resampled. Vegetation and invertebrate sampling were conducted in the same manner as in 2017, except that it was conducted using a 40 m^2 grid instead of a 100 m transect.

Laboratory methods

Identification of the collected invertebrates was conducted using high-throughput DNA metabarcoding. This is done by homogenizing invertebrate tissue in liquid nitrogen using a mortar and pestle (Beng et al., 2016). The DNA was extracted from the homogenized tissue using a Mag-Bind® Blood and Tissue Kit from Omega Bio-tek Inc. A 450 base-pair region of the mitochondrial cytochrome c oxidase subunit 1 gene was amplified in two rounds of polymerase chain reaction (PCR) using the universal PCR primer pair MHemF and dghHCO2198 (Beng et al., 2016). The amplicons were sequenced on an Ion S5™ sequencing platform using an Ion 520™ and Ion 530™ Chip Kit. The bioinformatic pipeline, AMPtk, was used to cluster sequences into operational taxonomic units (OTUs) at an identity threshold of 97% (Palmer et al., 2018); one OTU represented the sequence of one species (Ji et al., 2013). Taxonomies were assigned to each OTU using the Barcode of Life Data System (BOLD) downloaded at the time of analysis (Yu et al., 2012).

Statistical Analysis

The 2017 Highland Valley Copper and New Afton data were analyzed using three types of statistical analyses: one-way analysis of variance (ANOVA), analysis of similarity percentages (SIMPER; Clarke, 1993) and nonmetric multidimensional scaling (NMDS). Data used in the NMDS and SIMPER analyses were rarified data subsampled to 10 000 reads and converted into presence-absence data. The NMDS diagram was created using Euclidean distances among the five sites (Highland Valley Copper 'control', Highland Valley Copper 'old', Highland Valley Copper 'new', New Afton 'old', New Afton 'new') being compared. Calculations carried out using SIMPER were based on the Bray-Curtis dissimilarity index. One-way ANOVA was used to compare species richness between the sites. Log-transformed data were tested for normality, using the Shapiro-Wilk test, and for homogeneity, using the Bartlett's test. There was a gap in New Afton 'old' data as a result of samples still being processed for sequencing; therefore, the mean of the five sites was calculated and applied to the sixth sample when performing the ANOVA test to measure species richness. All the statistical analyses were conducted in RStudio (RStudio, 2015), a free, open-source integrated development environment for the R software system for statistical computing.

Table 1. Site description (years since reclamation from 2019, reclaimed materials and reclamation methods) of the two mines (Highland Valley Copper and New Afton) sampled for invertebrates and vegetation data in summer of 2017.

Mine	Site	Year reclaimed	Years since reclamation	Reclaimed material	Reclamation method
Highland Valley Copper	New	2014	5	Waste rock and overburden	Biosolids
	Old	2000	19	Waste rock and overburden	Seeded (crested wheatgrass)
	Control	n/a	n/a	n/a	n/a
New Afton	New			Tailings	Fertilizer and cattle manure
	Old	2001	18	Tailings	

Figure 2. Pitfall trap set up in 2017 to collect epigeal invertebrates in the study area.

Figure 3. Malaise trap constructed in 2017 to capture flying invertebrates in the study area.

Results

The NMDS diagram illustrates distinct clustering between sample sites; however, the Highland Valley Copper 'control' and New Afton 'new' sites show distinct variation in invertebrate assemblages (Figure 4).

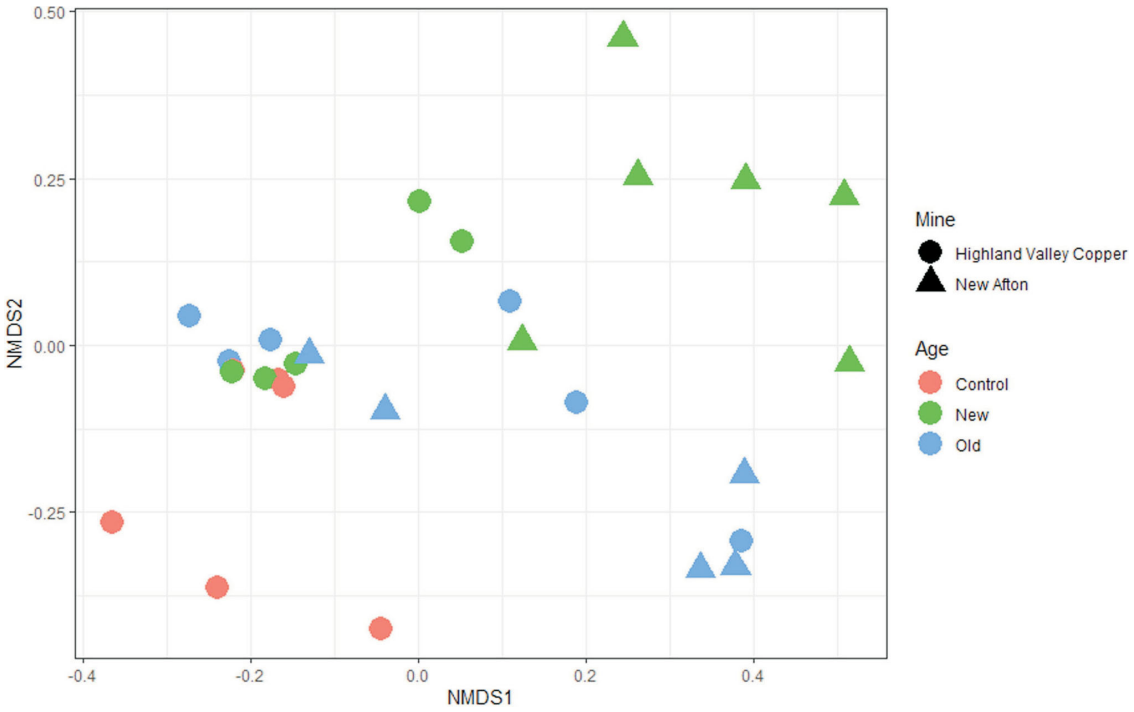

Figure 4. Nonmetric multidimensional scaling (NMDS) diagram created using Euclidian distance, illustrating invertebrate assemblages of different ages ('new', 'old', 'control') between 2017 samples from the Highland Valley Copper and New Afton study sites.

The SIMPER analysis describes the species that are responsible for the difference between the New Afton 'new' site and the Highland Valley Copper 'control' site. Figure 5 highlights the OTUs that define the cumulative top 20% contribution to the difference in invertebrate assemblage between sites. The invertebrate species that explain the distinction between sites are primarily *Hymenoptera* (order of insects that includes sawflies, wasps, bees and ants), *Trichoptera* (caddisfly) and *Phaonia apicalis* (Table 2). It should be noted that there are multiple OTUs annotated as *Phaonia apicalis*, which is a result of genetic variation within the species.

The results of an ANOVA test comparing species richness between sites revealed that there was no significant difference in species richness between sites ($p = 0.448$; Table 3). Figure 6 shows that the New Afton 'new' site had the lowest number of species, whereas the Highland Valley Copper 'old' site contained the highest number of species; however, the variability in species richness for each site was high.

Discussion

The effects of postmining reclamation on recovering invertebrate assemblages were examined in BC. Sequencing of invertebrate DNA metabarcodes showed differences in composition between mine sites and different age diagrams.

Invertebrate assemblage similarity of age diagrams

Understanding the reclamation trajectory of fauna assemblages postmine reclamation is an important objective on the road to achieving a successful end land use. In this study, a separation between age sites ('control', 'old', 'new') is visible in the NMDS diagram (Figure 4). Most notably, there is a difference between the Highland Valley Copper 'control' site and the New Afton 'new' site, indicating separate invertebrate assemblages between three age plots. This could, in part, be due to a body of water near the New Afton 'new' site, which is unique to that site. Furthermore, a small cluster of 'old' sites (both Highland Valley Copper and New Afton) formed together (Figure 4) It should be noted that the New Afton sites are also located on a historic mine-tailings storage facility. Comparatively, the Highland Valley Copper treatment sites are located on wasterock and overburden, whereas the Highland Valley Copper 'control' site is located near the road in a fenced enclosure.

Invertebrate taxa characterizing reclamation age diagrams

Invertebrate DNA metabarcode analysis can be used to generate a profile for all the site assemblages; however, the focus of this study is on the recognition of species that differentiate sites; more specifically, on the most noticeable difference between the Highland Valley Copper 'control'

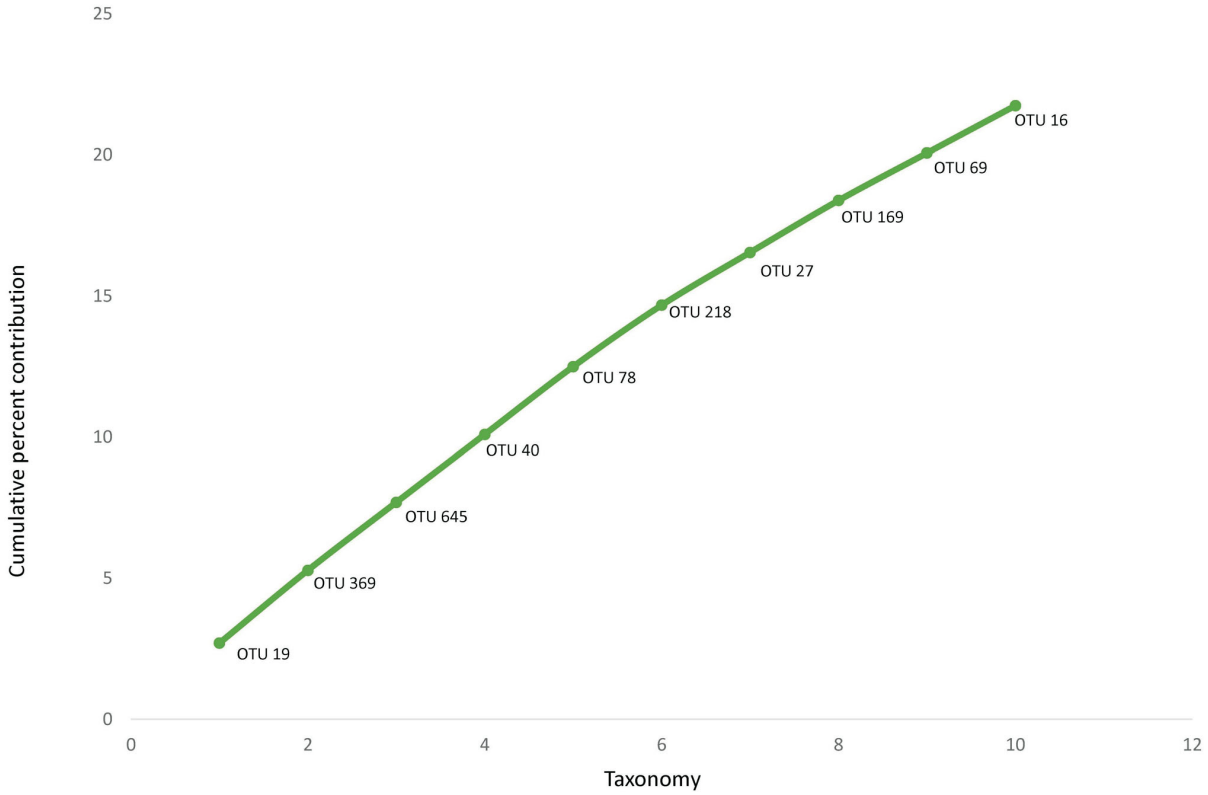

Figure 5. The top ten operational taxonomic units (OTU) explaining variation in community composition between the New Afton 'new' and Highland Valley Copper 'control' sites, as determined by SIMPER analysis based on the Bray-Curtis index of dissimilarity between samples. These top ten species account for 20% of the difference observed between the two sites.

site and the New Afton 'new' site. The taxon that was the most responsible for the difference between sites was *Hymenoptera* (OTU 19; Figure 5), which is an order of invertebrates that includes wasps, sawflies, ants and bees. In this case, the OTU 19 taxa were found predominantly on the New Afton 'new' site. Another species accountable for disparity between the two sites is *Trichoptera* (OTU 369, OTU 40, OTU 78, OTU 169). Four of the ten taxa responsible for the greatest cumulative percent contribution to assemblage difference between the two sites were *Trichoptera* taxa. The multiple OTUs may comprise multiple species or genetic variations of caddisflies. The trichopteran taxa were found primarily in the New Afton 'new' site. Interestingly, *Trichoptera* are used as a bioindicator for good water quality (Pereira et al., 2012) and their presence on the New Afton 'new' site is likely explained by the aforementioned body of water in the vicinity.

Species richness characterizing age diagrams

Data showed no significant difference with regard to species richness between the sampled sites. Despite the New Afton 'new' site appearing to have fewer species detected on site, the variation between the replicates was too great to identify a significant result.

Table 2. List of species responsible for the top 20% of the difference in invertebrate assemblages recorded between the New Afton 'new' site and the Highland Valley Copper 'control' site.

OTU	Taxonomy
OTU 19	*Hymenoptera*
OTU 369	*Trichoptera*
OTU 645	*Phaonia apicalis*
OTU 40	*Trichoptera*
OTU 78	*Trichoptera*
OTU 218	*Phaonia apicalis*
OTU 27	*Phaonia apicalis*
OTU 169	*Trichoptera*
OTU 69	*Phloeostiba lapponica*
OTU 16	*Suillia nemorum*

Table 3. One-way analysis of variance results, comparing species richness defined by the number of operational taxonomic units between each of the five study sites: Highland Valley Copper 'new', 'old' and 'control' sites, and New Afton 'new' and 'old' sites, where 'f' represents the ratio of the two mean-square values and 'p' is the probability of finding the obtained results given that the null hypothesis is true. Abbreviation: d.f., degrees of freedom.

Species richness	d.f.	Mean square	F-value	P-value
Mine sites	4	0.7923	0.958	0.448

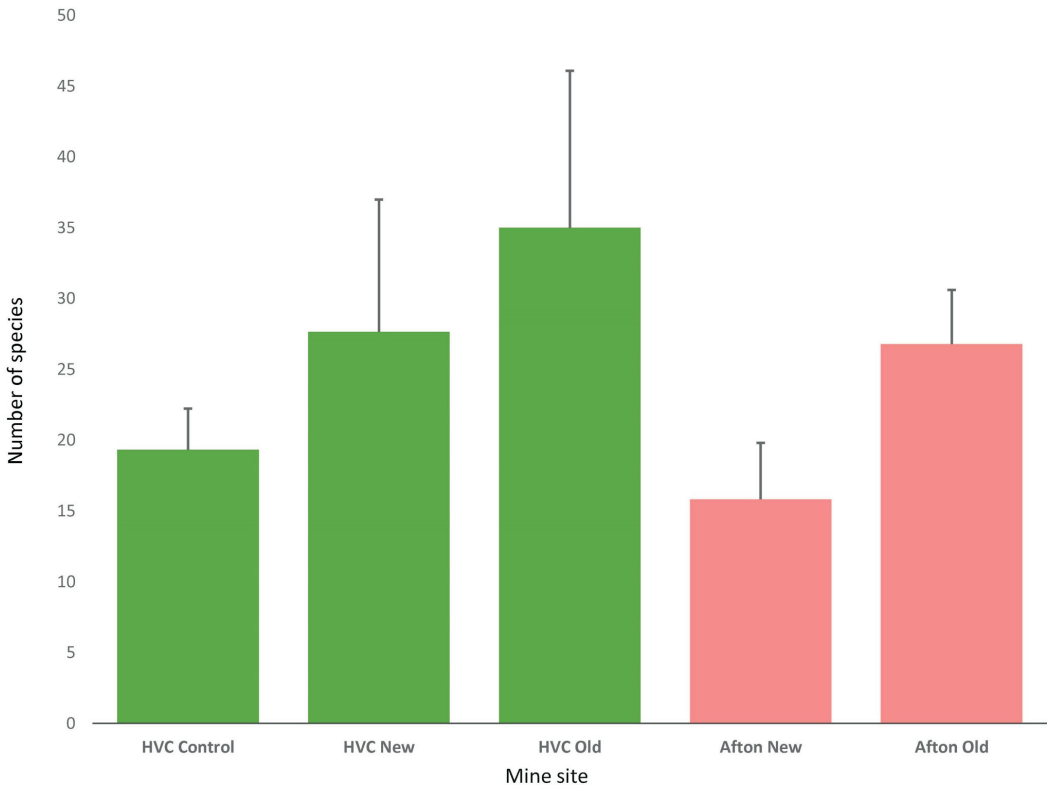

Figure 6. Distribution of species richness between the Highland Valley Copper (HVC) 'new', 'old', 'control' and New Afton (Afton) 'new', 'old' study sites.

Conclusions and Ongoing Work

The above results and correlations are based on data from 2017; additional analyses are underway as the remaining 2017 samples are currently being sequenced. The 2018 samples are also being sequenced and future papers will address the effects of biosolids as a soil amendment.

This study should significantly enhance the knowledge base guiding responsible development and reclamation of mineral extraction sites, factors that are important for the continued growth of the economy and the protection of the environment. Future studies identifying the environmental variables associated with invertebrate recovery may help land managers facilitate restoration through simulation of the relevant conditions. Further development of DNA metabarcoding will make monitoring reclamation via invertebrates more assessable.

Acknowledgments

Funding for this project is provided though Geoscience BC as well as through the Natural Sciences and Engineering Research Council of Canada Industrial Research Chair in Ecosystem Reclamation, with industry partners: Genome BC, Arrow Transportation Systems Inc., the Real Estate Foundation of BC, New Afton mine, Highland Valley Copper mine, Kinder Morgan Canada Limited, Metro Vancouver and the British Columbia Cattlemen's Association. Special thanks to the student researchers who helped in the field and laboratory: J. Foster, B. McAmmond, C. Stephens, M. Coghill, J. Paulson and S. Vogel. The authors also thank peer reviewer A. Fischer.

References

Bassett, E. and Fraser, L. (2015): Effects of cattle on the abundance and composition of carabid beetles in temperate grasslands; Agricultural Studies, v. 3, no. 1, p. 36–47, URL <https://doi.org/10.5296/jas.v3i1.6731> [November 2019].

Beng, K.C., Tomlison, K.W., Shen, X.H., Surget-Groba, Y., Hughes, A.C., Corlett, R.T. and Slik, J.W.F. (2016): The utility of DNA metabarcoding for studying the response of arthropod diversity and composition to land-use change in the tropics; Scientific Reports 6, art. no 24965, URL <https://doi.org/10.1038/srep24965> [June 2019].

Buchori, D., Rizali, A., Rahayu, G.A. and Mansur, I. (2018): Insect diversity in post-mining areas: investigating their potential role as bioindicator of reclamation success; Biodiversitas, v. 19, p. 1696–1702, URL <https://doi.org/10.13057/biodiv/d190515> [August 2019].

Clarke, K.R. (1993): Non-parametric multivariate analyses of changes in community structure; Australian Journal of Ecology, v. 18, p. 117–143.

Gaston, K.J. and Spicer, J.I. (2004): Biodiversity: An Introduction (2nd edition); Blackwell Publishing, Oxford, United Kingdom, 191 p.

Gerlach, J., Samways, M.J. and Pryke, J.S. (2013): Terrestrial invertebrates as bioindicators: an overview of available taxonomic groups; Journal of Insect Conservation, v. 17, p. 831–850, URL <https://doi.org/10.1007/s10841-013-9565-9> [August 2019].

Government of British Columbia (2019): Reclamation & Closure; Government of British Columbia, URL <https://www2.gov.bc.ca/gov/content/industry/mineral-exploration-mining/permitting/reclamation-closure> [May 2019].

Ji, Y., Ashton, L., Pedley, S.M., Edwards, D.P., Tang, Y., Nakamura, A., Kitching, R., Dolman, P.M., Woodcock, P., Edwards, F.A., Larsen, T.H., Hsu, W.W., Bendick, S., Hamer, K.C., Wilcove, D., Bruce, C., Wang, X., Levi, T., Lott, M., Emerson, B.C. and Yu, D.W. (2013): Reliable, verifiable and efficient monitoring of biodiversity via metabarcoding; Ecology Letters, v. 16, p. 1245–1257.

Majer, J.D., Brennan, E. and Bisevac, L. (2002): Terrestrial invertebrates; *in* Handbook of Ecological Restoration;, M.R. Perro and A.J. Davy (ed.), Cambridge University Press, Cambridge, p. 279–294.

McGeoch, M.A., Sithole, H., Samways, M.J., Simaika, J.P., Pryke, J.S., Picker, M., Uys, C., Armstrong, A.J., Dippenaar-Schoeman, A.S, Engelbrecht, I.A., Braschler, B. and Hamer, M. (2011): Conservation and monitoring of invertebrates in terrestrial protected areas; Koedoe, v. 53, p. 1–13.

Mining Association of Canada (2019): Reclamation; Mining Association of Canada, URL <http://mining.ca/reclamation> [February 2019].

Palmer, J., Jusino, M., Banik, M. and Lindner, D. (2018): Non-biological synthetic spike-in controls and the AMPtk software pipeline improve mycobiome data; PeerJ 6:e4925, URL <https://doi.org/10.7717/peerj.4925> [September 2019].

Pereira, L.R., Cabette, H.S.R. and Juen, L. (2012): Trichoptera as bioindicators of habitat integrity in the Pindaíba river basin, Mato Grosso (Central Brazil); International Journal of Limnology, v. 48, no. 3, p. 295–302.

RStudio (2015): RStudio: Integrated Development for R; RStudio, Inc., Boston, Massachusetts, URL <http://www.rstudio.com/> [September 2019].

Samways, M.J., McGeoch, M.A. and New, T.R. (2010): Insect Conservation: a Handbook of Approaches and Methods; Oxford University Press, Oxford, United Kingdom, p. 312–313.

Yu, D.W., Ji, Y., Emerson, B.C., Wang, X., Ye, C., Yang, C. and Ding, Z. (2012): Biodiversity soup: metabarcoding of arthropods for rapid biodiversity assessment and biomonitoring; Methods in Ecology and Evolution, v. 3, p. 613–623.

Post-Mining Reclamation in South-Central British Columbia: Investigating Microbial and Geochemical Changes in Topsoil Stockpiles in Opencast Mining (NTS 092I/09, 093A/12)

A.M. Fischer, Department of Natural Resource Science, Thompson Rivers University, Kamloops, British Columbia, granta18@mytru.ca

L.H. Fraser, Department of Natural Resource Science, Thompson Rivers University, Kamloops, British Columbia

J.D. Van Hamme, Department of Biological Science, Thompson Rivers University, Kamloops, British Columbia

E.M. Bottos, Department of Biological Science, Thompson Rivers University, Kamloops, British Columbia

W.C. Gardner, Department of Natural Resource Science, Thompson Rivers University, Kamloops, British Columbia

Fischer, A.M., Fraser, L.H, Van Hamme, J.D., Bottos, E.M. and Gardner, W.C. (2020): Post-mining reclamation in south-central British Columbia: investigating microbial and geochemical changes in topsoil stockpiles in opencast mining (NTS 092I/09, 093A/12); *in* Geoscience BC Summary of Activities 2019: Minerals, Geoscience BC, Report 2020-01, p. 167–172.

Introduction

Environmental laws and regulations govern mining and oil-and-gas extraction in Canada, including reclamation. Prior to development, resource-extraction companies are required to post a bond as a promissory that their activity and closure will meet approved government environmental standards. Despite the rising demand for restoration management, there is limited research on environmental restoration and there are few dedicated university postgraduate training programs in Canada to address the complexities of ecosystem reclamation. There is a critical need to work with the mining and oil-and-gas industries, in partnership with governmental agencies, to develop better management practices for successful ecosystem restoration.

The easiest way to replace soil and microbial communities after mine closure to their full pre-closing health status (i.e., equivalent soil characteristics, and microbial community composition and function), and therefore the most likely route to achieve fully functional reclamation, would be to simply replace the excavated topsoil with stockpiles of these materials kept on site. Unfortunately, it is known that microbial composition and functions degrade significantly over time, likely depending on factors such as stockpile depth, exposure to sun, and weather, temperature, chemical and microbial interactions (Abdul-Kareem, 1984; Stahl et al., 2002; Ghose and Kundu, 2004). Stockpiles can reach up to 30 m in height and may sit for the entire duration of mine operation, which could be decades. A major question is, "for how long does topsoil stored in piles remain viable?" In order to address this question, it is to characterize topsoil-stockpile viability over time at various depths. Furthermore, strategies must be developed to increase the viability of stored stockpiles.

Current restoration plans and mine-closure proposals for land reclamation are generally not based on sound scientific evidence. They are more likely to be based on past practice and administrative and logistical constraints. In order to rectify this, optimized reclamation methods that allow for a more harmonious coexistence between industry and environment are needed, and this need can be met, in part, by research focused on understanding and mastering ecosystem-reclamation processes.

Objectives

This project investigates factors that affect changes to soil health in topsoil stored in stockpiles by evaluating stockpiles at two gold operations in British Columbia (BC; Figure 1). The aim is to model changes in factors affecting soil health and function with depth, including: microbial communities, geochemical properties and the ability to support plant growth. By characterizing these stockpiles in the field and with greenhouse experiments, the study will improve understanding of the role of bacteria and fungi in restoration.

The working hypothesis is that the topsoil-stockpiling practices at the New Afton mine (Figure 2) and QR mill (Figure 3) have had adverse effects on soil properties and that amending stockpiled topsoil with native soil promotes restoration goals. Consequently, it is predicted that

This publication is also available, free of charge, as colour digital files in Adobe Acrobat® PDF format from the Geoscience BC website: http://www.geosciencebc.com/updates/summary-of-activities/.

1) there will be significant differences in soil composition between depths within the topsoil stockpiles;
2) the variations in composition will result in significant differences in plant growth, with deeper soils being less viable than shallower soils; and
3) the addition of native soil to the topsoil stockpile will result in a significant increase in plant growth and colonization by mycorrhizal fungi.

Sampling

New Afton Mine (New Gold Inc.)

The New Afton Cu-Au mine of New Gold Inc. is located approximately 10 km west of Kamloops in BC's southern interior. The mine is located within the traditional territories of the Tk'emlúps and Skeetchestn Indigenous groups. The topsoil stockpile of interest (Figure 2) is approximately 6 years old and 25 m high, and contains 250 600 m^3 of topsoil materials. Sampling of the topsoil stockpile and the corresponding reference soil occurred during September 2018. Four soil cores were extracted from the stockpile via solid-stem auger drilling by Geotech Drilling Services Ltd. Soil samples were collected at various soil depths and amalgamated into four intervals (0–60 cm, 61–152 cm, 152–610 cm, 610–1372 cm) until the bottom of the stockpile was reached. The corresponding reference soil sample (0–10 cm) was collected from an undisturbed grassland site close to the New Afton mine.

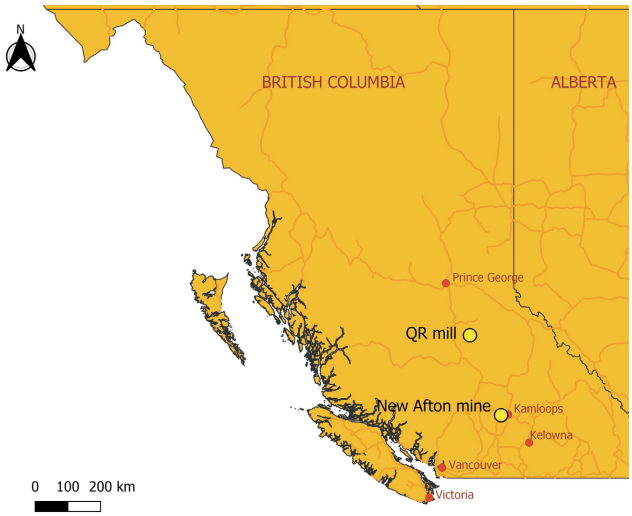

Figure 1. Sampling locations in south-central British Columbia.

QR Mill (Barkerville Gold Mines Ltd.)

Sampling at the QR mill of Barkerville Gold Mines Ltd. in Cariboo, BC was completed in May 2019. Barkerville Gold Mines has a 20-year-old, 6 m deep topsoil stockpile at the QR mill (Figure 3). Three holes were dug using an excavator to access various layers of the stockpile (0–10 cm, 10–20 cm, 60–120 cm, 200–260 cm, 350–390 cm and 500–575 cm). A corresponding reference soil sample (0–10 cm) was collected in an undisturbed forest site adjacent to the mill.

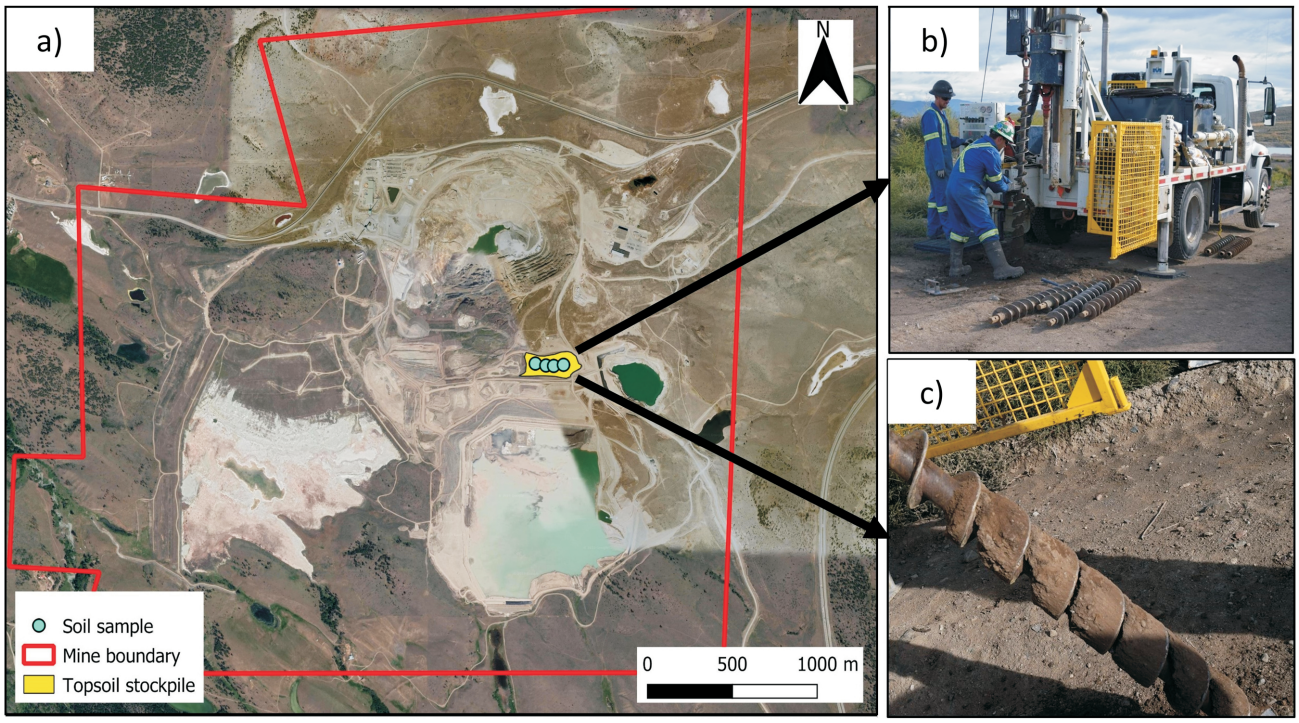

Figure 2. Location of the New Afton mine study area: **a)** aerial view, showing the New Afton mine boundary with the topsoil stockpile and four sampling locations; **b)** auger drill used to access different layers of the topsoil stockpile for sampling; **c)** section of a core sample from the topsoil stockpile.

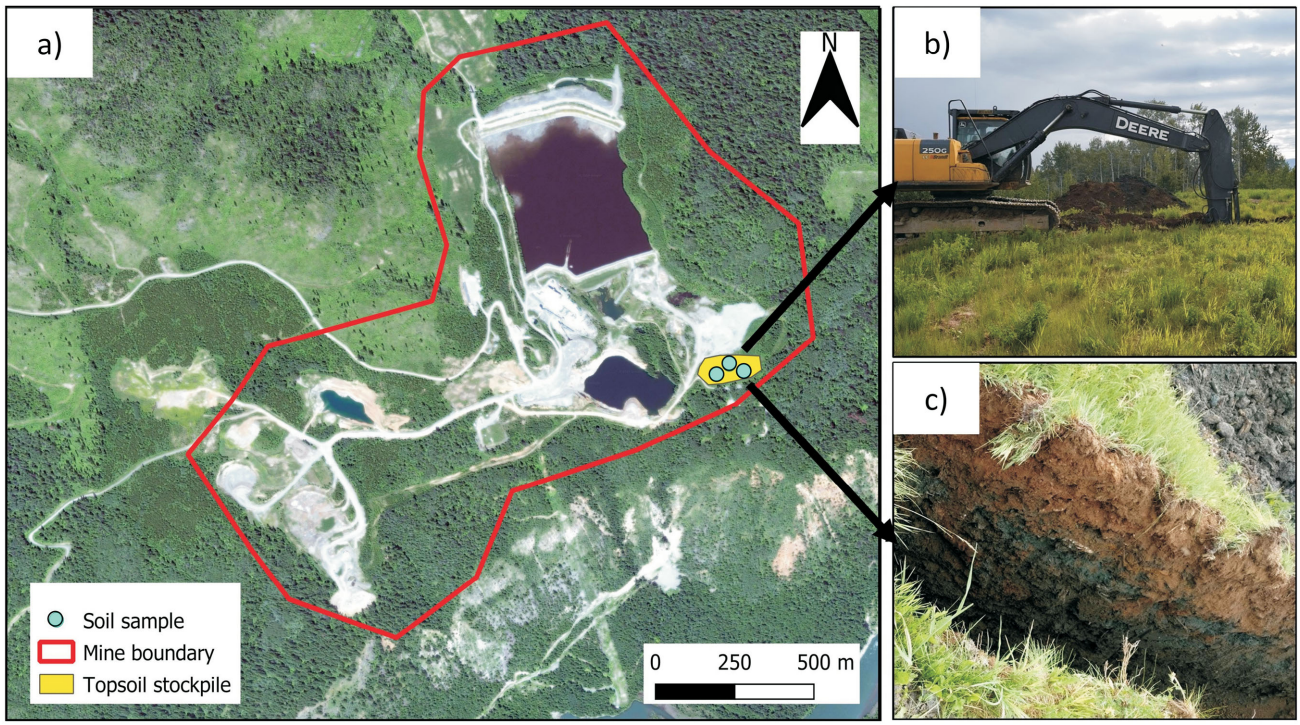

Figure 3. Location of the QR mill study area: **a)** aerial view, showing the QR mill boundary with the topsoil stockpile and three sampling locations; **b)** mechanical digger used to access different layers of the topsoil stockpile for sampling; **c)** hole left by excavator, exposing different layers of the topsoil stockpile.

Soil Properties Methodology

Microbial

The DNA from the soil samples was extracted using a MagAttract PowerSoil DNA Kit (QIAGEN, Hilden, Germany), and a portion of the bacterial 16S rRNA gene was amplified by Polymerase Chain Reaction (PCR) using primers 341F and 806R. For fungi, the primers ITS86F and ITS4R were used to amplify the second internal transcribed spacer of the nuclear ribosomal DNA (ITS2) region between the 5.86S rRNA and 28S rRNA genes. Amplicon libraries were prepared for sequencing during a second round of PCR with indexed primers, and purified with AgenCourt AMPure (Beckman Coulter Inc., Brea CA) magnetic beads to remove DNA under 100 base pairs in length. Sequencing was carried out using 400 base-pair chemistry on an Ion Torrent S5 XL platform (Thermo Fisher Scientific, Waltham, MA). Counts were rarefied as outlined in McKnight et al. (2019). Operational taxonomic units (OTU) clustering and taxonomy assignment were carried out using the bioinformatic pipeline AMPtk (Palmer et al., 2018).

Chemical

The major-element composition of soil samples was measured at the Analytical Laboratory of the Ministry of Environment and Climate Change Strategy in Victoria, BC. The samples were dried at 70°C for 24 hours, then sieved through a 2 mm pan. A complete profile of Al, B, Ca, Cu, Fe, Mg, Mn, P, K, S and Zn is being carried out. In the Thompson Rivers University (TRU) greenhouse lab, organic matter (OM) content was measured using loss-on-ignition (LOI), and pH and electrical conductivity (EC) were determined using a Palintest® 800 meter. Additionally, C, S and N were measured with a Thermo Scientific CHNS Elemental Analyzer.

Greenhouse Experiment

The greenhouse trial examines whether the depth of stockpile soil will impact its ability to support vegetation. Bluebunch wheatgrass is grown in pots of soil from varying depths in the stockpiles for three months. The cores or holes collected at the topsoil stockpiles are combined and mixed, and each depth is replicated ten times. The plants will be analyzed for dry-shoot weight, dry-root weight, shoot height, root height, chlorophyll content and mycorrhizal fungal colonization. Colonization will be measured using the root-clearing and -staining methods described in Vierheilig et al. (1998).

Data Analysis

For analyzing the effect of depth on soil geochemical and microbial properties, a repeated measures design was used. The cores or holes collected at the topsoil stockpiles will be treated as replicates for analyses, except for the greenhouse experiment, where soils were combined. All errors are re-

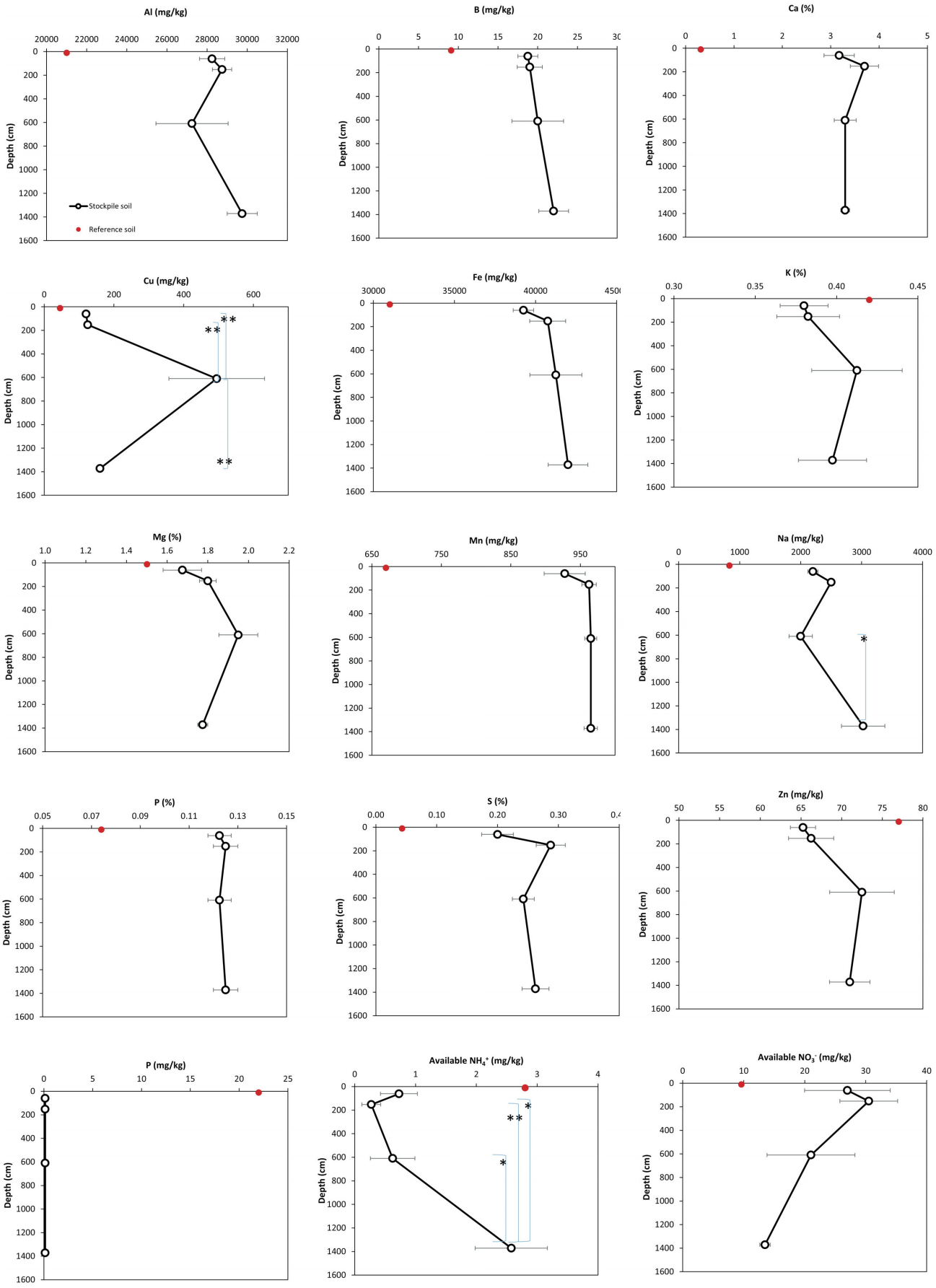
Al (mg/kg)
B (mg/kg)
Ca (%)
Cu (mg/kg)
Fe (mg/kg)
K (%)
Mg (%)
Mn (mg/kg)
Na (mg/kg)
P (%)
S (%)
Zn (mg/kg)
P (mg/kg)
Available NH4+ (mg/kg)
Available NO3- (mg/kg)
Depth (cm)
Stockpile soil
Reference soil

ported at standard error. One-way and repeated measures ANOVA will be used to test significance between depths. A non-metric multidimensional scaling (NMDS) plot will be used to understand the similarities or differences between bacteria and fungi communities with depth. The relationship between soil parameters and depth will be summarized using principal-component analysis (PCA) in R software.

Preliminary Results

Analyses for this project are ongoing. All results reported below are preliminary and should not be taken as complete. The microbial-community analyses are currently in progress, so there are no results available to report.

Elements and Nutrients

Soil-nutrient profiles and elemental properties for the topsoil stockpile at the New Afton mine, when compared to the grassland reference soil, showed that the stockpile has notably higher levels of Al, Ca, Cu, Fe, Mn, Na and available NO_3^- (Figure 4), and is higher in pH and EC (Figure 4). In contrast, the reference soil was found to be substantially higher in P. Significant differences (one-way ANOVA) were observed between depths in the stockpile for Cu, Na and NH_4^+ ($p = 0.006, 0.023, 0.025$ and $F = 6.91, 4.62, 7.12$, respectively). The 152–610 cm depth interval for Cu and the 610–1372 cm depth interval for NH_4^+ were significantly different from all other depths, whereas the 152–610 cm depth interval for Na was significantly different from the 610–1372 cm interval.

Figure 5 shows the profiles for soil nutrients and elemental properties in the topsoil stockpile at the QR mill of Barkerville Gold Mines Ltd. The OM content in this stockpile varied from 5 to 10%, and the 0–10 cm depth interval was significantly higher in OM than the other intervals ($p = 0.00148$, $F = 7.293$). The corresponding forest reference soil fell within the range of the stockpile for OM, pH and EC.

Discussion

Results show that some soil properties appear to change with depth in stockpiles due to storage. For example, the New Afton mine stockpile had higher levels of Na at the bottom (610–1572 cm depth). In addition, a significant increase in Cu occurred at 152–610 cm. Whether varying properties such as these will impact plant growth is being investigated

Interestingly, OM in the New Afton mine and QR mill stockpiles remains generally unchanged below the 0–10 cm depth, even after 6 and 20 years of storage, respectively. It is hypothesized that the lower OM levels in the New Afton mine stockpile (2%) and in the QR mill stockpile (5%) should be sufficient for plant growth; this is currently being evaluated in greenhouse experiments.

Another interesting finding is the significant increase in available ammonium (NH_4^+) with depth and a somewhat parallel decrease (not significant) in available nitrate (NO_3^-) in the New Afton mine stockpile. This may indicate a

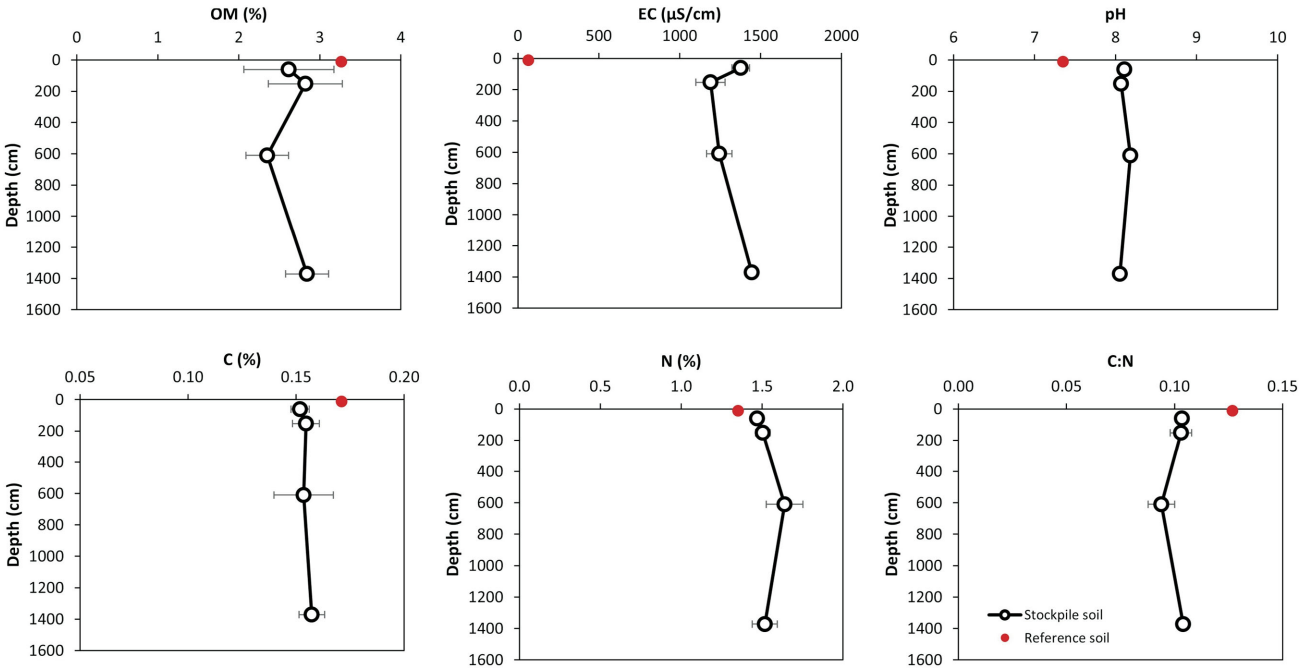

Figure 4. [to left and above] Depth profiles (n = 4) for various analytical parameters in a topsoil stockpile at the New Afton Cu-Au mine of New Gold Inc. and a corresponding grassland reference soil (mean ± standard error of the mean). Significance between depths denoted by * ($p < 0.05$) or ** ($p < 0.01$).

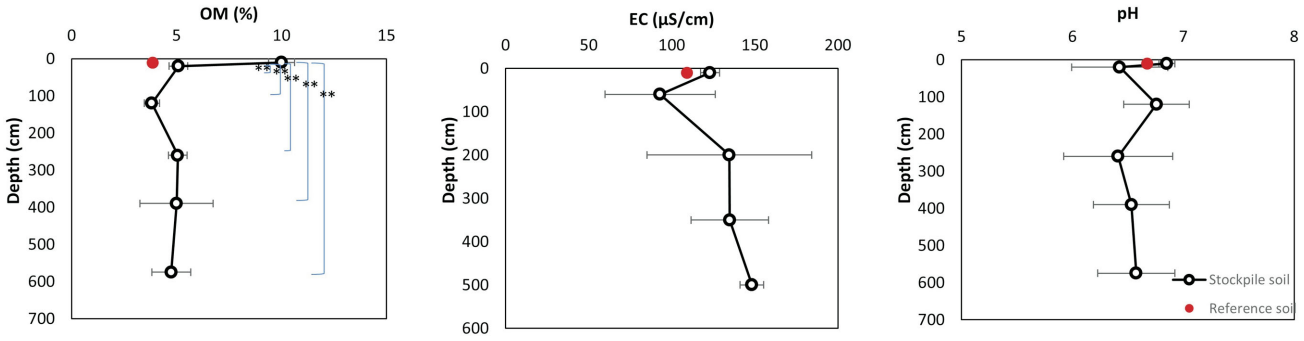

Figure 5. Depth profiles (n = 3) for various analytical parameters in a topsoil stockpile at the QR mill of Barkerville Gold Mines Ltd. and a corresponding forest reference soil (mean ± standard error of the mean). Significance between depths denoted by ** (p <0.01).

change to anaerobic conditions at the bottom of the stockpile, since NO_3^- can be reduced to NH_4^+ in the absence of oxygen (Buresh and Patrick, 1978).

Although statistical significance is shown with some analyses, it should be noted that, with only four replicates (cores) from the New Afton mine and three replicates (holes) from the QR mill, the power of this significance, as determined from a one-way ANOVA, is limited.

Overall, results indicate that there do not seem to be any substantial indicators, based on the preliminary chemical and nutrient profiles of the two stockpiles, that either would be unfit for use in revegetation during reclamation, particularly with respect to OM content. Major-element and nutrient measurements are being completed for the QR mill samples, allowing for additional analyses. For both the New Afton mine and QR mill soil samples, analysis of total C, H, N and S, the greenhouse experiment and microbial analysis are in progress.

Conclusions

This research provides new information on post-mining reclamation, with an emphasis on above-ground–below-ground linkages, thus potentially allowing industry to improve reclamation practices. The project addresses knowledge gaps in industry by exploring the compositional nature of topsoil stockpiles and their ability to facilitate post-mining revegetation.

Acknowledgments

In addition to Geoscience BC, this project is funded through an NSERC Industrial Research Chair in Ecosystem Reclamation with the following industry partners: Metro Vancouver, New Afton Mine, Highland Valley Copper Mine, Barkerville Gold Mines Ltd., Genome BC, Arrow Transportation, the Real Estate Foundation of BC, Kinder Morgan Canada and the BC Cattlemen's Association. Thanks go to J. Singh, who peer-reviewed this submission. Additional thanks go to all the researchers who helped in the field and the lab: B. McAmmond, S. Vogel, C. Gervan, M. Coghill and S. Kega.

References

Abdul-kareem, A.W. and McRae, S.G. (1984): The effects on topsoil of long-term storage in stockpiles; Plant and Soil, v. 76, URL <https://link.springer.com/article/10.1007/BF02205593> [November 2019].

Buresh, R.J. and Patrick, W.H. (1978): Nitrate reduction to ammonium in anaerobic soil; Soil Science Society of America Journal, v. 42, no. 6, p. 913, URL <https://doi.org/10.2136/sssaj1978.03615995004200060017x> [November 2019].

Ghose, M.K. and Kundu, N.K. (2004). Deterioration of soil quality due to stockpiling in coal mining areas; International Journal of Environmental Studies, v. 61, no, 3, p. 327-335, URL <https://doi.org/10.1080/0020723032000093991> [November 2019].

McKnight, D.T., Huerlimann, R., Bower, D.S., Schwarzkopf, L., Alford, R.A., and Zenger, K.R. (2019): Methods for normalizing microbiome data: an ecological perspective; Methods in Ecology and Evolution, v. 10, no. 3, p. 389–400, URL <https://doi.org/10.1111/2041-210X.13115> [November 2019].

Palmer, J.M., Jusino, M.A., Banik, M.T. and Lindner D.L. (2018). Non-biological synthetic spike-in controls and the AMPtk software pipeline improve mycobiome data; PeerJ 6:e4925, URL <https://doi.org/10.7717/peerj.4925> [November 2019].

Stahl, P.D., Perryman, B.L., Sharmasarkar, S. and Munn, L.C. (2002). Topsoil stockpiling versus exposure to traffic: a case study on in situ uranium wellfields; Restoration Ecology, v. 10, no. 1, p. 129–137, URL <https://doi.org/10.1046/j.1526-100X.2002.10114.x> [November 2019].

Vierheilig, H., Coughlan, A.P., Wyss, U. and Piché, Y. (1998). Ink and vinegar, a simple staining technique for arbuscular-mycorrhizal fungi; Applied and Environmental Microbiology, v. 64, no. 12, p. 5004-5007, URL <https://www.ncbi.nlm.nih.gov/pmc/articles/PMC90956/pdf/am005004.pdf> [November 2019].

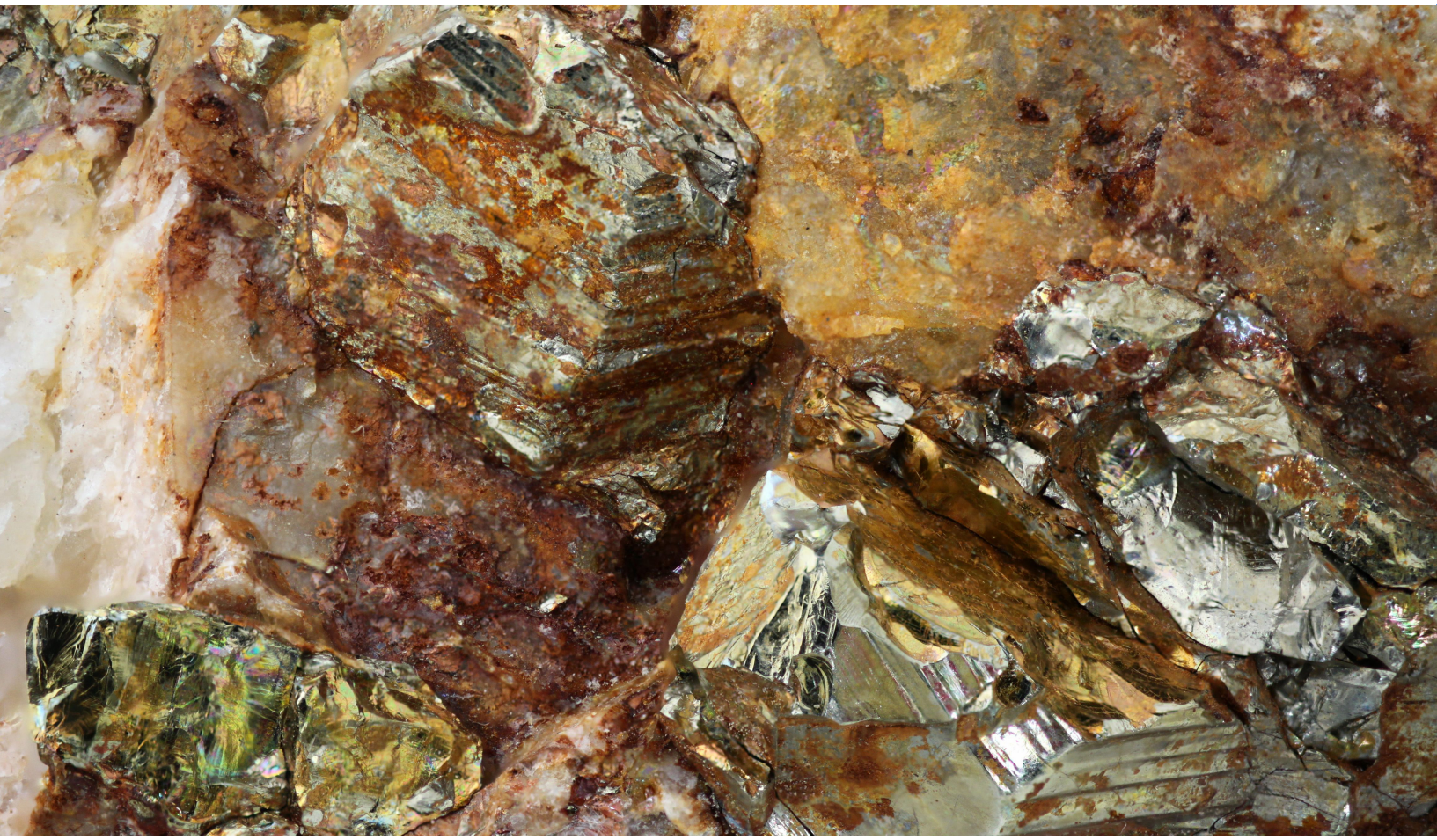

Geoscience BC

t: 604 662 4147
e: info@geosciencebc.com

SUITE 1101–750 WEST PENDER ST
VANCOUVER, BC V6C 2T7

www.geosciencebc.com